Observations of Glitches in PSR 0833-45 and 1641-45.

THESIS

submitted in fulfilment of the

requirements for the degree of

Doctor of Philosophy

of Rhodes University.

by

Claire S. Flanagan

December 1995

Abstract.

An eleven-year series of radio timing observations of 0833-45 (Vela) and PSR 1641-45 is presented. During this time, five large spin-ups ("glitches") were observed in 0833-45 and one in 1641-45. The stellar response to these events is investigated, and the three relatively long complete inter-glitch intervals in 0833-45 are modeled.

The results are of relevance to studies of the interiors of neutron stars. The initial aim of the project — to obtain good observational coverage of large glitches in the Vela pulsar — was successfully achieved, and high quality observations of the periods between glitches were obtained as a by-product. The results of the analysis presented here provide support for the existence of both linear and non-linear coupling in the Vela pulsar, and put a limit on the former in PSR 1641-45. The recently observed existence of a rapidly recovering component of part of a glitch in Vela was verified in the subsequent glitch, although there is now evidence to contradict the suggestion that this component involves a particular region of the star that is implicated in every glitch. Observations of a recent glitch in the same pulsar have resolved a small component of the spin-up; such a component has not been reported for any other large glitch.

Acknowledgements.

I would like to thank the following people:

my supervisors, George Nicolson and Eddie Baart, for their endless patience;

the staff of the Hartebeesthoek Radio Astronomy Observatory, who maintain the telescope, passed on glitch alarms, did thousands of observations, argued over the results, and encouraged me;

the Director of HartRAO, George Nicolson, who initiated the project and was excited about the results;

my family and friends for tolerating this thesis.

Contents.

Appendices.

Figures.

Tables.

1 Introduction.

The subject of this thesis is an eleven-year series of radio pulsar observations of PSR 0833-45 and 1641-45, made at the Hartebeesthoek Radio Astronomy Observatory (HartRAO) near Johannesburg. This chapter attempts to put these observations into perspective; more detailed and balanced reviews of pulsar astronomy can be found in Krause (1986), Taylor & Stinebring (1986), Srinivasan (1989), and Lyne & Graham-Smith (1990).

1.1 Manifestations of Neutron Stars.

Over the last 60 years, neutron stars have developed from an exotic figment of the imagination of theorists (fig. 1-1), to a realistic stellar model that has withstood the rigours of observational testing. Many of the observations that have driven the refinement of this theory have been of pulsars, especially radio timing observations such as those described in this thesis.

Legend has it that neutron stars were first proposed by Landau in Copenhagen, on the same day (in 1932) that the news of Chadwick's discovery of the neutron reached Copenhagen (e.g. Hewish 1986). Neutron stars were first formally described in 1934 by Baade & Zwicky, who also suggested their formation in supernovae. Landau was also the first to propose another star made of cold degenerate matter, this one supported by electron pressure — the white dwarf. The enormous differences between white dwarfs and neutron stars are mainly because neutrons (a) are much heavier and (b) interact through the strong force, compared with the degenerate electrons that support the white dwarfs.

Although thermal emission has been detected from the surfaces of few if any neutron stars (i.e. direct observations of neutron stars are still tenuous), these stars have been detected or proposed in a variety of stellar systems:

Radio pulsars (PSR): The accepted definition of a radio pulsar is probably: a non accreting compact star from which radio pulses are observed. However, pulsed optical, infrared, X-ray and 7-ray emission has also been detected from a small number of the radio pulsars. The large magnetic field of these objects gives rise to a narrow beam of coherent radio emission, believed to originate above a magnetic pole. Mis-alignment of the magnetic and rotation axes enables a favourably located observer to detect regular radio pulses.

X-ray binaries: About 10% of the rest mass of matter accreting onto the neutron star component of a binary system is converted into X-rays, at

the neutron star surface. Over 100 such X-ray binaries are known. They are generally classified according to the companion-star mass, into high-mass X-ray binaries (HMXB; M, $10\ M_e$), low-mass X-ray binaries (LMXB; $2M_®$), and Be binaries (in which the companion is a B emission star, with a mass intermediate between the LMXB and HMXB). The X-ray binaries are also classified according to their emission characteristics, into X-ray pulsars and X-ray bursters. See White (1989) for a review.

7-ray bursters (GRB): There is little consensus on the underlying source of these enigmatic signals, even on whether they are at local or cosmological distances (e.g. Blaes 1994). Neutron stars in an extended Galactic halo are implicated in some of the proposed models; recent work by Lyne & Lorimer (1994) implies that pulsars can be born with velocities greater than the escape velocity from the Galaxy, thus addressing the problem of the source of these neutron stars.

Soft 7-ray repeaters (SGR): Three of the 7-ray bursters have been observed to repeat, one at least 100 times. The association of two of these with supernova remnants (e.g. Kulkarni & Frail 1993) is strong evidence for an underlying neutron star. Models involving neutron stars, summarised by Paczpiski (1989), include starquakes and mass accretion,

SS433: SS433 is a strange galactic optical, X-ray and radio source, which appears to have a high-velocity jet. Although there has been speculation that this object is a black hole, recent measurements by D'Odorico et *al.* (1991) put its mass at $0{,}8 \pm 0{,}1\ M_{d}p$, i.e. below the upper limit for a neutron star. Recently, jets have been discovered in two more galactic X-ray sources (e.g. Tingay *et al.* 1995); it has been suggested that these may be black holes.

Geminga: The status of this object evolved recently from a mysterious -y-ray source to a young (3×10^5 yr) isolated pulsar that would be a radio pulsar if it were more favourably aligned, when pulsations were discovered in X-ray observations (Halpern & Holt 1992) and confirmed in archival -y-ray data (Bertsch *et al.* 1992, Bignami & Caraveo 1992).

Alpar, ogelman &r Shaham (1993) have suggested that the relatively large value of St obtained from the 7 yr span of COS-B data is reminiscent of the interglitch behaviour of the Vela pulsar.

Thorne-4tkow objects: These hypothesized objects are massive stars with degenerate neutron cores (Thorne & Zytkow 1977).

Figure 1-1: First published Neutron Star Model.

First published model of neutron star formation in supernovae, January 1934_ Reproduced in Nature 356, 485 (1992).

1.2 Observations of Radio Pulsars.

The name "pulsar" describes the discovery observation of this remarkable class of stellar object - a train of fast (?-, 1Hz), extremely regular radio pulses (Hewish *et* at. 1968). Soon after the announcement of their discovery, pulsars were recognised by Gold (1968) as manifestations of the hitherto purely theoretical concept, the neutron star. The discovery, which is both a classic example of serendipity and a spectacular confirmation of theoretical prediction, is described vividly by Jocelyn Bell-Burnell (1978), one of the discoverers. Observations of pulsars have since provided insight into fields as diverse as degenerate neutron matter, general relativity, the interstellar medium, and SET! (see review by Blandford 1992). In addition, such studies regularly throw up complete surprises - such as millisecond pulsars and pulsars that are ablating their companions - that keep reminding us that there is still much to be discovered about these amazing objects.

The diverse applications of pulsar studies are due to the unusual properties of pulsar emission - the time-marker, the regularity and sharpness of the pulses, and the small size of the emission region. The data presented in this thesis are relevant to the study of the neutron star interior. Here, the radio pulsar has advantages over other manifestations of neutron stars - they are relatively well understood (compared to gamma-ray bursters for instance); they are numerous (over 560 are listed in the pulsar catalogue at Princeton, and there are a number of pulsar searches currently adding to this); they are relatively "clean" systems compared to X-ray binaries, for which the torques associated with accretion must be separated from those due to internal processes.

Fig. 1-2 shows the observation parameters most relevant to this area of study, for many of the major pulsar timing projects. Not listed are the few single-object programs, which observe objects such as the Hulse-Taylor binary pulsar and the Crab pulsar. At the time the HartRAO project was initiated, in 1982 (observations started in 1984), most large pulsar timing projects were no longer operating. The re-kindling of interest in this type of project in the late 1980's (note the large number of pulsars currently observed from major observatories) is due to a number of factors:

- the discovery (in 1982) of a new class of pulsar - the millisecond pulsars - members of which often occur in binary systems and appear to have an evolutionary link with X-ray binary systems;
- the existence of high-energy observatories (currently ASCA and ROSAT (X-ray) and the Compton Gamma-ray Observatory); pulsar observations made with these instruments require rotational ephemerides, best acquired at radio frequencies, for their reduction;

- the ongoing discovery of new pulsars, especially rapidly rotating millisecond and young pulsars.

A major motivation for initiating a pulsar timing project at HartRAO was the possibility of "catching" a glitch until the Vela glitch of 1981, the epoch of none of the glitches was known to better than a week; it was suspected that the observations of the more immediate post-glitch response would be valuable. The project also targeted a number of other southern pulsars (initially five; this number has grown to 27 over the years). The advantages of this project (more relevant at the time than now) were:

- better time resolution (observations were initially made once per week, a significant improvement on the once per month typical at larger observatories);
- dual-frequency observations;
- access to southern pulsars.

An additional factor, still relevant, is the flexible scheduling policy followed at HartRAO, which enables approaches such as the glitch detection system described later to operate effectively.

1.3 Pulsars 0833-45 and 1641-45.

PSRs 0833-45 and 1641-45, the objects of this thesis, are two of the strongest known radio pulsars at the relatively high observing frequencies used at HartRAO. A brief summary of what is known of them is given below.

PSR 0833-45 (Vela) was discovered in 1968 by Large *et at.* in the Vela supernova remnant, with which it was associated. This makes it one of the dozen or so cases of such associations (e.g. Caraveo 1993). Although there has been some controversy over the exact birthplace of the pulsar (e.g. Bignami & Caraveo 1988), recent X-ray observations of both the supernova and "explosion fragments" by Aschenbach *et at.* (1995) now place the pulsar at the centre of the remnant. At a distance of '--500pc, it is one of the nearest young pulsars. The pulsar has an optical counterpart (Cache *et al.* 1969); optical pulsations from this star were discovered in 1977 by Wallace *et al.* Pulsations in medium energy -y-rays were discovered by Turner *et al.* (1984). At X-ray energies, various nebulae are seen around the pulsar (e.g. Ogelman & Zimmermann 1989); pulsed X-rays were also recently reported, by Ogelman *et al.* (1993).

Besides its association with a 12000yr old remnant and its 11300yr spin-down age, the pulsar has another feature attributable to youth - it doesn't

Figure 1-2: Pulsar Timing Projects,

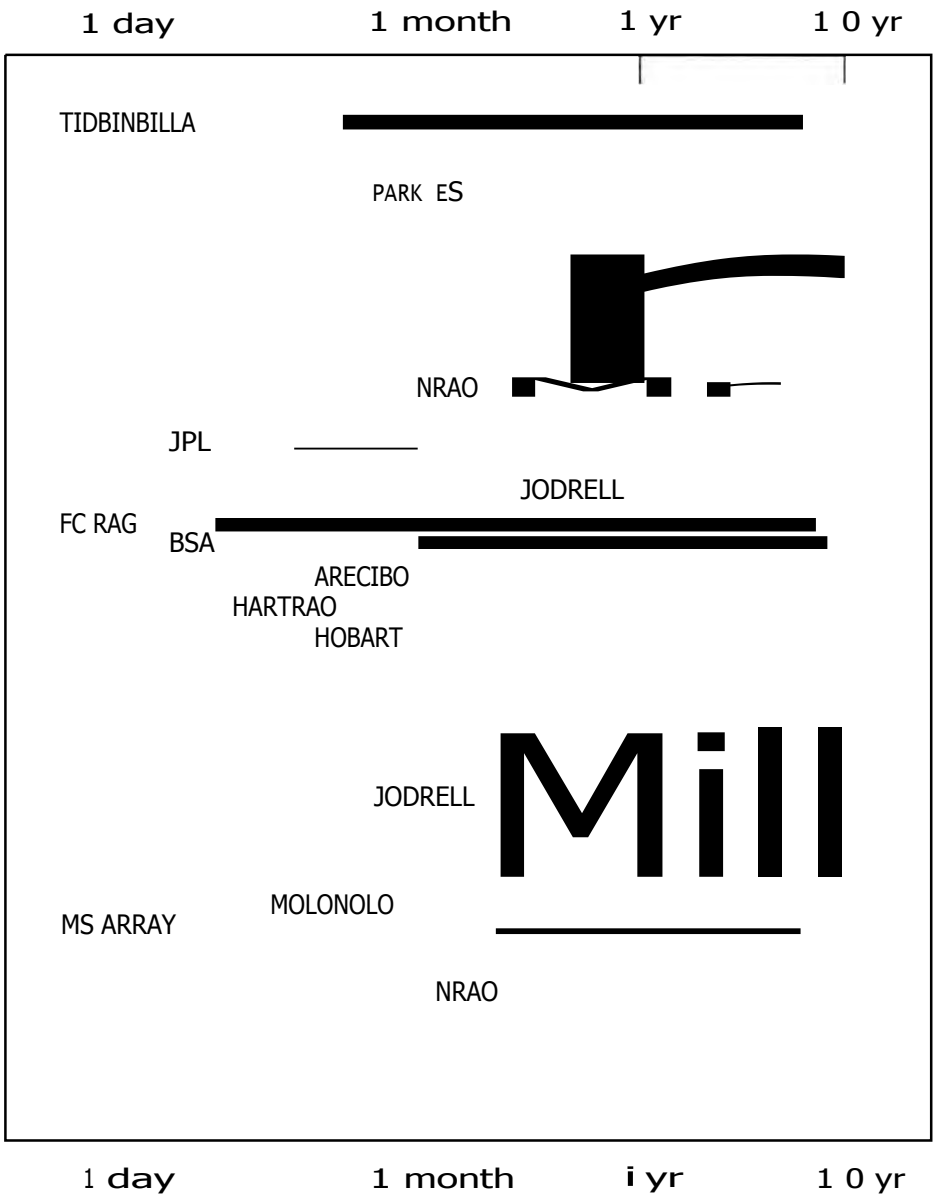

Parameters of most radio pulsar observing projects reported in the literature: the vertical extent of each block is proportional to the number of sources observed; inter-observation spacing and duration of project (i.e. shortest and longest timescales investigated) are indicated on the logarithmic horizontal axes.
Those projects that commenced prior to 1984 are shown above the bar corresponding to the HartRAO project; most of these had been terminated by 1984. Many of those that commenced since 1984 (lower half of the diagram) are ongoing.

appear to null (nulling fraction < 8 x 10^{-6}; Biggs 1992). Vela is also well-known for its timing noise, and was recently subjected to chaos analysis by Harding *et al.* (1990; the results could not distinguish between random noise and non-linear dynamics as the underlying source). Its velocity is around 90km s^{-1} (Ogelman *et al.* 1989).

In contrast, **PSR 1641-45** seems to have been rather neglected - discovered in 1973, it was only included in the JPL timing program 8 yr later. Timing noise *was* not apparent in the short length of these observations (Downs & Krause-Polstorif 1986), but was noted by Manchester et *al.* (1983). At a distance of 3.9-5.3kpc (Frail & Weisberg 1990), it is not a promising candidate for high-energy or proper motion studies. It also has a low fraction of nulls (< 0.4%; Biggs 1992).

1.4 This Thesis.

This thesis discusses glitches observed in the two pulsars 0833-45 and 1641-45. A summary of published glitch observations is given in chapter 2. Chapter 3 describes the current status of models developed to explain these events. In chapters 4 and 5, the equipment and analysis methods used at HartRAO are described. HartRAO observations of six large glitches are presented in chapter 6. Various aspects of these observations are discussed in subsequent chapters: searches for glitches of intermediate size in chapter 7, the inter-glitch behaviour of the Vela pulsar in chapter 8, transients observed following the Vela glitches (chapter 9), and an investigation into dispersion variations accompanying the most recent two Vela glitches (chapter 10). The timing behaviour of PSR 1641-45 is discussed in chapter 11. Chapter 12 summarises these results_

Some of these results have already been published in the astronomical literature: the hitherto unobserved transient following the 1988 glitch in Vela (Flanagan 1990), and the events in PSR 1641-45 (Flanagan 1993). HartRAO observations of the 1985 Vela glitch were combined with those from Hobart for presentation at a conference, by Klekociuk *et at.* (1986). In addition, the success of the glitch detection system has enabled rapid notification of the astronomical community of these events via the IAU Circular system (Flanagan 1988, 1991, 1994, 1994a).

2 Glitch Data.

In this chapter, glitches are described, and all glitch observations published in the literature are assembled.

2.1 General Trends.

As the time span covered by observations increases, it is becoming apparent that all pulsars undergo continuous small, random variations in rotation frequency and its derivative, known as timing noise (e.g. Groth 1975, Cordes & Helfand 1980). A glitch is a sudden change in the rotation frequency that is clearly above the level of this timing noise.

Only those events which are clearly glitches are discussed here - changes in spin-rate which have been reported as glitches but are not above the level of timing noise, or appear to occur slowly, are not included. Examples of such rejected events are the spin-ups of PSR 1508+55 (Manchester Sz Taylor 1974) and PSR 1951+32 (Foster *et al.* 1990), and the "slow glitches" identified by Gullahorn Sz Rankin (1982).

The first two pulsars in which glitches were observed are the Vela and Crab pulsars_ Both have since undergone additional events. Glitches in these two pulsars differ in both magnitude and post-glitch response: the spin-up, $\Delta\nu/\nu$, of Crab events is typically 10^{-8}, and most of $\Delta\nu$ decays within weeks of the glitch. Vela glitches, on the other hand, are two orders of magnitude larger, and typically 95% of the spin-up in Vela remains as a permanent feature (or decays over timescales > 50yr). The classification of glitches into "Crab-type" and "giant", or "Vela-type", in the early years of pulsar observing has persisted, although glitches of intermediate size have since been observed. Interestingly, at least three pulsars (Vela, PSR 1641-45, PSR 0355+54). have undergone both Vela- and Crab-type glitches, differing in magnitude by two to three orders of magnitude; for comparison, ΔS_{2152} of the first nine giant glitches in the Vela pulsar falls within the range $(1.1 — 3.1) \times 10^{-6}$. PSR 1737-30, however, exhibits an apparent continuum of glitch sizes.

A trend becoming apparent now that larger numbers of pulsars are being monitored is an age-dependence of pulsars that glitch. McKenna & Lyne (1990) have defined a "glitch activity" parameter - the fractional amount of change in rotation frequency per year. They note that the "youthful" pulsars, of age $(10— 20) \times 10^3$ years, have by far the greatest glitch activity; this activity appears to decline with increasing age (Lyne 1995). Only Crab-sized glitches have been observed in the very youngest pulsars (age 10^3 years), and these are relatively infrequent. Vela-sized glitches have been observed in

Table 2-1: Parameters of Glitching Pulsars

Pulsar	ν Hz	10^{13} Hz s^{-1}	Age 1000yr	Discovered
0355+54	6.4	-1.6	630	1972
0525+21	0.27	-0.029	3 000	1968
0531+21	30.2	-3850	1.2	1968
0833-45	11.2	-156	12.6	1968
1325-43	1.9	-0.11	2 800	1978
1338-62	5.17	-68	12	1985
1535-56	4.11	-0.82	800	1992
1641-45	2.20	-0.97	400	1973
1706-44	9.76	-89	17	1992
1727-33	7.17	-44	26	1992
1736-29	3.10	-0.75	650	1986
1737-30	1.65	-13	20	1986
1758-23	2.41	-6.5	58	1985
1800-21	7.48	-75	16	1986
1823-13	9.86	-73	21	1986
1830-08	11.7	-13	150	1986
1859+07	1.55	-0.058	4 300	1986
2224+65	1.47	-21	1 000	1973
Median*	1.6	-0.063	3 800	

"Age" is calculated in the standard way, from $1/f^3/.f^5$.

* Median is of the total known pulsar population, excluding the millisecond pulsars.

Parameters "on the wrong side" of this median, according to the apparent trend that glitches occur in faster, rapidly decelerating, younger pulsars, are underlined. At least half of the glitching pulsars listed above fall within the extreme 10% of the fastest spinning, the fastest slowing down (largest IV), and the youngest of the canonical (non-millisecond) pulsars.

Parameters are from the catalogue maintained on pulsar.princeton.edu (as at 25/09/1993) (Taylor et al. 1993).

Figure 2-1: Distribution of glitching pulsars.

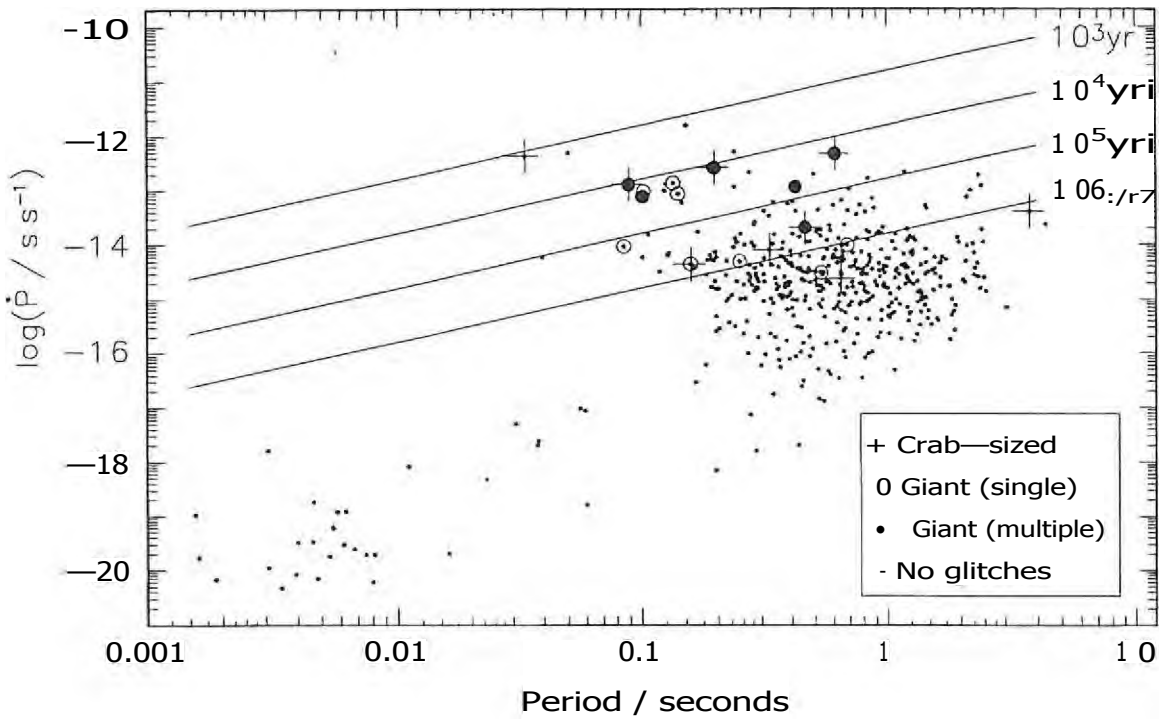

The distribution of glitching pulsars in P and $\dot{p}$ is compared with that of the general pulsar population.
Pulsars in which Vela-sized glitches have been observed are circled (0), those experiencing multiple Vela-sized glitches are marked with large dots (e), and pulsars that have undergone at least one Crab-sized glitch are marked with --F.
Solid lines mark ages, according to the definition age =

Figure 2-2: Schematic of a Glitch in a

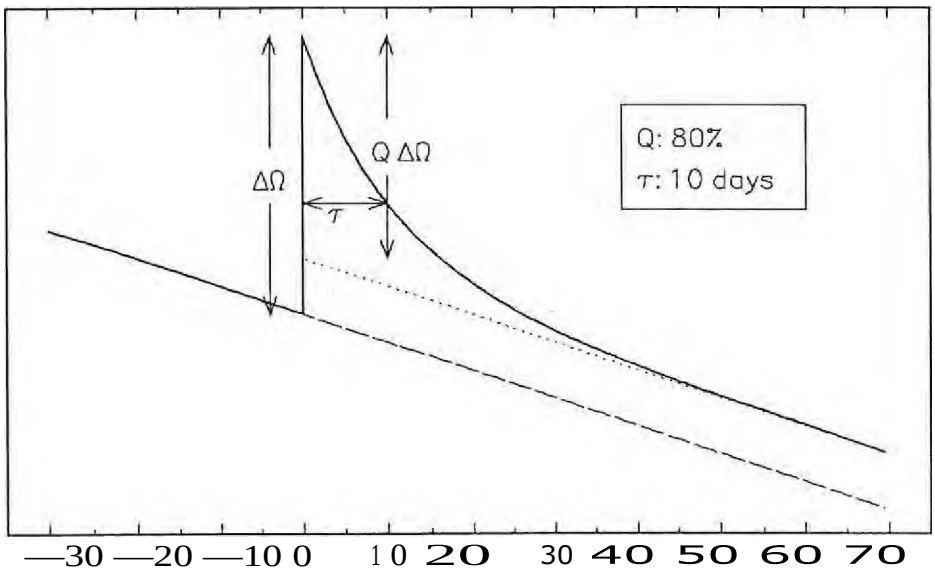

The parameters used to describe a glitch are:

the glitch epoch;
Aft the magnitude of the spin-up;
Q, the fraction of the spin-up that recovers;
r, the timescale of this recovery;

Up to three recovery components have been seen; for clarity, only one is shown here. The glitch is also apparent in ***f(t),*** exhibiting a sudden change (A11) and recovery over the various timescales

older pulsars, but again infrequently. Parameters of pulsars in which glitches have been reported are listed in table 21. Their distribution in period, period-derivative, and age is compared with that of the general population in fig. 2-1.

2.2 Glitch Parameters.

The parameters generally used to describe a glitch are shown in a schematic of a typical glitch, in fig. 2-2.

Table 2-2 summarises an attempt at a complete collection of all published glitches. That more of these are "Vela-sized" than "Crab-sized" may be due to the confusion between real glitches and timing noise, or because the

Table 2-2: Published Parameters of Glitches.

Pulsar		Epoch MJD	A12111 x10^{6}	AM2, x10^{2}		ref
0355+54	1985	46079(3)	0.00562(8)	0.15(2)		20
	1986	46 497(8)	4.37(2)	6.2(3)	0?	11,20
0525+21	1974	42 057(7)	0.0013(2)	0.46(9)		17
0531+21	1969	40493.4	0.006(2)	0.0035(2)	94(1)	15
(Crab)	1975	42 448	0.0383(7)	0.0217(1)	70(16)	15
	1981					24
	1986	46 664.42(5)	0.0092(1)	0,25(2)	100	16
	1989	47 768.40(2)	0.067(2)			19
	1992	48945.5				24
0833-45	1969	40 280(4)	2.34(1)	1.0(1)	3(1)	1,18
(Vela)	1971	41192(8)	2.05(3)	1.5(6)	3.5(1)	1,18
	1971'	41 312(4)	0.012(2)	0.19(6)	5511	1,18
	1975	42683(3)	1.99(1)	1.06(7)	8_8(8)	1,8,18
	1978	43693(12)	3.06(6)	1_8(9)	2.4(5)	1,8,18
	1981	44 888.0707(2)	1.145(3)	4_9(4)	18.3(1)	2,1,9
	1982	45 192(1)	2.05(1)	2.3(1)	4.4(3)	1,9
	1985	46 257.2284(8)	1.601(1)	1.7(1)	15.8(1)	3,9
	1988	47 519.803(1)	1.8071(8)	12(1)		4,5
	1991	48 457.382(1)	2.715(2)	60(6)		6
	1994	49 559.057	0.835(2)			28
	1994A	49 591.158	0.199(2)	12(2)		29
1325-43	1978	43590(24)	0.116		0?	13
1338-62	1990	47 989(22)	1.504(3)			23
	1991	48 453(12)	0.023(6)			23
	1992	48 645(11)	0.993(1)			23
1535-56	1990	48 165(15)	2.793(1)	0.11(6)		25
1641-45	1977	43390(62)	0.191(1)	0.2(1)	0?	8,7
	1986	46 453(35)	0.8036(1)	0.05(3)		10
	1989	47 589(4)	0.00161(4)	0.11(1)		10
1706-44	1992	48 775(15)	2.057(2)	0.40(1)		25
1727-33	1990	48 000(10)	3.033(8)	0.35(6)		25

cont 'd

Table 2-2: *eont'd*

Pulsar		Epoch MJD	AQ/5/ x10^{6}	Aft/12 x10^{2}	Q %	ref
1736-29	1987	46956(4)	0.00308(6)	0.03		26, 27
1737-30	1987	47 003(50)	0.42(2)	0.28(8)		14
	1988	47281(2)	0.033(5)	0.2(4)		14
	1988A	47 332(16)	0.007(5)	-0(1)		14
	1988B	47458(2)	0.030(8)	0.0(4)		14
	1989	47 669.7(2)	0.6009(6)	0.20(4)		14
	1990	48 191.9(2)	0.71(2)	0.13		26, 27
	1991	48 426.4(5)	0.0178(1)			21
1758-23	1987	46 907(43)	0.20(3)			22
	1989	47855(49)	0.2312(9)			22
	1991	48 454(10)	0.34768(8)			22
1800-21	1990	48 245(21)	4.08(2)	0.82		26, 27
1823-13	1986	46 507(57)	2.7			26, 27
	1993	49 014	3.1	1		26
1830-08	1990	48 041(19)	1.8647(4)	0.11		26, 27
1859+07	1987	46 859(4)	0.0303(8)	4		26, 27
2224+65	1976	43 072(38)	1.71(2)		0?	12

References: (1) Cordes *et at.* (1988); (2) McCulloch *et at.* (1983); (3) Klekociuk *et at.* (1986); (4) Flanagan (1990); (5) McCulloch *et at.* (1990); (6) Flanagan (1991); (7) Manchester *et at.* (1978); (8) Manchester *et at.* (1983); (9) McCulloch *et al.* (1987); (10) Flanagan (1993); (11) Lyne (1987); (12) Backus *et at.* (1982); (13) Newton *et al.* (1981); (14) McKenna &z. Lyne (1990); (15) Lohsen (1981); (16) Lyne & Pritchard (1987); (17) Downs (1982); (18) Downs (1981); (19) Lyne & Pritchard (1989); (20) Shabanova (1990); (21) D'Alessandro *et at.* (1993); (22) Kaspi *et at.* (1993); (23) Kaspi et at. (1992); (24) Lyne *et at.* (1993); (25) Johnston et *al.* (1995); (26) Lyne (1995); (27) Shemar (1994); (28) Flanagan (1994); (29) Flanagan (1994a).

less spectacular events are less likely to be published. Fig. 7-7 shows the distribution of glitch sizes, including previously unpublished data presented in this thesis. The glitching pulsars are discussed individually below.

2.2.1 PSR 0833-45: the Vela Pulsar.

The Vela pulsar was the first pulsar observed to spin-up (Radhakrishnan & Manchester 1969, Reichley & Downs 1969). This pulsar has become the classic glitching pulsar: it has undergone eleven giant glitches since its discovery by Large *et al.* (1968), and two smaller Crab-type glitches. Much of the data for these glitches was obtained at the Jet Propulsion Laboratory (JPL) in a 14-year monitoring program (Downs 1981, Downs *igr* Krause-Polstorff 1986). Weekly observations of this pulsar were also made from Tidbinbilla from 1975 to 1981 (Manchester et a/. 1983). Continuous observations have been made by the University of Tasmania Physics group at Hobart since 1981 (e.g. McCulloch *et al.* 1983). An important result of this effort is sets of observations with two-minute time resolution of the 1988 and 1991 glitches, in which the spin-up is unresolved (McCulloch *et al.* 1990, Chau *et at.* 1993), implying that the spin-up is complete within two minutes. The Vela pulsar has also been a primary target of the HartRAO pulsar observing project, which started observations in 1984.

Initial reports of glitches of necessity present only the immediately observable glitch parameters: AO and the glitch epoch. Long glitch recovery times can be inferred from the reported 1S1/6,12 -years, but no actual observations of the long-term behaviour were published for over a decade. The first analysis of Vela data to include analyses of both the glitches and the interglitch epochs was that of Downs (1981). It covered twelve years of observations that included four large glitches (1 - 4) and one smaller glitch (2'). Downs drew the following conclusions from his investigation:

- the glitch recovery can be modeled as a simple exponential decay of AP, on a timescale of 40 - 80 days;
- e by day T_O + 200, - 2% of the jump in P has recovered, and P has returned to a value of 1.247+1 x 10^{-13} s s^{-1} = 156.6+1 x 10^{-13} Hz s^{-1});
- following this short-term recovery, P continues to decrease throughout the entire interglitch period, at a rate $\dot{P}$ at least 20 - 50 times that expected for slow-down solely due to electromagnetic braking or particle-loss;
- $\dot{P}$ differs from one interjump era to the next, but remains nearly constant within a particular interjump era;

Table 2-3: Published Analyses of Glitch Recoveries in the Vela Pulsar.

Glitch	Alqii 10^{-3}	T1 days	10^{-3}	T2 days	AU3/1 10^{-3}	73 days	ü 10^{-22} Hz s^{-2}	Method
1969		75(20)					+7(2)	PALL
1969	2.9(2)	120(6)	3.8(4)	10(1)			+530(1)	Li VALL
1969	2.91	34.6	2.02	3.4			+8.0	VALL
1969	3.0	33/	1.95	3.2[1]	0.001	0.4[1]	+7.87	VALL
1971		60(10)					+7(1)	PALL
1971	2.4(3)	94(5)	6.7(4)	4(1)			+8.602(8)	ii VALL
1971	3.09	32.6	6.25	3.4			+9.46	VALL
1971	3.3	33[1]	6.06	3.2[1]	0.0002	0.4[1]	+9.50	VALL
1971a		80(20)						PALL
1971a			1.6(2)	10.0(5)				V VALL
1975		40(5)					+12(1)	PALL
1975	1.7(1)	35(2)	1.8(2)	4.0(4)			+13.19(8)	Li i/ALL
1975	8.0(2)	412(10)						^{41}160
1975	7.2(2)	610(16)						O450
1975	13(5)	1210(200)						O1000
1975	2.06	30.3	1.67	3.0			+12.5	VALL
1975	2.22	33[1]	1.60	3.2[1]	0.0	0.4[1]	+12.5	VALL
1978		55(5)					+7(1)	PALL
1978	3.9(2)	75(3)	10(1)	6.0(6)			+8.04(1)	V. VALL
1978	9:0(7)	300(23)						O160
1978	7.6(3)	525(18)						O450
1978	6(4)	2700(1000)						O1000
1978	7.31	38.8	4.87	3.3			+8.61	VALL
1978	7.13	33[1]	4.98	3.2[1]	0.0004	0.4[1]	+8.7	VALL
1981	1.3(2)	14(2)	1.3(1)	6.0(6)			+21.1(1)	ii VALL
1981	7.20(4)	233(1)	40(10)	1.6(2)				040
1981	0.75	32.5	4.00	3.4			+19.0	VALL
1981	0.93	33[1]	3.84	3.2[1]	0.49	0.4[1]	+18.4	VALL
1982	4.4(6)	22(2)	14.1(3)	3.0(6)			+16.0(8)	LL
1982	10(2)	60(9)	50(10)	3.2(5)				040
1982	6.29	30.0	5.9	3.0			+6.95	VALL
1982	6.17	33[1]	6.01	3.2[1]	0.27	0.4[1]	+7.29	VALL
1985	62(2)	332(10)	8(2)	6.5(5)				040
1985t	6.12(3)	397(2)	11.3(5)	6.1(1)				040
1985	2.9	31.1	4.81	3.4			+12.1	VALL
1985	2.97	33[1]	4.73	3.2[1]	0.91	0.4[1]	+12.1	VA LL

cont 'd

Table 2-3: cont'd

Glitch	10^{-s}	days	AI/2/i/ 10^{-3}	12 days	10^{-3}	days	10^{-22} Hz s^{-2}	Method
1988	2.91(6)	96(5)	16(3)	4.0(5)	200(90)	0.4(1)		1/320
1988[1]	7.18(4)	351(1)	17.4(1)	4.64(2)				090
1988[1]	7.18	351	13	5.1	45	1.0		090
1988	4.61	29.0	6.9	3.5	21	0.4	+5.40	"ALL
1988	4.40	33!	7.04	3.2[1]	21.5	0.4f	+5.90	11,4 LL
1991	8.6	29.0	10,52	3.0	29	0.5	+12	11A LL
1991	7.37	33!	10.55	3.2[1]	31.8	0.4f	+11.6	11,4 LL

The parameters are of an exponential decay: (A///ii)e⁻t/T.

PALL: estimated by eye from plots of P(t), obtained by dividing each pair of cb(t) measurements by their separation in time; at least 800d of data is available for each glitch; Source: Downs (1981)

i/ALL: longer decay from fit to v(t), obtained by dividing each pair of 0(0 measurements by their separation in time; short decay from plots of iqt), obtained by fitting low-order polynomials to short lengths of OM data; data from 1968.9 to 1983.3 was fitted; Source: Cordes et al. (1988)

O_{Th}: Ave⁻qr fitted to OM over n d of post-glitch data;
Source: Manchester et al. (1983)

040: Ave⁻OT fitted to 0(t) over 40 d of post-glitch data;
Source: McCulloch et al. (1987)
t This analysis included HartRAO data; there is evidence for an unmodeled fast 1 d) recovery component (Klekociuk et al. (1986)

090: AVe⁻ᵗʰ fitted to OM over 90d of post-glitch data;
Source: McCulloch et al. (1990), McCulloch & Hamilton (1992)
t A damped sinusoid and offset in DM were included in this model.

1/320: model fitted to i(t), up to T_G + 320d; Source: Flanagan (1990)

I/ALL: model fitted to i/(t); data of the entire interglitch period werefitted, except the 1991 glitch for which 200d of post-glitch data were fitted.
f these parameters restrained to a common value for all glitches.
Source: Alpar et al. (1993a), Chau et at. (1993)

- there is a correlation between the magnitude of P during a particular interglitch interval and the size 6..P of the next glitch;
- *Q,* the fraction of AP that recovers, is — 4.5% for the four large glitches, and — 55% for the small glitch.

Cordes et *al.* (1988) report an intensive re-evaluation of the JPL Vela data, which by then included six glitches. Their conclusions differ from those of Downs as follows:

- in addition to the 60 day recovery of AP, there appears to be a faster (--days) recovery component present in all glitches;
- the correlation between P and AP disappears with the extension of the data set.

The other results of Downs (1981) were confirmed by this work.

The JPL observations were made approximately weekly. Two days after the Tasmanian group started daily monitoring of Vela in 1981, the fifth giant glitch occurred, accompanied by the fastest post-glitch recovery yet observed (1.6d) (McCulloch *et al.* 1983). The Australian Vela data of glitches 5-7 are analysed by McCulloch et *at,* (1987); HartRAO data covering the seventh glitch are not included in this last analysis, but were combined with the Tasmanian data in a poster paper (Klekociuk *et al.* 1986). Modeling of HartRAO data of the eighth Vela glitch, which occurred 1988, revealed a third decay component, with a recovery time of 0.4d (Flanagan 1990), and amplitude larger than any previously observed. The analysis by McCulloch *et at.* (1990) of the same event revealed a further two features not previously noted:

- a damped sinusoidal oscillation of period 25 days and damping time-constant — 50 days, evident in $0_R(t)$ and *i/(t);* and
- an increase in the delay between pulse arrival times at 635 and 950 MHz, equivalently an increase in DM of 0.016pc cm^{-3}, around the time of the glitch.

McCulloch & Hamilton (1992) do however note that the last of these may be coincidental. In a subsequent re-analysis of the 1988 glitch, the 0.4 d decay evident in HartRAO data is included; McCulloch Si Hamilton obtain a decay timescale of L5 ± 0.2 d.

Alpar *et at.* (1993a) and Chau *et at.* (1993) have analysed all Vela data up to (and including) the ninth glitch; as well as fitting the standard linear long-term decay *(ii)* plus two or three exponential decays to data of each glitch

independently, they successfully modeled the data with a consistent fit in which the three decay timescales (T -= 33d, 3.2d and 0.4d) do not vary from glitch to glitch.

Table 2-3 shows glitch recovery parameters reported in the literature. Some of these reports analyse the decay in terms of v (or, equivalently, *P),* rather than In table 2-3, all decay amplitudes have been converted to i> for easy comparison.

Interglitch Behaviour:

The JPL data analysed by Cordes et *a?.* (1988) included five entire interglitch intervals; Cordes et a/. stress that the behaviour throughout these periods, from $TG \pm 200$d until the subsequent glitch at To,i_{+i}, is adequately modeled by a linear decline in I *z>(t)* I (equivalently, a constant

> "There is *no* evidence for a *long-term exponential* decay in the data; if the long-term decay is in fact exponential, then the time constant must be at least 50yr. Fluctuations in i away from linearity appear to be due entirely to microjump fluctuations." (Emphases in the original).

Downs (1981), in his analysis of the first twelve years of the same JPL data, agrees:

> "There is no evidence of a deviation from a linear decay in P at more than 300 days beyond the jump epoch."

Cordes *et al.* obtain relaxation times for the glitch recovery $T < 120$ d. This is in contrast to other analyses, in which recovery times of up to 400d are obtained. Analyses of the interglitch behaviour are included in table 2-3, which includes details of the method of analysis. The main features of the approach taken by Cordes *et at.* not generally used by others, are:

- the entire interglitch interval is analysed (as opposed to e.g. 40 d of post-glitch data analysed by McCulloch *et al.* (1983), from which a recovery time of 233d was obtained, although the authors point out that a cubic polynomial provides an equally plausible model); and

s models are fitted to /./(t), as opposed to v(t).

Manchester *et al.* (1983) have fitted exponentials to a range of lengths (160 - 1000d) of OM in order to demonstrate the sensitivity of the model parameters to the length of data fitted.

It is apparent from the widely different recovery timescales listed in table 2-3 that the parameters of the post-glitch model, particularly of the long-term behaviour, depend on both the method of analysis used and the length of data analysed.

HartRAO observations of the 7th - 11th Vela glitches are (re-)analysed in chapter 61f; the form of the interglitch behaviour is investigated in chapter 8.

2.2.2 PSR 0531+21: the Crab Pulsar.

The Crab pulsar was the second pulsar observed to glitch **(Boynton** *et al.* **1969). It** has undergone six events that are widely regarded as glitches since its discovery in 1968 by Staelin & Reifenstein (1968); the parameters are listed in table 2-2. There is some argument over the identification of additional Crab pulsar glitches - the change in rotation frequency, Aft/SI, is 10^{-9} - 10^{-8}, making possible events difficult to distinguish from the timing noise that is present at a high level in this object. Lohsen (1981), for instance, identifies a further three events that he regards as being of the same type as the 1969 event. Groth *(ibid.* and 1975), however, disagrees, arguing that the 1969 event is fundamentally different in that it occurs over a short time and is followed by a decay of the jump. Such confusion is partly due to low sampling rate of the earlier observations, although this object was the subject of a number of timing programs (summarised by Derniariski Proszyriski 1983) in the first decade following its discovery. Continuous (14 hours per day) observations of the Crab pulsar have been made since 1982 at Jodrell Bank (Lyne *et al.* **1993);** major successes of this program are observations of the 1986 glitch within an hour of its occurrence (Lyne & Pritchard 1987) and observations during the 1989 glitch (Lyne et *a/.* 1992).

The Crab glitches show clear differences from the Vela glitches: besides being less frequent and two to three orders of magnitude smaller, much of the jump in frequency decays away within weeks. Demialiski & Pr6szyriski (1983) also note that the 1975 glitch was accompanied by a persistent increase in the magnitude of of magnitude 0.02%. Recently Lyne et *al.* (1993) have assembled all available timing data for this pulsar; a careful analysis of the 23 yr span has revealed that:

- the persistent increase in appears to accompany all glitches;
- a slow 100d) asymptotic increase in rotation rate is evident following at least four of the six glitches - all except the first (for which the sampling rate was very low) and the last (which occurred too near the end of the data span for the recovery to be complete);

- part 25%) of the spin-up in 1989 is an asymptotic increase occurring over 20 hr.

This was the first report of the spin-up being resolved. The results of this re-analysis are given in table 2-4.

Interglitch Behaviour:

Lyne *et at.* (1993) find that, after removal of the glitches, the data are consistent with a constant value of the braking index n, implying that the glitch recovery is adequately described by the models of table 2-4 and is complete within less than a year. In addition, a quasi-periodic oscillation of period 1 - 2yr and amplitude in v of 5×10^{-8} Hz is present. This oscillation had previously been interpreted as wandering in v, i.e. timing noise.

Lyne et *al.* (1993) specifically report no abnormalities during the month prior to each of the six glitches.

Seargle & Harlan (1970) observed structural changes in the "wisps" of the Crab Nebula around the time of the 1969 glitch, leading to speculation that the two types of event were related; no further such coincidences have been reported in this pulsar, however.

2.2.3 PSR 0525+21.

PSR 0525+21 is one of the most slowly rotating (P--'3.7 sec) pulsars, but has a fairly large spin-down rate. Downs (1982) has published twelve years of observations of this pulsar, which include a Crab-type glitch. There is evidence of a 150 day decay of AS, involving —50% of the jump in frequency; a persistent change in f of 0.03% is also seen. A second spin-up, occurring nearly five years later, probably falls within the definition of timing noise (it is very small, and is not accompanied by a significant change in a). The first glitch was also observed from Arecibo by Gullahorn & Rankin (1982), who obtain a glitch magnitude half that reported by Downs; the Arecibo data appear to be less well sampled than that of Downs, though.

2.2.4 PSR 1737-30.

This pulsar was discovered during the Clifton & Lyne survey for younger pulsars (Clifton & Lyne 1986), and has a characteristic age of 2×10^4 years, similar to that of the Vela pulsar. Three years of monitoring at Jodrell Bank has uncovered five glitches, three of which are nearly as large as those of the Vela pulsar (McKenna & Lyne 1990). Unfortunately, the post-glitch behaviour is not clear, because of the low observation rate. Timing observations at Jodrell Bank have been stepped up in the hope of catching a glitch,

Table 2-4: Parameters for Crab Pulsar Glitches.

Glitch	$\Delta\nu_{oi}/\nu$ 10^{-9}	$\Delta\nu_{o2}/\nu$ 10^{-9}	τ_{02} days	$\Delta\nu_i/\nu$ 10^{-9}	τ_i days	$\Delta\nu_2/\nu$ 10^{-9}	τ_2 days	$\Delta\dot{\nu}_p/\nu$ 10^{-4}
1969	4.0(3)			2.3(3)	19(2)			+0.04(1)
1975	43.8(7)			34(4)	18(2)	23.5(3)	97(4)	+2.40(3)
1981						9.3(3)	222(20)	+0.10(2)
1986	4.1(1)			4.1(1)	9.3(2)	3.7(3)	123(40)	+0.19(4)
1989	61.7(2)	23.4(2)	0.8	76.1(3)	18(2)	70.4(3)	265(5)	+4.10(5)
1992								

Data are from the recent analysis of Lyne *et at.* (1993). The model fitted is:

$$\Delta\nu(t) = \Delta\nu_{oi} + \Delta\nu_{o2}(1 - e^{-t/\tau_{o2}}) - \Delta\nu_1 e^{-t/\tau_i} + \Delta\nu_2(1 - e^{-t/\tau_2}) + \Delta\dot{\nu}_p t, \quad (2 - 1)$$

where:

$\Delta\nu_o = \Delta\nu_{oi} + \Delta\nu_{o2}$ is the total size of the spin-up;

$\Delta\nu_{oi}$ and $\Delta\nu_{o2}$ are the unresolved and resolved components of this spin-up respectively;

$\Delta\nu_i$ is the component of $\Delta\nu_o$ that decays over a few weeks, evident since the first glitch observations;

$\Delta\nu_2$ is a "delayed" slow increase in spin-rate; and

$\Delta\dot{\nu}_p$ is the persistent change in $\dot{\nu}$.

Alternatively, the last two components above could be regarded as a persistent change in ν which builds up slowly.

however, and other timing programs are now targeting this very interesting pulsar (e.g. Nice 1990, D'Alessandro *et at.* 1993); a total of seven glitches have so far been reported.

2.2.5 PSR 0355+54.

This pulsar has undergone two spin-ups with the classic [+,-] signature of [6,11, AO] (Lyric 1987). The first of these is a Crab-sized glitch, in which part of the spin-up 20%) occurred over 60 - 70 days (Shabanova. 1990). Shabanova also reports a possible precursor to this event, in the form of a marginal decrease in I O I of relative magnitude $2 \pm 1 \times 10^{-4}$.

The second event has the largest value of AIVO observed in any pulsar. The recovery has been well-observed: most of the jump in decayed over a timescale of 44 days, leaving a persistent increase in of $+(6.2 \pm 2) \times 10^{-3}$ (Lyne 1987). There has been no noticeable recovery of AO.

2.2.6 PSR 2224+65.

This pulsar appears to have undergone a Vela-type glitch during the gap between two observing programs (Backus *et at.* 1982). No other information about this glitch has been published.

2.2.7 PSR 1325-43.

As for PSR 2224+65, only the magnitude of the spin-up has been published (Newton *et at.* 1981). Only two pre-glitch observations are available.

2.2.8 PSR 1641-45.

This pulsar underwent a Vela-type glitch in 1977 (Manchester *et at.* 1978). The four-month gap in observations at the time of the glitch probably precluded observation of any post-glitch recovery. HartRAO observations, reported in this thesis, have uncovered a second glitch of similar size in 1986, followed three years later by a Crab-sized spin-up. Further details are given in chapters 6 and 11, and in Flanagan (1993). The 1986 glitch was also noted by Siegman *et at.* (1993); it occurred during a 7,1 yr gap in their data.

2.2.9 PSR 1758-23.

Three moderate-sized glitches have been observed within six years in this youngish pulsar, which may be associated with a supernova remnant in W28 (Kaspi *et at.* 1993). Unfortunately, the paucity of observations precludes any determination of the change in *12* or of the post-glitch behaviour.

2.2.10 PSR 1338-62.

This young pulsar, probably associated with SNR G308.8-0.1, underwent two large and one small glitches during a 27 month period (Kaspi *et al.* 1992). Again, the poor observational coverage precludes the determination of any glitch parameters besides the approximate epoch and size of the spin-up.

2.2.11 PSR 1800-21.

The second-largest glitch ever observed occurred in this youngish pulsar (Lyne 1995). PSR 1800-21 is monitored at three-month intervals at NRAO (Arzournanian *et at.* 1994); one pre-glitch measurement is available. A recovery time of 259 ± 6 d and amplitude 14.6 ± 0.5P was obtained from a fit to phase residuals *(ibid.)*

2.2.12 PSR 1736-29, 1859+07.

Parameters of a small glitch in each of these two pulsars are listed in Lyne (1995). A recovery time of 1400d is reported for 1859+07, the oldest pulsar in which a glitch has been observed; the increase in was unusually large in this event.

2.2.13 PSR 1535-56, 1706-44, 1727-35

One large glitch has been observed in each of these pulsars during a two-year timing program (Johnston *et at.* 1993). Observations are too sparse to fit glitch recoveries.

2.2.14 PSR 1823-13.

Two large glitches have occurred in this pulsar; a recovery time of 560d is reported for the first of these (Lyne 1995).

2.2.15 PSR 1830-08.

One large glitch has been observed in this pulsar (Lyne 1995).

2.2.16 PSR 0540-69?

A report of a large glitch in this young 50 ms pulsar (Ogelman *et al. 1991)* was later retracted (Ogelman, private communication).

2.3 Summary.

To date, 31 large ($\Delta\nu/\nu \geq 10^{-7}$) and 15 small ($10^{-9} \leq \Delta\nu/\nu \leq 10^{-8}$) glitches have been reported in the literature, involving 18 pulsars. Eleven of the large glitches occurred in the Vela pulsar. The database of glitches has increased sharply in the past few years, due to (a) pulsar searches successfully targeted at discovering faster (and generally younger) pulsars, the group most prone to glitches, and (b) the resuscitation of a number of pulsar timing programs. Programs aimed specifically at "catching" glitches have recently had some success in obtaining good coverage of these events. Examples of such projects are; Jodrell Bank (Crab pulsar), Hobart (Vela) and HartRAO (Vela).

Trends now becoming apparent with the increase in data include:

- pulsars of age ,-- 10000yr (e.g. Vela) undergo the largest and most frequent glitches; the glitch rate decreases with increasing age; and
- very young pulsars (e.g. Crab) either do not glitch or undergo small and less frequent glitches;

New features of glitches observed during the last decade'include:

- a large (Z10%) increase in $\dot{\nu}$ which decays rapidly (within ,---, 1 d), in the most recent Vela glitches;
- components of the increase in v which are slow enough to be resolved by observations, in two pulsars;
- persistent increases in $\dot{\nu}_{1/1}$ in at least three pulsars.

There have been reports of dispersion events apparently coincident with glitches in both Vela and the Crab pulsars, although it is not clear whether these are real connections between the two types of event. Only one report mentions a possible glitch precursor (associated with the small glitch in PSR 0355+54); on the other hand, such signals have unsuccessfully been sought in the well-sampled data sets of recent Crab and Vela glitches.

3 Glitches as Probes of the Neutron Star Interior.

Glitches are sudden and relatively large changes in pulse rate that imply a change in the stellar spin-rate, and thus constitute a major disturbance to the star. A primary motivation for the observation of glitches (and thus for this project) is their consequent value as probes of the neutron star interior: the rotation rate can be measured to an accuracy of 10^{-10} over 12hr; the response to a glitch of magnitude 10 is thus easily measurable.

This chapter summarises generally accepted knowledge of the neutron star interior, and outlines some of the models proposed to explain observations of glitches. The area of glitch models is currently one of heated debate, to which, hopefully, the results of this project contribute. Published glitch observations are reviewed in chapter 2.

Notation: A summary of the symbols and notation used in this chapter is given in appendix 1.

3.1 Neutron Star Structure.

Fig. 3-1 shows two recent neutron star models, and illustrates some of the variety of models proposed. Two important transition densities are:

- ρ 4.3 x 10^{11} g cm', the "neutron drip point", when nuclei are so neutron-rich that neutrons start leaking out of them; and
- ρ_{c} 2.8 x 10^{14} g cm^{-3}, the density of nuclear matter, at which point the nuclear structure has dissolved.

Superfluidity: A recent review of superfluidity in neutron stars is given by Sauls (1989). Two types of superfluidity, with different dynamical properties, are believed to occur in neutron stars:

$^{1}S_{0}$ at lower densities, where the inter-particle spacing is greater than the range of the repulsive component of the strong force; and

$^{3}P2$ at densities —> po 'L.,' 2.8 x 10^{14} g cm^{-3}.

The model of fig. 3-la is calculated using a stiffer equation of state (EOS) than that of fig. 3-1b. A stiffer EOS incorporates a larger repulsive component of the strong interaction at short inter-neutron distances. The effect of a stiffer EOS is a more distended star with a more uniform density distribution

Figure 3-1: Cross-section of a 1.4$M_{\odot}$ Neutron Star.

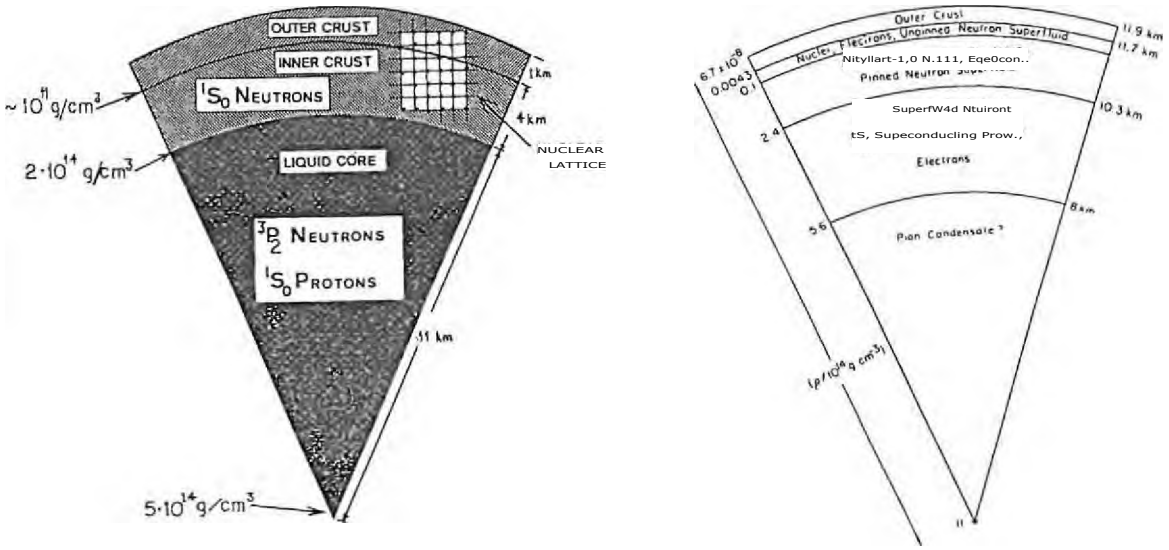

a

Fig. 3-1a: Based on the relatively stiff EOS of Pandharipande, Pines and Smith.
Source: Sauls (1989), fig. 1.

Fig. 3-1b: Based on a softer EOS.
Source: Alpar (1989), fig. 1.

— note the solid core in the softer EOS model. A stiffer model can support a larger mass — up to 4 or 5M_{e}, as opposed to 0.7 - 1$M_{®}$ for the softest viable EOS. Measured lower limits on neutron star mass will therefore rule out softer EOS.

Exotic Matter and Solid Cores: At very high densities, exotic matter such as pion condensates, quark matter and "abnormal matter" may occur (Baym & Pethick 1979). The first of these is the most widely discussed; if present (at densities p $2p_0$), it would soften the EOS, enhance cooling by neutrino emission, and possibly facilitate the formation of a solid core. Measurement of an unexpectedly low neutron star temperature, as is apparently the case in Vela (Ogelman & Zimmermann 1989), is thus evidence for exotic matter in the core; such interpretations are however complicated by separation of the thermal stellar component from other emission and the choice of

thermal evolution and heat transport models. Some glitch models, e.g. the starquake model, require a solid core in some pulsars.

Quark Stars: The possible existence of a stable cold star supported by the degeneracy pressure of unconfined quarks has been mentioned (e.g. Baym & Pethick 1979). Such a star would be more compact than a neutron star; the upper limit on its rotation speed would thus be higher. The observation of a half-millisecond pulsar would be evidence for such an object. Alcock *et at.* (1986) point out that the observation of ASI/ft 1% accompanying a glitch may be proof that pulsars (at least those that glitch) are neutron stars, .as opposed to quark stars, since it implies the existence of a stellar component with moment of inertia 1%. In quark stars, the only possible second component, the crust, comprises at most 10^{-5} of the total moment of inertia.

3.2 Dynamics of Superfluids in Rotating Neutron Stars.

Current neutron star theory, combined with the observation that post-glitch recovery occurs over a range of timescales, suggests the presence of a number of dynamical components; these are summarised in fig. 3-2.

3.2.1 Quantisation of the Rotation into Vortices.

Laboratory experience with superfluid helium (e.g. Donnelly 1988) suggests that the rotation of the superfluid is quantised into vortices running parallel to the stellar axis of rotation. These vortices have cores of normal matter. The superfluid then appears to rotate as a solid body, i.e. classical concepts such as moment of inertia can be applied to the system.

The rotation rate of a superfluid is described by

$$= \frac{1}{2}\text{-nn rad s}^{-\blacksquare} \qquad (^{3} - {}^{1})$$

where n, the vortex area density, is 10^{5} cm^{-2} for the Crab pulsar.

Eqn. 3-1 implies that for the rotation frequency of the superfluid to change, the vortex density must change. In particular, for the superfluid to follow the steady deceleration of the crust that is observed in all pulsars, the vortex density must decrease, presumably by outward migration of the vortices.

Figure 3-2: Hypothesised Dynamical Components of the Neutron Star

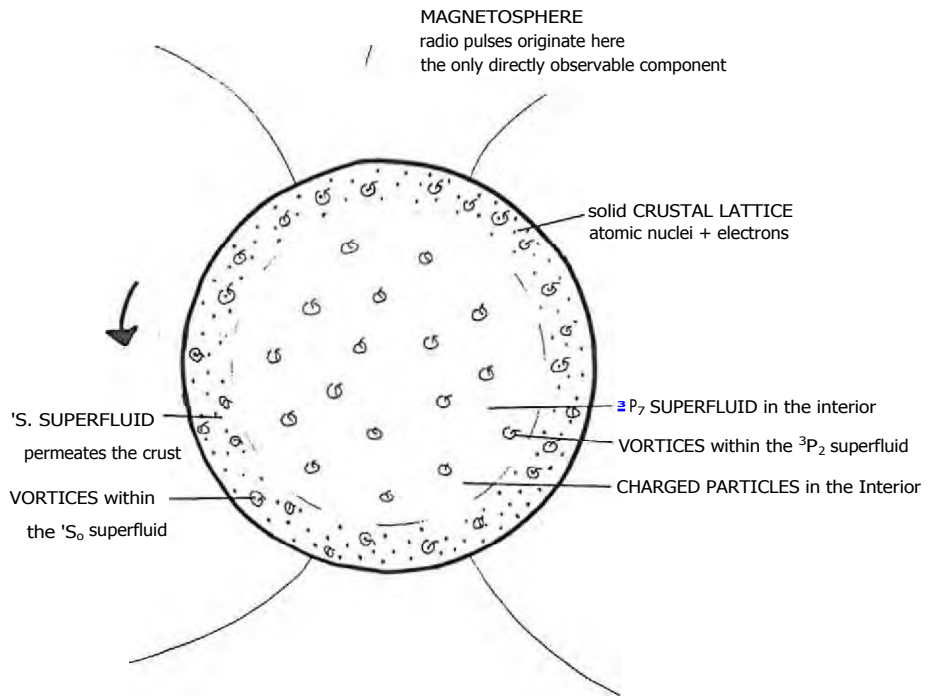

3.2.2 Inter-component Coupling.

Some of the interactions mentioned in the literature are listed below; a summary follows.

Coupling between Charged and Normal (Non-superfluid) Components: The inner part of the pulsar magnetosphere is electromagnetically anchored in the normal matter of the crust. The charged particles of the interior plasma are coupled to those of the crustal lattice on timescales of

10 sec, due to the enormous magnetic field. Recoupling following a large disturbance such as a glitch also occurs rapidly, within (-30sec (Easson 1979). This dynamical response may be mediated by the large magnetic field or, in cooler stars, by plasma viscosity; in either case it is expected to be too fast to observe. The magnetosphere, crust and core plasma thus effectively respond as a single component to perturbations of the system. This is the component we observe, via radio emission from the magnetosphere. It is also the component on which the external spin-down torque operates.

Scattering Processes: Where two components co-exist and rotate at different rates, e.g. superfluid and normal matter in the inner crust, scattering processes will transfer momentum from the more rapidly rotating to the

slower component. Such processes result in a force which may be described as a frictional force, with a characteristic timescale 7, for example by (Harding *et al.* 1978):

$$P = pip2(gv)\ I\ pr, \qquad (3 — 2)$$

where

p ==. $pi + p_2$ is the total density, and

Ev is the relative velocity of the two components.

The importance of each scattering process can be determined by calculating the interaction timescales, given estimates of factors such as temperature and densities; processes with shorter timescales will dominate. A variety of scattering processes have been proposed (e.g. Harding et *al.* 1978, Bildsten SI, Epstein 1989, Jones 1990a, 1992). Most involve constituents of the crustal lattice and therefore do not operate in the core. An exception is the **Feibelman mechanism (scattering** of electrons off thermally excited normal neutrons of the vortex cores). The Feibelman mechanism is an example of the current lack of consensus on which of the many processes is dominant: originally proposed to explain the recovery times (~ months) observed in the earliest glitches (e.g. Baym *el al.* 1969), recent calculations by Sauls (1989) give the interaction time as 10^{12} yr, i.e. completely irrelevant; Takatsuka & Tamagaki (1989) however include it in a recent version of the starquake glitch model to explain coupling times of ~-years.

Forces between Vortices and Superfluid: A free vortex line in a rotating superfluid will move with the superfluid, since any imbalance between the superfluid and vortex velocities results in a large radial force on the line, the **Magnus force:**

$$f = pi' \times (V_L — V) \quad \text{per unit length of vortex line,} \qquad (3 — 3)$$

where

is the velocity of the ambient superfluid, and

Cq.. is the velocity of the vortex line.

Forces between Vortices: According to Link & Epstein (1991), these can be disregarded, since the spacing between vortex lines is relatively large. Mochizuki & Izuyama (1995) have however invoked inter-vortex repulsion in a region of high vortex density as a glitch initiator.

Coupling between Superfluid Neutrons and Non-superfluid (Normal) Components: The coupling between normal neutrons and protons is mediated by the strong interaction. The timescale for this is r_m, 10^{-11} sec at $T = 10^6$ K.

Introducing superfluidity removes the strong interaction, and extends the interaction time to i -+ oo at T 10^6 K (see review of superfluidity in neutron stars by Sauls 1989). Since this is far too long to explain glitch recovery observations, additional coupling mechanisms are required.

Crustal versus Core Superfluid: Since the crust and core (a) are very different environments, and (b) involve different superfiuids ($^1S_0$ and $^3P2$ respectively), different types of interactions have been hypothesised in the two regions.

Coupling between Core Superfluid and Normal Matter: Initially, coupling of the interior superfluid to the crust was believed to be mediated the Feibelman mechanism. Early estimates of the timescale for electron scattering were yr, which accorded with the first observations of glitch recovery times of weeks (Crab pulsar) to months (Vela pulsar) (Baym *et al.* 1969), and led to the original two-component model: the core superfluid as component 1, and everything else as component 2.

Alpar *et al.* (1984) have investigated the effect of the superfluid, superconducting protons in the neutron star interior. They conclude that the proton drag current induces a vortex magnetic flux, which reduces the electron-vortex coupling times to around 1 sec. This mechanism operates only if both neutrons and protons are superfluid (above densities of 2.8×10^{14} g cm', i.e. only in the interior). Alpar & Sauls (1988) later extended this to a prediction of dynamical coupling timescales of 400P - 10^4P (depending on the stellar density and the (uncertain) proton effective mass) — minutes at the most.

Sedrakian & Sedrakian (1995) suggest that clusters of proton vortices will form around each neutron vortex in the interior; scattering of electrons off the large (- 10^{14} G) local magnetic field couples the clusters tightly to the normal component. This restricts the outward motion of the neutron vortices, resulting in dynamical coupling times of days to months. The coupling times are density dependent, independent of temperature, and cc $.l^{32}$ (in contrast to coupling involving scattering off neutron vortices, for which τ oc P).

Greenstein (1970) pointed out that tangling of the core superfluid vortices as they migrate outwards would introduce immense complications.

Since Ruderman & Sutherland (1974) argued (rather convincingly, apparently) that this would not happen, this issue has been disregarded.

Since the spin and magnetic axes of a radio pulsar are not parallel, the outward-migrating superfluid vortices must encounter **proton flux lines.** The consequences of any such interaction, and its effect on the rotational dynamics of the pulsar, are unknown (Sauls 1989), but are now being investigated (e.g. Chau *et al.* 1992).

Vortex Pinning within the Crustal Superfluid: The core superfluid is generally assumed to comprise a homogeneous medium, with no normal matter to restrict movement of the vortices. Within **the** crust, however, the crystal lattice is expected to impede the free motion of the vortices. Specifically, the vortices may pin to nuclei in the lattice, and be forced to move with the lattice rather than with the superfluid. Differential rotational velocities of 1 - 10 rad s^{-1} can be maintained between the pinned superfluid and the lattice (SanIs 1989).

Pinning is described by Alpar *et al.* (1984a) and by Jones (1991). The inner crust (density — 4 x 10^{11} g cm^{-3} to 2 x 10" g cm^{-3}) comprises nuclei which are bloated, neutron-rich, and contain superfluid neutrons. A vortex will pin to a nucleus if the energy cost of creating the normal core of the vortex is thereby reduced. This results in a **pinning force** which opposes the Magnus force.

The type of pinning is highly density-dependent - some of the possibilities are illustrated in fig. 3-3. Weak and superweak pinning will occur in regions of higher densities, i.e. in the inner regions of the crustal superfluid; strong pinning is expected to occur at greater radial distances, if it is present at all.

Fig. 3-4 shows the extent of the region where conditions are favourable for pinning, for a variety of EOS, according to Datta & Alpar (1993).

How prevalent is pinning? Jones (1990) has argued that vortices will pin only to those microcrystals of the crustal lattice that have a specific geometric orientation, since the vortices are expected to be rigid. He argues that Alpar *et al.* have ignored this fact, and that although some vortices will be pinned, and in fact *must* be pinned in order to explain the occurrence of glitches, these comprise a small fraction of the crustal superfluid.

A counter-argument to the above is that if the crustal melting temperature $T_{„}$ is less than the superfluid transition temperature T_c, the lattice will form after the vortices and may be favourably aligned for pinning (Ruder-

Figure 3-3: Possible Pinning Configurations.

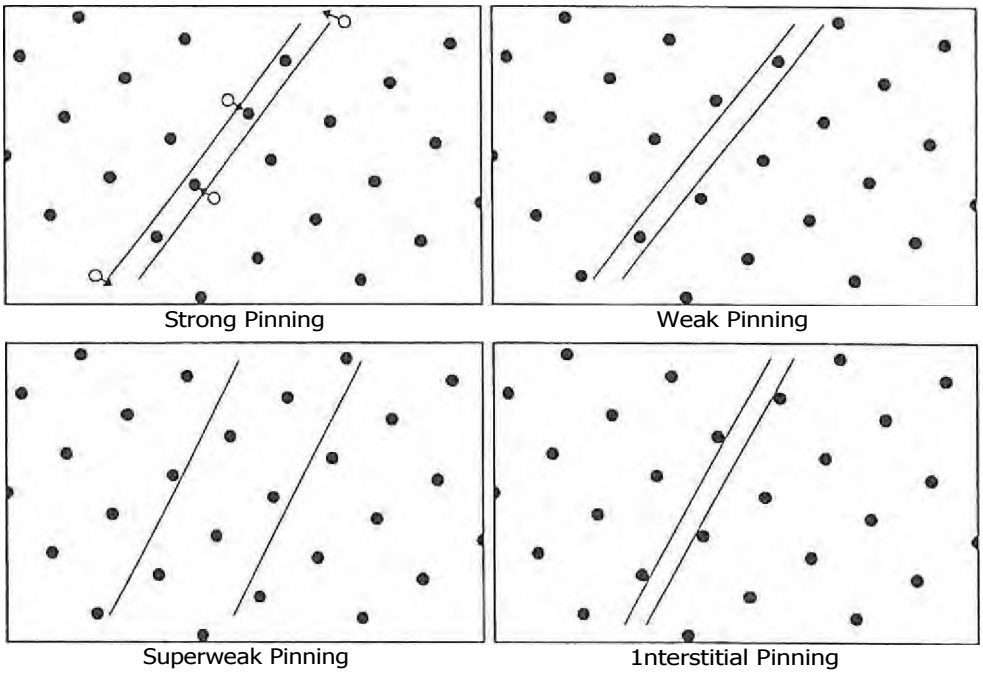

The geometry of various pinning configurations:
Strong pinning, where the pinning force is great enough to dislodge nuclei from their equilibrium positions in the lattice. Vortices in this region will not unpin easily.
Weak pinning, where the vortex pins only to those nuclei through which it passes.
Superweak pinning, where the vortex radius is comparable to the lattice spacing; very little energy is required to move the vortex.
The above are proposed by Alpar et al. (e.g. 1984a).
Interstitial pinning (as opposed to nuclear pinning), which occurs at densities $p < 10^{13}$ g cm^{-3}. Here, repulsive forces between lattice nuclei and vortex lines cause the path of minimum energy for a vortex to be between the crustal nuclei (Link & Epstein 1991).
Pinning to defects, such as vacancies or "impurities" in the crustal lattice, has also been suggested at densities $p \geq 10^{14}$ g cm^{-3} (e.g. Chevalier 1993).

Adapted from Alpar et al. (1984a) fig. 2.

Figure 3-4: The Extent of the Crustal Pinning Regime.

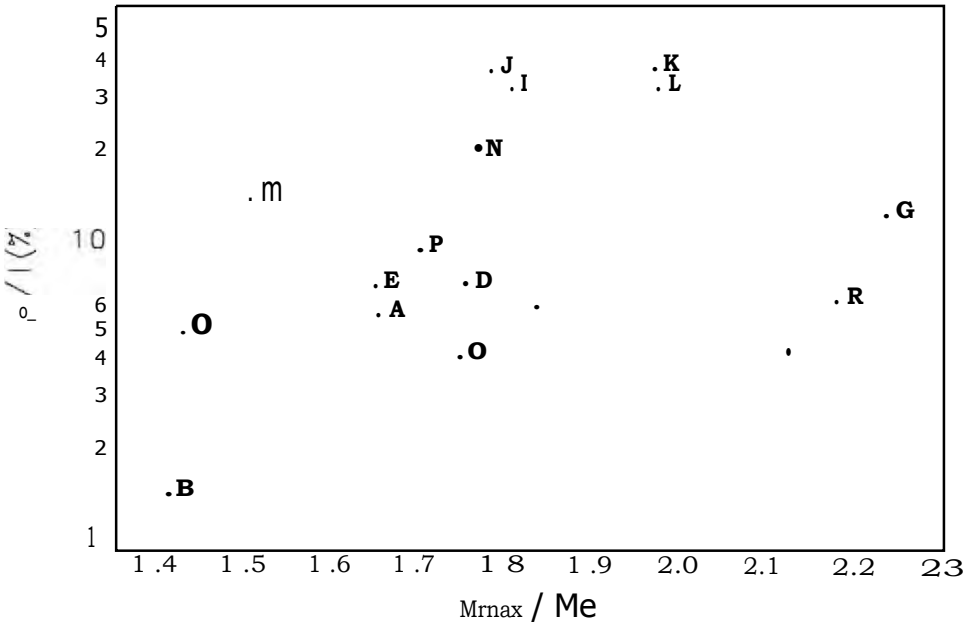

Letters refer to [OS listed by Datta & Alpar (1993).

I_p/I is the relative moment of inertia for the region $2 \times 10^{13} < p < 2 \times 10^{14}$ g cm^{-3}, the region where pinning may occur, for $M_{\text{„}} = 1.4\ M_{a}$, and M_{inax} is the maximum possible mass for this [OS.

The very soft EOS F and H have masses < 1.4 $M_{®}$; they are omitted.

Pulsar observations can rule out some of the models: a lower bound on I_p/I rules against the softest EOS for a given mass, and supports lower masses for a given EOS. While the crustal thickness increases with ft, I_p/I is relatively insensitive to Q. For instance, if the application of vortex creep to Vela glitches by Alpar et at. (1993a) is accepted, model **B** must be discarded, since $I_p// > 3.4\%$. In fact, models B, F, H and 0 are in contradiction with the measured mass of the pulsar in the PSR 1913+16 system (1.442 + 0.003) M (Taylor & Weisberg 1989).

Source: Datta & Alpar (1993)

man 1991a). This situation ($T_{ni} < T_c$) is debatable, and may be altered by subsequent motion of vortices or lattice (Jones 1993).

Also, systematic variations in the timing residuals of the Crab pulsar and Her X-1 have been interpreted as precession of the neutron star, implying that a very small fraction 10^{-7}) of the crustal superfluid is pinned (Jones 1988 and Triimper *et al.* 1986 respectively). However, Jones (private communication) has recently expressed doubts about this inference.

Vortex Creep within the Crust: Should vortices remain **pinned** within the crustal lattice, changes in the vortex density and hence rotational velocity of a component of the crustal superfluid will be prevented, thus completely decoupling this component from the stellar spin-down. The differential velocity that results is w(t) = $Ii_5(t)$— 1 (i), where subscripts S and C refer to superfluid and crust respectively; the time dependence of w and fli is implied below. A non-zero value of 14.1 creates a radially-directed Magnus force (eqn. 3-3), which is opposed by the pinning force. Thermal activation will cause pinned vortices randomly **to** unpin and move to another pinning site. The Magnus force lowers the energy barrier for vortex unpinning, and introduces a bias to the subsequent vortex motion. in a radio pulsar, nc decreases with time as the external torque spins down the crust. Thus w increases, a Magnus Force directed radially outwards builds up, and any vortices which unpin will tend to move outwards, reducing the local superfluid density and thus decelerating the superfluid (eqn. 3-1). The opposite would occur in stars that are spinning up. Thus "vortex creep" couples the crustal superfluid to the remainder of the star. The creep rate will be greater for larger temperature and larger w,

Much has been written about vortex creep, particularly within the context of the vortex creep model (below), and features such as a linear and nonlinear dependence of the creep rate on to have been invoked to explain glitch observations.

In Summary: The component we observe is the magnetic field, where the radio pulses originate. All charged and normal components — the crustal lattice and all plasmas of the crust and interior — are widely believed to be tightly coupled to the magnetic Reid.
The relatively long time taken for Aft/Si. to recover following a glitch is evidence for a component that is far more loosely coupled. The simplest way to increase coupling times is to include superfluidity, which is predicted at high densities in any case. Two distinct superfluid components exist: the core and the crustal superfluid; they have different properties and exist in different environments,

A mechanism for tightly coupling the core superfluid to the normal matter has been proposed (Alpar *et* a/. 1984) and appears to be generally accepted, although recently stronger interactions which (paradoxically) increase the coupling time, by restricting the response of this superfluid, have been suggested. Factors such as the interaction of vortices and flux lines in the core are also now being addressed. The role of this component has thus recently been attracting more attention.
The inhomogeneous inner crust, where crustal lattice and superfluid co-exist, is often regarded as the most promising candidate for the "loose" component. Here there are two widely supported possibilities: either (1) most of the superfluid vortices are "pinned" to the crust, large differential velocities develop, and coupling of the superfluid and normal components is via vortex creep; or (2) while part of the superfluid is pinned, much of it virtually co-rotates with the superfluid, and is coupled to the crust via one or more of a variety of possible "frictional forces".
A number of glitch recovery models have accordingly been developed; some are described below.

3.3 Glitches.

Glitch theories address two distinct issues: the cause and mechanism of the event, and an explanation of the subsequent response of the star. The following sections outline current theories for each of these phenomena.

Any glitch model needs to explain the following features of the observations:

- All glitches observed to date have been spin-ups, i.e. Af is positive. So far, all measured values of Ah./S accompanying a glitch are **O.**
- The glitch occurs suddenly, within 2rnin (the eighth Vela glitch, observed by McCulloch *et at.* 1990). However, at least part of the most recent (and much smaller) Crab pulsar glitch was resolved, the spin-up occurring over a few hours (Lyne *et at.* 1992).
- Glitches occur at different rates in different pulsars. The average interglitch interval for the Vela pulsar is 3 years. Glitch activity appears to be age-related, though, and around 97% of the general pulsar population have not glitched since their discovery. More specifically: the very young pulsars (e.g. the Crab) undergo small, if any, glitches, while larger and far more frequent glitches occur only in the "adolescent" pulsars (McKenna & Lyne 1990).
- **The fraction of the spin-up that recovers** varies from pulsar to pulsar. For smaller glitches, such as those seen in the Crab pulsar, a

fairly large fraction (Q-70%) of Al recovers; in the larger glitches of the Vela pulsar, Q-5%.

- The recovery of All: while AQ tends towards complete recovery in the large Vela glitches, a general feature of Crab glitches appears to be a permanent shift in Q.
- Detailed observations show recovery of All occurring in distinct components (at least three in Vela).
- Other features — pre-cursors, ISM-related changes, and damped sinusoidal oscillations in the rotation rate — have either not been convincingly exclusively connected to the actual eta and have been ignored, or have only been seen recently and are not yet accommodated in the models.

3.4 Early Glitch Models.

The remainder of this chapter deals with the more persistent glitch models. Some early suggestions are mentioned here for historical interest. Most suffered from major flaws such as failure to predict that All would be positive. Among the proposals were:

- a planet in an eccentric orbit around the pulsar (e.g. Michel, 1970);
- dumping back to the star, or complete ejection from the system, of gas accumulated from the stellar surface in the magnetosphere (Roberts & Sturrock, 1972). An increase in dispersion measure accompanying the 1969 Crab Pulsar glitch lent support to this idea, but this coincidence was not repeated (Rankin & Counselmart, 1973);
- magnetic field instability (Chau *et al.* 1971);
- a massive body falling onto the pulsar (13Orner & Cohen 1971);
- superfluid instability, resulting in a mixing of differentially rotating interior layers (Greenstein 1970);
- hydrodynamic model with thermal instabilities (Greenstein 1979), in which a small increase in temperature shortens coupling times, which in turn further increases the temperature, resulting in a "seize-up" of the star.

3.5 Glitch Triggers.

A brief overview of some of the possible triggers of glitches is given here.

3.5.1 Crustquakes.

The glitch mechanism invoked after the first Vela glitch in 1969 was suggested by Ruderman (1969) and described in more detail in a paper that has become a classic (Baym *et al.* 1969): the crustquake. The solid crust of a young, rapidly rotating neutron star would be expected to be slightly oblate. As the (rigid) crust spins down, the centrifugal forces on it decrease, and stresses build up, until the crust cracks, decreasing the oblateness and temporarily relieving the stress. 'The change in oblateness decreases the moment of inertia of the crustal component, which therefore spins up in order to conserve angular momentum.

Even in 1969, Ruderman remarked on the disconcertingly short time after its discovery that Vela glitched. Twenty-seven years and eleven glitches later, it, is obvious that the giant Vela glitches cannot be crustquakes — the change in oblateness Af = $AI\,I\,I =$ 10^{-6} involved in each glitch is a substantial fraction of the expected total oblateness (c $\mathbf{1O^{-4}}$).

3.5.2 Corequakes.

A solid core could support a larger oblateness than a crust, and, being more "brittle", would be expected to build up to a critical strain faster than the crust would (the core would be coupled to the crust via the magnetic field, and would thus follow its deceleration). Soon after the second Vela glitch, Pines and co-workers (1972) argued that these spin-ups were corequakes in a solid neutron core. Unfortunately, the heat released in such events should render the star a stronger X-ray source than it is (Ruderman 1976). More recently, however, Takatsuka & Tainagaki (1989) have developed the starquake **model,** which includes both crustquakes and corequakes, with a pion condensate core. The pion condensate solves the problem of removing excess heat caused by corequakes by invoking accelerated neutrino emission.

3.5.3 Vortex Unpinning.

Large-scale unpinning of vortices within the crustal superfluid was first proposed as a glitch mechanism by Anderson & Itoh (1975). The unpinning would result in the sudden outward motion of the vortices, due to the Magnus force, and a consequent slow-down of the superfluid (eqn. 3-1), The angular momentum thus lost from this superfluid is transferred to the crust and all parts of the star that are tightly coupled to it, causing it to spin-up — this is the observed glitch. The number of vortices involved in the unpinning would be (Chau Sz Cheng 1993)

$$\mathrm{AN} \quad 3.2 \times 101°\mathrm{R11t1}\,[\frac{\mathrm{Aft}}{,\mathrm{S1}\ -\mathbf{6}} \qquad (3 — 4)$$

where R_1 is the stellar radius in units of 10^1 km, SZ_I is in units of 10^1 rads^{-I}, and the relative size of the glitch is in units of 10^{-6}. It appears to be somewhat of a mystery how such a large number of unpinnings can be co-ordinated (e.g. Epstein & Baym 1992); Mochizuki & Izuyama (1995) propose "self-trapping" of vortices, which they suggest could result in regions of such high vortex density that inter-vortex repulsion would eventually cause a cascade of unpinning. Cheng et *al.* (1988) earlier suggested a similar scheme, involving vortex "accumulation" and "depletion" regions, although they had difficulty producing the larger Vela glitches with this mechanism.

A mechanism to transfer the momentum to the crust within the required timescale (2 min in the 1988 Vela glitch), involving "kelvons", has been suggested by Epstein & Baym (1992).

In this model, the glitch is due to a transfer of momentum between components; in the starquake model it is due to a change in moment of inertia of one component.

3.5.4 Crustquakes inducing Vortex Unpinning.

Cha.0 & Cheng (1993) calculate that there is sufficient energy in a starquake-induced spin-up of relative size $10^{-1\circ}$ to unpin the number of strongly-pinned vortices given by eqn. 3-4 required to cause a giant glitch in the Vela pulsar. The energy of the starquake would be transferred by vortex oscillations (kelvons).

3.5.5 Lattice Breaking.

Ruderman (1991, 1991a) has investigated the possibility of the crustal breaking **strain** being exceeded before vortices unpin. He points out that some of the assumptions made about parameters such as the pinning energy *Ep* may not be justified; allowing for this can increase $w_{„}$ by a factor of 20. If vortices exist when the lattice crystallises, an "aligned lattice" may form, with $co_{„}$ an order of magnitude larger.

Extrapolating maximum strains ($9_{„}$) obtained in laboratory crystals to conditions in neutron star crusts implies that crust cracking will occur before vortex unpinning for spin-period $P < 10$ms. However, this involves an extrapolation of the scale-length over about 17 orders of magnitude. Depending on the effects of for example crustal dislocations and fault planes, $0_{7„„„}$ could be two or **three** orders of magnitude less, which would extend the period range of **affected** pulsars to 6 see, thus including even "dead" pulsars.

3.6 Glitch Models: General.

3.6.1 Equations of Motion.

The following equations of motion are useful:

The equation of motion of a rotating superfluid:

$$= \qquad (3 — 5)$$

The equation of motion of the observable crust:

$$= N_{ext} — \mathrm{E} \qquad (3 — 6)$$

where N_{ext} is the external torque, subscript C refers to the crust and all components coupled to it on unobservably short timescales, and subscript i refers to a loosely coupled interior component.

3.6.2 Approximations:

The following approximations are generally made:

- I, lc, i.e. Ic $I_{,otat}$ =
- N, the external torque, is constant on the timescale under investigation (days to years);
- 0 is large compared to fluctuations in SI, and is thus approximated by a constant, 0_0; for all glitches observed so far, A1l/0 < 5 x 10';
- is usually approximated by $0._c$, since the long term change in 0 introduced by a glitch is 1%;
- because of the dependence of angular velocity on r, the distance from the rotation axis, conditions at the equatorial crustal regions dominate the glitch dynamics;
- the radial extent of the crustal superfluid, $6r$, is small compared to r; r can be treated as constant in this region;
- cylindrical symmetry w.r.t. the rotation axis.

3.7 The Starquake Model.

starquakes were assumed to occur in the crust (section 3.5.1), and the only other component involved was the superfluid core; electron scattering off superfluid vortices would couple the two components. A sudden change in ft (a glitch) perturbs the coupling. The recovery back to steady state is observed as a decay of AC/ and the consequent An, over a timescale T

Observations such as the large glitching rate of the Vela pulsar, and the small fraction of Act that recovers in the same pulsar, prompted the incorporation of quakes in a solid core for some pulsars (Vela). The re-named starquake model has recently received renewed attention from Takatsuka Tamagaki (1989), who replace the solid neutron core proposed by Pines *et at.* (1972) with a pion condensate, and extend the model to include two distinct regimes of superfluid: the core ($^3P_2$) superfluid and the crustal ($^1S_0$) superfluid. Takatsuka & Tamagaki apply the revised starquake model to data of the Crab and Vela pulsar glitches. Coupling times T_s of 2 - 11 yr are deduced for the interaction between the crustal superfluid and the normal component. The Feibelman mechanism is suggested; glitch-to-glitch variations in r_s are explained by the sensitive temperature dependence of this process. The core-superfluid-crust interaction, on a timescale of T_p 6 d, is attributed to spontaneous vortex core magnetisation (Alpar *et al.* 1984). A component of the crustal superfluid with a larger energy gap would be responsible for the very long re-coupling that causes the observed excessive I/ between Vela glitches. The post-glitch behaviour is described in the notation of Takatsuka & Tamagaki by:

$$\mathrm{Al}(t) = -\frac{\mathrm{Ano}}{z-1}\exp(-t/\mathrm{Ti}) - \frac{Q2}{T_2}\mathrm{A.Clo\ exP}(-t/\mathrm{T2}), \qquad (3 - 7)$$

where

An_0 is the observed magnitude of the spin-up;

$T2$ are the timescales of the observed long and short recovery components respectively, and are distinct from Ts and T_p, which describe the interaction times of physical interior components; and

$Q1, Q2$ are the fraction of Al_o involved in each recovery component.

The interpretation of the Qi as structural parameters follows from assumptions about the relative moments of inertia of the various components of the star, and a basic assumption of the starquake model: that angular momentum of the individual components is conserved during the glitch, i.e. $= -A/,/f_{\zeta,}$ Then

$$\frac{A^{1}=//'}{Arcfic} \qquad (3 — 8)$$

where

i = 1 is identified with the slowly-recovering component and the crustal superfluid;

i = 2 is identified with the rapidly-recovering component (the core superfluid); and

/c is the observed (normal) component, and does not necessarily constitute the bulk of the star.

Factors invoked to explain the distinctly different characteristics of the Crab and Vela glitches are, briefly:

The lighter Crab pulsar dues not have a solid core, and thus its major component is the $^{3}P_2$ core superfluid. The glitch occurs in the crust, and the effect on the thin layer of crustal superfluid is far greater than that on the mass of core superfluid below it. The observed recoupling is that of the core superfluid.

The Vela pulsar, with a solid core, has a much smaller fraction of core superfluid. Although glitches may involve crustquakes, they are all (including the small glitch of 1971) accompanied by corequakes. Since these occur in the deep interior of the star, the effect on the core superfluid is far more noticeable. Takatsuka *Sz* Tamagaki follow Alpar *et a/.* (1993a) in assuming the same timescale 3 d for all the large glitches. They do not mention the possible existence of the more rapidly recovering component.

3.8 The Vortex Creep Model.

In this model, developed over the last decade by Alpar *et al.* (e.g. 1984a, 1989, Pines Rz Alpar 1985), the only component not tightly coupled to the external torque is a layer of superfluid within the crust, the crustal superfluid. This component comprises at most a few percent of the moment of inertia; the remainder of the star is assumed to effectively (Le. on observable timescales) constitute a single component.

Vortex pinning and motion within the crust dominate the interaction between the two components. At steady state, the difference in spin-rates drives a vortex creep current in the crust, which enables the superfluid there to share the external torque. The glitch may or may not be triggered by a break-down

of this coupling mechanism; in any case, it is a massive perturbation to the coupling. The response of the coupling gives rise to the observed post-glitch behaviour. Vortex creep provides a range of forms and timescales for the subsequent recoupling.

Transfer of Angular Momentum:

Due to the finite coupling time of the "loose" crustal superfluid with the remainder of the star, this component will always lag the slowdown imposed on the star by the external torque, and will always (except possibly immediately after a glitch) be rotating faster. The model assumes that the angular momentum gained by the crust in a glitch is delivered by this superfluid component. Conservation of angular momentum then gives:

$$\text{icAf/c} = \qquad (3 — 9)$$

where

An, is the observed change in crustal spin-rate,

i refers to a superfluid region that contributes angular momentum to the glitch;

(5f1, is the presumed but not directly observable decrease in ft of such a region; and

/c includes the crust and all components coupled to it on unobservably short timescales; Ic P‡, *I*.

Coupling:

The strength of the coupling between the two stellar components is determined by Lo, the difference between their rotation rates. At steady-state, ftc = ft_s = $Si_{c°}$, the superfluid and crust share the external torque, and = 0. Two different types of creep are distinguished, with fundamentally different types of behaviour both at steady state and following a perturbation. They are described in detail by Alpar *et at.* (1989); a brief outline is given here.

The Linear Creep Regime:

In this regime,

$$w \qquad = \text{ı ''' ICX1 T1911} \qquad \text{Wcr} \qquad (3 — 10)$$

where *TIM* is the response time of the region, so **glitch initiation by unpinning cannot occur here.** Each linearly-coupled component contributes an observable post-glitch recovery component:

$$= \frac{5w(°))}{(\ Tun_{,,}} \exp \quad , \qquad (3 — 11)$$

where

$$6Wi(0) = \quad — w(0) \qquad (3 — 12)$$

is the initial perturbation in w,

$$_{Tiin} = \frac{krf\ \ \underline{w_{cr}r}}{^{41}Q0^{1)}0}) \exp (\frac{EP}{kT} \qquad (3 — 13)$$

is a relaxation time, and the subscript i distinguishes between regions of the crustal superfluid with different response times and initial perturbations.

The crustal response is thus a simple exponential decay, with **amplitude** linearly proportional to the size of the local perturbation in w, 6w(0) — hence the term "linear" creep.

The Non-Linear Creep Regime:

Here, w,t w_{cr}, i.e. at steady-state w of this regime is close to its critical value **of** w, for unpinning. Thus **a glitch could be triggered here** via unpinning of vortices.

The non-linearity of the coupling refers to its exponential dependence on Sw(0). This gives rise to a glitch response with a Fermi function form:

$$\cdot nZ^2c,k(t) = \frac{ik}{jO\ \ 1} \left[\frac{1}{1 + [\exp(t^2_{\cdot}) — 1] \exp\left(-\frac{t}{\tau_{nl,k}}\right)} \right], \qquad (3 — 14)$$

where

$$to,k = \frac{8wk(0)}{\cdot} \qquad (3 — 15)$$

is the "offset time" of the k^{th} sub-component, caused **by the non-linearity** of the response in this regime; and

$$_{Tra} = \frac{kT\ \underline{w}}{Ep\ 01.} \quad I \quad \frac{\underline{k}\quad \underline{T}}{pkr(b\ )} \qquad (3 — 16)$$

is the response time of the region. $\cdot r_{ni}$ will thus vary throughout the star, and is smaller for larger b, i.e. in regions of weak or superweak pinning. in cooler

stars, T_ra should also be shorter (w_{o},,,i is nearer w_{e}., and the bias "seen" by the creep rate is greater). However, in older (and presumably colder) stars, 7_{ra} is expected to be larger because of the 1 dependence.

The Observable Crustal Response:

The response of a particular sub-component of the crustal superfluid will depend on:

- whether or not the region participated in the glitch by contributing angular momentum to the crust. This determines the size of the perturbation, *Scd:*

  f5w = AC + 611 > Alta if the region did participate
  Afic if the region did not participate

  Since glitches cannot originate in regions of linear creep, these components are not expected to participate in the glitch. In a region that *does* participate by contributing angular momentum, conservation of momentum (eqn. 3-9) amplifies the perturbation.

- whether coupling of the region is linear or non-linear; this depends on the temperature, the external torque, and pinning parameters; it affects the form of the response;

- the type of pinning prevalent in the region; this is determined by *Ep* and *b,* and determines features of the response such as timescales. Alpar and co-workers consider only weak and superweak pinning in their more recent investigations (e.g. 1993a).

The glitch response is most naturally observed in the evolution of the crustal deceleration, St_c (i), given in eqn. 3-11 and 3-14. This is illustrated in fig. 3-5 for non-contributing regions of crustal superfluid.

Fitting the Model to the Data:

Over the years, A [par and co-workers have successfully fitted the vortex creep model to nine Vela glitches, two Crab glitches, and one glitch each of PSR 0525+21 and 0355+54. As improved observations have become available, the model has been refined to include features such as linear coupling and "capacitor" regions.

Figure 3-5: Vortex Creep Model: Linear and Non-Linear Glitch Response.

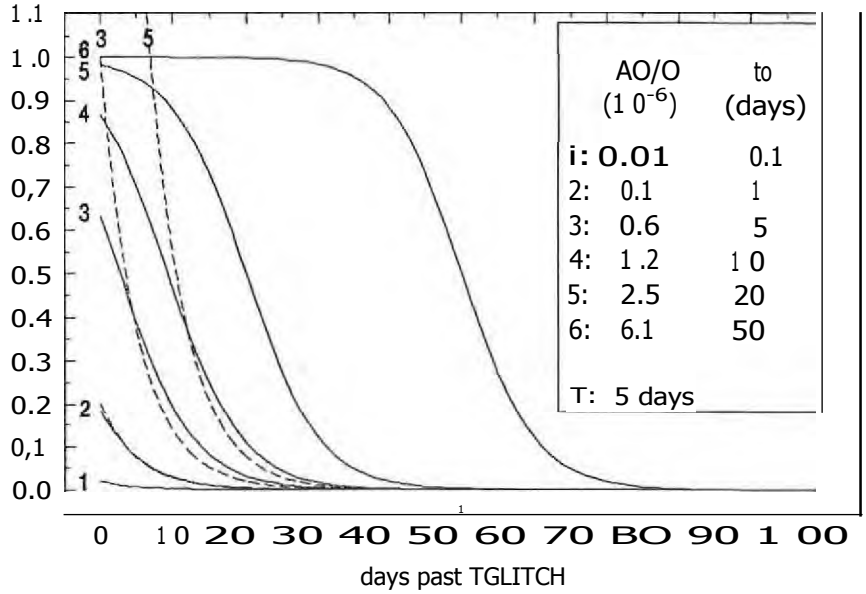

Observable crustal response to a glitch:
Solid lines: non-linear regime;
dashed lines: linear regime; only curves 2, 3 and 5 are plotted.

None of the regions contribute angular momentum to the glitch. The same response time (y = 5d) is assumed for all curves. The different glitch sizes and corresponding offset times t_o are listed in the panel.

The vertical axis shows the relative value of $A_c(t)$ contributed by a particular component, normalised by the relative moment of inertia of that component.

Note that:

- for smaller perturbations, the responses of linearly- and non-linearly-coupled components are indistinguishable (curves 2);
- for a large enough perturbation, a non-linearly coupled component (e.g. no. 6 in the figure) completely decouples, and recouples around a time to ± T;
- the amplitude of the response of a non-linearly coupled region is a non-linear function of the perturbation (eqn. 3-14, with t = 0) and is limited to a maximum AC/c/12 = /WI, corresponding to the case of a perturbation large enough to completely decouple the superfluid;
- in contrast, the response of a linearly coupled component is a linear function of the perturbation, and can be much larger.

Figure 3-6: Vortex Creep Model: Components of the Crustal Superfluid of Vela.

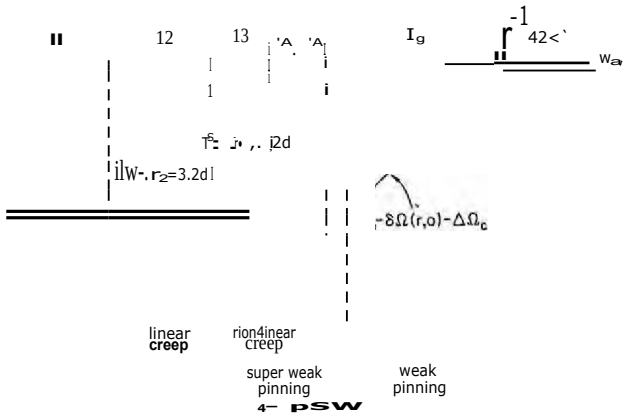

Solid lines indicate the value of *cc* at steady state (upper curve) and immediately after a glitch.
Dashed lines demarcate regions of different coupling and pinning, deduced from observations of eight glitches, as discussed in the text.
IP and *p$lii* indicate the transition densities for linear—non-linear creep and weak—superweak pinning respectively.

Source: Alpar *et* a/. (1993a) fig. 2.

PSR 0833-45 (Vela): The application of this model to the glitches in this pulsar is illustrated in fig. 2 of Alpar *et at.* (1993a), reproduced here as fig. 3-6. With reference to fig. 3-6, the proposed scenario is:

- Regions 1 and 2 are regions of linear creep proposed to explain the observations of the two shortest recovery timescales (10h and 3.2d respectively). Linearity is implied since the offset time for recoupling of a non-linearly coupled region (eqn. 3-14, 3-16) is $t_o > 10$ — 25d, i.e. > T, yet the recovery has the form of a simple exponential decay. The data are consistent with similar inertial moments 1_1 and $/_2$ being involved in each glitch,

- No glitch-related vortex motion takes place through regions 1 or 2. This is implied by the amplitude of the response: should vortex motion occur here, Al2/11 Af2,617 is expected. Thus the glitch-induced perturbation *5w(0)* = Anc(0) throughout this region.

- The observed recovery tirnescale for region 3 is 7_3 > so the simple exponential decay of Af/c observed could indicate either linear or non-linear coupling here. In either case, no vortex motion occurred

here — if the coupling is linear, and vortex motion took place, the response (A,Q/Q) would be far larger; if it were non-linear, recoupling would be delayed by months. Alpar *et al.* prefer non-linear coupling, in which case the short time-constant would imply superweak pinning. They find that it is not possible to simultaneously constrain all three inertial moments, and suggest that region **3** is at the boundary where the glitch is initiated and that the location of this latter region varies from glitch to glitch.

- Vortices unpin in A_1, move through **B,** and repin in A2. The simplest hypothesis is that A_i and A2 are regions of uniform vortex density, thus 6c.(0, r), and hence also $t_o(r)$, has a linear dependence on the radial distance r. This explains the observed monotonic decrease in *Aft$_c$(t)* I that appears to persist until the subsequent glitch — during each interglitch interval *[t,t* 8t1 there will be a part of this region ⟅1$_A$ which is in the process of recoupling ($t_o(r)$ = (Af2$_c$(0) Sw(0, r))/ SV1) (eqn. 3-14).

  Within this model, this implies non-linear coupling.

a Vortices move outward through **B,** but do not unpin or repin here; the size of the glitch perturbation is thus largest here, and is independent of r. There are two possibilities here: either (I) **B** is coupled by vortex creep to the rest of the star prior to the glitch, and would be expected to recouple some time after the glitch, or (2) **B** is never coupled to the star (i.e. this region does not sustain vortex creep; it acts as a "capacitor"). In the former case, one would expect a decrease in I ci$_c$(t) I when all of **B** recouples simultaneously, at a time t >> t_o after the glitch, At this time, recoupling in regions A should also cease, since &J(), r) here is less than 6w(0, r) of region **B.** Completion of recoupling in A would be observable as a decrease in SI Neither of these two features have been observed; hence Alpar *et al.* favour option (2): region **B** is never coupled to the crust, and so does not contribute to the observed behaviour of EI$_G$(t) during or after a glitch. Since vortices unpinned by a glitch do pass through **B,** this region does contribute angular momentum to the crustal spin-up.

- The angular momentum balance is thus:

$$Iccic = (\tfrac{1}{2} + IB)8a \qquad (3 — 17)$$

a Non-linear coupling in region A, and the assumption **B** was not coupled to the crust prior to the glitch, lead to:

$$/A.// = AS^4/c,/t \quad c, \qquad (3 — 18)$$

where Ak$_{it}$ refers to the amplitude of the long-term linear decline.

- The interglitch time calculated by assuming that a glitch occurs as soon as region A has recoupled is

$$tG = ASV,ft/ \qquad (3 — 19)$$

  where Af1 refers to the slope of the linear decay. These values of t_G agree fairly well (with an rms deviation of 33%) with the observed interglitch intervals.

- The next glitch will occur when the initial (unobserved) jump 62 is recovered, i.e.

$$\cdot t_G \quad {}^{fi}n/\,II?'11 \qquad (3 — 20)$$

  which enables the calculation of 6S1 and hence, via eqn. 347, of I.

One requirement of the above scenario is that the transition from weak to superweak pinning occurs at a lower density than the transition from linear to non-linear pinning. The requirement that the fraction of stellar mass in the form of superfluid in the superweak density regime be at least the measured $/_{13}// — 10^{-2}$ is satisfied by most neutron star models. The total measured moment of inertia involved in the glitch is 24% for the largest glitch, and requires a "moderately stiff' equation of state (fig. 3-4).

PSR 0531+21 (Crab): The most recent application of the vortex creep model to this pulsar is that of Alpar et *al.* (1994). Again, they model the four glitches for which there is sufficient data with the same recovery timescales. Two simple exponentials = 0.8d and 72 12d) and one non-linearly-coupled component (7_3 = 200d) were fitted. Component 3, involving negative Sw(0) (he. a spin-up) is only fitted to the most recent (1989) glitch by Alpar *et al. ;* a recent re-analysis of the Crab data by the observers (Lyne *et al.* 1993) incorporates a spinning-up component with a long timescale (7 200d) for all four of the glitches for which they had sufficient data. Lyne *et al.* fit fl(t), and *see* a fast (r = 0.8 d) component only at the 1989 glitch; Alpar *et al,* assume this component is present but unobservable following all the glitches.

Since the offset time t_o is not larger than 1.5 hr for the Crab, it is not possible to distinguish between linear and non-linear coupling for the simple exponential decays (components 1 and 2). Linear coupling is assumed for these two components; unless vortex motion occurs through region 2 the implied moment of inertia $1_2/1$ is unrealistically large. Negative values of (5w (components 1 and 3 in the 1989 glitch) imply an *increase* in superfluid rotational velocity, which Alpar *et al.* suggest is due to inward crust breaking (a

crustquake) accompanied by inward vortex motion. The angular momentum balance (eqn. 3-17) is thus modified:

$$= \text{lc AC2c} + \qquad \text{Ii6thi} + 113^{8}\text{CJB} \qquad (3 — 21)$$

where $A/_{c}$ is due to the crustquake and subscript B refers to a vortex depletion or capacitor region of the type invoked in the Vela pulsar glitches.

The crustquake should be accompanied by permanent changes in both l and SI, of size:

$$\left(\frac{\Delta N}{N}\right)_{res} = \frac{\text{AS)}_{c}}{\text{nc}\ )_{re.}} = \left|\frac{\Delta I}{I}\right| \qquad (3 — 22)$$

Since the observed Aftciftc < A.0/12, Alpar *et al.* assume that $A/_{c}$ contributed by the crustquake is negligibly small (e.g. in eqn. 3-22), and that the observed residual Aftc is due to the formation of a new capacitor region, with inertial moment i_{g}.

Both Crab and Vela glitches can thus be explained in terms of the vortex creep model; the very different glitch characteristics are due purely to the different ages of the two pulsars: Crab glitches are caused by starquakes; this pulsar is still hot enough that thermal creep effectively slows down the pinned crustal superfiuid. At each glitch, a new capacitor region is formed, and by the time the pulsar reaches the age of Vela it will have a network of such regions (region B in fig. 3-6). The response times $T_{,}$ of the crustal superfluid regions will lengthen with time as the pulsar cools.

PSR 0355+54: Both non-linear and linear creep are implied by observations of, respectively, a persisting shift in $S2_{c}$ and a prompt exponential decay of part of ASI_{c} over a timescale $44\text{d} < t_{o}$ 5 yr).

PSR 0525+21: The long relaxation times *(-r* = 150d and 3000d), persistent shift in Ste, long spin-down age and probable low temperature are all consistent with no regions of linear creep existing in this pulsar (Alpar *et at.* 1989).

Other Pulsars: Alpar & Baykal (1994) have compared the actual (19) and predicted numbers of glitches in a sample of 430 pulsars. The glitch models compared are:

- vortex unpinning model with the same Sh for glitches in all pulsars;

- vortex unpinning model with the same 89,/,Q for glitches in all pulsars, i.e. including a dependence on vortex density;
- corequake model.

The Vela glitches were omitted from the sample; parameters such as 811 were deduced from these glitches and compared with the sample average. They conclude that the second option above is a better match to the data.

In general: A major selling point of the vortex creep theory is its applicability to all neutron stars, using the same structural parameters (mass, pinning strengths); differences in the details of the fitted models are ascribed to evolutionary factors such as temperature. The starquake model, in contrast, requires a solid core for Vela and not for the Crab pulsar.

In early work, Alpar et *al.* (1984b, 1985) used eqns. 3-13 and 3-16 to estimate internal temperatures of Vela, the Crab and 0525+21. In more recent work (e.g. 1989) they have taken the more cautious path of using independent estimates of temperature to calculate pinning energies.

In addition, Alpar et *al.* (1984a) predict that vortex creep will dissipate energy, even more than the glitches themselves; this heating mechanism should be the primary heat source in older pulsars which have radiated away their original heat.

3.9 Co-rotating Vortex Model.

The vortex creep model assumes that the bulk of the crustal superfluid is pinned to the crustal lattice, and that the response of the vortex creep coupling mechanism to the glitch explains all features of the glitch recovery. Jones (1990a,b, 1991), on the other hand, argues that much of the crustal superfluid is not pinned. Since pinning forces are the only forces operative in the crust that are large enough to oppose the Magnus force, free vortices will very nearly co-rotate with the superfluid (hence the name of this model). Very small differential velocities are caused by frictional forces (section 3.2.2); it is these interactions that couple most of the crustal superfluid to the spin-down, and that are responsible for the form of the glitch recovery. The temperature-dependency of the coupling is thus different from that of the vortex creep model.

Jones argues that vortex pinning is restricted to a small part of the crust, as shown in fig. 3-7.

Figure 3-7: Co-rotating Vortex Model: Regions of Pinned and Co-rotating Superfluid.

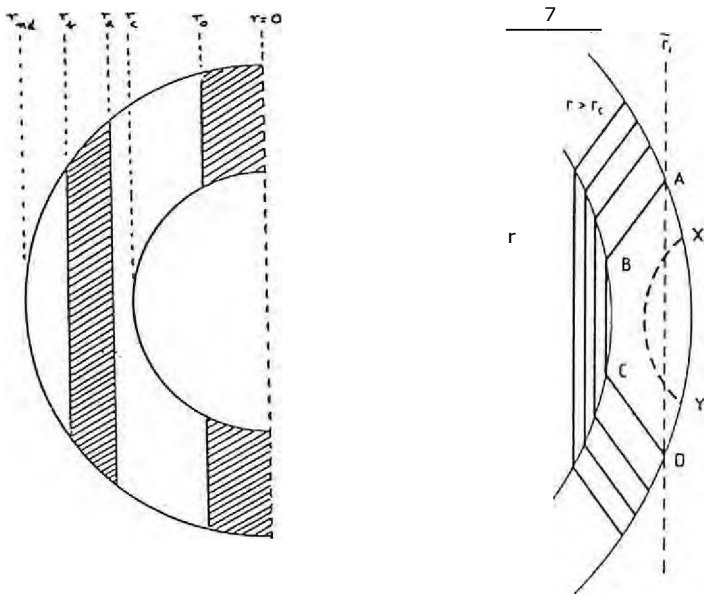

a

In these vertical cross-sections of a neutron star the crustal superfluid is bounded by spherical radii r_{nd} and r_c. A second boundary at r„ may separate $^1S_0$ and $^3P_2$ superfluids; Jones assumes $r_n < r_c$. The nature of these boundary layers is uncertain; however, a boundary layer of thickness 14 m at r = r, would have a non-negligible moment of inertia — 10^{-3}/.
The rotation axis is indicated by r =- 0. Shaded regions denote pinned superfluid, and heavy lines vortex geometry.

Fig. 3-7a The following two regions must exist in all pulsars:
a region of pinned superfluid extending from the rotation axis to cylindrical radius r_o, where the superfluid velocity is smaller; and
a region of unpinned superfluid at low superfluid density near the equator (r_d to r_e), where the superfluid coherence length is >> a, the lattice spacing.

In addition, a region r_b r_a in which the pinning energy is large enough for pinning to be present may also exist, around p_n — 10^{-13} g cm^{-3}.

Fig. 3-7b Should vortices be strongly pinned in the core, the pinning region in the crust could be distorted. Since co-moving vortices must be straight, this results in a vortex depletion region (ABCD) and a reduced co-rotating volume.

Source: Jones (1990b) fig. 1 & unpublished.

The frictional force acting on the vortex is

$$= \quad - \qquad (3 — 23)$$

where subscript L refers to the vortex line and C to the crustal lattice.

The force constant 7 is due to interactions involving the moving vortex line, the electron-phonon system of the crust, and crustal nuclei. The exact form of 7 appears to involve a large number of unknown factors, but according to the calculations of Jones (1990a) *b,* 1991):

- the dominant component of 7 is independent of temperature, and $\propto E2_{PS}$,
- the magnitude of the temperature-dependent term is difficult to calculate but probably relatively small;
- there is a term that is negligible at small differential velocities 1 m s^{-1}) but large enough at high velocities to be responsible for the relatively fast transfer of momentum from newly unpinned vortices to the crust; this term would explain the fast 2min) rise time of the Vela glitch observed by McCulloch *et al.* (1990).

Fitting the Model to the Data:

The response of the crust to a glitch is

$$A2_{,c}(t) = Af2_{,,}(t)\ AO_{,,,,,t}(t) \qquad di_{n}, \qquad (3\text{-}24)$$

where

- the term within the integral refers to pinned superfluid that is unpinned at the time of the glitch;
- *b,)* is the steady-state lag of the above superfluid component;
- the tilde implies a function of cylindrical polar co-ordinates (F, *z);*
- *.)* = SU is a function oft;
- **a** the subscript vc refers to the vortex creep response of the pinned superfluid region outside of I_N;
- the subscript *corot* refers to the response of the superfluid with co-rotating vortices.

Small Glitches in Vela, Crab, 0355+54, 1737-30: Jones (1993) suggests that these events constitute a class distinct from the large glitches. They are due to unpinning and re-pinning of vortices, in a region where vortex creep is operative. Jones calculates that the vortex creep relaxation times are unobservably short. The exponential form of the response is thus due entirely to the distribution of the perturbation *Sw(H)* and the consequent distribution of recoupling times $t_o(H) = {}^{8}b)(^{6}1)/$ 1C.21; it gives no information about temperature. The response is then described by the last term in eqn. 3-24; the terms describing the response of pinned superfluid not involved in the glitch and of the co-rotating component are negligible for this class of glitch. Jones expects that Aft„ = 0; the non-zero 6.12,„„ observed following the Crab glitches requires (within this model) extremely large c.o, and hence implies structural changes of the type suggested by Alpar *et al.*

PSR 0833-45 (Vela): Again, unpinning of vortices is the cause of the glitch. Recovery on timescales longer than a few days (specifically the "intermediate" and "linear" terms extracted by Cordes *et al.* 1988) is due to recoupling of this superfluid, and is described by the third term of eqn. 3-24. As is the case for the small glitches, the form of the recovery is due to the distribution of the unpinning, and is temperature-independent. In contrast to the Crab pulsar, Vela must have a superfluid component which is permanently pinned and hence decoupled from the star at all times (this is also required in the vortex creep model).

The response of any non-participating region of vortex creep is again unobservably fast.

Jones attributes the fast recoveries seen in large Vela glitches (7- 0.5 d and 4 d) to recoupling of the co-rotating component (the second term of eqn. 3-24). These components are of too large an amplitude to be explained by the response of a pinned superfluid component, unless either a low stellar mass, a very stiff eqn. of state, or a strange distribution **of** *Ep* is assumed. For the glitch of 1988, Jones infers $T_{ne}(r,) = 3.4$ d (combining the two fast responses observed by Flanagan 1990), but suggests that the data do not constrain this value severely.

PSR 0355+54: The deduced force constant for Vela, scaled by ,S1 of 0355+54, gives a predicted 7-„(r,) of 6.0d for this pulsar, in contrast to the observed 44 d recovery time. Possibly there is an un-accounted-for temperature dependence involved.

PSR 1641-45: An unusual feature of the most recent large glitch in this pulsar is that by the time of the first post-glitch observation (up to 70d

after the glitch), L1O/S1had decayed to (5 + 3) x 10^{-4}. Jones (unpublished) suggests that strong pinning of vortices within the core could (a) completely decouple part of the superfluid from the crust, and (b) create a "vortex depletion region" at the expense of the co-rotating component, as shown in fig. 3-7.

3.10 Crustal Plate Tectonics.

In this model (Rucierman 1991, 1991a), the crustal lattice yields before reaches the critical value for vortex unpinning (section 3.5.5). Ruderman envisions cracks developing in the crust, resulting in macroscopic crustal platelets being formed; these then migrate towards the spin equator or poles in pulsars spinning down or up respectively. Two forces are expected to strain the crust: pinned vortices of the crustal superfluid, which rotates faster than the crust, and migrating magnetic flux tubes which are anchored in the lower crust.

Pinned vortices of the crustal superfluid move with the platelets; a sudden release of strain of magnitude AO in a spinning-down pulsar will result in an outward displacement of vortices of rA0/2. The corresponding reduction in SI is

$$8,0 = \qquad (3 — 25)$$

By conservation of angular momentum, this results in a glitch in the crustal spin-frequency of size

$$\mathrm{AQ_c} = \frac{AOSZI_s}{} \qquad (3 — 26)$$

Setting $/_s$ 10^{-2}1 gives a breaking strain AO 10^{-4} for Vela, consistent with the assumptions of this work.

In the laboratory, a transition from a plastic flow to a "brittle response" (i.e. cracking) is observed at T 10% of the crystal melting temperature, Extrapolating this to neutron stars implies that stress release may be in the form of plastic flow for younger (and hotter) pulsars such as the Crab. Even in cooler pulsars, the response may be brittle on the scale of crustal grains "microscopic crumbling" rather than large-scale cracking along plate boundaries may occur.

The interglitch interval would be — *SOIS'1,* which gives values close to those observed for pulsars of age 10^4 yr, but predicts far higher glitch rates

than seen in younger pulsars, supporting the suggestion that an alternative stress-release mechanism such as plastic flow operates in these objects.

According to Rudermau, the stellar response to a glitch caused by sudden crustal plate motion would involve the following components:

- the strongly coupled core+crustal-lattice+crustal-electrons;
- the strongly pinned crustal superfluid, with moment of inertia ip 9 x 10^{-3}/, which remains pinned to the moving crustal lattice plates during the glitch; presumably this component contributes only to *Act* (and not to *Aft,* since it is never coupled to the star);
- the co-rotating superfluid component described by Jones (e.g. 1993), which contributes the fast recovery of Aft over days;
- the component of crustal superfluid in which continuous vortex creep is operative; Ruderman mentions that there are at least two different theories (of Jones and of Alpar *et al.)* regarding the response of this component.

Ruderman also mentions that the last of these could be supplemented or replaced by lattice creep or lattice crumbling, neither of which need involve movement of vortices among pinning sites; calculation of details of the response of such interactions would require better knowledge of the crustal lattice behaviour than is currently available.

3.11 Return of the Core Superfluid: The Core Shell Model.

In a return to the original two-component model of Baym *et* a/, (1969), Sedrakian *et al.* (1995) examine the role of clusters of proton vortices around the neutron vortices in the core. The resulting coupling of the core superfluid with the normal component is so strong that the Magnus force is effectively opposed, resulting in longer dynamical coupling times than is normally assumed. The behaviour of the crust is given by the sum of the responses of layers of core superfluid, indicated by subscript *k:*

$$\frac{Pk}{\text{id}\,(1 + Pk)}\{\delta_{wk}\,exp\,(-t\,TO]\;;\frac{1}{T} = \qquad (3-27)$$

where

$pk =$

$(sw_k\ is\ w_{ic}$ the departure from equilibrium in layer k.

Note that since in this model $I_{,,}$ the crustal component moment of inertia, includes only the crust and the region of the core with $R <$ 5km, pi, can be quite large, although it is assumed (and later demonstrated) to be < 0.5. The steady state lag is given by

$$co_{,k} = \frac{}{27rr,} (\, + Pk). \qquad (3-28)$$

Following a glitch, which must reduce co, the core shells can become:

- relaxation shells (bu.)(0+) < 0): I2, will decrease (I S't, I increase). A special case of relaxation shell is one in which the shell was in equilibrium prior to the glitch (bco(0^-) = 0) and the glitch decouples the shell.
- rise shells (S1,(0+) > 0): the glitch may originate in such a shell, in which for instance pinning has resulted in the build up of a large *co;*
- passive shells, in which either Aft, Sw, i.e. the shell is brought into steady state by the glitch, or (more likely) the shell remains pinned throughout the glitch; in either case no glitch response is observed.

PSR 0833-45: Sedrakian *et* a/. (1995) apply the model to the data of Cordes *et at.* (1988). The "linear" *(ii)* term of the latter analysis is assumed to be a decay term with T_t the interglitch time; the exponential is expanded in a Taylor series, of which only the linear term is retained. The consequent function to be fitted is then

$$f\mathrm{Mt}) = \frac{f2, \quad AI1_C / 5,}{T_C \quad T.\ le} \exp(i/7_3) \quad \frac{Af2,\ Li}{} \exp(-tir_i) \quad \frac{Aft,\ Li}{TI\ \ i^re + Isl}(1 \quad t/T_i) \quad IC \frac{(w}{g} \frac{To^{c}}{T}) \frac{eXP\ HIrg)}{g} 7 \qquad (3-29)$$

where

- subscripts i and *l* refer to the short, intermediate and long recovery components identified by Cordes *et at.*, and
- the last term is the "rise shell" in which the glitch originates, where $c.0_g >$ (1?47-,)r_g.

Sedrakian *et at.* fit the model by

- selecting a neutron star model;

Figure 3-8: Core Shell Model: Vela Glitches.

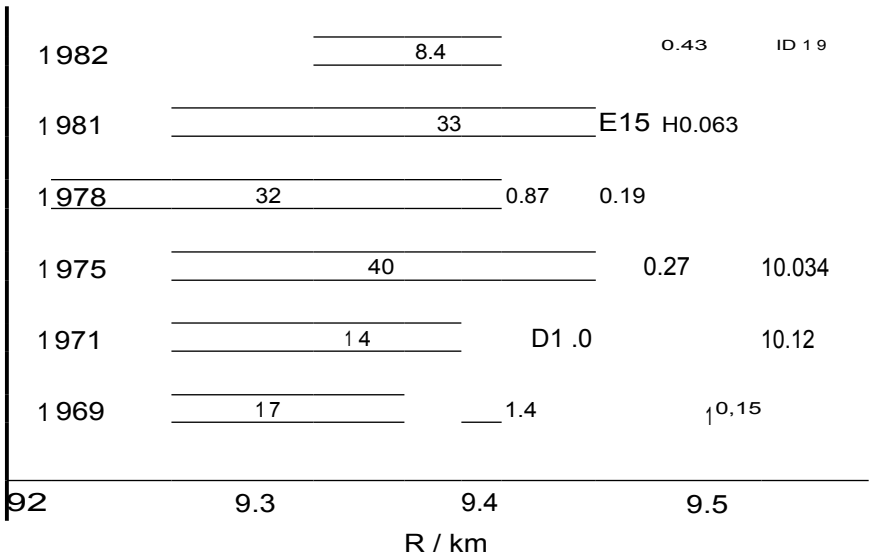

The radial location and extent of each core shell involved in the glitch response after each of the first six Vela glitches.
The numbers give relative moment of inertia 'k/I, in units of 10.

Source: Sedrakian *et al.* (1995) fig. 3 and table 1.

- using the parameters $\mathbf{I_k}$ $\mathbf{T_k}$ of Cordes *et al.;*

- **a** fitting further parameters such as density and location for each shell by integrating over regions of the inner crust until a matching total */I,* and mean *rk* are obtained.

The resulting shells identified in each of the first six Vela glitches are shown in fig. 3-8. Features of these results include:

- the locations of the shells change from glitch to glitch;

- the *1*-, i- and s-shells are at progressively smaller density (larger radius);

- the /-shell is by far the most extensive;

- there are large portions of the outer regions that do not participate in the glitch; pinning is presumably more likely in these regions, where the pinning force (at the crust-core interface) is shared over a shorter length of vortex.

From observations of the eighth glitch, τ_g f^2 3 min. Such a shell is possible in the outer region of the core *(R* 9.62 - 9.64km), with $/_g//$, = 0.02. A lag w_g - 6 x 10^{-6} Hz > $\mathbf{co_{cd}}$ **0,1** τ_2 3 x 10^{-9} Hz must accumulate in this shell, presumably by pinning. This requires an interglitch period of $t_g > c0_g / 11\bar{1}1 \rightarrow$ 450d, which is feasible.

Other Pulsars: In this model, coupling times are independent of temperature and scale with P^2 (assuming the mass and other structural parameters are the same for all neutron stars).

For **PSR 1737-30,** the short interglitch interval 1 yr) and small (, 0.1 IQ *!VELA)* pose a problem for accumulating sufficient excess w in the g-shell. This could be resolved by involving different g-shells for each glitch — observations of a range of rise times in future glitches would support this idea.

Resolved increases in SI observed in some **Crab** glitches are attributed to rise shells; the P^2 scaling factor explains why such features have not been observed in Vela glitches — for shells at similar locations, coupling times of 5 yr are predicted. The wandering of WO over timescales of **400d** observed in **PSR 1641-45** can be explained as a superposition of rise and recovery shells located at density 2.6 x 10" g crn^{-3}_ The amplitude of the 44 d relaxation of the large jump in **PSR 0355+54** requires averaging over a fairly large range (9- 90d) of **T.**

The above shell model is an approximation — Sedrakian *et at.* note that post-glitch recovery should preferably be modeled with a continuous *T(p).* They also predict that rapid post-glitch transients should not be observable in long-period pulsars; neither should observable (T days) recoveries be seen in millisecond pulsars.

3.12 Return of the Core Superfluid cont'd: Creep against Magnetic Flux Tubes.

Chau *et al.* (1992) have suggested that superfluid vortices of the core will be pinned by magnetic flux tubes associated with the superconducting protons of the interior. Thermal creep will couple the neutron superfluid to the crust; Chau *et* al. calculate that this coupling will be non-linear, with cd,,,, <
A glitch will decouple the entire region from the spin-down; recoupling will occur after a time

$$t_o = \ /0\ |\ \underline{\min(AS/}_{\subseteq}, 2w, \qquad (3 — 30)$$

If $t_o >> T_{\mathbb{h}}i$ (the recoupling timescale), the decoupling of the interior should be apparent as a large and persistent increase in Inc 1, AfICIfloo >> 1. Sincethis is not observed following the 1988 Vela glitch (for which to 2l hr), they infer that either (a) the internal magnetic field is smaller than previously assumed (i.e. $B < 10^{12}$ *G)* or (b) an exotic EOS is implied.

3.13 Energy Release in Glitches.

Part of the stellar rotational energy extracted in a glitch will be released as heat. The amount of heat depends on the glitch mechanism: Van Riper *et al.* (1991) calculate that Vela glitches originating in a region of strong pinning, in a region of interstitial pinning, and smaller glitches caused by starquakes will release 10^{43}, 10^{40} and 10^{3}" erg respectively. The magnitude and evolution of the consequent increase in surface temperature depends on factors such as the equation of state, the stellar temperature, and the depth at which the heat is released; it may persist for hours or months. Van Riper *et* a/. have constructed a simple one-dimensional model, from which they conclude that giant glitches due to superfluid unpinning may be observable in nearby pulsars with the current generation of X-ray telescopes such as ROSAT.

3.14 Glitches and ry-ray Bursts?

One of the models for 7-ray bursts (GRB) summarized by Hartmann (1995) involves a sudden transfer of angular momentum from the crustal superfluid to the crust of a neutron star. As well as causing a glitch, such an event

could excite surface waves which would generate strong electric fields parallel to the magnetic field, providing the plasma density is low enough. Particle acceleration in these fields could produce a GRB.

Searches for 7-ray bursts coincident with glitches are only feasible if the glitch epoch is known accurately (within minutes); this knowledge is only available for the most recent Crab and Vela glitches. Vela is closer and has larger glitches, which makes it a better candidate. Hartmann *et al.* (1992) have searched data from the Phobos 2 spacecraft around the time of the 1988 glitch. Two burst detectors were operating, in the 6 - 1000keV and 120 – 1400keV range — no likely events were found. Hartmann (1993, private 'communication) also reports that no event coincident with the 1991 glitch was seen in Compton GRO data.

An upper limit of conversion efficiency of energy into -y-rays of 10^{-4} was obtained for the 1988 glitch. The implications are:

- the burst was confused with the steady or pulsed 7-ray emission; or
- it was beamed away from Earth; or
- the plasma density is too high for this model (Vela has not yet evolved into a 7-ray burster); or
- the model is wrong: bursts and glitches are not related.

3.15 Summary.

The status of glitch models is now at an interesting stage — the developers appear to be incorporating features of each other's models as new features are uncovered in the data. For instance, the starquake and vortex creep model initially had very little in common; the current version of the starqu.ake model incorporates crustal superfluid dynamics to explain the range of recovery times observed, and the vortex creep model now invokes crustquakes to explain the resolved component of the Crab pulsar glitches.

To an observer, the many uncertainties currently involved in linking observed timescales to stellar model parameters such as temperature make for a depressing situation. However, the quality and quantity of glitch observations has been increasing in recent years, which has already had an impact on some predictions of the models. For instance, rapidly recovering components of the Vela glitches strongly imply linearly-coupled stellar components. The rise time of the glitch, now limited (at least for the Vela pulsar) to ;-.2rnin, puts fairly strong constraints on the models. The remainder of this thesis presents glitch observations that hopefully contribute to this effort; aspects

of the analysis prompted by the above reading of the theory include: to what extent are distinct recovery components involved? what is the form of the long-term behaviour of the Vela pulsar? and are any of the recovery parameters common to all glitches?

4 Observations.

All observations were made at the Hartebeesthoek Radio Astronomy Observatory (HartRAO), near Johannesburg. HartRAO was originally Deep Space Station 51 of the NASA Deep Space Network, and is currently operated by the-Foundation for Research Development as a national facility. The author was involved in the early stages of the pulsar observing project. Observing commenced in January of 1984, and continues at the date of writing (1995). In this chapter, the equipment used for the observations, and the observing strategy developed for observing the immediate post-glitch behaviour of the pulsars, is discussed.

4.1 Hardware.

The hardware used for the observations consists of:

- 26m Cassegrain radio telescope;
- 1.6 GHz and 2.3 GHz receivers;
- antenna control computer;
- station time-keeping and frequency-generation systems;
- intermediate frequency (IF) section;
- pulsar timer.

The first four items listed above are used by other observatory projects, and were in use before the pulsar timing project began. Receivers are configured in total power mode for pulsar observations. System parameters are listed in table 4-1. Relevant upgrades implemented since the start of this project are listed in table 4-2. The IF section is used only for pulsar observing, and is composed mostly of standard components. The pulsar timer was custom-built for this project.

Fig. 4-1 shows how the pulsar signal is processed by the above hardware. The pulsar signal path is indicated with a heavy line. A number of observing frequencies are simultaneously available - all receivers and feeds are permanently mounted at the secondary focus, and the Cassegrain reflector can be manually tilted to optimise illumination by individual feeds. Selection of a particular receiver involves adding the corresponding feed offset to the telescope position. Pulsar observations are made at the two lowest frequencies, 1.6 GHz and 2.3 GHz, shown in fig. 4-1.

Figure 4-1: Pulsar Observing Hardware.

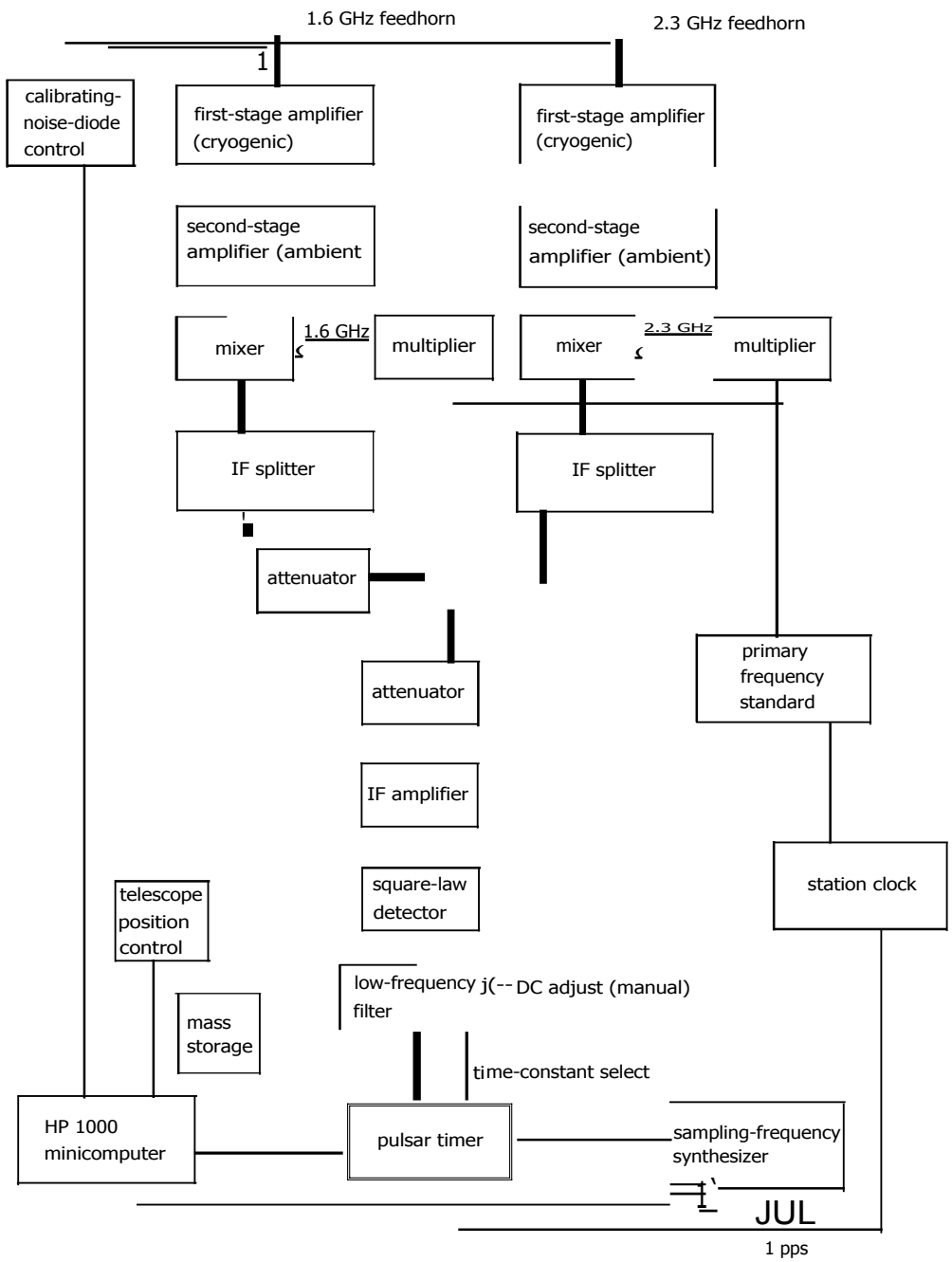

The pulsar signal path is indicated with a heavy line.
The pulsar timer is shown in more detail in fig. 4-2.

Table 4-1: Receiver System Parameters

system:	1.6 GHz (tilted)	1.6 GHz (untilted)	2.3 GHz
centre frequency (GHz):	1.668	1.668	2.3256
system temperature (K):	40	45	42
point-source sensitivity (Jy/K):	10.4	13.8	9.9
polarisation:	left circular	left circular	right circular

Narrow band mixers convert signals received at all observing frequencies to a standard intermediate frequency (IF) of 60 MHz. At the splitter, the signal is distributed to the equipment utilised by the different observing projects. A manually adjustable IF attenuator is installed in one signal path to equalise the signal levels, in order to allow computerised switching between the two channels. The attenuator, IF amplifier, and square-law detector of the IF section are standard components. One of six low-pass post-detection filters, listed in table 4-3, can be selected by the pulsar timer.

The pulsar timer was designed by F. Gull, under supervision of M. Marsh, both of the (now defunct) National Institute for Telecommunications Research (NITR), and was assembled, programmed and installed by the author, with the assistance of M. Marsh. The low-frequency filter and hardware to divide the sampling frequency by 1000 are modifications added by the author. The pulsar timer is described in more detail below.

4.1.1 The Pulsar Timer.

The pulsar timer design is based on equipment used by Downs & Reichley (1980, 1983) of the Jet Propulsion Laboratory at various NASA Deep Space Network stations for a similar observing program. The hardware is shown in fig. 4-2_ It comprises a Motorola microprocessor, a block of memory, hardware for sampling the analogue input signal, timing-control hardware, interfaces to the HP-1000 control computer, an analogue signal-display meter, and an LED status-display. The software was written in 6800 assembler code, as speed and timing are critical. More detailed information is available in the HartRAO Pulsar Timer Manual.

Table 4-2: System Upgrades to the 1.6 and 2.3 GHz Systems since 1984M.

Date	MJD	Receiver	Upgrade
1984/01/04	45 704	2.3 GHz:	pulsar observing started, using linear polarisation and ambient GaAsFET receiver
1985/04/24	46 180	2.3 GHz:	ambient GaAsFET replaced with cryogenically cooled GaAsFET
1985/05/16	46 202		station frequency standard upgraded from rubidium to hydrogen maser
1985/06/05	46 223	1.6 GHz:	cryogenic GaAsFET receiver installed, with left circular polarisation
1985/12/19 — 1986/02/18	46 419 — 46 480		telescope re-configured for prime focus: no pulsar observing possible
1988/11/28	47 494		on-site GPS receiver installed
1989/04/20	47 637	2.3 GHz:	feed changed from linear to right circular polarisation
1990/08/17	48 152	1.6 GHz:	tilting subreflector installed to improve efficiency
1991/10/16	48 546	1.6 GHz:	cryogenically cooled H EMT receiver installed
1992/01/16	48 638	2.3 GHz:	cryogenically cooled HEMT receiver installed

Figure 4-2: The Pulsar Timer and its Interfaces.

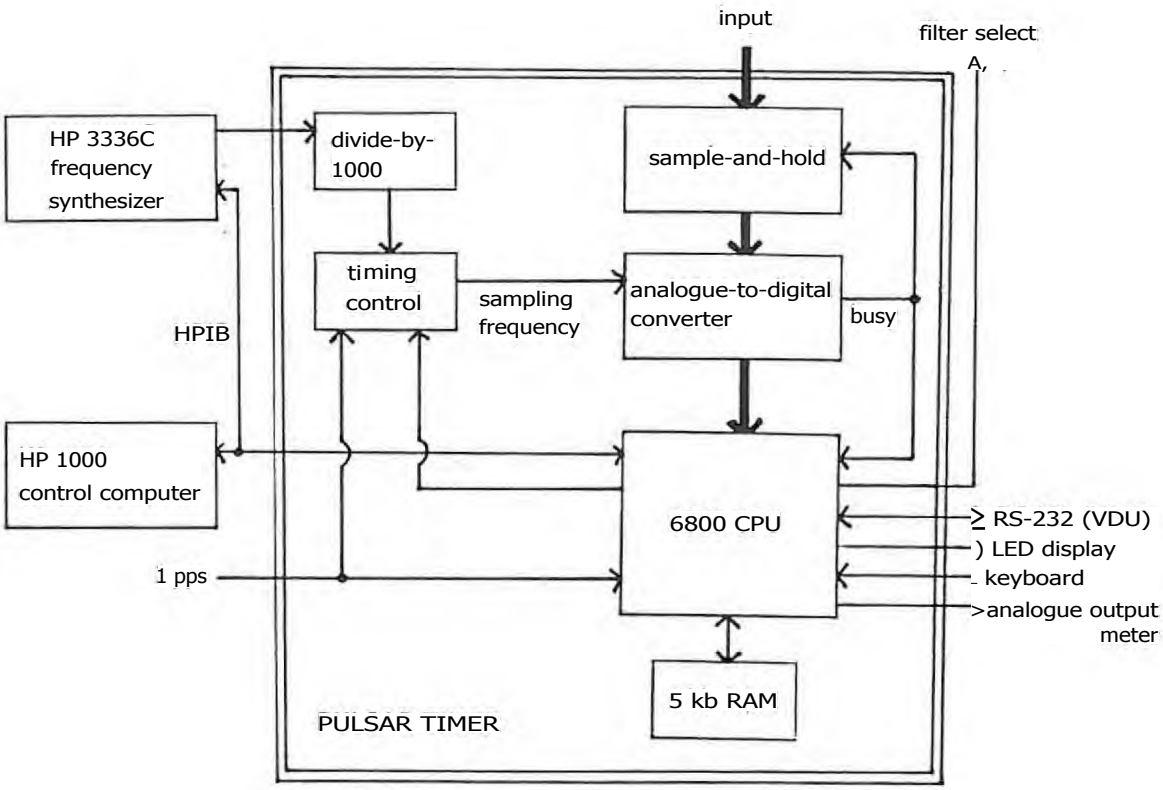

The pulsar timer is enclosed in a double line.
During normal operation, the timer is controlled by the HP1000 via the HPIB; the VDU, LED display, keyboard and meter shown on the right-hand side are used for de-bugging and status monitoring only.

Table 4-3: Post-detection low-pass Filter Time-constants

Filter number	Nominal value psec	Actual value psec
1	50	49
2	100	104
3	150	159
4	200	190
5	250	265
6	500	445

The main purpose of the pulsar timer is to sample the received signal synchronously with the apparent rotation period of the pulsar, integrating the samples from successive periods into memory. This on-line integration is carried out over *Np* consecutive periods, at an accurate and known rate of N_s samples per period. *Ne* and *Ns* vary from source to source, and are programmable. The pulsar timer software imposes an upper limit OD NS:

$$PI\ Ns > AT_{,s}, \qquad (4 — 1)$$

where *P is* the apparent rotation period, and *ATs is 113 its,* the time taken for the pulsar timer to execute one sample-and-add-into-storage cycle.

The sampling software of the pulsar timer is shown in appendix 2. The output from the timer, after an integration, is this on-line integration, the start-of-integration time and the parameters *(Np* and *Ns)* of the integration.

4.2 Time-keeping.

Accurate time and frequency control is needed for

- the sampling rate;
- the start-of-integration time;
- the local oscillator.

An accurate and stable local oscillator is essential because pulsar signals are dispersive in the interstellar medium, i.e. the pulse arrival time is dependent

Figure 4-3: Timing Control

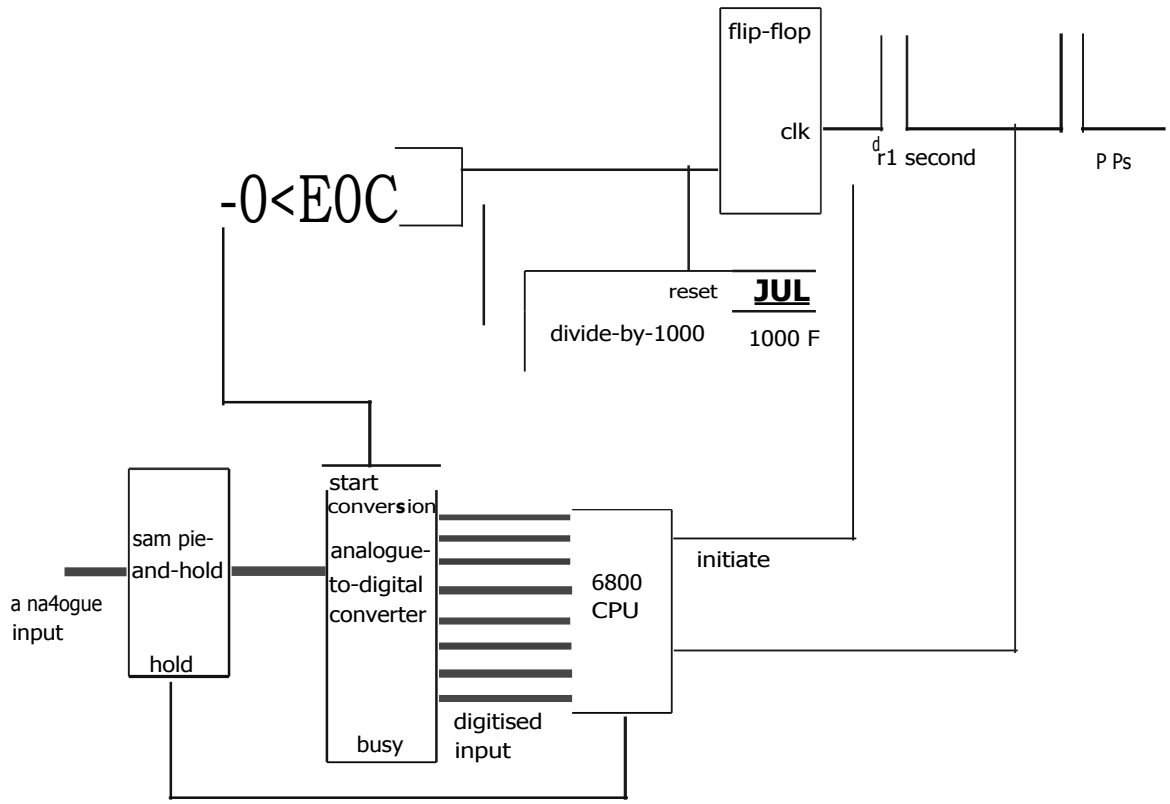

on the observing frequency. An unknown observing frequency offset will cause an unknown and hence uncorrectable offset in pulse arrival time,

Fig. 4-3 illustrates the time keeping hardware of the pulsar timer. The station 1 Hz time signal is used to update the pulsar timer software clock. This clock is synchronised with that of the HP1000 before each integration, and is suspended when the integration starts. The integration starts at time $t_o = ts + (1/F_s)$, where t_s is an integral number of seconds, as shown in fig. 4-3 and appendix 2. The sampling frequency, F_s, is generated by an HP3336C synthesizer, under control of the HP1000 control computer. The synthesizer is set to 1000F, and divided down to Fs, in order to improve the accuracy of t_o. Since the frequency generated by the HP3336C can be set to +1 mHz, the resulting smear over a typical integration is insignificant (<1 *ps*).

The station 1 Hz time signal is generated by the station clock, which is based on the station Primary Frequency Standard (PFS), currently a hydrogen maser. Prior to 1985, the primary standard was a rubidium oscillator. All local oscillators are derived from the PFS. The PFS also provides a reference frequency for the HP3336C, which produces the pulsar timer sampling frequency, and for the HP1000 computer clock.

Linking the PFS to the clock, the local oscillators, and the pulsar timer sampling frequency ensures the required level of short-term stability of these signals. The two remaining links required in the time-keeping chain concern the absolute time: ensuring that the integration occurs at a known time, and linking this time to an internationally accepted timescale. The first problem is made easier by starting each integration on the second, and thus reduces to resolving ambiguities at the level of the second. This is done by requiring the operator to check the HP1000 time against the station clock. Fortunately, pulsar observing itself provides a check on this: the observation time can only be wrong by an integral number of seconds; since pulsar rotation frequencies are not phased to terrestrial seconds, any error is immediately obvious as a very large offset in pulsar pulse phase.

The second problem (connecting the HartRAO time to Universal Coordinated Time, or UTC) is dealt with by allowing the HartRAO clock to run free, and comparing it regularly with UTC. The frequency standard is adjusted approximately once every three months, to keep the frequency within $+2 \times 10^{-12}$ of UTC, and corrections are applied in the data processing. The HartRAO clock is always behind UTC, so the time correction applied is always in the same sense. The comparison has been done in a number of ways:

- Time was transferred to HartRAO from the Omega network of navigational transmitters (Gaede 1988). This has been done at various intervals (monthly to daily) since the early 1980's; time-transfer from Omega was terminated in 1992.
- Time was transferred every working day from 1982 to 1991 from the South African National Time Standard, based in Pretoria, via the local television transmitter. Offsets between this standard and UTC are published monthly.
- From 1988 to late 1990, an on-site receiver was used to transfer time every 15 minutes from the Global Positioning Satellite (GPS) network.
- From mid-1991 until early 1993, HartRAO time was compared weekly with that of the neighbouring Satellite Application Center (SAC), via travelling clock. SAC has an on-site GPS receiver.

- A GPS receiver was installed at HartRAO in early 1993. Time transfer is now done under computer control every 2 hours.
- Throughout the time period covered by this project, HartRAO has participated at least monthly in global VLBI experiments. By-products of these experiments are a check on the stability of the local oscillator, and hence the PFS, and a check on the actual time.

All the above time-transfer methods are accurate to a microsecond or better, which is more than adequate for the pulsar timing observations carried out at HartRAO. The drift rate of the HartRAO clock is never allowed to exceed 200 ns per day, far better than that required for a 20-minute pulsar integration.

4.3 Observing Software.

The observatory "control computer", an HP1000, commands the pulsar timer, sets up synthesizers, turns calibrating noise-diodes on and off, controls the telescope positioning and reads and stores data from the pulsar timer. The Fortran-77 programs (written by the author) that do this are:

PLS77 the main observing program, described below.

PGDET on-line glitch detection — calculates the pulse arrival time t_{obs} of the latest observation, compares this with the predicted pulse arrival time t_{pred}, obtained from the current ephemeris in the PULSAR source file, and flags an alarm if $t_{obs} - t_{pred}$ exceeds the allowed value.

QPLT7 plots the latest integration, together with the predicted pulse arrival time calculated by PGDET.

PLOG maintains a log of the observations.

PPRNT prints out the log produced by PLOG.

SRCFL allows manual updating of the PULSAR source file, e.g. addition of a "new" pulsar, or updates of rotation ephemerides, and produces an observing schedule for a given source-list and a particular date.

ETAPE extracts a block of the PEP 740R planetary ephemeris from the tape supplied by the Center for Astrophysics and writes it to a disk file on the control computer. The ephemeris tape covers many years; only about six months of data is kept on the control computer at any time.

BACKP backs up observations from the control computer disk to a 9-track tape for off-line analysis.

DTOPC transfers data from an HP1000 computer to the station PC+Sun network, where the data is analysed, and from where a second backup to tape streamer is done.

4.4 Observing Method.

The observing program, PLS77, can be run in a number of modes, specified by parameters in the run-string. These modes are:

- Standard mode, which runs a 24-hour source list; default equipment is used.
- Schedulable mode, for a single observation of Vela or PSR 1641-45; this mode is fully automated, i.e. no operator intervention is required.
- Fully interactive mode, in which alternative equipment and non-standard options (e.g. disabling of calibrations, if the noise-diode is not functioning) can be selected.

A variety of equipment checks are carried out before and during observing. These are:

- test of the memory of the pulsar timer;
- test for the presence of the station 1Hz signal;
- test that the sampling frequency is present and correct;

The above three checks are done once each time the program is run.

- signal-level check;
- time check of the HP1000 control computer;

The above two checks require operator intervention, and are only done when the program is run in standard mode (i.e. once every week or two).

- measurement of the offset between the station 1Hz signal and the HP1000 clock;

This test is done before each integration in order to monitor the stability of the HP1000 clock, which is derived from the PFS.

- Calibration of the signal level: the increased signal introduced by firing the calibrating noise diode is measured;

This check is done before and after at least one integration per source.

- Calibration of the noise diode against a standard radio astronomy calibrator.

This check is done at least once per fortnight, when the program is run in standard mode, and at intervals in between.

As many functions as possible have been progressively automated throughout the years, in order to avoid the errors associated with manual intervention. These functions include computer control of the local oscillator frequency and of the sampling frequency.

The sequence of operations carried out by the observing program (PLS77 and associated sub-programs) during an observing session is described in appendix 3.

4.5 Glitch Detection.

The two pulsars monitored for this thesis have both undergone large, sudden spin-ups ("glitches"). Since a glitch is a major perturbation of the star, observations of the stellar response are of great interest. Consequently, a major aim of this project is to observe the rotational behaviour of a pulsar immediately after a glitch. Observations during a glitch would obviously be extremely interesting. However, given the probable short duration minutes) of the event, the limited amount of observing time available for this project, and the unpredictability of the occurrence time of a glitch, such observations are unlikely to be obtained at HartRAO. In order to make maximum use of the observing time available, the "glitch detection" strategy described below was instituted in 1985.

Short observations can be "scheduled" frequently and entirely automatically, by the scheduling program SCHDL. SCHDL, written by D.C. Bramwell of HartRAO, interrupts the current observing program at specified times and schedules a pulsar observation. If no glitch occurred between this observation and the previous one, control is returned to the current observing program after the pulsar observation. If a glitch was detected, the pulsar observing program retains control of the telescope, making continuous observations until the pulsar has set. The Vela pulsar has glitched roughly every two to four years since its discovery in 1969, and is currently the best candidate for such a project. Observations are scheduled at least once every six hours while the pulsar is visible, up to once every hour as the time since the previous glitch increases above three years. Observations of PSR 1641-45 are scheduled once a day when possible. Fortunately, these two pulsars are relatively strong -

a Vela observation takes about 10min, and an observation of PSR 1641-45 around 15 mm. Much of this time is taken up in moving the telescope to and from the pulsar, as Vela observations are often made when the pulsar is low in the sky, while most other astronomical observations are done when the source is near its meridian transit.

This strategy of automatically-scheduled observing works well at HartRAO, since the allocation of telescope usage is reviewed and finalised weekly, and involves the cooperation of all observing staff. Thus, for example, the frequency of scheduled pulsar observations can be increased at short notice, should other demand on observing time allow.

The glitch detection algorithm is described in appendix 4.

The success of this strategy is shown in fig, 4-4, which shows the gap between the calculated glitch epoch and the first post-glitch observation. Frequent observations, and use of the glitch-detection method, enabled continuous observations to commence within 35min and 7min of the 1988 and 1991 Vela glitches respectively. These observations are analysed in a later chapter.

4.6 The Sample.

The sample observed for the pulsar timing project comprises twenty-nine pulsars, selected for their high flux at the available observing frequencies. Preference was given to southern pulsars, which are out of reach of the northern observatories from which most timing programs have been operated. The sample was limited by the restriction of the total observation time to twenty-four hours, the standard timeslot allocated at HartRAO. Observations of only two of these pulsars, PSR 0833-45 and PSR 1641-45, are reported in this thesis.

Table 4-4 lists the observation details (sampling resolution, filter time-constant, and length of integration), and table 4-5 lists spin-periods and other properties of the two pulsars.

4.7 Observing Strategy.

PSR 0833-45 and 1641-45 have been observed at least weekly since 1984, when the pulsar project was allocated one 24-hour observing slot per week More recently, pressure on observing time has reduced the frequency of 24-hour slots available to the project to fortnightly- However, the two pulsars reported on in this thesis have been observed daily when time allows, because of the importance attached to observing glitches. The only significant gaps in observations are: a ten-week period at the beginning of 1986, during

Figure 4-4: Time of first post-glitch Observation for eleven Vela Glitches.

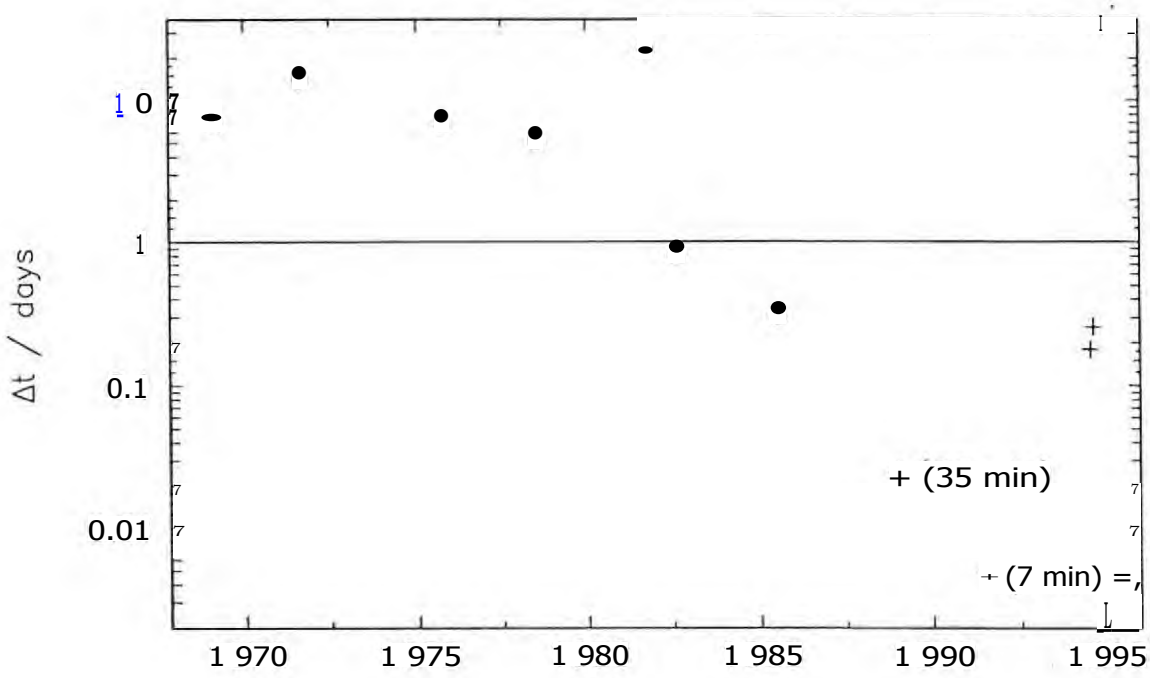

Time delay between glitch epoch and first post-glitch observation for all observed glitches in the Vela pulsar.
Glitches observed using the glitch-detection strategy are marked with
References are: 1969, 1971, 1975, 1978 and 1982 glitches: Cordes et al. (1988); 1981 glitch: McCulloch et al. (1983); 1985, 1988, 1991 and 1994 glitches: this thesis.

Table 4-4: Observation Parameters of PSR 0833-45 and 1641-45.

PSR	Ns	ATs /ZS	r /Ls	NINT	TINT min
0833-45	512	173	150	500	0.7
1641-45	2048	222	200	100 (500)	0.8 (4)

Ns is the number of samples per rotation period integrated;

AT_s is the sampling resolution;

7, is the filter time-constant;

NiNT is the number of pulse periods integrated per integration;

TINT is the corresponding integration time.

Table 4-5: Other Parameters of PSR 0833-45 and 1641-45.

PSR	Period ms	DM cm^{-3} pc	Linear polarisation	Circular polarisation
0833-45	89	68.26	88%	14%
1641-45	455	478.2	21%	4%

Polarisation values are from Manchester *et al.* (1980), and are measured at 1.6 GHz.

which time the telescope was reconfigured to prime focus and only VLBI observations could be done; and a three-week period early in 1990, when the secondary reflector was upgraded.

Each observation consists of three (1641-45) or four (0833-45) consecutive integrations of duration given in table 4-4. Each of these integrations results in an independent arrival-time estimate. A noise diode calibration is carried out at the start and end of the first of these integrations. Multiple short integrations are used for a number of reasons: any interference will hopefully affect only one out of three integrations; pulsar fluxes fluctuate appreciably on time-scales of minutes; an error estimate can be obtained empirically from the scatter of the three arrival times; and pulse-smearing due to changing velocity of the antenna relative to the source is kept to a minimum.

When observations started early in 1984, the lowest observing frequency available at HartRAO (and the only practical one for observing pulsars, which have steep spectra) was 2.3 GHz (13cm). A 1.6 GHz (18cm) receiver system was installed in 1985. A tilting secondary fitted to the telescope in 1990 resulted in a 30% improvement in antenna efficiency for this system. The observing frequency is alternated each day when practical, for observations of PSR 0833-45 and 1641-45.

The advantages of dual-frequency observing are:

- if one receiver system is unavailable, the other can be used;
- in order to combine measurements made at different frequencies, the dispersion measure (DM) for the pulsar must be known. The DM must be measured from a series of observations made at at least two frequencies. Thus if the occasional 2.3 GHz observation is to be included in an analysis of mainly 1.6 GHz observations, regular observations at both 2.3 GHz and 1.6 GHz must be made in order to keep track of the (varying) DM;
- this monitoring of DM variations is itself useful as a probe of the ISM;
- O at the high observing frequencies available at HartRAO, the timing behaviour of the pulsars is expected to be independent of observing frequency (except for small variations due to DM changes); however pulsar fluxes may be affected by their passage through the interstellar medium (ISM) on timescales that are frequency dependent. This provides another probe of the ISM. In order to separate intrinsic flux variations from those caused by the ISM, flux measurements at more than one frequency are needed.

5 Data Processing.

A pulse arrival time and flux measurement can be extracted from each integration by modeling the integration with a pulse template of unit height. This chapter describes the building of the templates, the use of this template to extract pulse arrival times from the observations, and the fitting of further parameters such as rotation rate and source position to these data. Particular attention is given to the assignment of errors.

5.1 The Data.

A typical integration is shown in fig. 5-1. Each such integration is a set of Ns equally-spaced data. Initially, $Ns = 2$, with n the largest integer satisfying the time constraint imposed by the finite sampling speed of the pulsar timer. This choice of Ns was necessary to enable cross-correlation in the frequency domain, making use of the FFT. An alternative method of arrival time extraction, not involving the FFT, was implemented in 1993; the number of samples per pulse period no longer has to satisfy the condition of integer n, and has been increased. This gives an increase in sampling rate of 1.5 for PSR 0833-45 and 2.0 for PSR 1641-45. Sampling rates for the two pulsars are given in table 4-4. The integration signal-to-noise ratio is 3 - 4 for PSR 1641-45, and 20 - 30 for PSR 0833-45.

5.2 Extracting Arrival Times and Fluxes from the Data.

Extracting a pulse arrival time and a flux measurement from these observations involves locating the pulse among the measurement noise and measuring its position and height respectively. This suggests a matched filter approach, using a filter that closely approximates the actual pulse shape. There are a number of ways of implementing this:

- Each integration can be cross-correlated with a pulse template. This is the "standard" method of extracting arrival times and fluxes (e.g. Downs & Reichley 1983). The template is an accumulation of a large number of observations. An FFT routine is generally used to transform both data and template to the frequency domain, where the correlation reduces to a simple multiplication. The result is then transformed back to the time domain, where the position of the maximum correlation coefficient is interpolated from a fourth order polynomial fitted to the largest coefficients. A parameter scaling the template to the data is easily obtained. Improved results can be obtained by filtering the template and setting the off-pulse values to zero in order to decrease the noise level.

Figure 5-1; Typical HartRAO Pulsar Integration.

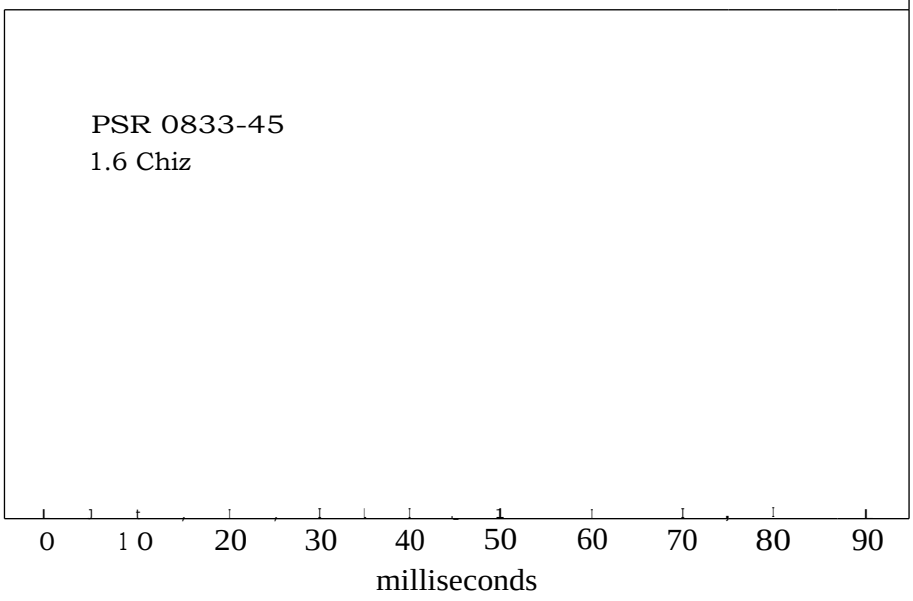

A 500-period (45second) integration of PSR 0833-45.

- Equivalently, the integration can be written as

$$d(t) = a + bp(i — t_o) + €(0, \qquad (5— 1)$$

where

p(i) is the actual pulse, approximated by the template;

t_o is the pulse position within this integration;

c(t) is a random process including receiver and other noise;

b is a scaling factor;

a is a constant offset.

The parameters a, *b* and t_o can be obtained from a least squares fit of *p(t)* to the integration *d(t)*. Taylor (1990) points out that discrete sampling of both *d(t)* and *p(t)* necessitates interpolation of the template. Since the integration is band-limited, a sinc(x) function, rather than the commonly used polynomial, should be used for this. Taylor presents simulations showing that interpolating by polynomial limits the accuracy of the measurements to about 5% of the inter-sample time. This limit is a problem only for integrations with signal-to-noise

ratio $\geq$ 50. Taylor presents an alternative implementation, in which the least squares fitting is performed in the frequency domain, where the parameter t_o becomes a linear slope in phase. Although this method is equivalent to the cross-correlation described above, the problem of interpolating is avoided and the accuracy does not seem to be limited for SNR 300.

- Alternatively, the pulse can be approximated by a continuous analytical function, such as a Gaussian. This function can then be fitted to each integration. This is the method currently used at Hartebeesthoek. It has a number of advantages:

  —using a continuous instead of a discrete function avoids the problem of interpolation;

  —fitting is done in the time domain, so the FFT is not used and there is no need to limit the number of samples to $2^?$ as is often done for pulsar timing observations;

  —additional parameters such as pulse width can easily be obtained from the data, by merely increasing the number of free parameters of the fit;

  —a more objective definition of the pulse zero phase can be used;

  —estimates of the parameter uncertainties can be obtained, as output from the standard least-squares fitting routine used.

5.3 The Pulse Templates.

Each of the above methods requires an approximation of the actual pulse shape. This is generally obtained from a pulse template, which is a high signal-to-noise ratio pulse, built up from aligning and accumulating a series of the integrations to be processed. This is done in a bootstrap fashion, as follows:

- A number N_{NICE} of integrations with high signal-to-noise ratio are selected;

- An estimate of the pulse position in each of these integrations is made by either cross-correlating the integration with a triangle of similar width to the pulse, if the cross-correlation method is used, or using a first-guess template model, if the analytical model is used;

- These pulse positions are used to re-align the *NAlicE* integrations, which are then added to each other to form an **initial template;**

- Refined estimates of the pulse position in each of the *NNI0E* integrations are obtained either by cross-correlation of the integration with the initial template, or by fitting an improved template model to the integrations;
- The refined estimates are used to line up the *NivicE* integrations, which are then added into the final template.

The resulting templates are then normalised to unit height. Two such templates are constructed for each pulsar, one for each observing frequency. The templates used for PSR 0833-45 and 1641-45 are presented in fig. 5-2.

5.4 The Template Model.

The **template model** is an analytical pulse model fitted to the final template described above. Up to thirteen free parameters are fitted, using the least squares fitting routine described in appendix 6.

The thirteen free parameters describe a baseline and up to three Gaussians. There are a number of reasons for using Gaussians: they have a simple functional form; they are physically meaningful — pulse profiles seem to consist of a number of separate, superimposed components which one would expect can be approximated by Gaussians. But the most compelling reason for using them is that they describe the pulse well: a combination of symmetric and asymmetric Gaussians provides a good fit to all the Hart **RAO** pulsars, as judged by the lack of broad features in the template-minus-model residuals.

The two types of Gaussian used to model components of the template are:

- Symmetric Gaussian:

$$F(x) = H\exp\left[\tfrac{1}{2}\left(\frac{x - 71^{\circ}}{0.}\right)^2 1\right]$$

- Asymmetric Gaussian

$$F(x) = \begin{cases} H\exp\left[\quad\quad\right] & \text{for } x < T_0 \\ H\exp\left[\tfrac{1}{2}\left(\frac{-70}{a\mathrm{RIGHT}}\right)^2 1\right] & \text{for } x > T_o \end{cases}$$

where

H is the height of the component,

T_o is the position, and

σ is the width.

Parameters of the template models used to approximate the pulse templates of PSR 1641-45 and 0833-45 are listed in table 5-1. The template models are shown overlaid on the template data in fig. 5-2.

Another reason for fitting Gaussian models is that the Gaussian components should correspond to individual components within the pulse. This enables the timing reference, or fiducial point, *TREF,* to be more sensibly defined than is usually possible. While rotational variation measurements are not affected by the incorrect choice of *TREF,* measurements of dispersion measure *(DM)* depend on a definition of *TREF* that is not dependent on observing frequency. Ideally, *TREF* should correspond to emission from the closest point to the magnetic pole. In order to determine where this point is, we need to understand how the observed pulse is related to the geometry of the emission region.

5.4.1 Pulsar Beam Shapes — Defining *TREF.*

While pulsar emission can vary remarkably from pulse to pulse (e.g. Krishnamohan 86 Downs 1983), integrated profiles, such as those observed from HartRAO, are generally very stable. This is interpreted (e.g. Smith 1991) as emission from discrete sources distributed over a circular area above the magnetic pole; each such "hot spot" corresponds to a component of the integrated profile. In an attempt to synthesize observations of the frequency-dependence of the polarisation and shape of the integrated profiles of nearly 100 pulsars, Rankin (1983) has identified two types of emission region: central (core) components and a ring of outer (cone) components; the two types of component have different emission characteristics. Variations among the pulse-shapes of individual pulsars are due to (1) different distributions of the emitting regions, and (2) variations in our orientation as observers relative to the pulsar magnetic pole. Variations in the beam shape with frequency are likely due to the lower-frequency emission being emitted at higher altitudes — for example, canal components appear to bifurcate with decreasing observing frequency. Core components, which have steeper spectra, become less prominent and develop conal "outriders" at higher frequencies.

There has been some controversy over the necessity to involve two distinct types of emission: Lyne *86* Manchester (1988) prefer a more continuous transition of emission characteristics between core and conal regions. The latter view derives from their collation (the most complete to date) of 800 integrated profile observations from over 200 pulsars. Lyne *St* Manchester classify

Table 5-1: Parameters of template models fitted to PSR 0833-45 and 1641-45.

PSR:	0833-45	0833-45	1641-45	1641-45
Frequency (GHz):	2.3	1.6	2.3	1.6
FREF (mP):	-11.63	-11.74	0.00	0.00
Q:	0.007	0.221	0.004	0.003
SNR:	219	250	62	55
Component 1:				
Left width (mP):	5.14 + 4	6.43 + 9	5.30 ± 9	6.0 + 2
Right width (mP):	9.9 + 3	10.1 + 1	9.9 + 1	8.1 + 4
Position (mP):	-(11.63 + 7)	-(11.74 + 9)	0.00 + 9	0.0 ± 2
Height:	0.994 + 8	0.94 ± 2	0.94 + 1	0.67 ± 4
Component 2:				
Width (mP):	4.5 + 2	4.7 + 4	16+2	13.2+4
Position (mP):	-F(11.6 + 1	+(11.7 + 3)	-(11 ± 2)	+(5.8 ± 4)
Height:	0.18 + 2	0.067+ 9	0.068+ 7	0.37 + 4
Component 3:				
Width (mP):	11 + 1	15.0 + 7	—	
Position (mP):	+(16 1 2)	+(8 + 2)		
Height:	0.13 + 2	0.14 1 2	—	

Flux reference points, positions and component widths are given in milliperiods.
Heights are relative to the value of the model at the flux reference point.
Component positions and flux reference points are relative to the timing reference point.
Errors are in the last digit of the result.

Figure 5-2: HartRAO Templates.

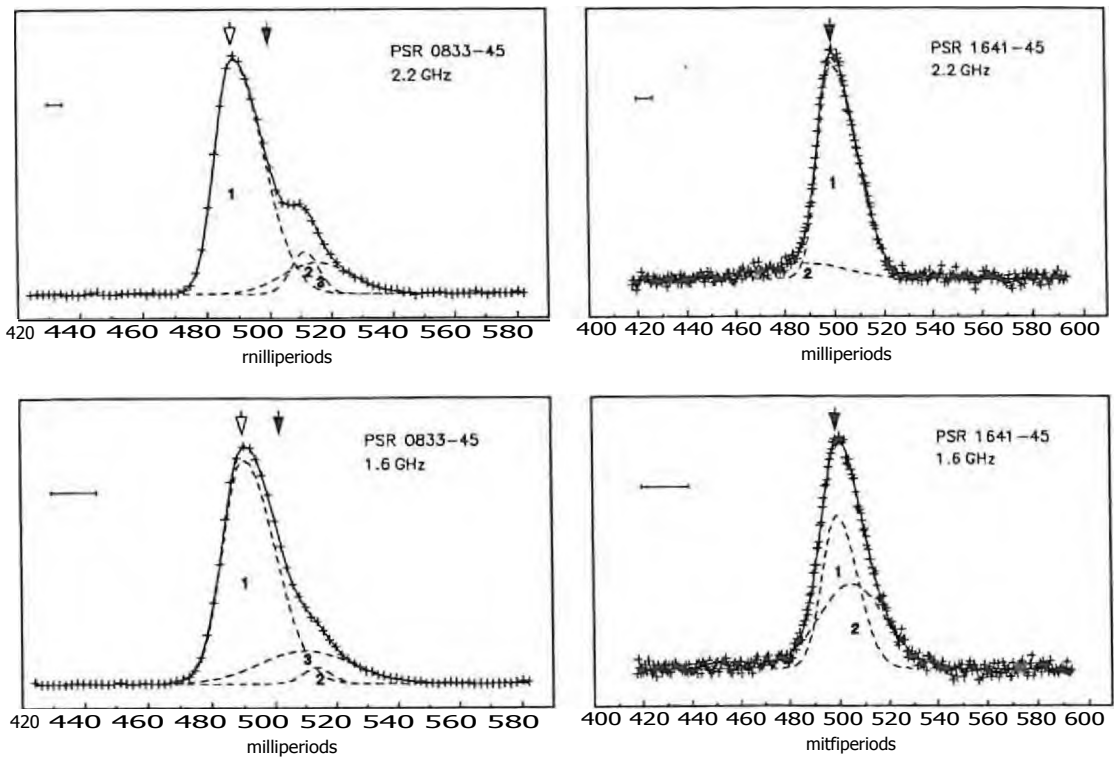

The fitted Gaussian models, described in the text, are overlaid on the templates. 2.3 GHz templates are shown in the upper panels, 1.6 GHz templates in the lower panels. For PSR 0833-45, the timing reference point *TREF* is marked with a solid arrow, and the flux reference point $_{PREF}$ with an open arrow. For PSR 1641-45, the two coincide and only $_{TREF}$ is marked. The horizontal bar in the upper left of each graph shows the amount by which the signal is smeared through the 10 MHz observing bandwidth, according to eqn. 5-3.

each pulsar according to our orientation with respect to the pulsar beam — this classification is used to determine *TREF* for the HartRAO pulsars.

It thus makes sense to choose *TREF* to be at the midpoint between the two conal components, where these are visible. Phillips (1991) has used a similar Gaussian profile model and choice of fiducial point to satisfactorily align profiles of six pulsars over a wide range of frequencies. This implies that the simplest model for pulse dispersion (the cold plasma dispersion law) is adequate, in contrast to previous reports, using measurements of the same pulsars, in which super-dispersive delays were reported at low frequencies. Phillips suggests that incorrect choice **of** fiducial point may be a contributing factor to such apparent discrepancies.

5.4.2 PSR 0833-45.

Models comprising an asymmetric main pulse, a smaller, symmetric trailing pulse and a broader trailing pulse fit both 2.3 and 1.6 GHz templates adequately. Krishnamohan & Downs (1983) have made an intensive analysis of the beam shape of this pulsar, using polarisation observations of over 87000 single pulses at 2.3 GHz. Their resulting decomposition of the pulse into four symmetric Gaussian components is very similar to the template model used at HartRAO. Components **1** and **2** of Krishnamohan & Downs are replaced by the asymmetric component **1** of HartRAO. Lyne & Manchester (1988) classify the beam of PSR 0833-45 as "cone-dominated", i.e. both sides of the conal emission are observed. The timing reference point is thus taken to be midway between the main component and the narrower (better defined) of the trailing components.

5.4.3 PSR 1641-45.

The template of PSR 1641-45 is successfully modeled with an asymmetric main pulse, and a broad underlying component that is more prominent at 1.6 GHz than at the higher frequency. Signs of a precursor at approximately the same position have been noted by Manchester *et al.* (1980).

Lyne & Manchester classify the beam of this pulsar as "partial cone emission," with emission from the leading side of the beam. If so, the timing reference point should be between the observed component and an unobserved component corresponding to the trailing side. Rankin (1993), on the other hand, classifies the main pulse as core emission. At HartRAO, timing and flux reference points are both taken to be the centre of the main pulse.

5.5 Fitting the Template Model to the Data.

The template model is fitted to the data using a standard least squares method (appendix 6). When fitting the template model to the data, as opposed to fitting the model to the template, only three free parameters are allowed: baseline, position and a scaling factor. These are the same free parameters fitted by the cross-correlation method; allowing extra parameters such as heights of individual components increases the parameter uncertainties, as would be expected when the fitting function is over-specified. In practice, the baseline is estimated from the off-pulse mean, and the remaining parameters are obtained from a fit to the on-pulse data with the baseline kept fixed. An initial pulse position within the integration is obtained by cross-correlating the central section of the template model with the integration. A refined estimate is obtained by least-squares fitting the model to a section of the data around this pulse position. The resulting arrival time is:

$$t = t_o + St + \frac{t_{int}}{2}, \qquad (5 - 2)$$

where

t_o is the start-of-integration time;

St is the offset of the pulse within the integration, obtained by the process outlined above; and

t_{int} is the total integration time.

5.6 Evaluation of the Template Model Fitting Method.

The cross-correlation method and the model-fitting method were compared by applying them to the data of three pulsars:

- PSR 0833-45 (Vela), which has a pulse duty cycle of 2.2%; the signal-to-noise ratio of the integrations is 20;
- PSR 1641-45: pulse duty cycle is 2.4%; SNR is 6;
- PSR 1054-62: pulse duty cycle is 5%; SNR is 2.

The method of fitting Gaussian models resulted in a slight (5-10%) improvement in measurement of both arrival times and fluxes, as judged from the reduction of scatter in the measurements. In addition, the Gaussian model successfully located the pulse in the one integration for which the template-correlation method failed to find a pulse.

The template-model fitting procedure was also tested on simulated observations with a wide range of signal-to-noise ratio, described in the next section, generated from a 785-sample 1.6 GHz PSR 0833-45 template (as opposed **to** from the template model). The pulse arrival times were also perturbed by a small amount (0.01 mP). These data were processed as described above; the resulting measured scatter in arrival time versus mean observation stir is shown in fig_ 5-3. The persistence of the $(snr)^{-1}$ trend over the entire range of snr investigated shows that this method is not limited by sampling effects, at least for snr 200. It also implies that the template **model is** an adequate model.

The use of Gaussian components to model pulsar observations has been described elsewhere (e.g. Foster *et al.* 1991); the above implementation was developed independently at HartRA 0.

5.7 Simulated Integrations.

Simulated observations are generated by adding random noise with a Gaussian distribution to either a template or to the model fitted to the template. As well as this measurement noise, timing noise can also be added to the arrival times of the simulations. The random noise generator used is GASDEV, of Press *et al.* (1986). Prior to generating a block of observations, GASDEV is pseudo-randomly initialised by calling it a number of times that depends on the millisecond counter of the computer clock. Even if no timing noise is added to the simulated arrival times, the position of the pulse within the simulated integration will vary among simulations, since data are generated relative to a specific pulsar ephemeris and must (like real data) commence on the second. This also applies to the offset between the pulse and the nearest sample; simple linear interpolation is used to generate the simulated data, the sampling times of which will fall between sampling times of the template.

5.8 Reduction of Arrival Times to an Inertial Reference Frame.

Before modeling the pulse arrival times, it is necessary to convert them to a dynamical timescale (TDB) and an inertial reference frame (the Solar System barycentre). This procedure **is** outlined in fig. 5-4. Basically, it comprises two stages:

- removal of local instrumental effects, resulting in a UTC site arrival time, and
- conversion of the site arrival time to a location-independent arrival time.

Figure 5-3: Results of Template-model Fitting.

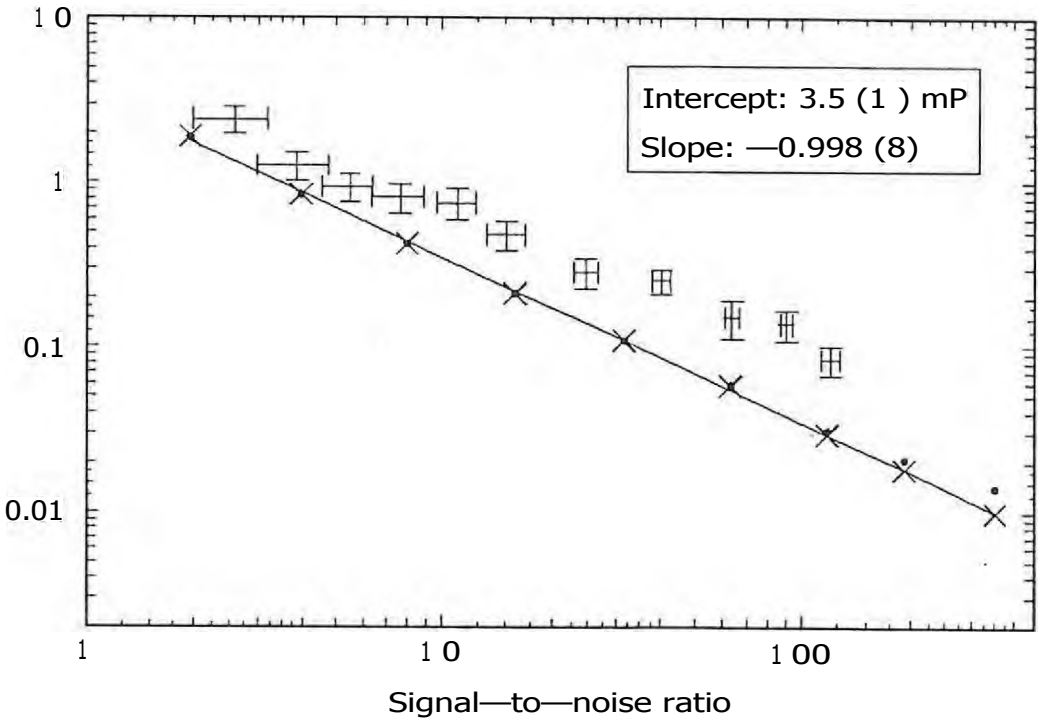

Variance of the phase-residuals extracted from simulated (x) and real (+) Vela data, for a range of integration times.
Errors for the simulated data are roughly the size of the symbols, and are not plotted. The simulations are described in the text. White noise of 0.01 mP was added to the simulated data; this has been quadratically subtracted from the variance of the data plotted with x. Small dots (•) mark data prior to this correction. The solid line is a fit to the corrected simulated data, and has a slope of —(0.998 + 0.008).
Axes are log-log plots.

Corrections involved in the first of these are described in more detail below. The second stage of the conversion is accomplished using software provided by the Smithsonian Center for Astrophysics (CfAps) (J.F. Chandler, private communication), and is documented in this software. It is also described by Backer (1989).

5.8.1 Correction for Dispersive Smear.

No pre-integration hardware correction is made for the effect of dispersive smear of the pulse through the bandwidth (10MHz) of the pre-detection filter. The amount of pulse smearing is given by Downs & Reichley (1983):

$$\text{ismear} = 8.29846 \times 10^{3} B\ DM\ f^{-3} \quad \text{seconds,} \qquad (5 - 3)$$

where

B is the observing bandwidth, in MHz;

DM is the pulsar dispersion measure, in pc czn^{-3};

f is the observing frequency, in MHz.

Calculation of this effect strictly should be done by monitoring the exact shape of the bandpass filter response. This was not done; however, no changes were made to this hardware during the project, and the corresponding correction is approximated by assuming a constant 10 MHz bandwidth throughout the project. It is implemented by subtraction of $1_{\bar{2}}\mathrm{i}_{smear}$ from the arrival times. Fig. 5-2 shows values of $_{t\ \$mear}$ for PSR 0833-45 and 1641-45.

5.8.2 Correction for incorrect Integration Period.

Downs & Reichley (1983) suggest correcting pulse arrival times for the delay caused by integrating the signal using an incorrect assumed pulse period. For the HartRAO data this correction is $(Np12)a^{2}P$, where a is the fractional error in the pulse period P. In the worst case (observations made immediately after a large glitch) this correction amounts to 2 x 10^{-9}P, some five orders of magnitude below the measurement error; it is not applied.

5.8.3 HartRAO Clock Correction.

The HartRAO clock is free-running, and is corrected approximately once every three months to track UTC. The clock offset w.r.t. UTC is obtained by time-transfer from UTC(USNO), as described in chapter 4. This offset is well-modeled by a second-order polynomial, the coefficients of which correspond to initial time and frequency offsets, and a clock aging rate. A file of these

Figure 5-4: Stages in the Correction of Data to a Dynamical Timescale and an Inertial Reference Frame

start-of-integration + pulse-position-in-integration + (integration-time) + correction for dispersive smear + (= correction for pre-detection filter smear)

HARTRAO SITE-ARRIVAL-TIME

- HartRAO clock correction 100 μs]

UTC SITE-ARRIVAL-TIME

+ leap-second correction [integer number of seconds]

TAI SITE-ARRIVAL-TIME

+ correction for gravitational redshift and time dilation effects due to the Earth **moving** in an elliptical orbit around the Sun [annual term, up to 1.6 ms]

TDB SITE-ARRIVAL-TIME

+correction for light-travel time [annual term, up to 8 minutes]

TDB ARRIVAL-TIME AT SOLAR SYSTEM BARYCENTRE

+ relativistic delay H 40 μs]
+ delay due to interstellar and interplanetary dispersion t< 1 second]

TDB BARYCENTRIC ARRIVAL TIME AT INFINITE OBSERVING FREQUENCY

Approximate values of the corrections are given in square brackets.

coefficients, together with the epochs of the station clock adjustments, is maintained on the HartRAO computer system. The correction from station time to UTC is thus simply a matter of accessing the correct set of coefficients, and evaluating the polynomial. This is done by the program TCRCT.

Correction of some of the early data by +1 second is also necessary, due to incorrect clock setting of the observing computer. Only a very small amount of data needs this correction, which is also done by TCRCT.

5.9 Modeling Pulse Arrival Times.

The timing behaviour of a pulsar is modeled with a rotational ephemeris:

$$0(0 = o + v_o(t - t_o) + \qquad -t_o)^2 \qquad -t_0)^3. \qquad (5-4)$$

In the above, $0(t)$ is the rotational phase of the pulsar, and v_o the rotational frequency. The parameters 00, vo, //0 and t_0 are adjusted using a standard weighted least squares fitting routine'. In practice, 0_0 is calculated and then the ephemeris epoch, t_o, is adjusted to reset 0_0 to zero, i.e., t_o corresponds to the fiducial point of a pulse. For short enough data spans, a second-order model $(0_0,$ $ii_o)$ suffices.

Eqn. 5-4 may also include terms describing a source position offset, dispersion measure (DM), and a glitch recovery. Modeling of each of these terms is described later.

Since HartRAO observations are made at two frequencies, **they are usually** combined by including the DM term in models.

5.10 Fitting a Position Correction.

Since pulsar signals are so accurately time-tagged by their narrow pulses, and are reduced from the telescope site to the Solar System barycentre at an early stage of the processing, a slight error in source position introduces an annually varying term into the arrival times. Proper motion causes the amplitude of this term to change over the years. Conversely, source positions and proper motions can theoretically be obtained from the arrival time data by modeling this term, although timing noise affects the accuracy of results, especially the proper motion measurements.

A position correction is fitted to the HartRAO data at an early stage of the processing; the catalogue position is used for the initial reduction of the data

'*See* appendix 6

to the Solar System barycentre. All site arrival times are then re-reduced to arrival times at the Solar System barycentre using the corrected position. Position is not included as a parameter in models subsequently fitted.

The position offset, and proper motion, is fitted to the phase residuals as follows. Taking the Solar System barycentre as the origin, let:

RE {x) zi
be the position of the Earth;

flp = [cos a cos 6, sin a cos 8, sin S1
be a vector of unit length, towards the assumed source position, used for initial reduction of the arrival-time data to the Solar System barycentre;

Pdetta be the proper motion in right ascension and declination, respectively;

t_o be the source position epoch;

= [cos(a + *Aa* + p_{ω}*(t* — t_o) cos(O + AS + */Is@ − t_o),
sin(a + Aa + it_{ω}*(1* — t_o) cos(6 + L5 + it_{5}(t — t_o),
siri(8 + AS+ p_{ω}*s(i* — t_o)]
be the direction towards the true source position.

The annually varying component of the pulsar signal time-delay is then

$$= -\frac{1}{c} \vec{RE} \cdot \vec{Rp}, \qquad (5 — 5)$$

and the excess phase residual caused by an incorrect assumed position is

$$= vAt = \quad \cdot \quad — \qquad (5 — 6)$$

For a typical pulsar, observed with an accuracy of 0.2ms, timing positions can be measured to an accuracy of 0.1 arcseconds (Lyne & Graham-Smith, 1990) The final positions used for all data reduction of the two pulsars are given in table 5-2_

5.10.1 PSR 0833-45.

The position used for PSR 0833-45 is the optical position of Manchester *et al.* (1978a), since rotation variations in this pulsar completely swamp any sign of an incorrect position in the arrival times. Comparison of recent VLA position measurements with the optical position yields a proper motion not significantly different from zero (Fomalont *et al.* 1992). A comparison of optical observations, yielding a similarly small proper motion, has led to the

Table 5-2: Pulsar Positions used to reduce Arrival Times to the Solar System Barycentre.

PSR	RA	dec	source
0833-45	$08^h33'39,s312$	—45°00'10."296	1
1641-45	16h41m10.^{5}288 + 1	—45°33'38."61 + 2	2

Sources are:

1: Manchester *et al.* (1978a);

2: fit to HartRAO data from 1984.0 to 1986.0. Errors are 3-u errors in the least significant digit.

questioning of the assumed association of this pulsar with the Vela supernova remnant (Bignami &E Caraveo 1988). The optical position of Manchester *et at.* (1978a) is traditionally used to reduce observations of this pulsar, and is used here.

5.10.2 PSR 1641-45.

The position used for PSR. 1641-45 is obtained from a fit to the two years of HartRAO data prior to the large glitch of 1986. Timing noise during this interval appears to be low (or to mimic a positional offset); following the glitch, there are no other similarly "quiet" lengths of data. Proper motion is expected to be negligible, since the pulsar is so distant ($D > 3.9$ kpc, Frail Weisberg 1990); it is assumed to be zero. The position thus obtained is compared with other measurements in fig. 5-5. ft is very close to the only other timing measurement made from a comparable length of data. The discrepancy with the VLA position is not unusually large, compared with other such comparisons listed by Fomalont *et* a/. (1984).

Figure 5-5: Position Measurements of PSR 1641-45.

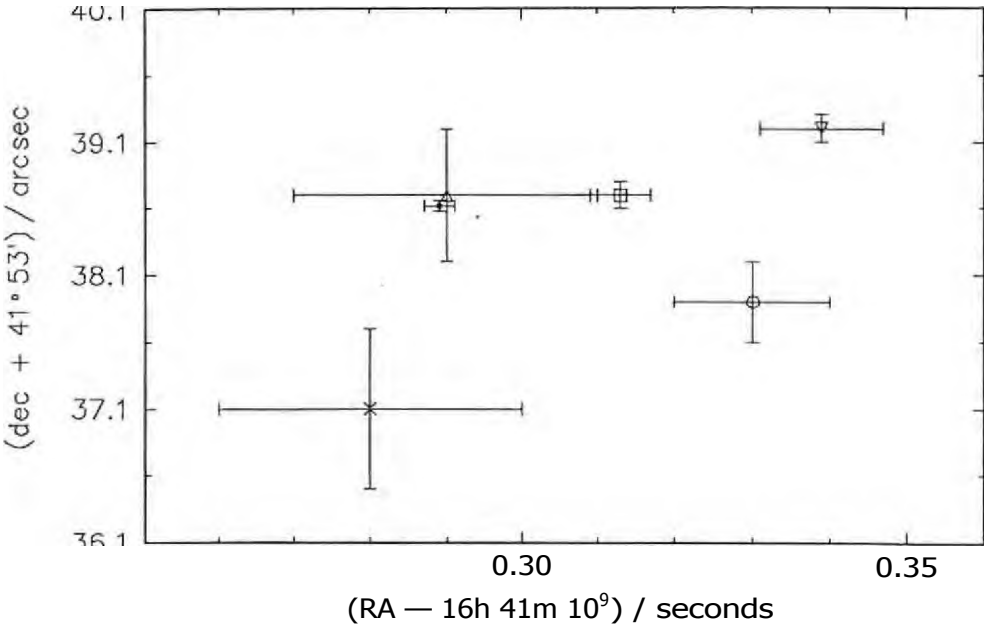

All positions plotted are in the standard reference frame used for pulsars: FK4, with e-terms of aberration removed. References for the positions plotted are given below.

Symbol	Range fitted	Reference
O	June 1975 — Apr 1976	Manchester *et al.* (1976)
CI	June 1975 — July 1977	Manchester *et al.* (1978)
A	June 1975 — July 1977	Manchester *et al.* (1983)
V	Aug 1981 — Oct 1982	Downs & Krause-Polstorff (1986)
	VLA	Fomalont *et al.* (1984)
•	Jan 1984 — Jan 1986	this thesis

5.11 Modeling Dispersion Measure.

The dispersion measure *(DM)* of a pulsar is the integral over the distance *1* to the pulsar of the local electron number density m_e:

$$DM = f\, n_e dl \qquad \text{pc cm}^{-3}. \qquad (5\text{-}7)$$

The delay caused by dispersion is

$$= 4.15 \times 10^3\, DM\, \mathbf{f} \qquad \text{seconds,} \qquad (5\text{-}8)$$

where f_{ob}, is the observing frequency, in MHz.

The delay given in eqn. 5-8 is removed during the reduction of the pulse arrival times to the Solar System barycentre. To avoid confusion, a constant value of *DM* is used for all such reductions. *DM* varies with time — these *DM* offsets are dealt with by including them as terms of the ephemerides fitted to various epochs of the data. This is in contrast to the procedure for dealing with (presumably constant) positions and proper motions, which at HartRAO are applied as corrections to the catalogue values, after which the new position terms are used to re-reduce the arrival times to the Solar System barycentre and no further position or proper motion fitting is done.

DM corrections are obtained by including a term

$$= 4.15 \times 10^3\, ADM\, f_{obs}^{-2}\, v \qquad (5\text{-}9)$$

in the model fitted to the phase residuals.

5.12 Editing of Data.

Data that lie more than - 5u from the model of eqn. 5-4 are deleted. Since the quantity of data is so large, no attempt was made to correct such "bad" data. The fraction of data edited out is very small — < 1% for Vela and < 2% for 1641-45. The most common reasons for data being flagged bad are: incorrect equipment settings (such as feed offset); observations made at extremely low elevation; and use of non-standard equipment configuration for test purposes.

5.13 Reduction of the Data to Averaged Arrival Times.

Each observation consists of three integrations (four for Vela observations), each of which yields an independent arrival time. The three (or four) arrival times of each observation are usually combined by averaging the phase residuals to the model of eqn. 5-4 and converting the result back to an arrival

time. This considerably reduces the time needed to access the data for further processing. The average phase residual is the unweighted mean residual; data at different observing wavebands are not included in the same average. Error assignment is described in the following section.

5.14 Errors in Arrival Times.

Evaluation of the parameter uncertainties and appropriateness of models fitted to the arrival times requires correct assignment of errors to the fitted data. Some methods of calculating errors of the averaged arrival times are listed in table 5-3 and discussed below; they are evaluated by counting how many data lie within lei, ±2ei and ±3e_i of a fitted model, where e_i refers to the error assigned to an individual point, and the length of data fitted is short enough that the model is adequate. The data used is described in the table caption.

The **formal error** returned by the routine that fits the template to the observations seriously underestimates the level of noise in the real data, but appears to be a good measure of the error of the simulated data. This implies that an additional source of noise other than flux noise contributes to the short-term scatter of the real data. This is not unexpected, and is due to effects such as interstellar scintillation, which causes the pulse strength to fluctuate within the integration time and bandwidth, and pulse-to-pulse "jitter" intrinsic to the pulsar (Cordes & Downs 1985). The amount of this short-term excess phase noise varies from pulsar to pulsar (ibid.); for the Vela pulsar, Downs *Sr,* Krause-Polstorff (1986) observe the same level of short term scatter using antennae that differ in aperture by a factor of 6.

For the purposes of model-fitting, a true estimate of pulse phase error must thus be made either by modeling these effects, as attempted by Cordes Downs (1985), or by directly measuring the scatter in the arrival times. For this project, the latter route was followed. Ideally, the error e_i assigned to each averaged arrival time should be obtained from the scatter of the data from which the average is obtained (i.e. from the internal scatter). The obvious estimator is the **standard error of the mean** ($\sigma/\sqrt{n}$, where n is the number of data per average). This appears to be a good estimate for most of the data: < e > rms scatter of the data, and 70% of the data lie within +le of the model. However, even when corrected for small-number statistics using the Student's-t distribution, this measure underestimates the number of outliers (see table 5-3). This is a serious problem — the least squares fitting routine used to fit models to the data is severely affected by incorrectly weighted outliers.

This is an unavoidable problem caused by the small number of data available

Table 5-3: Evaluation of methods of assigning errors to averaged data.

Errors assigned	No. of data per average (n)	±1e	±2e	±3e
SIMULATED DATA:				
formal error:	1	67.4%	947%	99.3%
RANDOM NOISE:				
std error in mean:	4	72.4%	90.2%	96.5%
std error in mean:	15	68.7%	94.7%	99.3%
Cbmaz cbmin, krrt:	4	86.7%	96.6%	98.4%
.(1/n(n 0E05- < ci)	4	90.0%	97.3%	99.2%
local scatter:	4	72.3%	96.1%	99.6%
REAL DATA:				
formal error:	1	35.2%	63.3%	82.4%
std error in mean:	4	68.1%	89.3%	96.6%
local scatter:	1	66.9%	95.2%	99.8%
local scatter:	4	69.1%	93.5%	99.4%
local scatter:	17	73.3%	95.0%	99.5%
GAUSSIAN DISTRIBUTION:		68.3%	95.4%	99.7%

Percentages given in the last three columns are the fraction of data points falling within one, two or three error bars of the model.

REAL DATA are 3444 data points collected on MJD 48462 - 48465 soon after the 1991 glitch. These data were chosen because they are approximately evenly spaced over the three days.

RANDOM NOISE is phase residuals generated from a Gaussian distribution with standard deviation equal to the rms of the above data, and at the same sampling times as the above data.

SIMULATED DATA are simulated observations generated from a 1.6 GHz PSR 0833-45 pulse template;

GAUSSIAN DISTRIBUTION refers to the expected results.

Methods of error calculation listed are described in the text.

(n = three or four). Averages of randomly generated phase residuals with varying n implies that n should be 25 in order to obtain a reliable measure of the internal scatter. Short term noise in the real data does appear to be randomly distributed: a cumulative distribution plot of the 3444 1.6 Gliz PSR 0833-45 data used in these tests is indistinguishable from a similar plot of randomly generated noise, and averaging successively longer spans of data results in the expected $n^{1}/^{2}$ dependence of the rms scatter. Also, similar four-data averages of random noise had the same problem. Using a more robust estimator of the scatter, such as a higher moment or a measure of the range, resulted in fewer outliers, but overestimated the error for the bulk of the data.

Since for most of the data it does not seem possible to estimate errors from internal scatter, a measure of the local scatter was used. Error estimates are obtained as follows:

- The two-sample variance $.\$_2$ is used as an estimator of the local scatter.

$$\text{³}\hat{2} = t \quad \frac{1}{2(m - 1)} \text{E(Oi -} \qquad (5 - 10)$$

  where m is the number of pairs averaged, and t_{m-2} is the 15% Student's-t correction for in - 1 degrees of freedom.

  This is a more practical estimator than the standard variance, since it is insensitive to low-order phase drifts (Aq5/At 30 mPid), as long as pairs separated by more than 12h are not included in the calculation.

- The unaveraged data are divided into successive blocks of length AT, so that each block includes 25 - 30 pairs of data satisfying the above requirement. For PSR 0833-45, AT varies from 25 min straight after a glitch to 1 week for the bulk of the data. For PSR 1641-45 AT is generally 30d.

- Each arrival time is assigned an error equal to the two-sample variance of the block within which it falls.

- The error assigned to each averaged arrival time is then the rms of the individual two-sample variances.

As shown in table 5-3, this appears to be a satisfactory estimate. This method unfortunately results in the data errors not being independent; this is partially alleviated by fitting models to lengths of data that are generally > AT.

5.15 The Effect of Changes in the Hardware.

Some types of hardware changes, for instance changes in receiver polarisation, are expected to affect the pulse-shape and hence the measured arrival times. This suspicion was confirmed by including a fourth parameter, the total width of the main pulse, in the fit of the template model to the data. The resulting plots of the evolution of pulse width with time are generally flat, with clear jumps corresponding to changes in receiver polarisation, installation of filters, change in local oscillator frequency, and the installation of the prime-focus S/X-band feed used for Mark III VLBI experiments. Plots of dispersion measure are also a useful tool for locating jumps in pulse phase. The effects of such equipment changes on the arrival time measurements could possibly be removed by analysing each inter-event length of data with a template model constructed from that data. This was not attempted. Instead, either (a) no models of rotational phase were fitted across the discontinuities, or (b) an offset in phase for the post- or pre-discontinuity data was included as an extra free parameter. Since the discontinuities cause steps in pulse phase (0), they will not affect measurements of v and higher derivatives of 0, or modeling of these parameters. The dates of the discontinuities are listed in table 5-4.

In addition to the jumps mentioned above, long-term trends of much smaller amplitude are visible in the pulse-width measurements. These are possibly due to refraction in the interstellar medium or intrinsic changes in the pulsar; such observations fall outside the scope of this thesis and are not discussed further. They are assumed to have a negligible effect on measurements of v.

5.16 Model fitting using Randomisation.

At each stage of the modeling — extraction of *v(t)* and *ii(i)* from *0(t),* and subsequent modeling of glitch response in *ii(t)* — a randomisation method is used for determination of the uncertainties in the model parameters. This is done as follows:

- One fit is made to the original data yi, using the original errors c„ resulting in a model *f (xi).* X^2 is obtained from this fit.
- If the perturbed data (V) is to be generated from the model, the errors (from which the size of the perturbation is obtained) are adjusted:

$$\mathbf{e_i} = \max(ei,1\ Yi \quad /(xi)\ 1)- \qquad (5 — 11)$$

✓ The fit is repeated ***NR*** = 200 times. Before each fit, a new data set is generated either from the original data set:

Table 5-4: Epochs of Equipment Changes causing Data Discontinuities.

Date (MJD)	Frequency	Cause
46287	2.3 GHz	polarisation change
46335	2.3 GHz	installation of 200 MHz bandpass filter
46480	2.3 GHz	polarisation change
46803 — 46882	2.3 GHz	SIX feed in use
47145 — 47188	2.3 GHz	SIX feed in use
47249 — 47254	2.3 GHz	??
47560 — 47565	2.3 GHz	??
47636	2.3 GHz	polarisation change
47664	2.3 GHz	??
[49148 .. 49159]	2.3 GHz	lo frequency changed
47190	1.6 GHz	??
47265	1.6 GHz	polarisation change
48355— 48360	1.6 GHz	polarisation change
48395 — 48405	1.6 GHz	polarisation change
48435 — 48440	1.6 GHz	polarisation change
48555	1.6 GHz	extra filters installed
		81 change in lo frequency
48700	1.6 GHz	??
[49301.3 .. 49305.3]	1.6GHz	??
[49307.3 .. 49308.9]	1.6 GHz	??
49582.3— 49590	1.6 GHz	polarisation change
49602 — 49607.3	1.6 GHz	polarisation change

Epochs are those of discontinuities in measured pulse-width. The probable causes are also listed. "Unknown" causes are probably polarisation changes that were not logged in the station log-book.

(5 — 12)

or from the model fitted in the first step:

$$f(xi) + 7e2, \qquad (5 — 13)$$

and the errors are adjusted:

$$ei == \qquad (5 — 14)$$

in the above, -y is a random number drawn from a Gaussian distribution with zero mean and unit variance. Prior to the randomisation, the random number generator is pseudo-randomly initialised by calling it times, where N_{init} is generated from the millisecond counter of the computer clock.

The errors are multiplied by „r2 since the perturbation introduces an additional source of error in the data. This error correction would only be necessary if the formal errors in the fitted parameters were used; goodness of fit measures (x^2, *Q)* are calculated using the original data and errors.

Ideally, the perturbed data should be generated from the best approximation of the underlying model, When fitting short lengths of phase residuals (e.g. to obtain *v(t), V(t)),* the length of data fitted is chosen such that the model is a good representation of the data. Tests show that it makes no difference whether the perturbed data is generated from data or model; it is computationally simpler to generate it from the data. Long spans of *v(t)* or V(i) data of both pulsars analysed here are affected by random timing noise, which cannot be modeled by a simple glitch-decay model. When fitting such models, the fitted model is usually used as a base for generating the perturbed data, and the size of the perturbation is increased (eqn. 5-11) in an attempt to include the effect of the timing noise on the model parameters.

- For each model parameter, the *NR* measured values are binned and fitted with a Gaussian distribution. The parameter value and its error are then the mean and standard deviation respectively of the fitted distribution.

Although parameter uncertainties are generally estimated by this method, care is taken to propagate good estimates of the data errors through each stage of the data reduction, since

s the size of the perturbations used in the randomisation depends on the error assigned to each individual data point; and

- the goodness-of-fit parameters, x^2 and Q, depend on the data errors.

5.17 Extraction of v(t), fi(t), **and** Dispersion Measure *(DM).*

Much insight into the pulsar rotational behaviour can be obtained by examining the evolution of the parameters v and z with time. hi particular, the response of the pulsar to a glitch is best investigated by looking at *i(t),* as described in chapter 9. The procedure for obtaining these time series *(v(t), zi(t))* is outlined below. The *DM(t)* data are a product of this analysis, but are not useful for studies of timing behaviour, and are not discussed further in this thesis. Demiariski & Pr6szyriski (1983) point out some of the advantages of using this approach, rather than fitting a single model to phase residuals: sudden changes in ri and V are more evident, and the contribution of timing noise to the parameter errors can be estimated directly from the scatter in *v* and V.

Series of v(i) and *140* are obtained by fitting eqn. 5-4 to short segments of the data, using the least-squares routine described in appendix 6. The segmenting of the data is a compromise between short lengths, which yield better time resolution, and longer lengths, which yield more accurate values of *v(t)* and V(t). Adequate time resolution is particularly important immediately following a glitch, where recovery timescales can be < 1 day. The uncertainties in *v(t)* and i/(t) should preferably be similar throughout the entire length of data analysed, as these are used as weighting factors in later stages of model fitting. The procedure is:

- Phase residuals plots are examined for discontinuities indicating sudden real changes in v(t) or *zi(t).* Epochs of discontinuities are noted; these should occur at segment edges only. An example of such a discontinuity in phase is shown in fig. 5-6a. The segments are also selected so that discontinuities caused by equipment changes listed in table 5-4 fall on segment boundaries; alternatively, an offset AO in the data on one side of the discontinuity is included as an extra free parameter.

- An initial segmentation and fitting of the data is done. Each fit is initially for a second-order polynomial plus *DM;* the polynomial order is then incremented to three if necessary. The criterion for rejection of the lower order fit is (Bevington 1969) F_x $Ax^2/(x^2/dof) > F_5$, where Ax^2 is the improvement in x^2 obtained by increasing the number of model parameters, the denominator refers to the higher-order fit, and

Figure 5-6: Examples of Phase Residuals indicating an Inadequate Rotation Model.

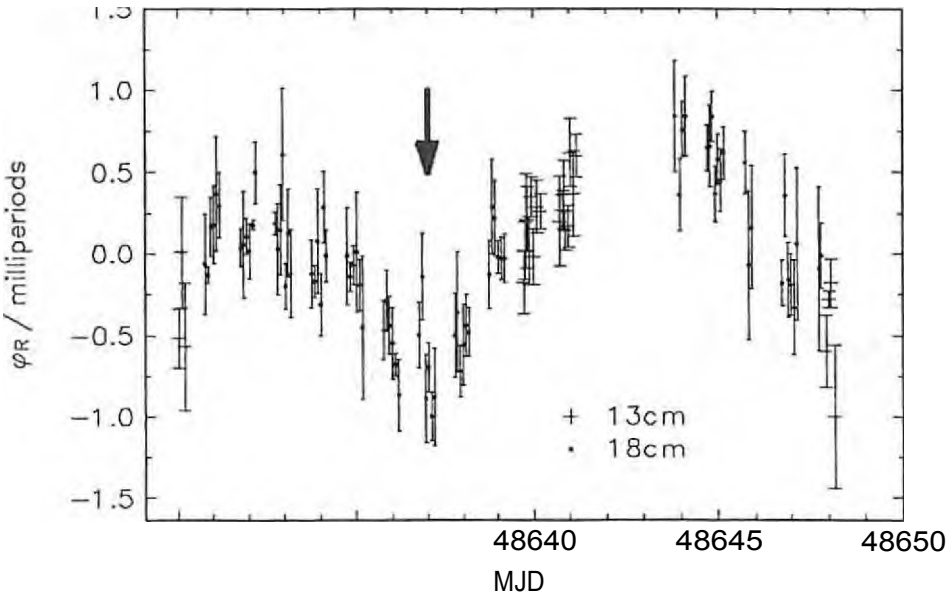

5-6a. Phase residuals for a 20 day length of Vela data which includes a sharp change due to a small change in frequency of size $\Delta\nu/\nu \sim 10^{-9}$ (arrowed). Segmenting will be adjusted so as not to include the epoch of this event within a segment.

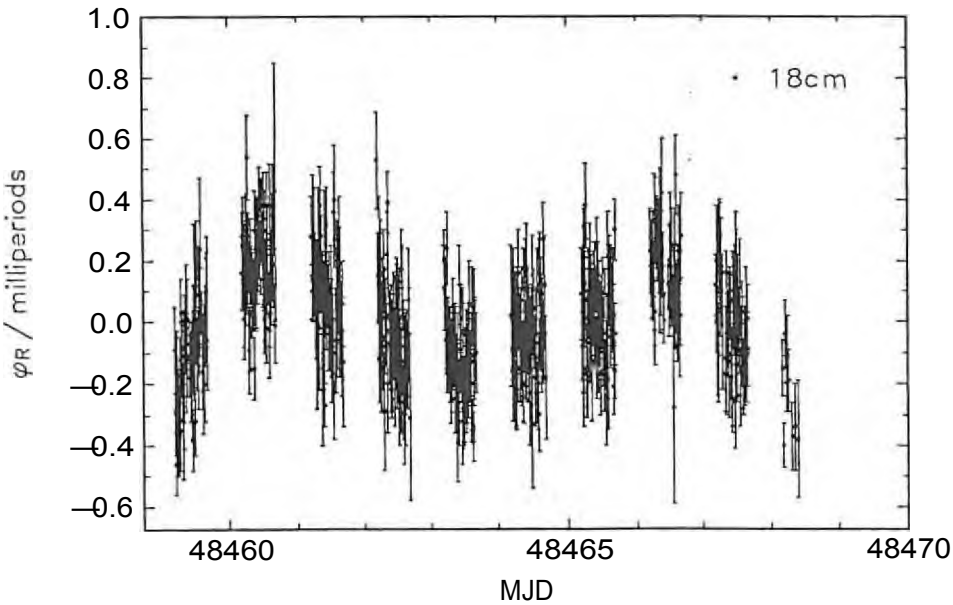

5-6b. A 10 day length of phase residual data showing structure due to timing noise. The segment length will be decreased so as to include the timing noise in the $\nu(t)$ and $\dot{\nu}(t)$ series.

F_5 is the 5%-ordinate of the F-distribution with one and *dof* degrees of freedom. The epoch of each fit is the unweighted mean time ordinate. This step is automated: because of the amount of data involved, it is tedious and hence susceptible to human error.

- The resulting *u(t)* or *ii(t)* are examined to ensure they satisfy the requirements of sufficient time resolution, small error values, and reasonably similar error values. Fits with low Q ($Q < 0.001$) are examined manually to determine the reason for the bad fit. This is usually either an outlier or structure in the residuals indicating an inadequate model. If the latter is the cause, the segment length is decreased.

  The previous step is repeated until these requirements are satisfied.

- When the final choice of segmentation has been made, a final pass is done in which the data are randomly perturbed and the fit repeated 200 times, as described in section 5.16, in order to estimate uncertainties in v(t) and il(t).

Table 5-5 summarises the *v(t)* and z>(t) series obtained in this way. Since the segments of arrival time data from which these series were produced do not overlap, these data are independent and thus suitable for statistical tests of the models.

5.18 Glitch Epochs.

The glitch epoch is obtained by fitting lengths of pre- and post-glitch data with the rotation ephemeris (eqn. 5-4), and extrapolating the two ephemerides to the point where they meet. An error estimate is obtained by repeating this process with a variety of lengths of data. The post-glitch data length is relatively short, since large transients following the glitch cannot be modeled with eqn. 5-4. Since continuous observations were made after most of the large glitches, this is generally not a problem.

An accurate glitch epoch can be obtained only if the gap in observations at the time of the glitch is short enough that there is no ambiguity in the pulse-numbering. For example, a typical Vela glitch has magnitude Aviv $1O^{-6}$. Since the spin period of Vela is --, 89ms, the post-glitch drift relative to a model fitted to the pre-glitch data is approximately one full rotation period per day. For a similar size of glitch in PSR 1641-45, the drift rate is one spin-period per 5.2 days. Observations must thus be made more frequently than this in order to determine the glitch epoch. This is why early reports of Vela glitches had epoch uncertainties of up to two weeks (the inter-observation gap).

Table 5-5: Time-series *v(t),*

PSR	Fit for	Block length
0833-45	v	8-11d
0833-45*	v	id
0833-45	zi	12-15d
0833-45*	V	2d
1641-45	ii	40-50d
1641-45		85-100d

*: Immediately following the large glitches, for periods when continuous observations are available, shorter segments are fitted. The first post-glitch value of is obtained from the first day of data following the glitch.

Figure 5-7: Obtaining the Glitch Epoch from Phase Residuals.

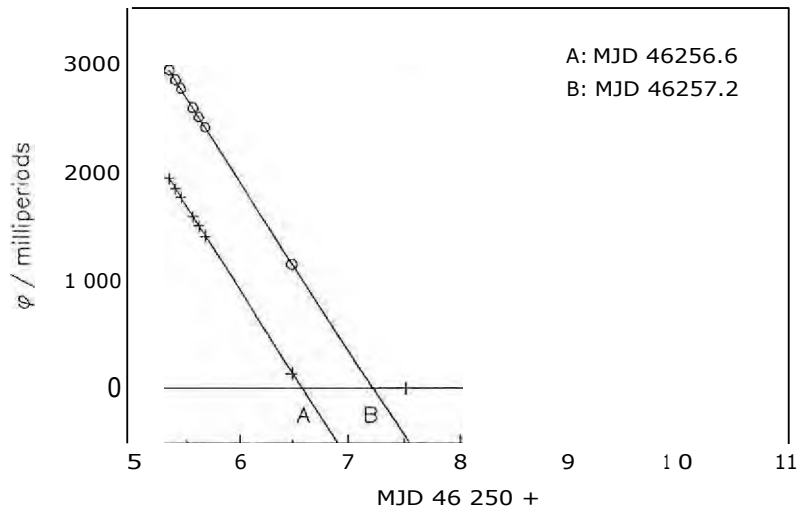

Phase residuals to a model fitted to four days of data following the 1985 glitch of the Vela pulsar (marked with +). The glitch epoch, and its uncertainty, is determined from a straight line fitted to the pre-glitch data. The gap in the data between KID 46256.5 and 46257.5 introduces an ambiguity in the glitch epoch, shown in the figure: the pre-glitch data could correspond to the points marked with crosses (+), or those marked with open circles (0) and separated by 1000milliperiods (one full rotation period). This yields two possible glitch epochs, marked A and B. Comparison with data recorded at Hobart, Tasmania, resolves the ambiguity: the true glitch epoch is that marked B.
Error bars fall within the symbols and are not plotted.

5.19 Safety Precautions.

Approximately 100 000 integrations of PSR 0833-45 and 10 000 integrations of PSR 1641-45 have been recorded and analysed so far. It is not feasible, nor necessary, to process this amount of data manually. However, the data reduction process listed in fig. 5-4 and in subsequent sections has potential for introducing errors that mimic the effects under study. For instance, if different parts of the data are reduced using different position corrections, an annual variation in v(t) which may be mistaken for timing noise will be introduced into sections of the data.

To avoid this and other types of error, an "audit trail" of the data is kept: each of the 110 000 data is tagged with information such as assumed source position and *DM,* and UTC-HartRAO clock correction. At each of the later stages of the analysis, checks are made that consistent values of the relevant parameters were used for reduction to the inertial reference frame, and that all necessary corrections were actually made.

Analysis is automated as far as feasible. Default values of parameters such as time range to process are offered to avoid errors. The process of fitting consecutive blocks of data, to obtain v(t) and *i/(t),* is entirely automated, as the routine of calculating phase residuals, locating the mean time ordinate, shifting the ephemeris epoch, recalculating residuals, fitting, adjusting the ephemeris, recalculating phase residuals, and repeating the procedure with a higher-order model is complicated, time-consuming, and boring. To guard against errors introduced by this automation, additional checks are built in. For instance, the combination of an unsuitable ephemeris and a gap in the data can result in a phase jump of ±1 rotation period, which will affect the fit. The high rms residual of such a fit halts the fitting procedure; manual intervention is required to continue. A minimum acceptable number of data points per fit is specified; again, the fitting procedure halts if this condition is not satisfied.

6 Glitches in PSR 0833-45 and 1641-45.

During the 11 years duration of the pulsar project, six large and two small glitches were observed in the two pulsars discussed here. In this chapter, observations of these glitches and of the post-glitch behaviour are presented.

Four of the large glitches, all of them in the Vela pulsar, occurred after the implementation of the "glitch detection" system described in section 4.5. The recovery of the pulsar was monitored continuously for 10d following each of these events, for the twelve hours per day that the pulsar is visible. The first day of observational coverage for each of these glitches is shown in fig. 6-1:

Figure 64: Observations of large Vela Glitches with the Glitch Detection System.

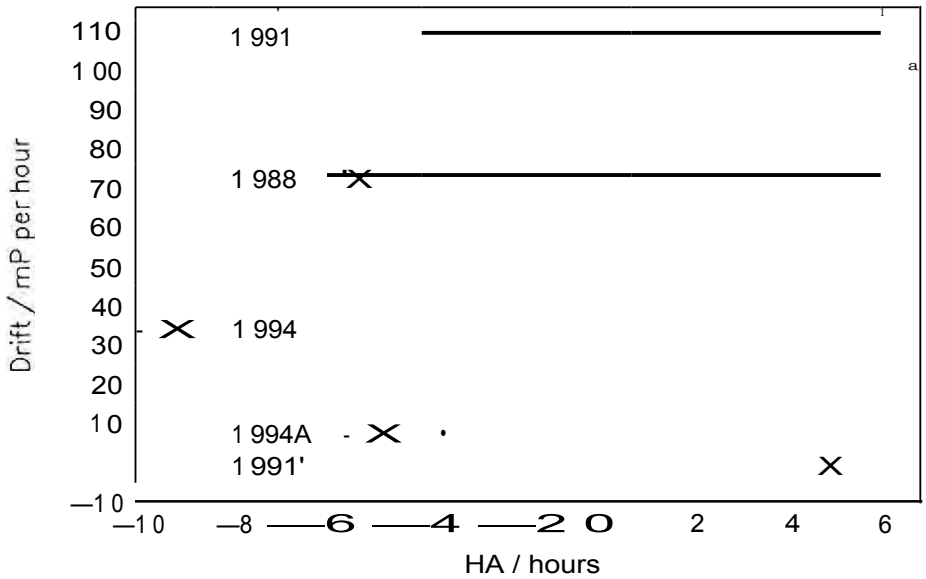

Extent of observations made on the first post-glitch day. Each dot marks an average of a number of observations; longer averaging times were used in 1994. "x" marks the glitch epoch. Ideally, observations should start immediately after the glitch and continue for as long as possible. The vertical scale shows the size of the glitch, as rate of phase-drift introduced by the spin-up. The glitch detection system is set to trigger on an accumulated drift of 10 mP since the most recent observation — for the smaller glitch of 1994A, continuous observations were initiated only after a h gap between observations.
The observing limits of the telescope are HA -6 h to +6 h,

Glitch Notation: Throughout this thesis, large glitches are referred to by the year in which they occur. When a glitch is not the first to occur in a particular year, a letter is appended to the year (e.g. 1994A). Smaller glitches are denoted by a prime (e.g, 1991').

6.1 Glitch Parameters.

The most obvious and easily measured event parameters are the epoch and size *(Aviv,* Ai/iii) of the spin-up; these are listed in table 6-1.

6.1.1 Glitch Epochs.

The method of determining glitch epochs is described in section 5.18.

PSR 0833-45 [1985, 1988, 1991, 1994, 1994.4 Three of these large glitches occurred between observations spaced 1h apart (fig. 6-1). The 1994 glitch occurred while the pulsar was below the horizon, but was small enough that no epoch ambiguity resulted. Fig. 5-7 shows phase-residuals for PSR 0833-45 at the time of the 1985 glitch. The ambiguity in the epoch caused by the gap in the HartRAO observations was resolved by including Hobart data, as explained in the figure caption.

PSR 1641-45 [1986]: Unfortunately, the gap at the time of this event was ten weeks; since the magnitude of -Iv was large enough to introduce an extra rotation each seven days, the glitch could have occurred any time during the ten week gap.

PSR 0833-45 [19911 PSR 1641-45 [1989]: Although there were no large gaps in the data at the time of these events, the errors in determining the epochs are relatively large because of the smaller sizes of the spin-ups.

Error in epoch determination due to missing transients: It appears from fig. 6-6 that short, large-amplitude transients occur after glitches and are only resolved in the most recent and better sampled events. How does this affect the epoch determination? Data following the 1991 glitch was sampled at approximately the same resolution as that following the 1985 glitch; the epoch determined from this edited data differed from that determined from the full data set by less than one minute (approximately the size of the formal error obtained for the 1985 glitch). Although the missed transient in *b(t)* is large, its amplitude in *O(t)* is only 20 rriP.

6.1.2 Glitch Sizes.

The magnitude of the spin-up *(Aviv,* is determined by fitting the standard spin-down model of eqn. 5-4 to short lengths of phase residuals immediately before and after the event, and extrapolating these models to the event epoch. The glitch magnitude is simply the difference between the post- and pre-glitch values of the rotation parameters. Choosing the lengths of data to model is not a simple matter: values of v and V obtained from a range of lengths of data exhibit a scatter that is (for the longer lengths) not reflected in the error estimates. This is presumably due to timing noise (i.e. the fitted spin-down model is inadequate). The following si,rategy was thus adopted:

- Where continuous data is available following a glitch (the most recent four large Vela glitches), post-glitch models were fitted to one or two days of data. Because of the rapid post-glitch recovery, longer spans of data cannot be adequately modeled with the simple ephemeris of eqn. 5-4.

- A 10 d gap in the data occurs four days after the 1985 Vela glitch. Since only five measurements were made in the first four days following the glitch, the post-glitch model was fitted to these four days.

- For all pre-glitch models, and for post-glitch models not mentioned above, plots of the fitted parameter value and its error versus length of fitted data were used to select a suitable length of data, such that the formal error in the parameter reflects the scatter introduced by the choice of data lengths. For Vela, data lengths of 20 d appear to be suitable; for PSR 1641-45, lengths of 40 - 60d are used. For the 1994A glitch, a shorter pre-glitch fit was used because of the high level of activity preceding the glitch.

Details of the models fitted are listed in table 6-2.

Table 6-1: Sizes of the Glitches in PSR 0833-45 and 1641-45.

PSR	Glitch	Epoch (MJD)	ti_{pre} x1 V Hzs^{-1}	Aviv x10^{6}	*Aii/i)* x10^{2}
0833-45	1985	46 257.2306(8)	—156.052(4)	+1.6051(5)	+2.4(2)
0833-45	1988	47 519.8035(4)	—155.822(2)	+1.809(2)	+15(7)
0833-45	1991	48 457.3823(4)	—155.722(3)	+2.715(1)	+53(6)
0833-45	1991'	48 550.4(4)	—156.61(2)	+0.0056(1)	+0.10(2)
0833-45	1994	49 559.060(1)	—155.827(4)	+0.8614(2)	+0.6(2)
0833-45	1994A	49591.157(2)	—156.53(1)	+0.197(1)	+8(2)
1641-45	1986	46453(35)	—0.970(1)	+0.804(1)	+0.4(4)
1641-45	1989	47591(6)	—0.971(2)	+0.0020(4)	+0,5(5)

Errors are 2-u in the least significant quoted digit.

Table 6-2: Glitch Ephemerides.

0833-45:

Range fitted MJD	*ii* Hz	ii 10^{-13} Hz s^{-1}	ii 10^{-20} Hz s^{-2}	Epoch MJD	X_R^2	TMS mP
46 237 - 46 257	11.201 678 849 64(8)	-156.052(4)		46 246.905	0.57	0.14
46 257.5 - 46260.6	11.201 680393(1)	-159.8(3)		46 259.052	0.76	0.17
47 499 - 47 519.8	11.199 992 694 18(4)	-155.822(2)		47 509.511	1.1	0.26
47519.8 - 47 520.22	11.199 998 751(3)	-180(10)		47 520.024	0.91	0.22
48 437 - 48 457.34	11.198 749 773 31(7)	-155.722(3)		48 445.398	1.0	0.26
48 457.39 - 48457.7	11.198 763 720(4)	-240(10)		48 457.543	1.2	0.20
48 530 - 48 550.3	11.198 651 207 5(2)	-156.673(3)	+0.7(2)	48 540.306	1.3	0.21
48 551 - 48 570	11.198 623 386 8(2)	-156.682(4)	+0.9(2)	48 560.903	0.95	0.16
49 539 - 49 559	11.197 288 651 09(8)	-155.827(4)		49 549.927	0.91	0.17
49 559.24 - 49560.7	11.197 284 757 4(5)	-156.7(3)		49 559.978	1.41	0.14
49 581 - 49 591.12	11.197 249 555 7(1)	-156.53(1)		49 586.010	1.40	0.14
49 591.20 - 49 592.6	11.197 243 521(2)	-156.9(7)	+1500(300)	49 592.069	1.14	0.13

1641-45:

Range fitted MJD	v Hz	V 10^{-13} Hz s^{-1}	i. 10^{-20} Hz s^{-2}	Epoch MJD	x_R^2	riir mt)
46 363 - 46 418.3	2.197 515 181 47(9)	-0.970(1)		46 388.974	0.82	0.32
46 487 - 46 526	2.197 515 985 6(1)	-0.974(4)		46 503.638	0.86	0.30
47 533 - 47 589.2	2.197 507 131 3(1)	-0.971(2)		47 559.742	L08	0.58
47 593 - 47 631	2.197 506 723 6(2)	-0.975(5)		47 608.789	0.36	0.34

x_R^2 is the reduced x^2.
Errors are 2-a errors in the least significant quoted digit.

6.2 Analysis: *O(t), υ(t),* or

Pulsar timing behaviour is analysed in terms of *ON, v(t)* or ii(t). Often, only one of these three available approaches is used, particularly for the analysis of im mediate post-glitch behaviour. There are advantages and disadvantages to each:

- Timing noise is present throughout the data, particularly for the Vela pulsar. It is noticeable as wandering in OM, *v(t)* and */1(0,* and small jumps in the latter two parameters. Much of the wandering in OW and *v(t)* is reduced to scatter in *1.(t),* which makes it easier to include in the models. In particular, the uncertainties in the glitch-recovery parameters are more easily determined from ⅈ/*M.*
- The amplitudes of the faster transients following the glitch are far more prominent in *i>(t)* and *v(1)* than in *OM,* as shown in fig. 6-2. In OW, the wandering due to timing noise is difficult to distinguish from the post-glitch transients, particularly the faster transients.
- Many of the theoretical models involving glitches are directly applicable to *ii(t),* and therefore require integrating to apply them to *v(t)* or *OM,* which is not always simple.
- Reduction of the original data to *v(t)* and *i)(t)* requires one and two steps of averaging respectively. These series therefore have poorer time resolution than the phase residual data, *OM.*

Because of the large amount of data gathered for this project, it is feasible to reduce arrival times through a double differentiation to *i/(t)* while retaining a reasonable time resolution. Unless otherwise mentioned, time-series of *independent* values of z> and v were used for the analyses described below, to enable correct evaluation of the fitted models. The procedure used to obtain these series is described in section 5.17.

Figure 6-2: Observability of Transients in 0(t), v(t) and //CO.

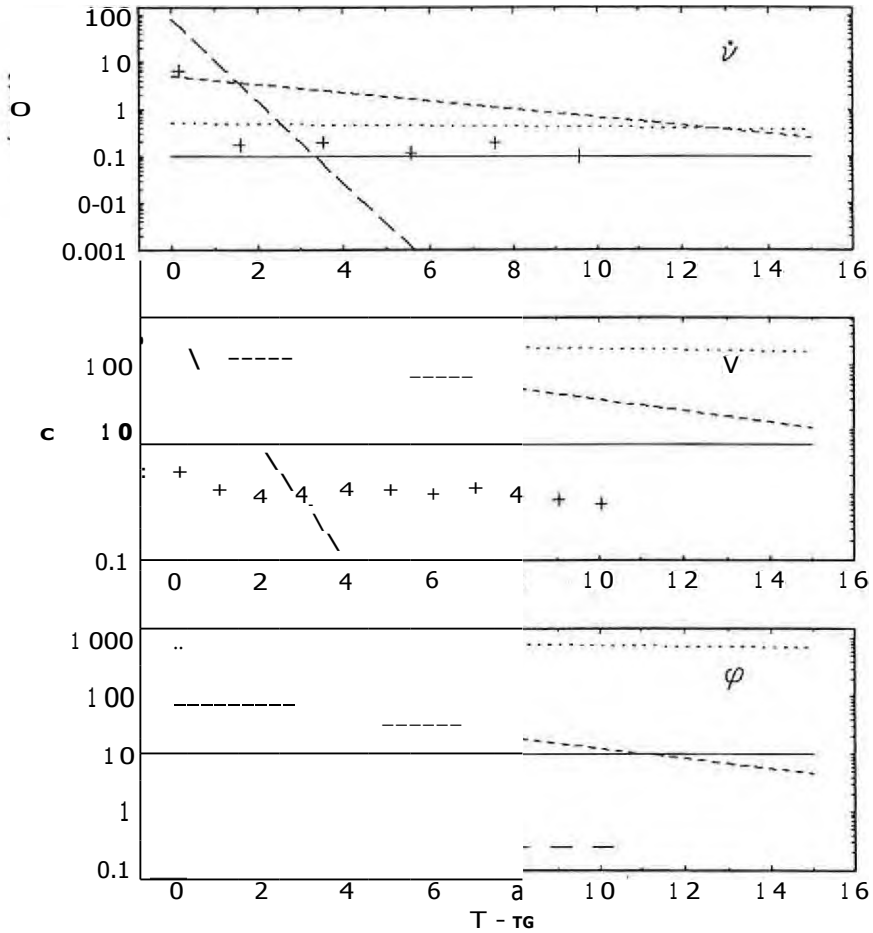

Dashed lines show the contribution of typical decay components in 1)(0 (top graph), v(t) (middle) and 0(t) (bottom). The transients are:

long dashed line: = 50%, T = 0.5d;
medium dashed line: = 3%, T = d;
dotted line: = 0.3%, r = 50d.

Pluses (+) in the top two panels show the formal data errors, at the sampling times following the 1991 glitch;
Dashes in the bottom panel show the typical error in 0(1), and indicate the observation times of the 1991 glitch;
Solid horizontal lines show the amplitude of timing noise typical over 250d.

The fastest transient is most prominent in V-data, and is at the level of the timing noise in 0-data.
The amplitudes of the three transients are similar in v-data, but differ by an order of magnitude in the i/-data.

6.3 Qualitative Features of the Glitches.

The evolution of v(t) and *V(t)* is shown in figs. 6-3 — 6-7. Features prominent in these figures are:

- Although the increases in v are large, about three orders of magnitude larger than the interglitch scatter visible in figs. 6-4c and 6-5, they are negligible compared to the overwhelming general spin-down, for both pulsars (figs. 6-3a and 6-4a).

- Very little of Av recovers, in either PSR 0833-45 (fig. 6-3b) or PSR 1641-45 (fig. 6-4a) .

- The (factor of ten) larger increase in I V observed for the Vela glitches of 1988 and 1991, compared to the less well resolved earlier events (e.g. 1985) (fig. 6-6), is due to the presence of a large amplitude, rapidly decaying component of AV for this pulsar. Any change in V of PSR 1641-45 at the time of the 1986 glitch has recovered during the 68d gap in observations (fig. 6-7).

- There appears to be a characteristic form of glitch recovery in *V(t)* for Vela: most of AV recovers within a day or two; the recovery continues at a slower rate until it settles into a roughly linear decay, describable by a positive value of U, which persists until the subsequent glitch (fig. 6-6b); noise in the form of wandering and small jumps in V appears to be present at all times, though at a much lower level than the recovery just described.

  In *i>(t)* of PSR 1641-45, however, there is no overwhelmingly clear trend visible that can be distinguished from the timing noise (fig. 6-7).

- Any transients following the smaller glitches are difficult to distinguish from the timing noise.

Figure 6-3: PSR 0833-45: v(i).

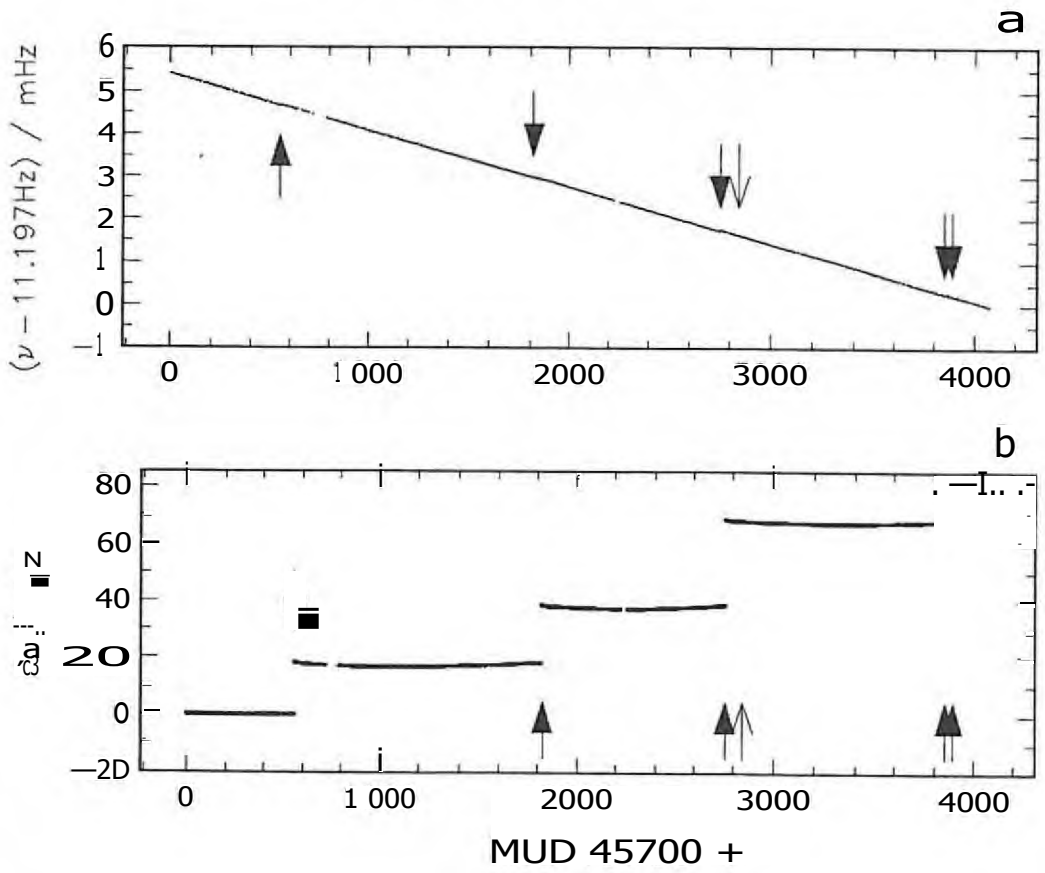

a Evolution of v(t) throughout the entire 11yr. The most dominant feature is the spin-down term, *ii,* which renders the spin-ups Av insignificant.

b A model (v, ii) fitted to all data prior to the 1985 glitch has been removed from the entire data span; the glitches are the dominant remaining feature.

Filled arrow heads mark the five large glitches. The open arrow head marks the smaller glitch of 1991. Error bars fall within the symbols and are not plotted.

Figure 6-4: PSR 1641-45: v(i).

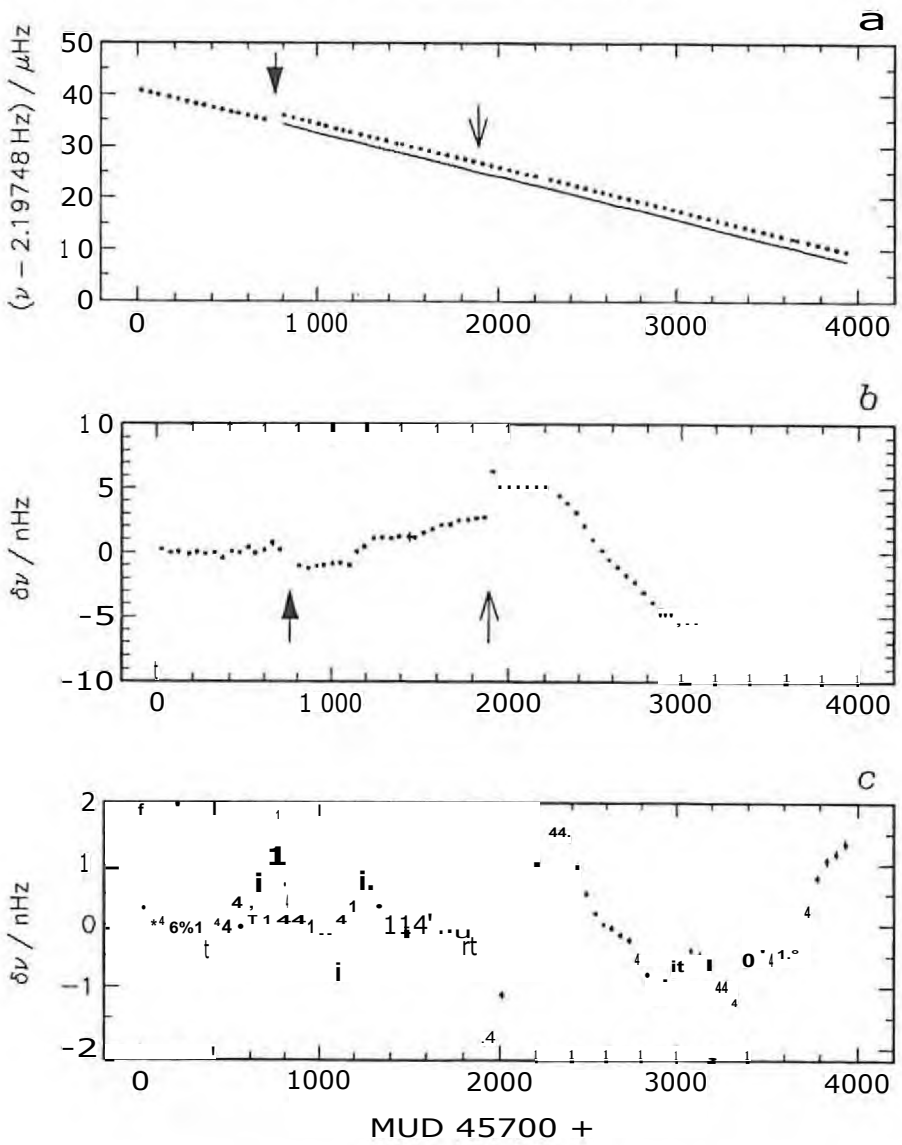

Evolution of *v(t)* throughout the project. The large glitch is marked with a filled arrow, the smaller glitch with an open arrow.

a Original data. The solid line is a *, id* fit to the pre-glitch data.

b A model *(ii,* fitted to the data prior to the large glitch of 1986 has been removed from all the data. The large glitch of 1986 (Av 1.767μHz) has been subtracted from the post-glitch data.

c Spin-down models have been fitted to and removed from each of the three interglitch data sets. For the last of these, a third-order term *(1)* = 9.7 x 10^{-25} Hzs^{-2}) was included.

Figure 6-5: PSR 0833-45: v(t) (expanded). (a) Pre-1985.

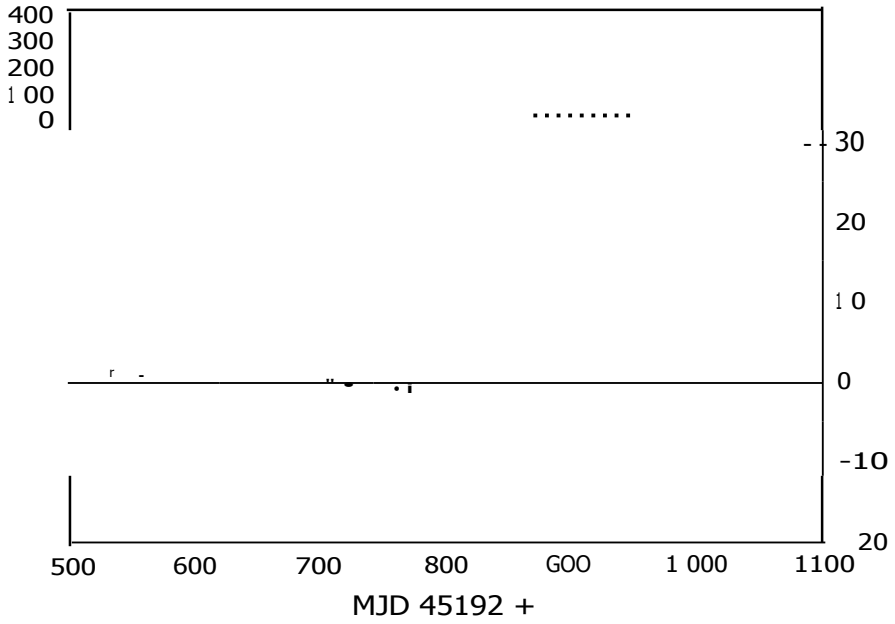

A running model [11, , id of length 300d has been removed from the data. Each interglitch period is processed separately; no fits were made across the small glitch of 1991. Upper panels show all data, so that the full extent of the transients can be seen; all these panels use the same scale. Lower panels are expanded views, showing the timing noise.

a 1984.0 to glitch of 1985.

b Glitch of 1985 to glitch of 1988.

c Glitch of 1988 to glitch of 1991.

d Glitch of 1991 to glitch of 1994.
The small glitch of October 1991 is marked with an open arrow.

e Glitch of 1994 to 1994,8.
The short length of data between the two glitches of 1994 was fitted with a first-order model , id; a second-order model [v, is, id has been removed from data following the second of these glitches. The second glitch (1994A) is a rrowed.

Figure 6-5: (b) 1985 — 1988.

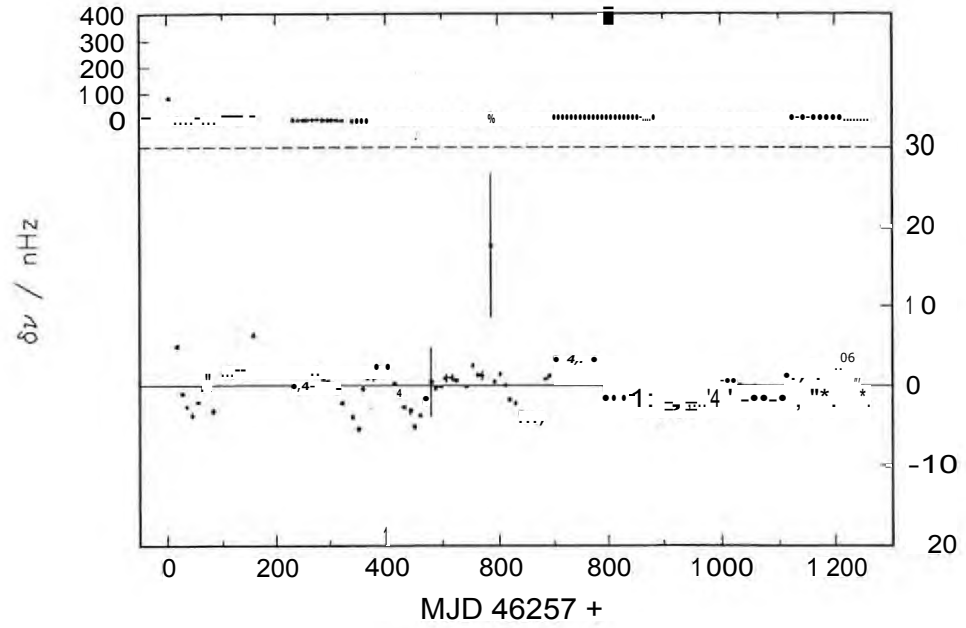

Figure 6-5: *(c.)* 1988 — 1991.

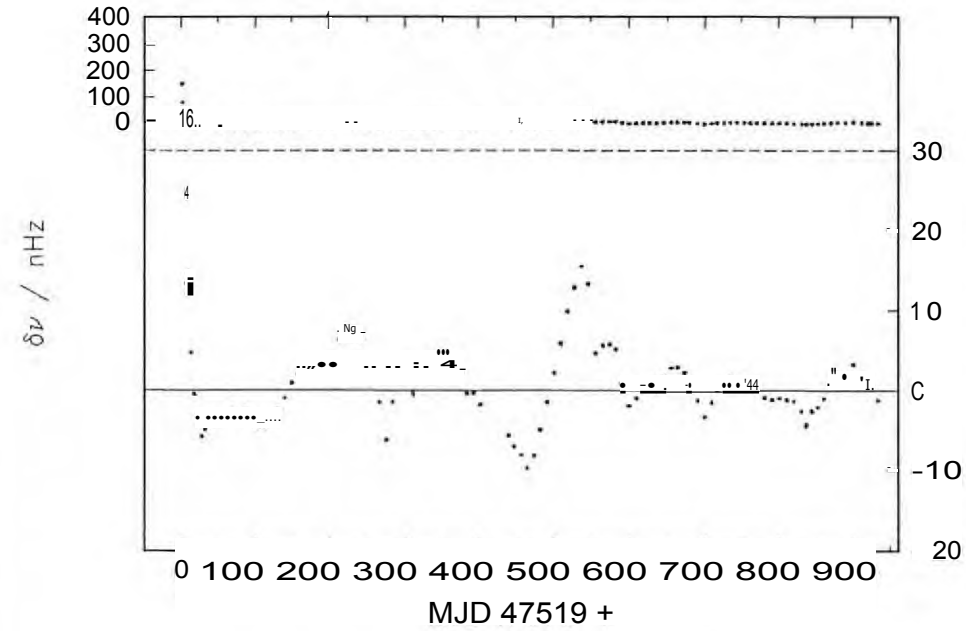

Figure 6-5: (d) 1991 — 1994.

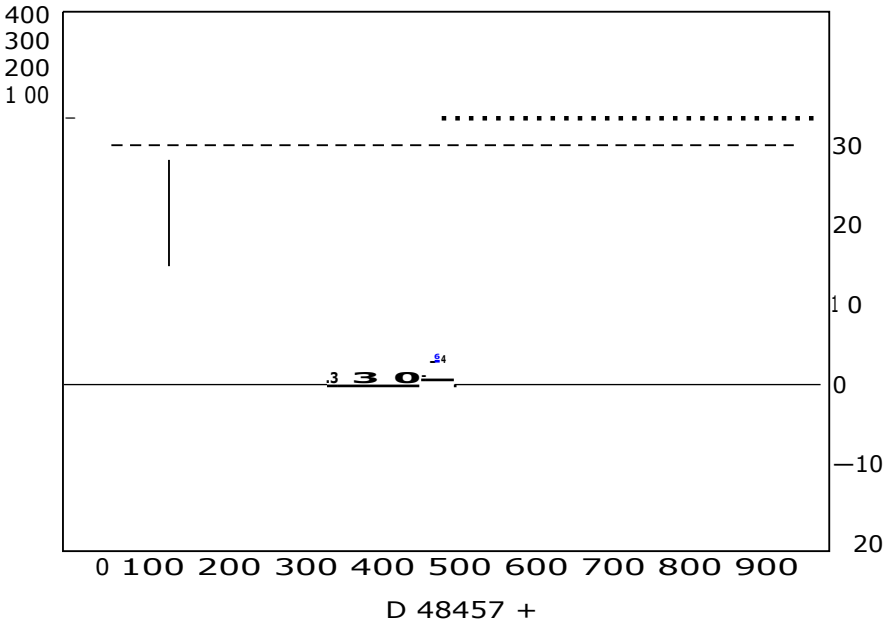

Figure 6-5: (e) Post-1994.

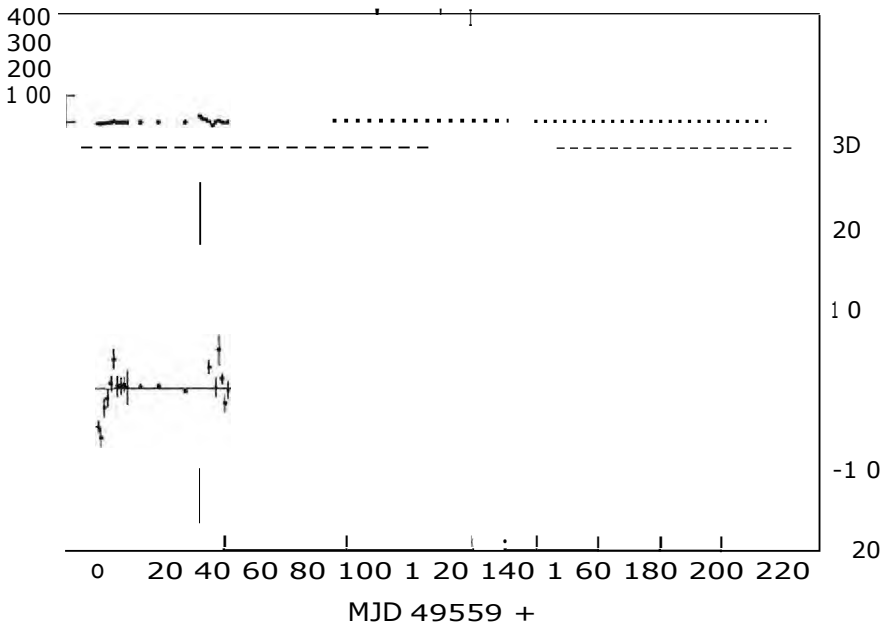

Figure 6-6: PSR 0833-45: (t).

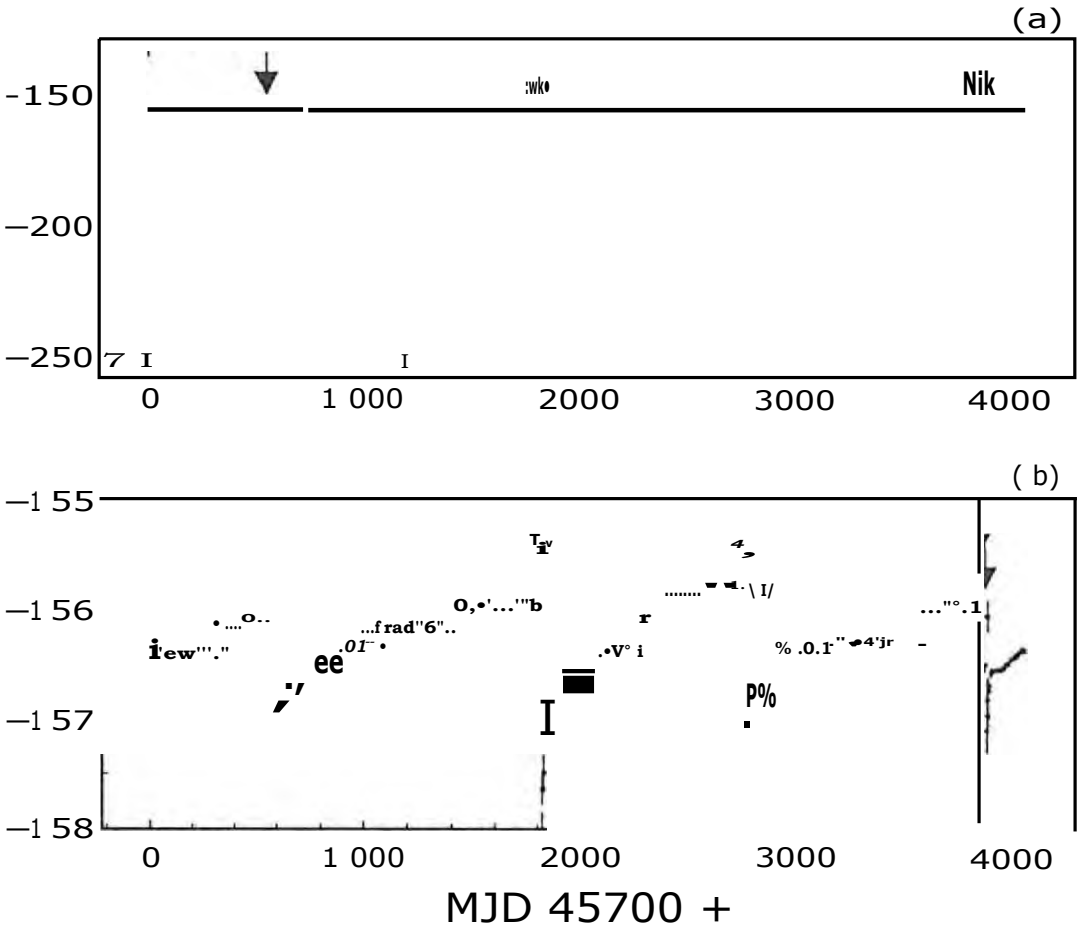

Evolution of li(t) throughout the entire period covered by this thesis. No models have been removed from the data. Large glitches are marked with filled arrows, and the small glitch with an open arrow.

a All data.

b Expanded version of (a).

Figure 6-7: PSR 1641-45: *ii(t).*

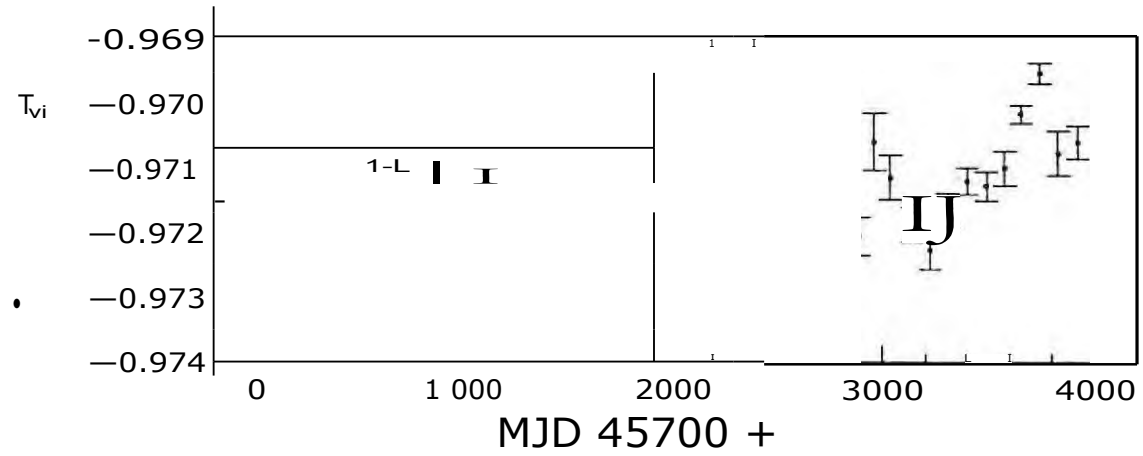

Evolution of 1984.0 — 1994.8. No model has been removed from this data. The large glitch of 1986 is marked with a solid arrow; the smaller glitch of 1989 is marked with an open arrow.

7 Glitch Sizes.

Large spin-ups such as those reported in chapter 6 are difficult to ignore. The question arises: have any smaller glitches been missed? A search of the data from 1984.0 to 1994.56 (glitch 1994) was thus made for abrupt changes in the spin-rate, either positive or negative. Three approaches were used; the methods and results are described here. The implications of the resulting distribution of glitch sizes are discussed in section 7.2.

7.1 Searches for Smaller Glitches.

7.1.1 Manual Search for Events in Phase Residuals.

Arrival times were blocked into lengths of 200d (Vela) or — 400d (1641), a 3^{7d}-order model removed from each block, and plots of residuals OW examined visually for sudden changes in slope. This process was repeated using blocks staggered with respect to the first set by half a block. For an event to be accepted, it had to be apparent in both sets of blocks. Nineteen candidate events were located in the Vela data, and one (the small glitch of 1989) in the 1641 data; on closer examination of the residuals around the time of the event, all but three of the Vela candidates were rejected as possibly being "slow glitches". Poor sampling over an event would result in it being rejected.

7.1.2 Manual Search for Events **in Frequency Residuals.**

Series of zi(t), created from independent blocks of arrival times, were examined for sudden changes. Three such series were created for each of the first four interglitch eras of Vela, **and** seven from the 1641 data. Block lengths were rs.' 10 d (Vela) and 50d (1641). The start times of the blocks were staggered from one series to the next for each pulsar, to avoid averaging out any small glitches. Fig. 7-1 and 7-2 show these series for Vela and 1641 respectively; candidate events are arrowed.

The arrival times for 150 d (Vela) and 800d (1641) at the time of each candidate event were modeled and the residuals examined for a sudden change in slope, indicating a genuine (sudden) change in spin-rate. The residuals are shown in fig. 7-3 and 7-4. All except four candidates in Vela **and one** in 1641 were consequently rejected.

7.1.3 Results of Manual Searches.

The parameters of all events located by the two procedures above are given in table 7-1. Epochs were estimated from plots of 0(0, and event sizes obtained from 25d (Vela) and 50d (1641) models. The larger two events would

Table 7-1: Parameters of Small Events.

Epoch (MJD)	Aviv x10^9	x10^2	Identified from
0833-45			
46110.5	+0.26(7)	+0.015(7)	$\nu(t)$, ϕ
48550.5	+5.58(6)	+0.072(7)	$\nu(t)$, ϕ
48 637	+0.85(5)	+0.016(5)	$\nu(t)$, ϕ
48985.2	+0.6(1)	-0.06(2)	$\nu(t)$
1641-45			
47 591	+2.0(4)	+0.5(5)	OM
49 060	+0.3(1)	-007(7)	v(t)

Errors are 2-o in the least significant quoted digit.
The last column shows the method by which events were identified.

be considered glitches in the Crab pulsar; they are listed as small glitches in table 6-1. The other events fall within the size range that is normally considered to constitute timing noise. All events are clearly spin-ups; except for the largest Vela event, measured changes in /*/ are small and dependent on the lengths of data fitted.

7.1.4 Automatic Identification of Events.

The above methods of searching for small glitches may not be objective enough - the eye may for instance pick out events with a preferred sign. An attempt was made to develop a more objective method of searching, as follows:

- a 5 d-length of arrival times was fitted with a 2-order model (0, *v*

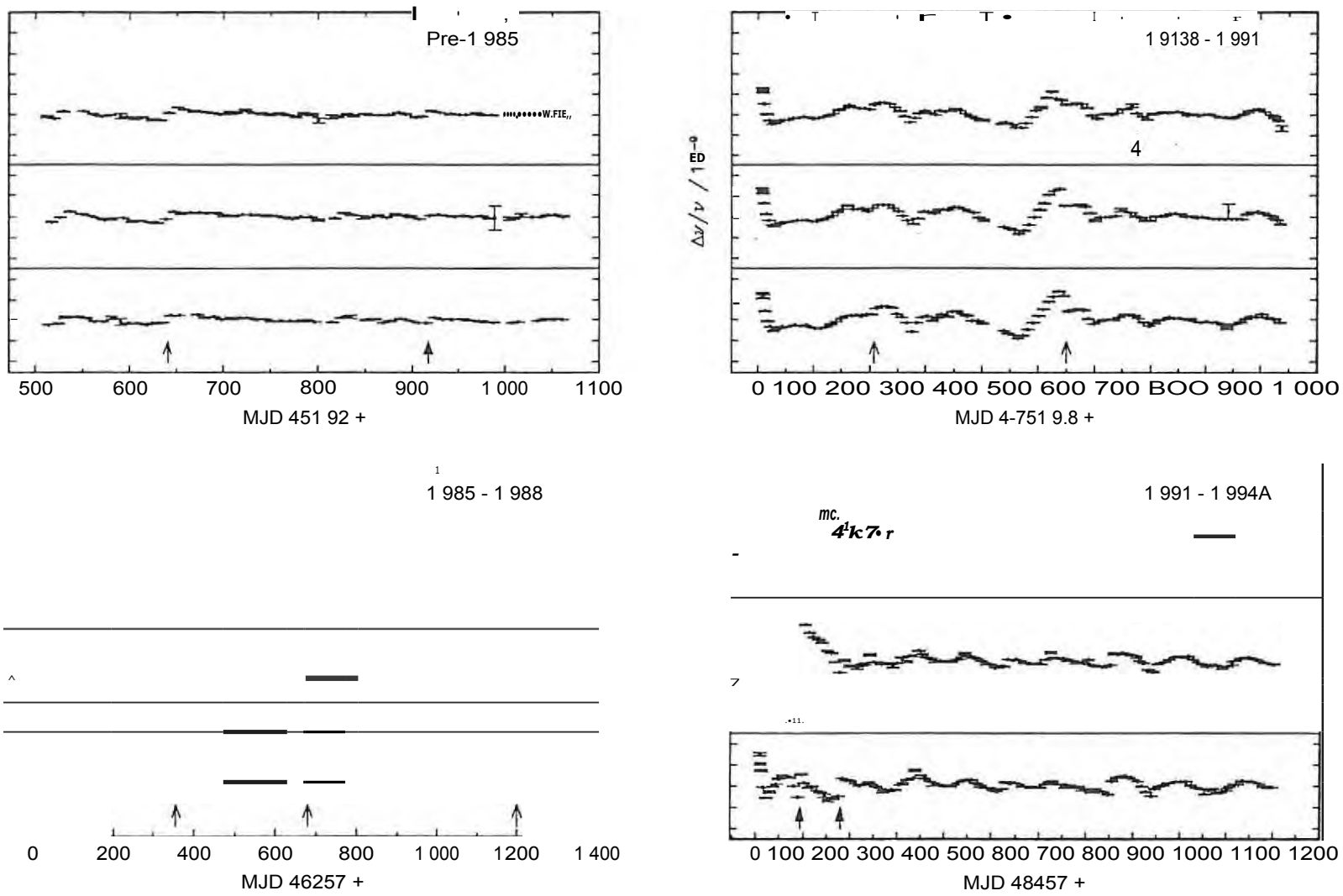

Independent v-series for four different inter-glitch eras. The time-ordinates (ti) in each series are approximately 1.0d apart; the t_i values are staggered by 3d from one series to the next. A running mean model has been removed from the data.

Candidate events identified by eye from these plots are arrowed; events that appear (from examination of phase-residual plots) to be genuine sudden changes in $\nu(t)$ are marked with solid arrow-heads.

Figure 7-2: PSR 1641-45: Searching v(t) for small Glitches.

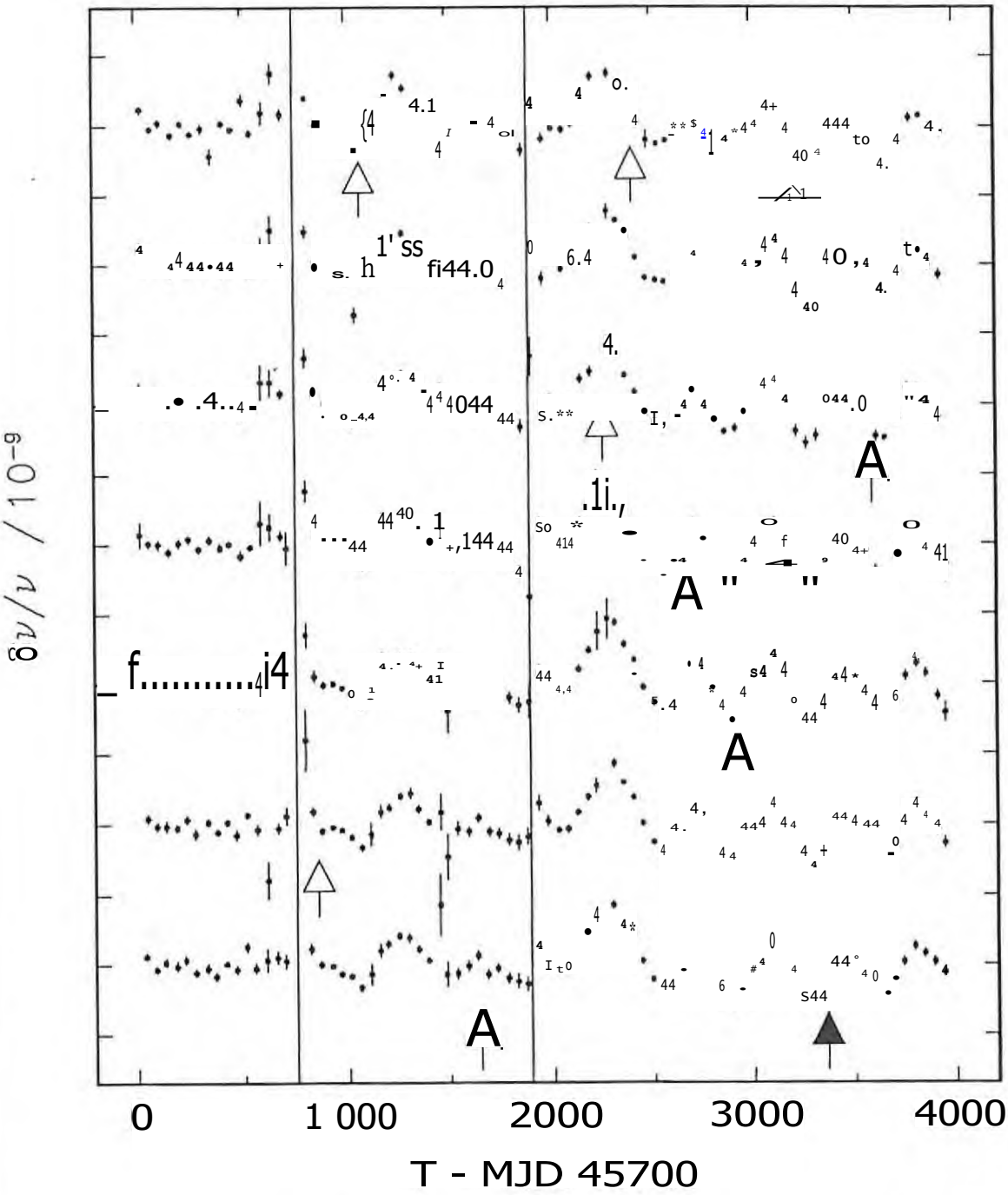

Independent v-series. The time-ordinates (t_i) in each series are approximately 50d apart; the /, values are staggered by 7d from one series to the next. A running mean model has been removed from the data, which were first divided into three eras, at the glitches of 1986 and 1989.

Candidate events identified by eye from these plots are arrowed; events that appear (from examination of phase-residual plots) to be genuine sudden changes in v(t) are marked with solid arrow-heads.

Figure 7-3: Vela: Candidates for small Glitches.

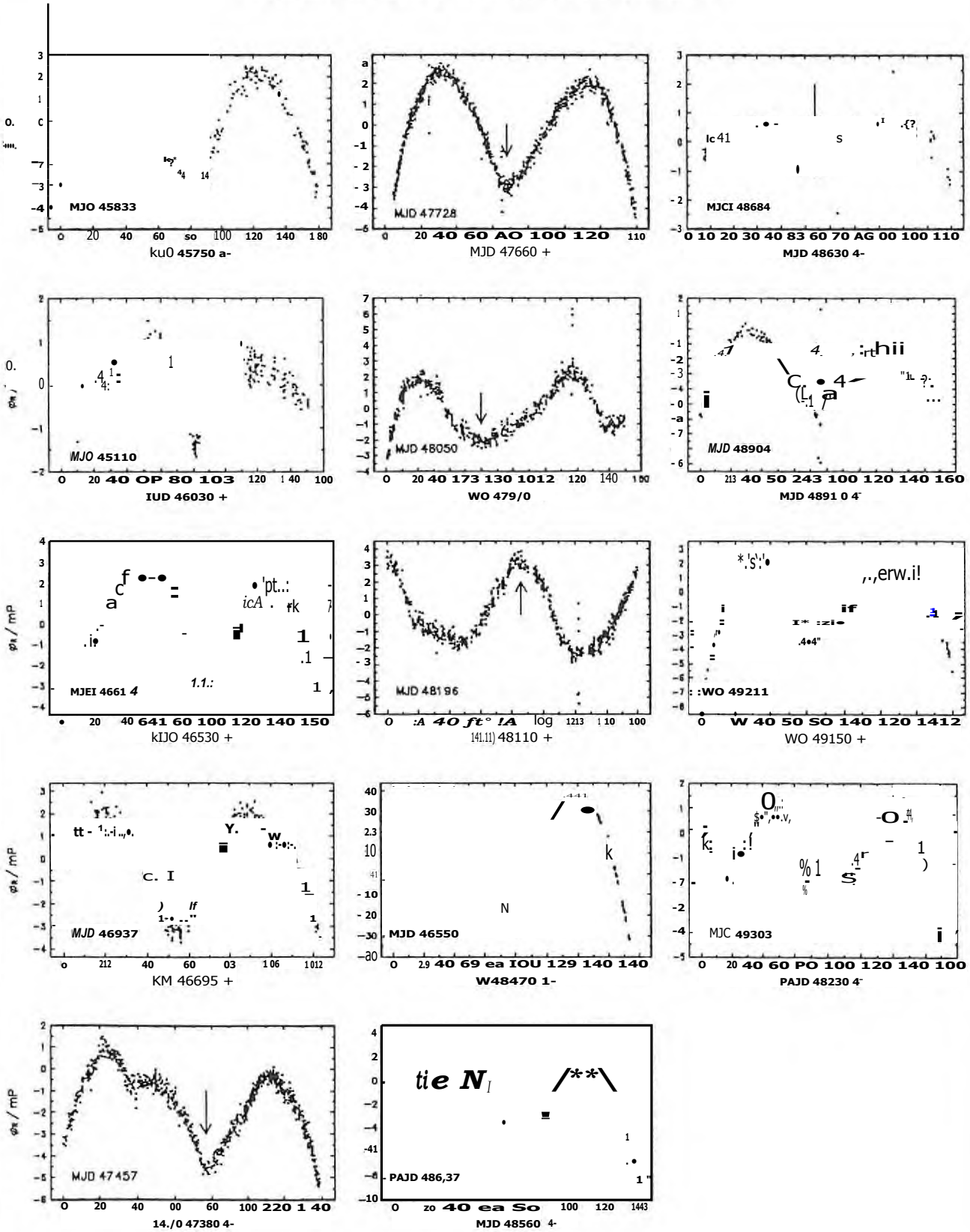

Phase residuals around candidate small glitches. The epochs of the events are marked — those rejected with open arrows and those accepted with solid arrows.

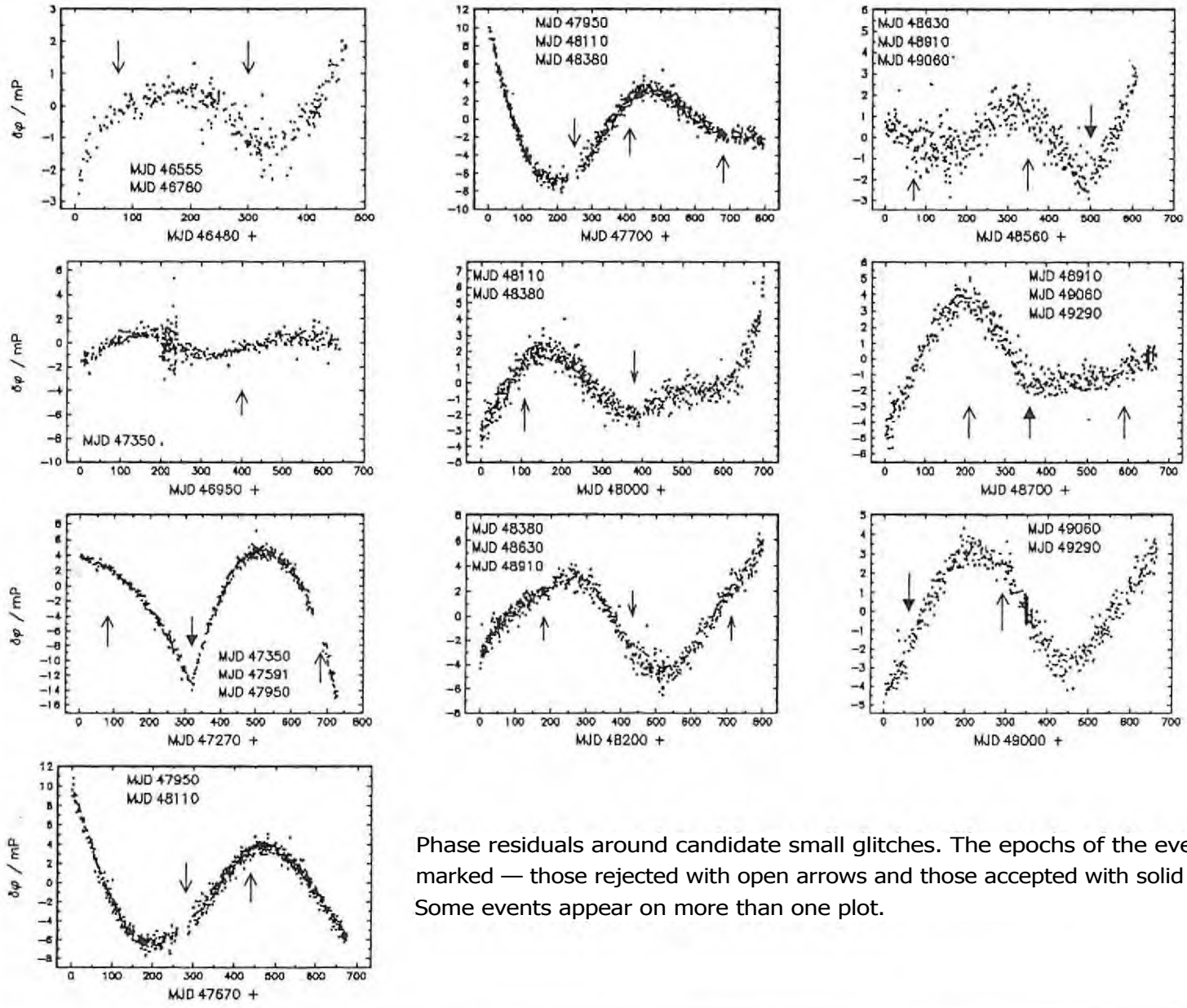

Figure 7-4: 1641–45: Candidates for small Glitches.

Phase residuals around candidate small glitches. The epochs of the events are marked — those rejected with open arrows and those accepted with solid arrows. Some events appear on more than one plot.

- this 5 d data length was lengthened by 2 d at a time, until the "goodness of fit" parameter Q (described in appendix 6) fell below 0.1 (i.e. a, possible event was located);

- the resulting ephemeris was written to a file, and the procedure repeated starting at this possible event;
  this method is referred to as 2F (2nd-order fits, forwards) below;

- the above procedure was repeated with 3rd-order fits; when the end of the block was located, a significance test was done on the ^{j2} term and it was omitted if necessary;
  this is referred to as method 3F below;

- the above two passes through the data were repeated starting at the end of the data and moving backwards;
  (methods 2R and **3R,** or 2nd- and 3rd-order reverse fits).

In the above, blocks were terminated at the large glitches.

This procedure resulted in four sets of spin-down models, extending between possible events. Event parameters were then calculated from the difference between consecutive models. **All** events for which Av < 2 , and Ai, < where c_{ap} is the formal error in Ap, were omitted from further analysis.

Forward **and** reverse passes were used in **the hope that** "real" events would show up in both passes - data points with underestimated errors, that would reduce Q below 0.1, should produce spurious events with different epochs in the two passes. In fact, very few events located by different passes had coinciding epochs, so this approach was abandoned and the four resulting sets of candidate events (one set from each of the methods 2F, 2R, 3F, 3R) were analysed individually and results compared. A fifth set of candidate events was created by merging all events from the initial four sets for which | A ii/v1> 10^{-9}, in case the original data set consisted of a large number of timing-noise events plus a few genuine small glitches. In this set, a number of groups of nearly-coincident events were found. For each such group, all except that with the largest value of 1 Av were deleted. The resulting data-set is referred to as **Large** below.

The analysis involved examining correlations between the parameters of the events, counting the number of events with [**6v/v,** Ai'/t'] signatures of [-I-, +1, [+, -], [-, +1 and [-, -], and examining plots of the event sizes. The event parameters examined for correlations were: event sizes $Aviv$, $Ai/0{,}16{\cdot}4/^{1}$ and Aii/i/ 1, time T since the most recent large glitch, time T^{-} since the previous candidate event, and time $T+$ to the next candidate event. T^{-} and $T+$ refer to the edited set of event epochs, i.e. after removal of insignificant

events. Should there be any real but small glitches in this collection of candidates, one might expect:

- s a preponderance of events with [Ay/ v, [+,+], as in the larger glitches;
- a negative correlation between the event size and $T+$, indicating post-glitch relaxation;
- a continuum of glitch sizes up to $Aviv$ 10^{-6}, the typical size of a large glitch.

The results are summarized in table 7-2 (correlations) and figs. 7-5 and 7-6 (event sizes and signatures). The only consistently large correlation was pa $Aviv_{1,I}$ $AVi\dot{v}$ $>$ 0.5. Since there appear to be a number of outliers that will affect PO Aviv LI this test was repeated on sets of data from which all events with lAvhil> 10^{-9} had been removed. The resulting correlations, listed in table 7-2, are reduced but stilt high. An interesting result is the marginal but persistent correlation of T^- with $T+$, implying regions of low activity (longer time between events); this is evident in plots of e.g. T+ vs time.

No trend in event signature [Aviv, AV/id was apparent in the small events; an excess of events with positive Av/v either sign) is apparent in the Large data set (fig. 7-6). However, the reality of these events needs to be carefully examined - when event parameters for the largest three (with 1.5 x 10^{-8}) were recalculated using 30d data lengths, the "events" were much reduced in size.

In summary, besides the "giant glitches", which are easily recognisable, the two manual searches located an additional four events in Vela and two in 1641-45 with 10^{-19}; interestingly, all these events are spin-ups. Only events which are well-enough sampled to rule out the possibility of them being "slow glitches" are accepted; other real small events occurring during the eleven years may have been rejected.

Although the automatic search located events with 10^{-8} <1 Av/v l< 10^{-6}, this method needs refining, and these events will be ignored for the meantime. There may be an excess of spin-ups relative to spin-downs among events of size 1 $Avivi$— $10';$ an improved automatic method of locating such events should be investigated but it may not be possible to identify individual events; a noise analysis along the lines of that used by Cordes & Helfand (1980) may be more productive. There are signs of some interesting trends (quiet periods,

Figure 7-5: Distribution of Sizes of small Events.

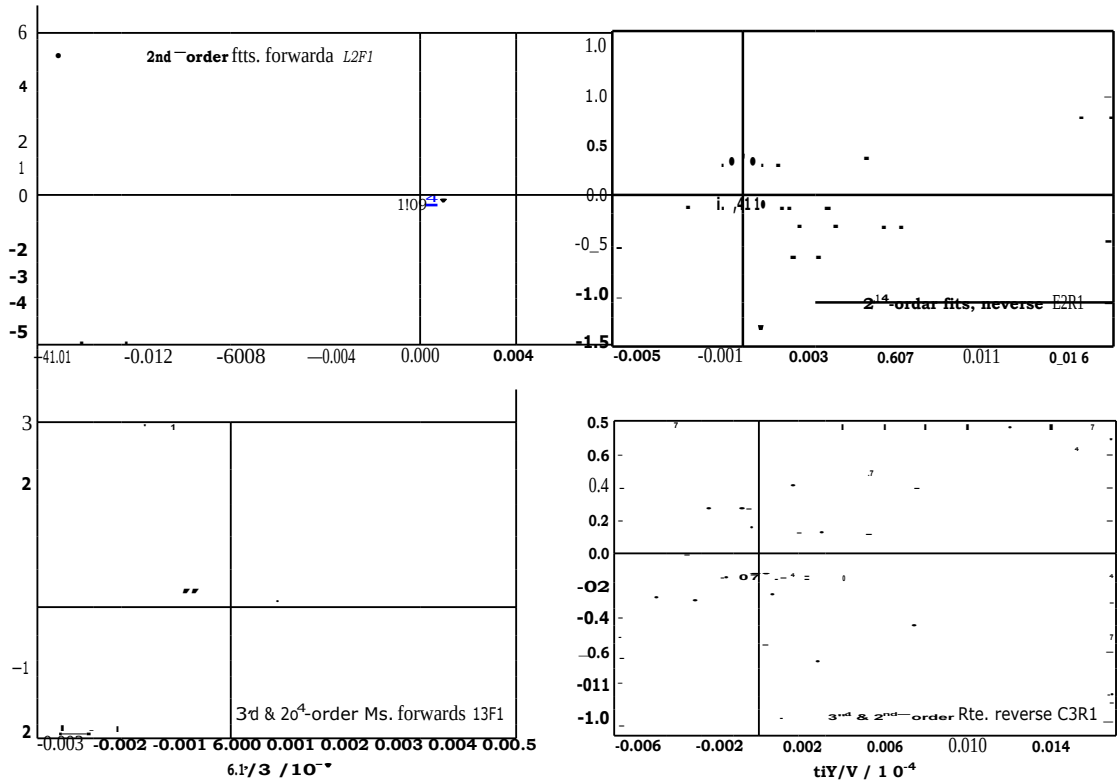

Each plot shows events located by one of the four methods (2F, 2R, 3F, 3R) discussed in the text. Proportions of events occurring in each of the four quadrants [+, +1, [+, [—,+] and [—, are given.

Table 7-2: Small Events in PSR 0833-45: Correlations.

Pass:	2F	2R	3F	3R	Large
No. of candidates:	157	156	137	113	58
[+, +] (%):	17	35	**19**	27	36
[+, −] (%):	45	21	26	24	33
[−, +] (%):	18	32	29	35	17
[−, −] (%):	20	12	26	14	14
p(Av I v, Az>/z>)	-0.34	+0.31	+0.01	+0.27	-0.09
Pa *Avii/* I, I Ailii;1)	+0.85	+0.60	+0.78	+0.56	+0.54
P(I Ali/yid ^{6,} $^{4^{11}}$ 1)*	+0.48	+0.28	+0.54	+0.37	
p(Av I v,T+)	+0.04	-0.11	-0.08	-0.07	+0.02
p(Aw, T+)	-0.22	-0.04	-0.03	-0.12	-0.24
P(! Av I v LT+)	-0.06	-0.12	-0.03	-0.01	+0.10
p(i Av I zd,T+)	+0.24	-0.11	-0.11	-0.06	+0.13
p(Az)/zi, T+)	-0.04	-0.03	-0.12	+0.12	-0.15
p(Ai/ I i. , T+)	+0.21	-0.06	+0.01	+0.06	+0.17
Pa Ai I 7%1, T¯)	-0.07	-0.25	-0.11	-0.20	-0.14
p(I Azi I ii I, T+)	+0.09	-0.17	-0.16	-0.17	+0.10
p(Az i I v,T)	+0.06	-0.01	+0.04	+0.08	-0.18
Pa Au I v I,T)	-0.05	-0.08	-0.16	-0.01	-0.15
p(6di I r i , T)	+0.01	-0.02	-0.03	+0.21	-0.10
p(L>/> I, T)	-0.01	-0.23	-0.18	-0.15	-0.22
p(T+ ,T)	+0.07	+0.09	+0.07	+0.01	-0.05
p(T+ ,T)	+0.16	+0.12	+0.19	+0.13	+0.23
p(T+ ,T¯)	+0.16	+0.20	+0.22	+0.28	+0.24

"Pass" refers to the method of locating events, described in the text.
[+, +1 is the proportion of events involving positive changes in $Av\ I\ v$ and *Aii/i,* respectively.
T is the epoch of the event relative to the most recent giant glitch.
T^- is the time since the previous event.
$T+$ is the time to the next event.

*: after removal of events with I Aviv I> 10^{-9}.

Figure 7-6: Distribution of Sizes of "Large" small Events.

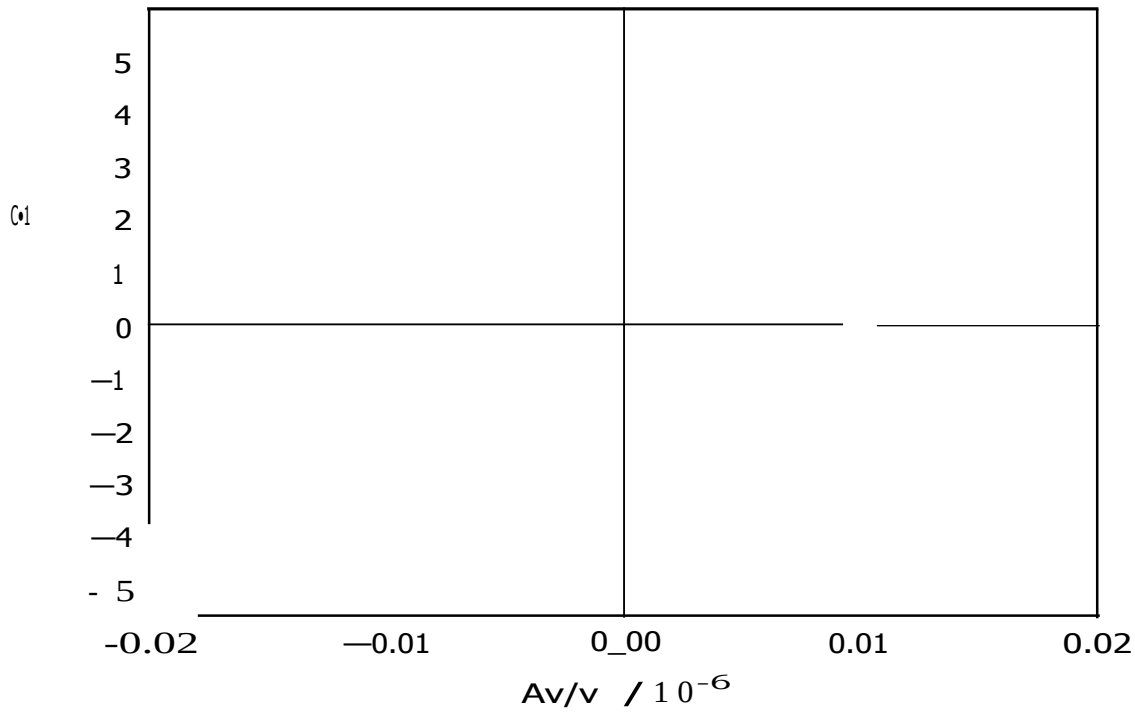

All events with lAvivi> 10 are plotted.
The largest of the events listed in table 7-1 is ringed.

and correlation of event magnitude in v and if); further investigation of these falls within the field of timing noise and is not pursued here.

7.2 Trends in Glitch Sizes?

Fig. 7-7 shows the distribution of all published glitches, plus those reported in this chapter. It is not a complete sample - many small glitches will not have been reported. Many of the glitching pulsars appear to experience spin-rate changes with a range of sizes. Cordes *et al.* (1988) note that there seem to be at least two different types of event: true glitches (all the larger events are spin-ups) and timing noise (events with 1 Av/v 1‹ 10^{-9}; both positive and negative changes are observed). So are the two Vela glitches with lAmiv1≈ 10^{-8} real glitches, part of the timing noise, or a different type of event altogether? Interestingly, both occur 100d after a giant glitch.

We may now have observed enough glitches in Vela to look for trends in their distribution in size and time. Fig. 7-8 shows the distribution of glitch

Figure 7-7: Distribution of Glitch Sizes - All Pulsars.

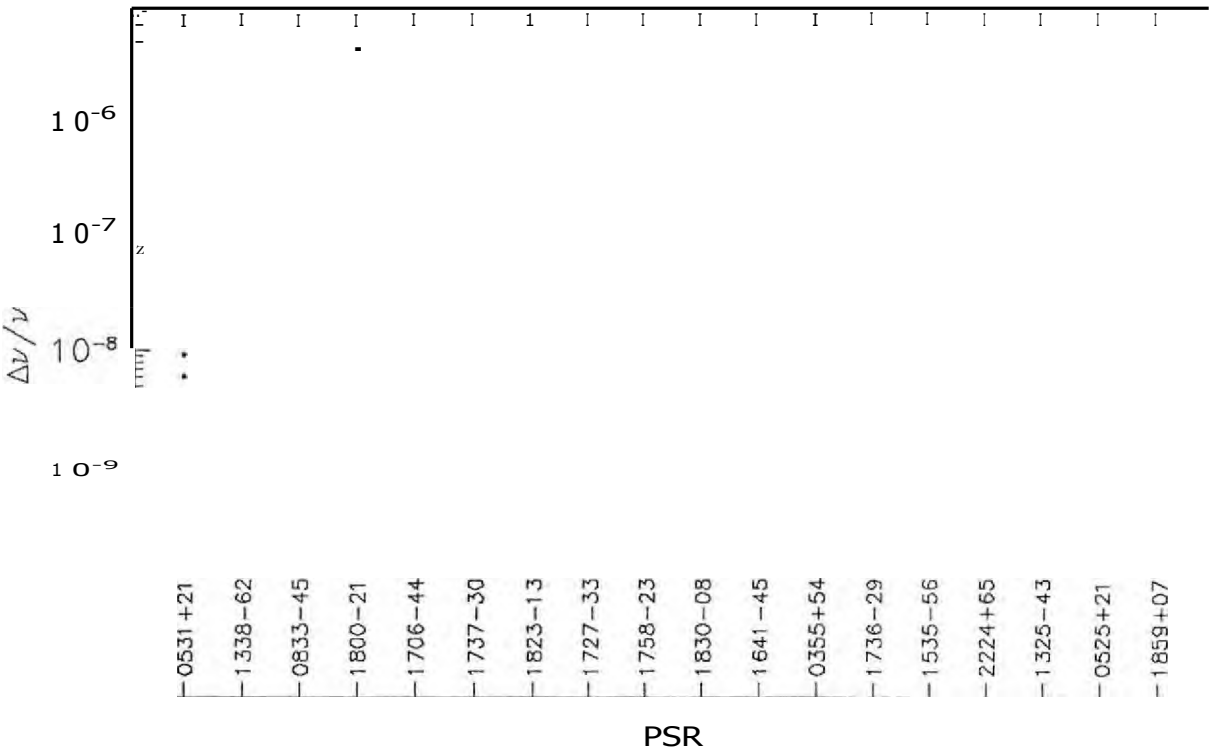

Relative glitch size versus pulsar, for all published glitches and those listed in table 7-1. Pulsars are ranked in order of age (youngest on the left). Glitches reported in this thesis are marked with +.

Figure 7-8: Glitch Size Distribution.

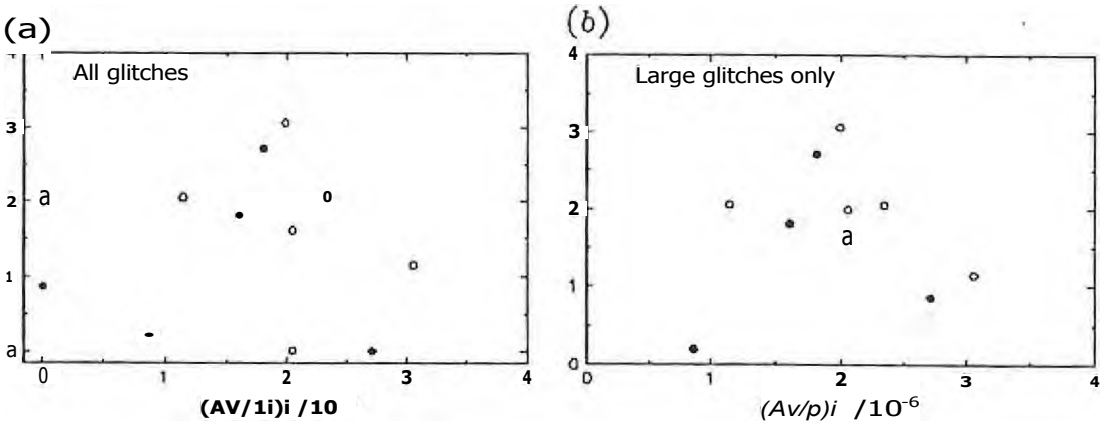

Size of glitch versus size of subsequent glitch.

a all glitches;

b after removal of glitches 1971! and 1991'.

Glitches observed from HartRAO are marked with solid circles (•).

Figure 7-9: Glitch Size versus Interglitch Interval.

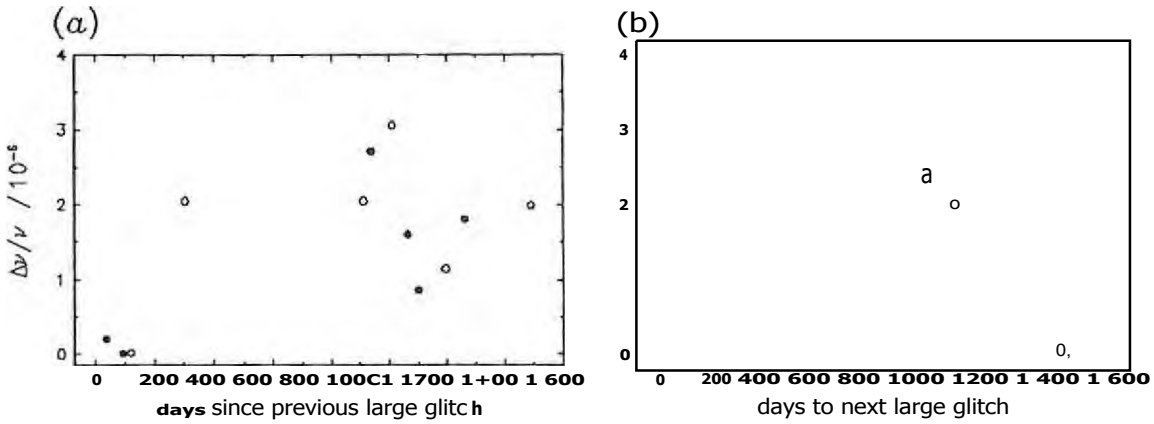

Size of glitch versus

a time since most recent large glitch;

b time until subsequent large glitch.

*: here, the glitches of 1971' and 1991' are not considered to be "large".
Glitches observed from Ha rtRAO are marked with solid circles (•).

size versus size of the previous glitch, for two sets of Vela glitches: with and without the two smaller events, 1971' and 1991'. The first of these data sets has a random distribution (p —0.05). The second set shows an interesting trend, in that a smaller glitch is generally followed by a larger glitch. The notable outlier (at [0.8,0.2]) can be removed if the most recently observed (and unusually small) large glitch should be classified with the two smaller glitches of 1971' and 1991'. In other words, the earlier glitch of 1994 is the most recent "giant glitch".

Fig. 7-9 shows glitch size versus time elapsed since the most recent large glitch (fig_ 7-9a) and versus time until the next large glitch (7-9b). One feature is prominent — the occurrence of all three small glitches (1971', 1991', 1994A) within --100d of a large glitch. Otherwise, there are no unambiguous trends in fig. 7-9. One would expect trends if the glitch size were related to stress build-up, for instance:

- the glitch releases stress built up since the previous glitch, in which case we should see a trend in fig. 7-9a;
- the glitch has a more or less random size, which causes a certain amount of stress relief; when this level of stress is regained, another glitch occurs; this should result in a trend in fig. 7-9b.

The apparent observation that glitches of size Au $\mathbf{1O}^{-7}$u occur only within -400d of larger glitches implies that these events are somehow related to the larger glitches — presumably stress released by the large glitches can accumulate elsewhere in the star. Then either the location of the newly-stressed region, or the short time since the previous glitch, is such that a large glitch is not likely (although the rather large glitch of 1982 occurred —300d after the previous event). The question arises: is this seen in other pulsars?

Fig. 7-10 shows the time elapsed since the previous large glitch for events in three other pulsars in which both large and small glitches have been seen. Although the (rather arbitrary) classification of events as either "small" or "large" biases these results, the "large" glitches all occur after longer periods of time than the "small" glitches, for individual pulsars. However:

- there is less of a clear bimodal effect for PSR. 1737-30 and 1338-62 than for PSR 0833-45 and 1641-45;
- a small glitch in PSR 0355+54 (not shown in the figure) occurred —400d *before* a large spin-up; no other glitches have been reported in this object, although it had been monitored for —13yr prior to these events (e.g. Lyne 1987).

Figure 7-10: Glitches in Pulsars with both large and small Glitches.

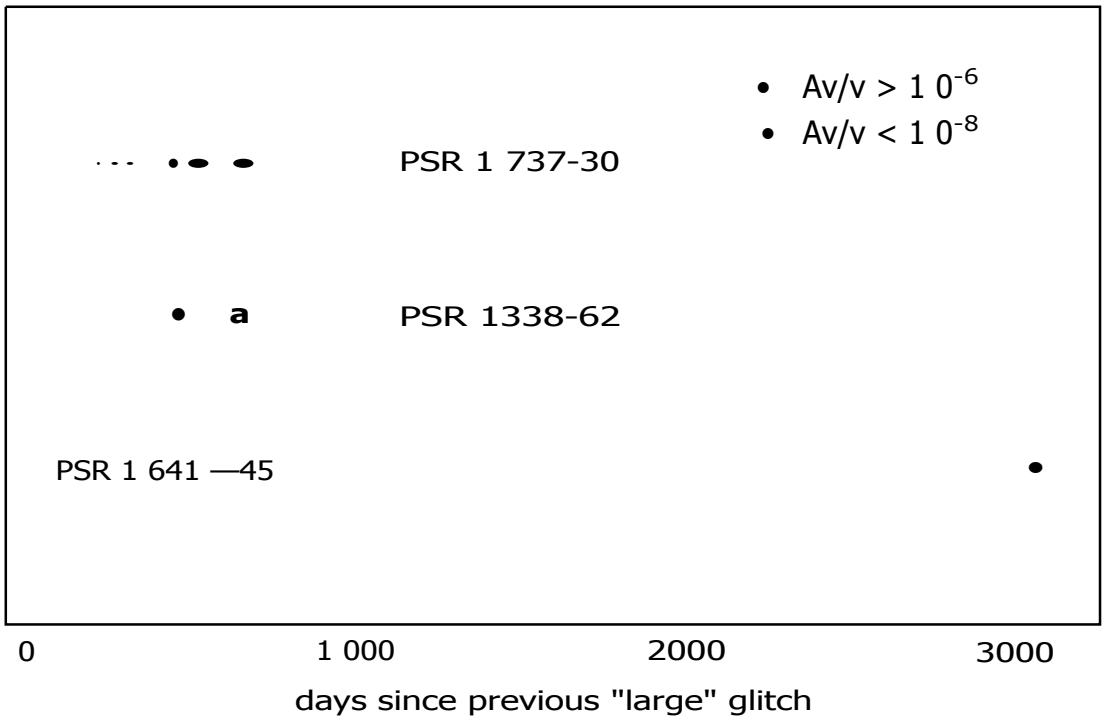

In the Vela pulsar, small glitches appear to occur within ---100d of a large glitch. This is an order of magnitude less than the typical interval between the (more numerous) large glitches. In order to investigate whether the same affect is seen in other pulsars, glitches are classified into "large" (At' 10^{-6}v) and "small" (At' 10^{-6}v) for three pulsars. The time elapsed since the previous "large" glitch is indicated on the horizontal axis.

Notwithstanding the above, the unusually short "build-up" time to the three unusually small glitches in Vela cannot be mere coincidence. It would seem that the glitch-triggering mechanism which releases stress in the large glitch must be one that can cause stress build-up in another part of the pulsar. If glitches are caused by large-scale unpinning of vortices, and pinning is widespread, this can be explained if the vortices move outwards and repin at a different radius, thus enhancing the vortex density at the new location. This supports the vortex creep model of Alpar *et al.*, since the environment at the location of repinning would be different, and a glitch initiated here would be expected to have different characteristics (e.g. involve a smaller moment of inertia or co,,, and thus result in a smaller Au). It may be difficult to explain within the co-rotating vortex model of Jones, since pinning is less prevalent and unpinned vortices are expected to remain **in their** new (co-rotating) state. Jones attributes small glitches to regions **where vortex creep** is sustained. Within the starquake model (according to Takatsuka Tam.agaki 1989), both the small and the large glitches in Vela are attributed to corequakes; the different characteristics of the smaller glitches could be due to heating effects of the preceding large glitch. Takatsuka & Tamagaki have no objection to a glitch in one part of the solid core transferring stress to another part, in fact they mention it as a mechanism for reducing predicted interglitch times to those observed.

8 Interglitch Behaviour: PSR 0833-45.

This chapter describes an investigation of the long-term (interglitch) rotational behaviour of Vela.

8.1 Overview of the Long-term Timing Behaviour.

From fig. 8-1 and from other analyses of Vela data, it seems the evolution of $i.(t)$ consists of three components:

- transients immediately following, and obviously induced by, the glitch;
- a long-term trend; and
- timing noise.

Each of these features is of interest; ideally we would like to model each separately.

An attempt to isolate the second component above was made as follows:

Estimate the time at which the transients have died out. 2nd-order models [i/$_o$, ii$_o$] were fitted to $\not/W$. The fits were of length 150d, shifted by 40d; the results are shown in fig. 8-1. From these plots, the first range of data over which i appears to be approximately constant (shown in fig. 8-1) was determined.

Estimate the magnitude of the timing noise. Removing the structure introduced by the timing noise is probably not possible, and certainly beyond the scope of this thesis. Since it is (generally) the least dominant of the three components, error estimates of the $z(t)$ data were adjusted so that uncertainties in model parameters allowed for the presence of the noise.

Estimate the number and magnitude of the transients. An estimate of was obtained from a fit to $ii(t)$ data over the range selected above. This model was subtracted from all ii(t) data following the particular glitch. Log-plots of the residuals were used to determine the range and approximate parameters of the next dominant exponential decay. This decay was then fitted to $ii()$ over the range determined, and removed from all data. This log-residuals, determine-range, fit-and-remove-decay process was repeated until all decay components were identified. The number and parameters of the components are listed in table 8-1. These values were later used as input for the model-fitting routine, when the parameters of the transients were refined (chapter 9).

Figure 8-1: Interglitch Behaviour of ii(t). (a) Pre-1985.

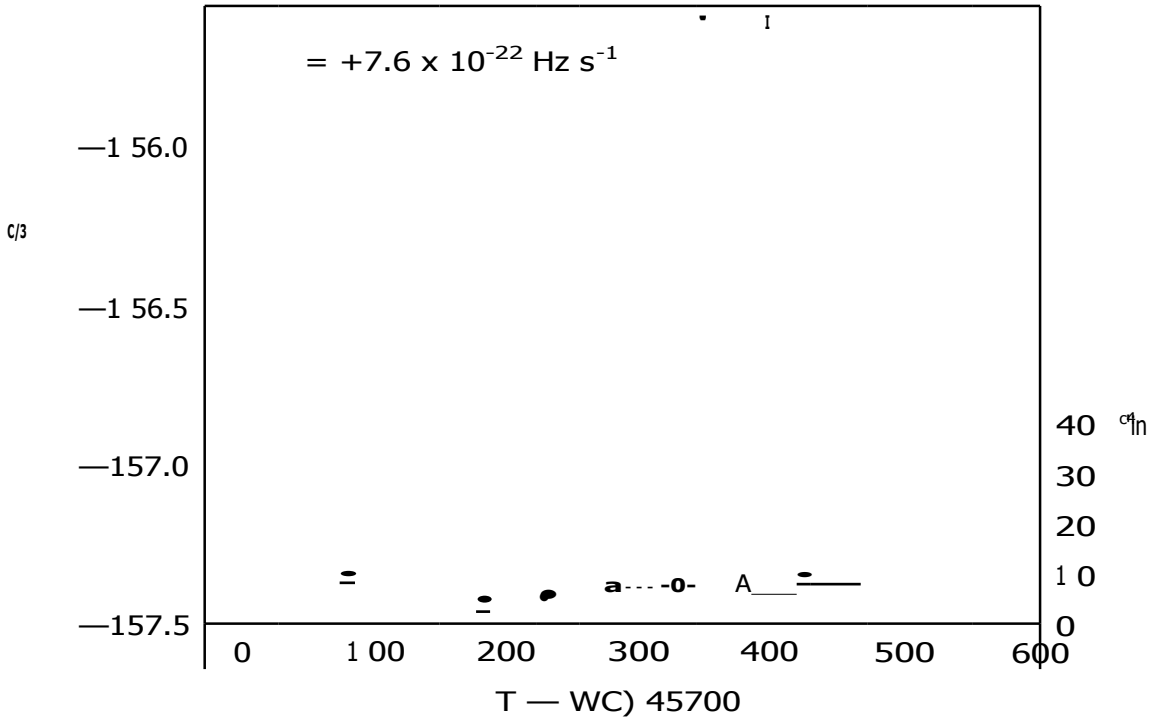

An expanded version of fig. 6-6. Large dots are values of I' obtained from -'150d blocks of data, shifted by 40d between fits (i.e. not independent), The dashed line indicates the earliest range over which this parameter appears to stabilize; the value obtained by averaging these data is given in the figure. The solid line shows a model with this slope, fitted to ii(t).
All graphs are plotted on the same scale.

a 1984.0 to glitch of 1985.

b Glitch of 1985 to glitch of 1988.

c Glitch of 1988 to glitch of 1991.

d Glitch of 1991 to glitch of 1994.
The small glitch of October 1991 is marked with an open arrow.

c Glitch of 1994 to 1994.8.

Figure 8-1: *(b)* 1985 — 1988.

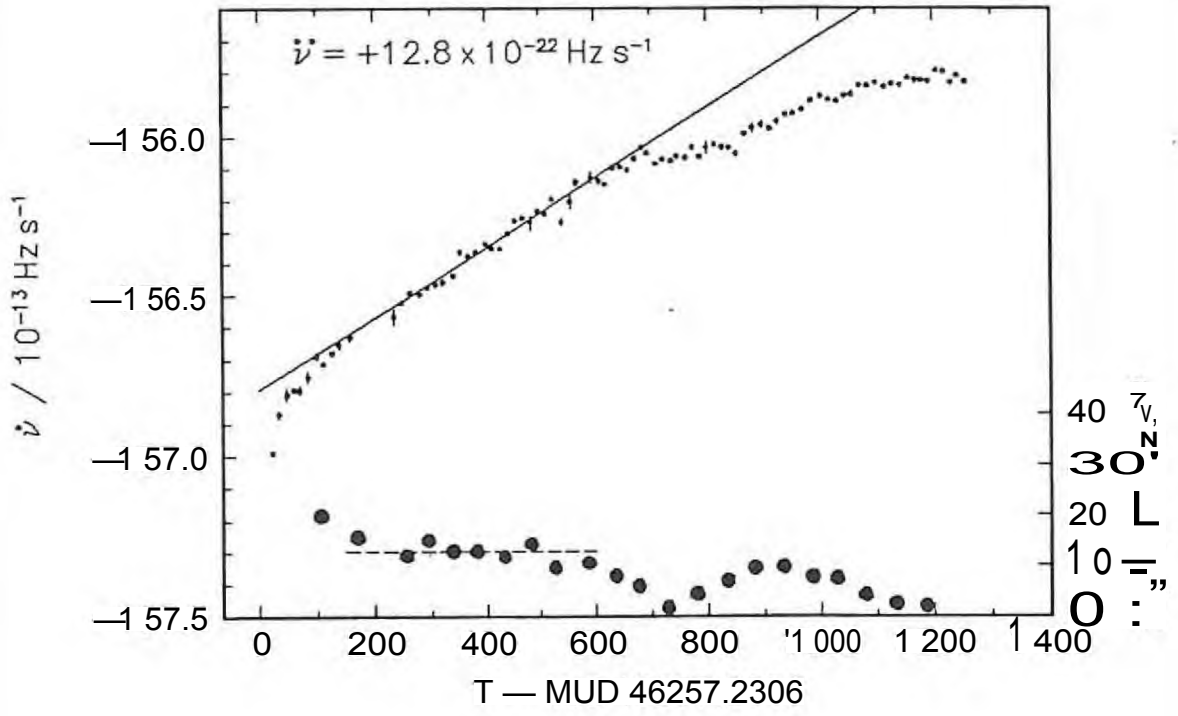

Figure 8-1: *(c)* 1988 — 1991.

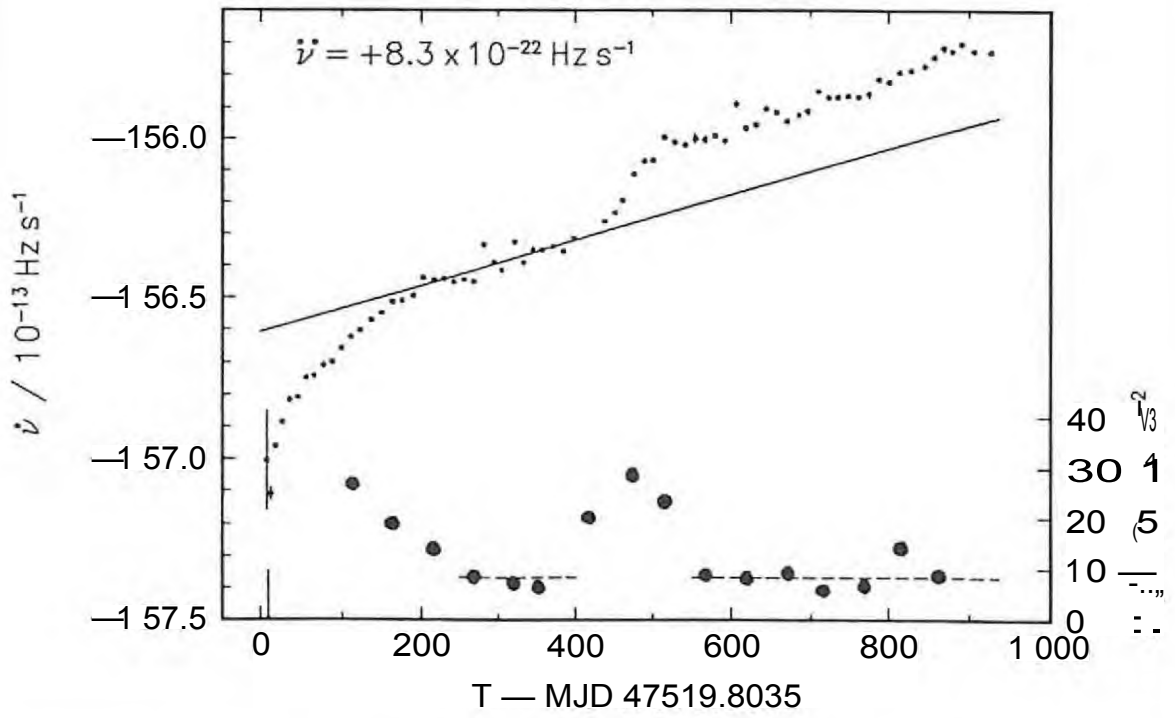

Figure 8-1: *(d)* 1991 — 1994.

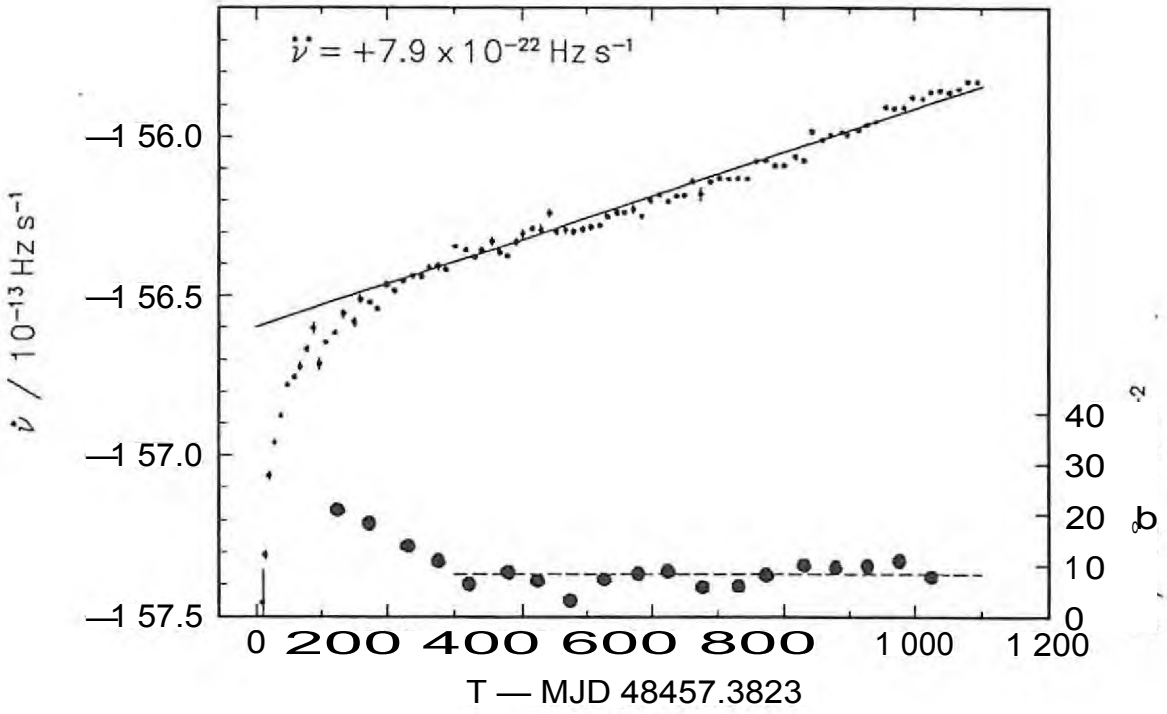

Figure 8-1: (e) Post-1994.

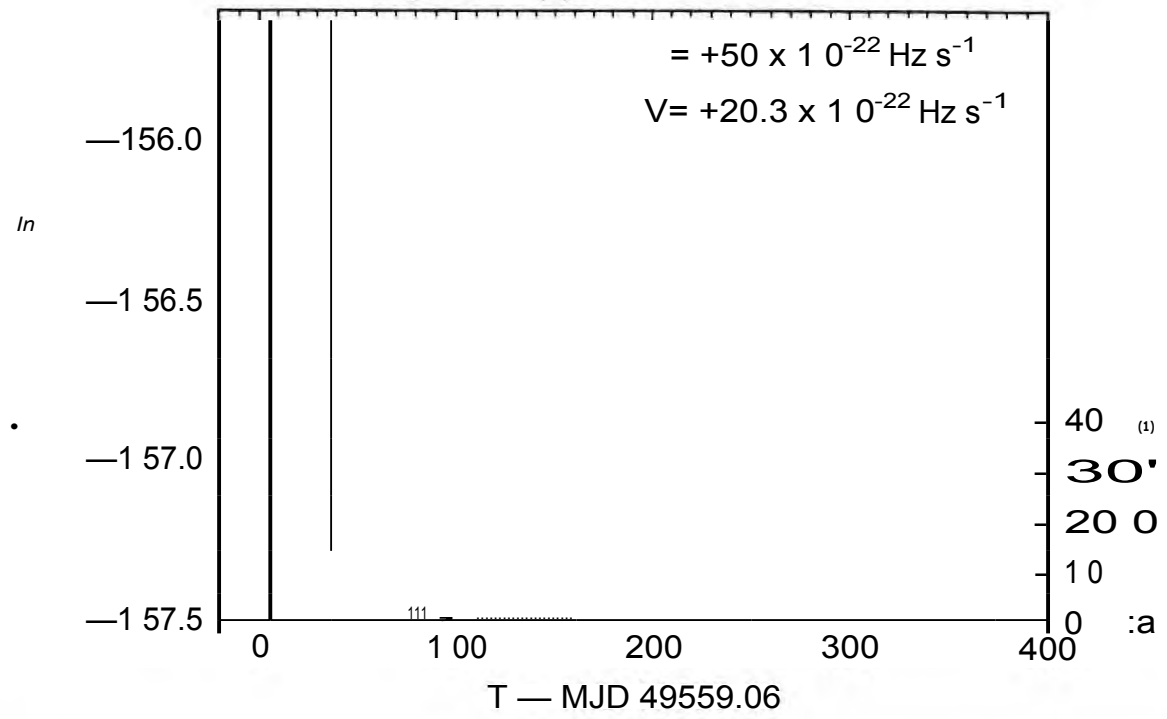

Table 8-1: Post-glitch Transients: Initial Fits.

Glitch:	1985	1988	1991	1994	1994A
σ_{TN} (10^{-13} Hzs^{-1}) :	0.013	0.022	0.014	0.02*	0.02*
(MJD) :	46450	47700	48687	49570	49 617
TN (MJD) :	46857	47930	49559	49591	49659
(10^{-22} Hzs^{-2}) :	+13.1	+8.3	+8.3	+50	+1.0
Log-plot estimates:					
(%) :	+0.26	+0.32	+0.38		
(d) :	40	70	60		
(%) :	+2.6 4	+1.9 4	+3.2 4	-0.64 4	+0.64 7
(%) :		+19	+64		+32
τ_3 (d)		0.4	0.5		0.4
X^2_R [1>1	209	84	356	2.4	6.2
X^2_R 1;1	14.5	25	55	2.5	5.6
x^2_R 1 decay] :	3.3	13.7	20.2	2.2	5.7
fif, i , 2 decays] :	2.1	3.3	4.8		6.0
xi [ii, i, 3 decays] :		1.4	2.8		

* The first row (σ_TN) gives the amount quadratically added to the error bars of the data in an attempt to compensate for the effect of timing noise on the model parameters. The first three values were estimated from the short-term scatter in during that particular interglitch era; the last two are based on the estimates from the earlier eras.

... TN is the range over which i first appears to stabilise following the glitch (marked in fig. 8-1).

is from a fit over the range T_t TN

"Log-plot estimates" refer to model parameters obtained from estimating successive decay components from log-plots of residuals, as described in the text.

The reduced X^2 (X^2_R) is calculated for various models fitted to the length of data from the glitch to $_{TN.}$ Comparisons between the various models are complicated by the fact that (a) different lengths of data following the various glitches are fitted, and (b) i) is kept constant for all fits.

Determine the form of the baseline. The form of the baseline (the long-term interglitch model) was investigated by comparing a number of different models fitted to lengths of data from TG,i + 300d to TG,i_{+i}, where TG,i is the epoch of the *ith* glitch. All transient components listed in table 8-1 have fallen below the noise level by this stage.

The remainder of this chapter deals with this last aspect of the analysis. Chapter 9 describes a more detailed investigation of the transients, which is best done once the form of the baseline has been determined.

8.2 Long-term Behaviour.

The data available for this project include:

- 555d prior to the 1985 glitch;
- three entire interglitch eras, of length 1 261, 937 and 1 102d respectively;
- e 32d data from the 1994 to the 1994A glitches;
- 186d of data following the 1994A glitch.

To avoid contamination by post-glitch transients, the 300d of data immediately following each of the 1985, 1988 and 1991 glitches were removed from the above data; the remaining data were then fitted with long-term models. The data following the 1994 glitches were not included in this analysis. The models fitted were:

Simple Linear Decay or i , i_0. This is the model convincingly fitted by Downs (1981) and Cordes *et* al. (1988) to 14yr of JPL Vela data, and used as a basis for theoretical interpretations by e.g. Alpar *et al.* (1993a).

Exponential Decay with a long time-constant, as fitted by e.g. Manchester *et al.* (1983) and assumed in the interpretation of e.g. Sedrakian *et at.* (1995):

$$Ali(t) \quad \text{Ai.exp(—tir).} \tag{1}$$

Third-order Polynomial or

Fermi Function as predicted by Alpar *et al.* (e.g. 1984a), and suggested by the behaviour of *i>(t)* following the glitch of 1988. No-one appears to have fitted this model to post-glitch data of any pulsar, and Alpar *et al.* (e.g. 1993a) seem to have discarded it. Such a term is described by

$$\mathrm{Ai/(t)} = \mathit{Al}\text{>}\ [\mathrm{i} \quad 1 + \quad \frac{1}{(e^{\cdot}\mathrm{toir} \quad 1)}] \qquad (2)$$

Segmented Model, in which the interglitch era is divided into a small number of segments, each of which is fitted with a $2\mathrm{Th}^{\mathrm{d}}$-order polynomial, resulting in a series of */Ai, i* $_{j}$. The end-points of the segments were selected as follows:

- remove a third-order polynomial (i/$_{0}$, i$_{o}$, *v$_{0}$)* from the data;
- run a median filter of length 100d across the data in steps of 10d, five times;
- use plots of these results to locate points at which a step, or the start or end of a slope, occurs, where the jump (instant or accumulated over the slope) is greater than the short-term scatter for that era;
- use plots of unfiltered residuals to refine the selection.

These apparent breakpoints are marked in fig. 8-2.

8.2.1 Timing Noise.

Timing noise is evident throughout the entire i(i) series, as scatter in the data well above the level of the error bars. Since the lengths of data fitted are generally at least an order of magnitude longer than the mean inter-data spacing, timing noise is dealt with by estimating a more realistic error from the scatter in the data and quadratically adding this to the formal error bars of each point. The scatter was measured for each interglitch era separately, from the three-sample variance (e.g. Rutman 1978):

$$\mathrm{a}TN = \frac{-}{9} \quad -21\mathrm{i}+1 + \quad . \qquad (3)$$

This estimate of the variance is insensitive to slow trends in the data. The error estimates are listed in table 8-2. They are very similar to the value of (51/ 0.02 x 10^{-13} Hz 5^{-1} obtained by Cordes *et al.* (1988) from an analysis of the variance of phase residuals for this pulsar.

This modification of the error bars compensates only for timing noise that is of the form of white noise in *i/(t.).* Noise of a higher order, such as steps (random walk) in *i'(t),* if present, will still affect the fitted models.

8.3 Evaluation of the Models.

The models were compared using:

plots of the residuals *(61/(t));*

weighted mean squared residual, or reduced x^2, $x_R^2 = x^2/dof$, where *dof* is the number of degrees of freedom of the fit; and

structure functions (1^3t- and 2nd-order); structure functions are described in appendix 7. They are a useful tool for discriminating between alternative underlying causes of the structure in residuals to a model — a slope in the structure function of order m that is also seen in the $(m+1)^1$h-order structure function indicates underlying noise. The type of noise determines the slope of the structure function. On the other hand, the effect of a polynomial of order m in the data will be apparent only in structure functions up to order 77Z

Model parameters and x_R^2 are listed in table 8-2. Plots of residuals and structure functions are shown in fig. 8-2. The results are discussed below.

CTTN 10^{-13} Hzs^{-1}	epoch MJD	Model	χ^2_R	N free	$\dot{\nu}$ 10^{-13} Hz s^{-1}	D_0 10^{-22} Hzs^{-2}	$\nu_{,0}$ 10^{-30} Hzs^{-3}	Ab_1iii %	T_i d	Ai/$_F$aIii %	T_{fII} d	t0,n1 d
Pre-1985: [Range fitted: 45 700 - 46257]												
0.022	45 970	1 i)	0.86	36	-156.69(6)	+6.9(9)						
		11 segment	0.86	36								
1985 - 1988: [Range fitted: 46 557 - 47519]												
0.013	47046.6	2 D, D	7.30	67	-156.58(1)	+7.7(2)						
		3 ii, exp	2.83	66	-155.54(6)			+0.88(1)	750(90)			
		4 D, v, ii	2.95	66	-156.81(2)	+7.7(1)	-11.4(9)					
		12 segment	1.83	55								
1988 - 1991: [Range fitted: 47 819 - 48457]												
0.022	48141.3	5 I>, I/	5.41	44	-156.70(2)	+13.1(3)						
		6 i, exp	3.00	43	-155.5(1)			+1.21(4)	460(90)			
		7 I/	2.91	43	-157.11(7)	+12.9(4)	-32(4)					
		8 D, D, FF	1.11	41	-156.45(4)	+9.3(8)				+0.12(1)	10(6)	466(6)
		13 segment	1.20	35								
1991 - 1994: [Range fitted: 48 757 - 49559]												
0.014	49147.5	9 I:, 1/	2.75	58	-156.621(7)	+8.2(1)						
		10 D, D,.1;	1.50	57	-156.47(3)	+8.1(2)	+9(2)					
		14 segment	1.58	55								

FE refers to a Fermi function.

*: D_0 is evaluated at the glitch epoch; it and ν_o are evaluated at the ephemeris epoch given in the table.

and T_i refer to model parameters of eqn. 8-1 (linear decay).

and $t_{o,ni}$ refer to model parameters of eqn.8-2 (non-linear decay).

Errors are 2c7 in the last significant digit quoted.

Figure 8-2: Models fitted to Interglitch Eras: (a) pre-1985.

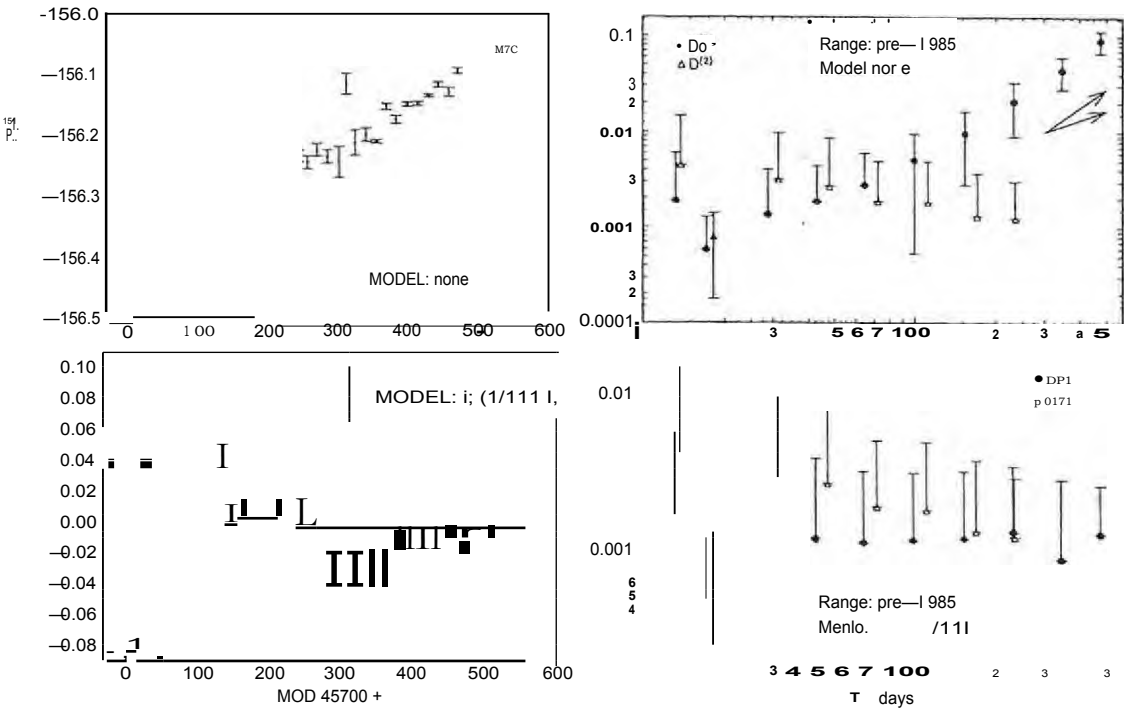

Residuals are plotted on the left, and structure functions of these residuals on the right

The model number following the model description refers to table 8-2.

Si- implies residuals to a model, as opposed to i> which refers to the original data;

Residual plots:

Original error bars are plotted; the amount by which this error has been increased prior to model fitting is the length of the thick bar following the model description in the residual plot (this value is given in table 8-2).

Arrows mark the points at which the data was segmented (for models 11 — 14).

Structure function plots:

First-order structure functions $D^{(1)}$ and $D_{5i}^{(1)}$ are indicated with circles (•);

Second-order structure functions $D_{2}^{(2)}$ and $D_{6i}^{(2)}$ are indicated with triangles (,L);

Upper error bars are the scatter in the mean for each bin (as opposed to the error in the mean);

Lower error bars are only plotted if they do not extend below zero.

Axes are log-log; slopes of 1 and 2 are shown with open-headed arrows.

Figure 8-2: *(b)* 1985 - 1988.

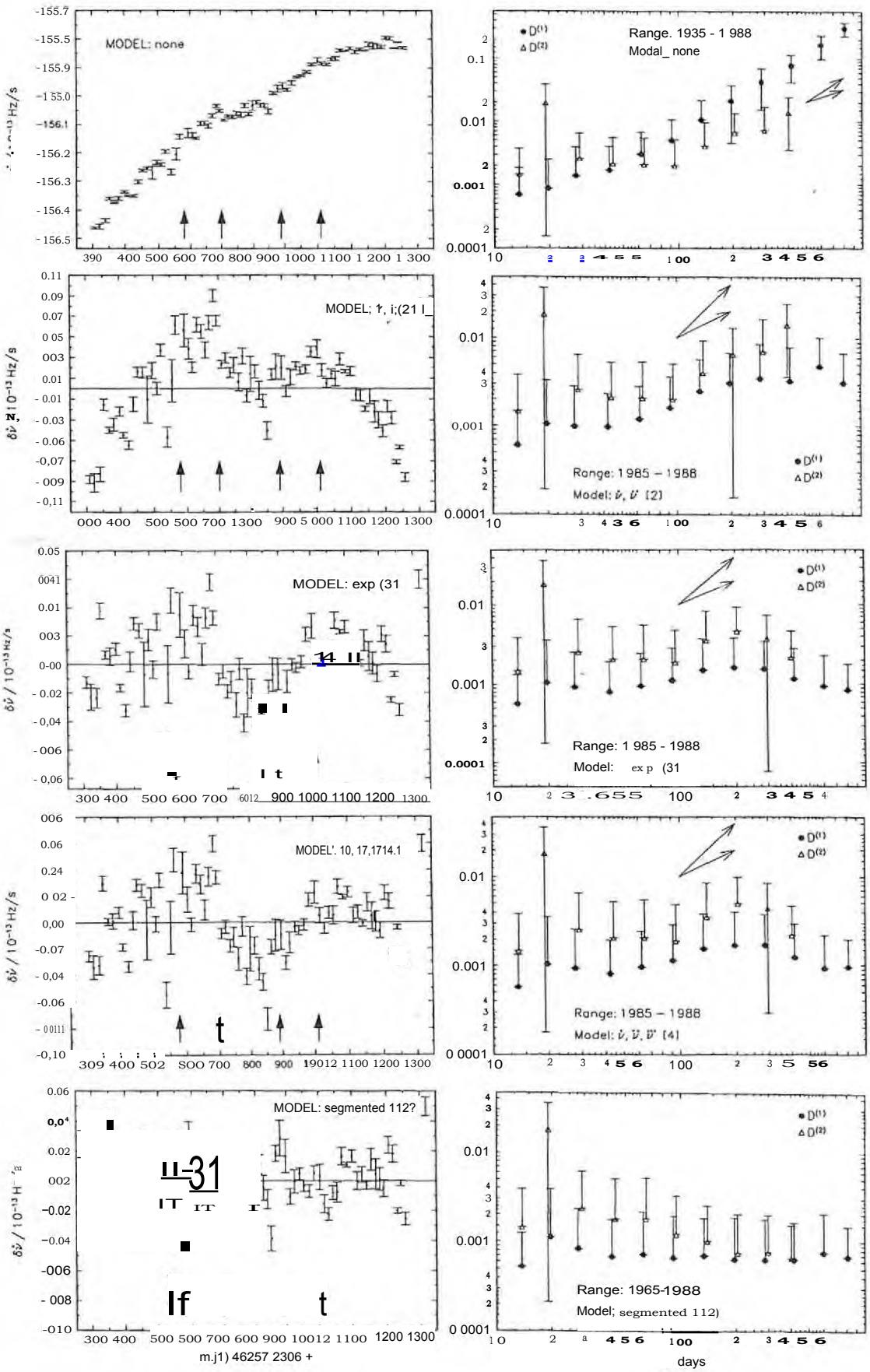

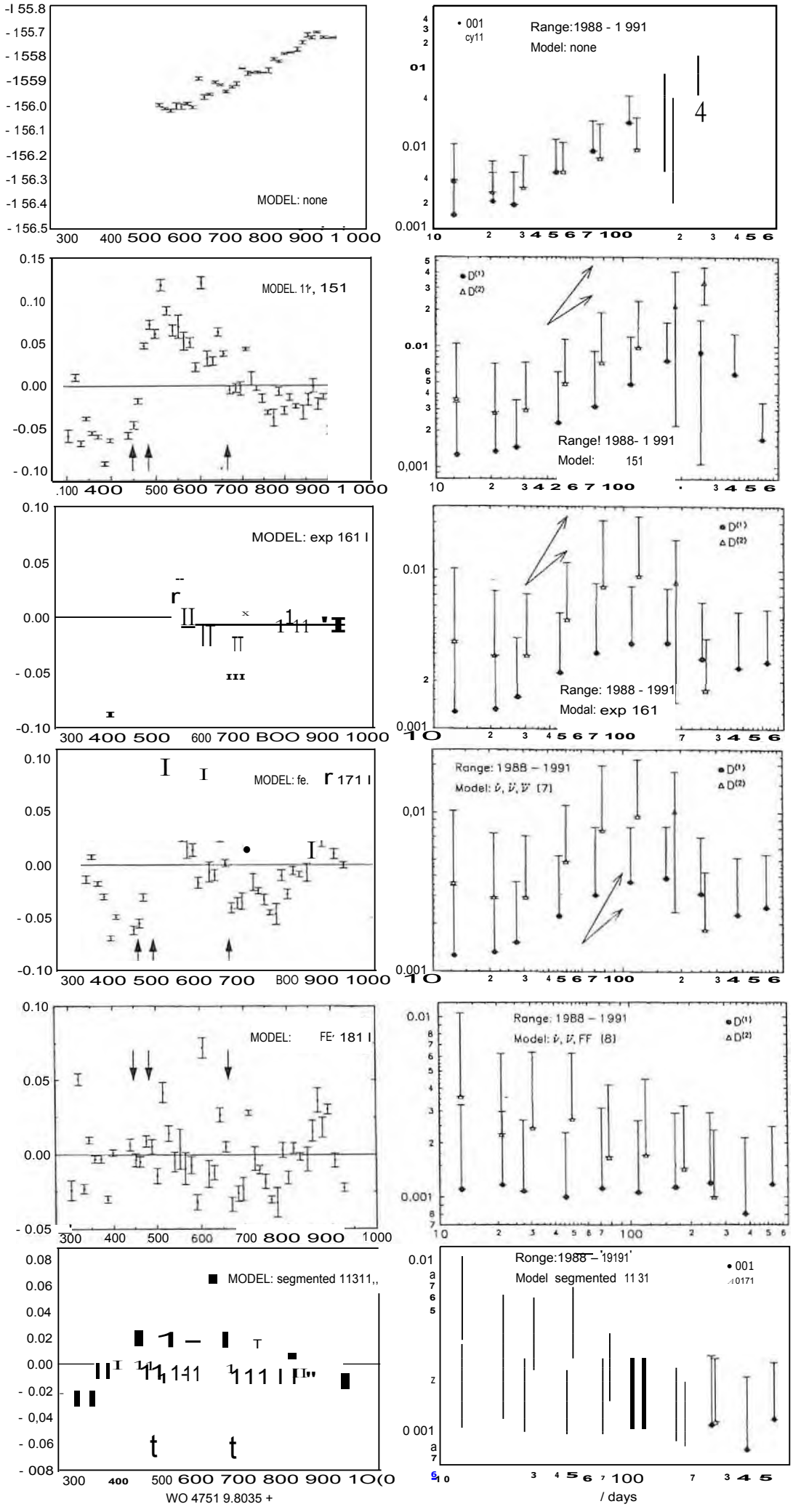
MODEL: none
Range:1988 - 1 991
Model: none
MODEL. 11r, 151
Range! 1988- 1 991
Model: 151
MODEL: exp 161 I
Range: 1988 - 1991
Modal: exp 161
MODEL: fe. r 171 I
Range: 1988 – 1991
Model: ν, ν, ν [7]
MODEL: FE· 181 I
Range: 1988 – 1991
Model: ν, ν, FF [8]
MODEL: segmented 11311,,
Ronge:1988 – 19191
Model segmented 11 31
WO 4751 9.8035 +
/ days

Figure 8-2: (d) 1991 - 1994.

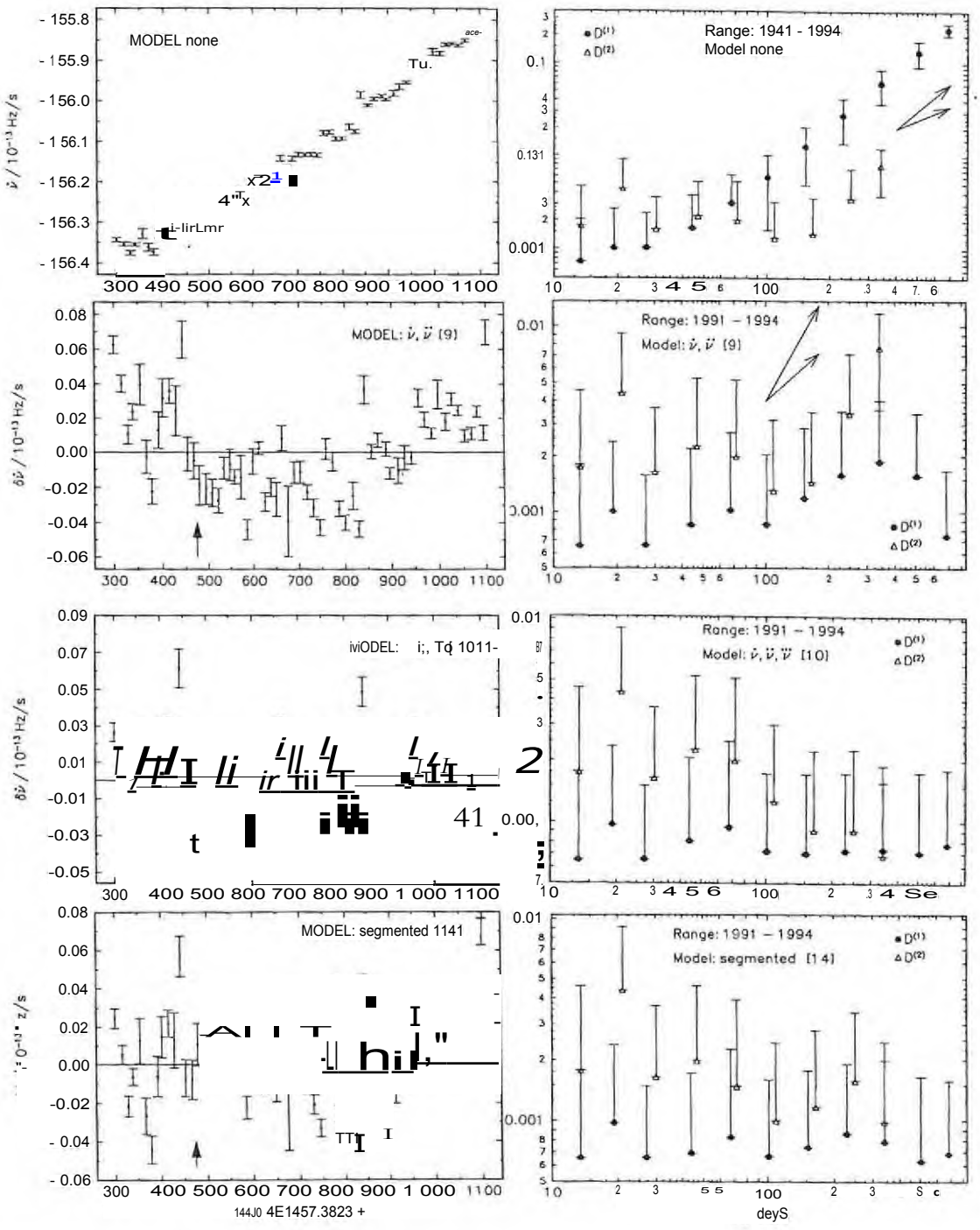

8.4 Results.

The simple linear decay model (1/, The only interglitch era for which this model is an adequate fit (as judged by x^2_R) is the pre-1985 era. The HartRAO data set includes only the data from *TG 4982+* 510 onward. For all other eras data from *TG* + 300 until the next glitch is analysed, generally around twice the length available following the 1982 glitch, and the linear model can be confidently rejected, since x^2_R is significantly improved by fitting one of the alternative models.

Third-order polynomial (I., F.", '**v**)**:** The inclusion of a term significantly reduces the residuals for the three interglitch eras- for which 900d of data is available. The justification for including an extra term can be evaluated by comparing x^2 for the fit with and without the extra term (Bevington 1969); for **all** three eras P(17= 0) < **0.001.**

Exponential Decay with a long time-constant: Where this model was successfully fitted (the interglitch eras following the 1985 and 1988 glitches), it was again significantly better than the simple linear decay model (as seen from comparing x^2) and indistinguishable from the third-order polynomial (the residuals are similar in shape).

Linear decay plus Fermi Function (i>, FF): This model was fitted to only the post-1988 glitch data, and was suggested by the apparently resolved step in *ii(t)* at around *TG* + 470. The fit appears to be excellent (x^2_R = 1.1) and the inclusion of an extra two terms is justified at the 3-cr level.

Segmented model (changes in *I/* **and** *ii):* The segmented model appears to be a fairly good fit for all four eras, which is not surprising considering the number of degrees of freedom sacrificed in the process of segmenting. Parameters of the segments are given in table 8-3, and plotted *(i;)* in fig. 8-3. Interestingly,

- of the eight segment boundaries, only three involve a significant change in all three involve an increase in magnitude;
- during two eras (post-1985 and post-1988) there appears to be a persistent value of *1)* 12 and 10 x 10^{-22} Hz s^{-2} respectively).

From the above, it appears that the linear (zi, model **is** inadequate, and that the correct model is either:

- exponential decay;

Table 8-3: Results of Segmented Fits.

T	$\Delta\nu/\nu$ 10^{-2}	$\dot{\nu}$ 10^{-22} Hz s^{-2}	T	$\Delta\dot{\nu}/\dot{\nu}$ 10^{-2}	$\ddot{\nu}$ 10^{-22} Hz s^{-2}
1982 + 510		+6.9(9)	1988 + 300		+10(3)
+1065			+446	+0.00(3)	+60(20)
1985 + 300		+12.8(8)	+483	—0.01(3)	+10(2)
+579	+0.01(1)	+12(3)	+664	+0.02(1)	+11(1)
+701	+0.03(1)	5(1)	+938		
+888	—0.01(1)	+11(3)	1991 + 300		+5.8(5)
+1009	+0.00(1)	+3.2(7)	+474	+0.020(5)	+9.1(2)
+1262			+1102		

Errors are *2-a.*

T gives the epochs of segment boundaries, relative to the most recent glitch epoch.
$\Delta\dot{\nu}/\dot{\nu}$ is the change in $\ddot{\nu}$ occurring at this epoch.
The third column gives $\ddot{\nu}$ for this segment.

- ll, i, 'v; or
- linear decay plus noise (jumps in I/ and

For the two eras where both the third-order polynomial and the exponential were fitted, the coefficients of the third-order polynomial are very close to those of the Taylor expansion of the exponential, evaluated at the mean of the era. These two models are thus equivalent.

The linear decay plus noise model appears to be the more likely model, since:

- 1 is negative for two eras and positive for the post-1991 era (or, the exponential for the post-1991 era involves an increase rather than a decay); this type of behaviour is (a) not encouraging when attempting to relate the model to physical behaviour of the star, and (b) expected if the higher-order terms are merely absorbing noise;
- The similarity in shape of the 1'- and 2nd-order structure functions, over the three eras in question, imply the presence of noise rather than higher-order polynomial terms, although the structure functions are marginal in many cases;
- When the slope of the fitted exponentials is compared to that of the data as shown in fig. 8-3 for the segmented models, it is apparent that the exponential is describing an average slope rather than convincingly modeling the data. In case the segmented model is biased towards extreme values of the slope, results of a second choice of segments are compared with the exponentials in fig. 8-4; the results provide further support for this conclusion.
- A noise event appears to have been resolved following the 1988 glitch.

8.5 Discussion.

The data thus suggests the long-term behaviour is a linear decline of accompanied by noise_ The persistence of a slope of —1 in the structure function plots is consistent with this noise being steps in *b(t).* There is some evidence for a persistent value of *1/,* of 10 + 2 x 10' Hz 5^{-2}. It would be worth looking for such behaviour in the 1 t yr length of JPL data.

The above supports the existence of a non-linearly coupled interior component. Should the long-term behaviour be due to the response of linearly coupled components, as for example in the "core shell" model of Sedrakian *et al.* (1995), one would expect the long term behaviour of *1)(0* to be an exponential decay, or superposition of such decays. In particular, the apparent existence of a persistent value of *i'* is in contradiction to this expectation.

Figure 8-3: Segmented Model: *i;.*

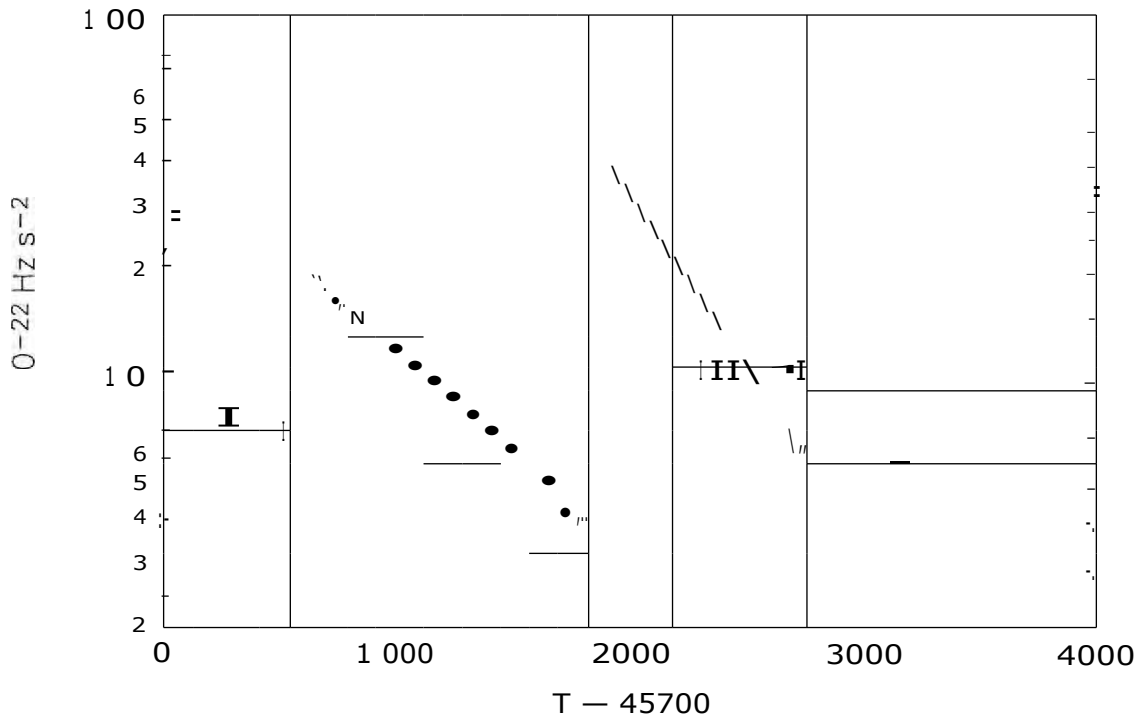

Segment slopes *(ii)* are plotted. Horizontal error bars indicate the range of each fit. Dashed lines show the slope of fitted exponentials.

Figure 8-4: i. from alternative Fits.

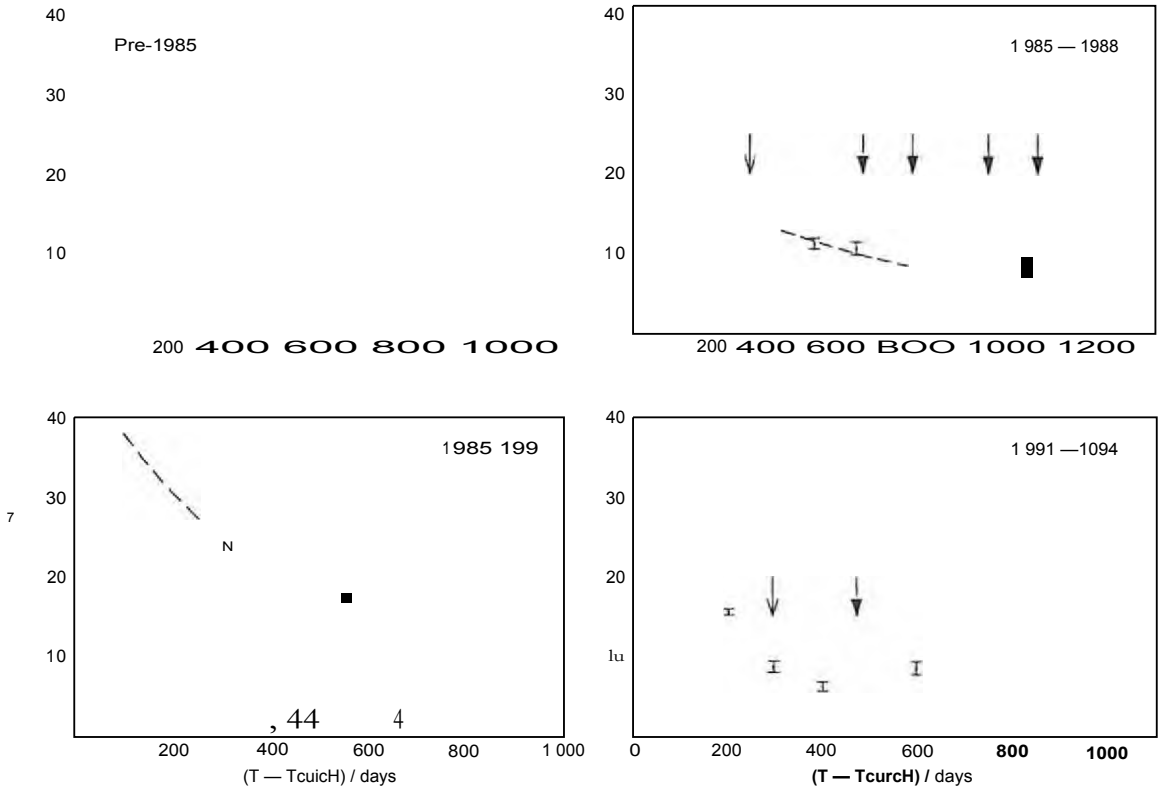

The plotted *i;* values were obtained by fitting 200d length blocks of i>(t) data with second-order polynomials. The blocks overlap by a factor of two (i.e. one value of every — 100d). Dashed lines show the slope of fitted exponentials. Arrows mark the boundaries of the segmented model discussed in the text and shown in fig. 8-3; open arrows mark the start of the first of these segments.

The discovery of the Fermi-function-type behaviour predicted by Alpar *el al.* (1984a) is a promising indication of non-linear coupling. According to Alpar *et al.* (1993a), the component in the post-1988 data would indicate recoupling of a fraction 0.12% of the total inertial moment of the star, over a timescale of 10 ± 6 d. This timescale appears to be rather short, compared to the value of r_{ni} = 32d obtained by Alpar et ad. (1993a) and associated by them with a region through which no vortex motion occurs. The fact that the offset time for the 10 d component is 466d > Afici I Si I— 15d implies that vortex motion *did* occur through this region. It must thus (within the vortex creep model) be located at a greater radial distance, i.e. in a region of lower density, than the 32d component. Alpar *el al.* associate such regions with longer timescales. Alternatively, the 10d component could be aSsociated with a previous glitch.

The rotational lag Lo of this region can be calculated from t_o I I; it is 4×10^{-3} rad s^{-1} if the region decoupled at the 1988 glitch; if it is associated with the previous glitch, the lag is 1.5×10^{-2} rads⁻i

However, the non-linear vortex creep interpretation is too simple to explain all aspects of this new feature: according to Alpar *et al.* (1993a), this type of behaviour corresponds to the recoupling of a finite extent of superfiuid, in the middle of the region of origin of a glitch - it should signal the complete recovery of the glitch, i.e. it should be followed by either (a) a reduction in ⅆ by an order of magnitude, *as* the surrounding regions become recoupled, or (b) another glitch. However, in the HartRAO data the recoupling event is followed by a resumption of the pre-event behaviour; in particular, i returns to within 20% of its prior value and remains at this value until the 1991 glitch.

The episodes of reduction in (e.g. following the 1985 glitch) may indicate the presence of non-participating regions, such as the "capacitors" proposed by Alpar et at., within the unpinning-repinning region. Or possibly non-axial symmetry could explain both these features.

8.6 Is there any Sign of the **underlying** ii0?

The standard energy-loss mechanisms predict i; nii^2/p, with n (the braking index) = 3. This gives a predicted 6.5×10^{-23} Hz s^{-2} for Vela. It has long been assumed that Vela is always in a state of glitch recovery. However, should this recovery be completed before the subsequent glitch, one would expect to see this underlying as a slope in the pre-glitch values of r_{p}. We now have nearly 26 yr of data, in which this value should be visible as a trend in Fig. 8-5 shows ii_{p} for the nine glitches for which sufficient data is available; the expected trend is not seen. Unsurprisingly, those glitches

which occur relatively soon after the previous glitch have a higher value of //pre, i.e. less of the jump in *ti* has recovered. A fit to all values of zi_{p},, yields = (4 ± 3) x 10^{-23} (1-o- error).

Interestingly, the rms scatter of the post-glitch values of ti *(i/p$_{ost}$)* plotted in fig. 8-5 is half that of the pre-glitch values //$_{pre}$ (0.10 compared to 0.19; Cordes *et at.* 1988 note that the latter value is interestingly low). This implies that ii_{pog}, rather than iip,,, indicates some sort of "baseline" behaviour of the spin-down. A straight line fitted to ii_{post} has a slope of +(2±2) x10^{-23} Hz s^{-2}, with a 3-o- upper limit of +7 x ^{1023} Hz s^{-2}. Thus i (and hence the braking index) may be smaller than the theoretically predicted value. This is consistent with the measured braking index of 2 n 3 of the handful of pulsars for which has been measured (e.g. Kaspi *et ad.* 1994).

The observation of a more stable long-term trend immediately after rather than before a glitch implies that glitches are triggered randomly, but return the pulsar to a particular state. For models in which the glitch results in the decoupling of interior components, this can be explained if the component responsible for the long-term behaviour is the same for each glitch — this component never fully recouples between glitches, and each glitch completely decouples it again.

8.7 A Comment on Exponentials.

At least one group (Sedrakian *et al.* 1995) has assumed that the linear model fitted by Cordes et *al.* (1988) approximates an exponential decay with a long time-constant. They obtain the decay timescale from the Taylor series expansion of the exponential (Sedrakian *et at.* 1995, eqn. 61) - *T* = where Ai› is the amplitude of the long-term linear recovery and thus also of the exponential decay. There are problems with this approach: firstly, as explained in the previous section, it seems that the pulsar never fully recovers from a glitch - it is thus not easy to estimate the amplitude of the decay. Also, the tirnescale of the long-term recovery, if interpreted as exponential decay, is similar to the interglitch time-span (although Sedrakian et *al.* explicitly state that the long-term decay time-constant is "much longer" than the interglitch time, in only one of the six glitches studied by them is the time-constant they obtain as much as 60% greater than the interglitch time; for three of the glitches, the time-constant is shorter than the interglitch time). Thus extra terms of the Taylor series expansion should be included, and i should be regarded as an average value of the decay slope, rather than (as Sedrakian et *al.* seem to have done) evaluating the slope at t = $_{t\,G}$•. Lastly, the investigation described in this chapter implies that the long-term recovery should not be modeled with an exponential decay.

Figure 8-5: Evidence for an underlying

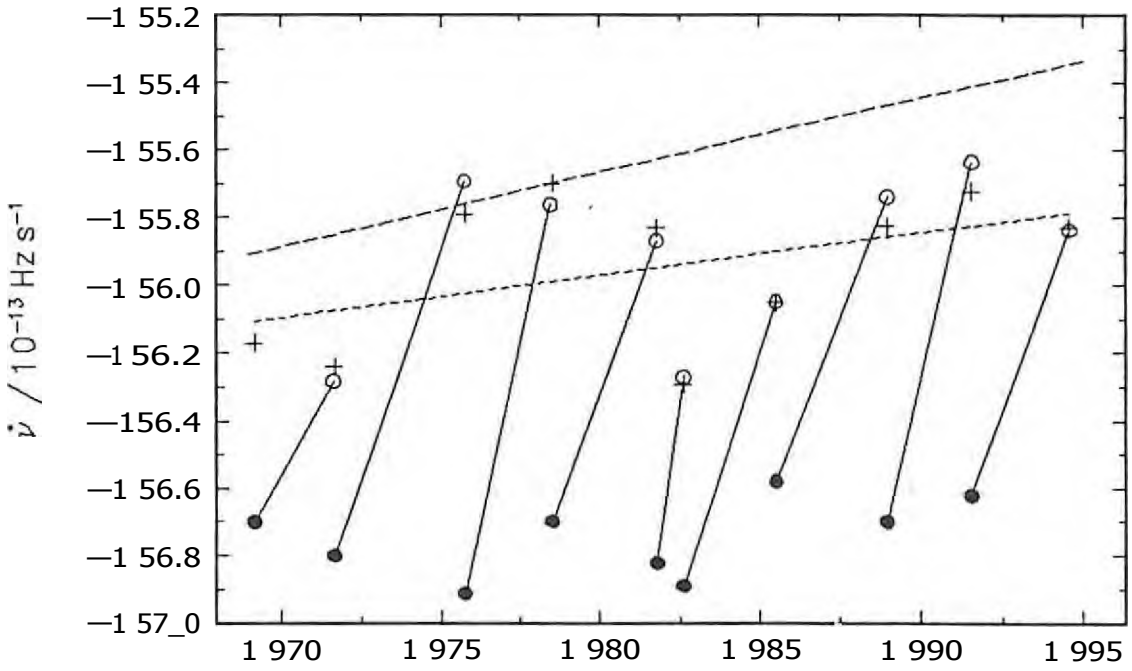

Solid lines are 2nd-order models fitted to Vela interglitch data. Parameters are from Cordes et al. (1988) table 2, and this thesis.

Filled circles (*) indicate post-glitch values of obtained by extrapolating the fits back to the glitch epoch.

Open circles (o) are pre-glitch values of $i/_{p'''}$, from extrapolation of the fits to the epoch of the subsequent glitch.

Pluses (+) mark observed values of $ii_{p'''}$, estimated from figs. 2 - 6 of Cordes et al., or obtained from 20-d fits to the HartRAO data.

The long-dashed line has a slope corresponding to the theoretically expected 6.5×10^{-23} Hzs^{-2}, and is drawn through the lowest of the observed pre-glitch points.

The short-dashed line is a fit to the observed $\mathbf{i}i_{p''}$ and has a slope corresponding to i) = $(4 \pm 3) \times 10^{-23}$.

Source: Cordes et al. (1988) and this thesis.

If (a) the long-term recovery is in fact an exponential decay and (b) the decay amplitude and timescale are the same after all glitches, then one should be able to determine both these parameters from a plot of slope (i)) of *ii(i)* versus the time t_s at which the slope is evaluated. Such a plot is shown in fig. 8-6, for the first nine glitches; t,, is the midpoint of the data range over which the straight line is a good fit. Fits to simulated exponential decays indicate that this choice of t_s is not correct, but is better than using $t, = t_G$. A decay time-constant T = 714Y5° d was obtained. Scaling these slopes by the presumed stimulus (glitch size Av) gives no improvement in correlation. This line of investigation was not pursued, since the JPL data set is available and it would be more productive to repeat the analysis described in this chapter on the original data.

8.8 Precursors?

Should a glitch be triggered by the completion of recoupling of an interior component, one would hope that a glitch precursor may be visible in the behaviour of 1/(t). For instance, an episode of rapidly decreasing I (increased *i..))* would be expected if the component is non-linearly coupled (Alpar *et al.* 1984). Fig. 8-7 shows i>(t) for the 500d preceding each of the five glitches observed from HartRAO. No such rapid recoupling is seen. In fact, four of the glitches occur after a short (-30 — 50 d) episode of *reduced i).* However, such episodes are common throughout the entire time-span plotted, for all four of these glitches. The smaller glitch of 1994A is noticably different in its pre-glitch behaviour.

Figure 8-6: Slow exponential Decay of Vela Glitches.

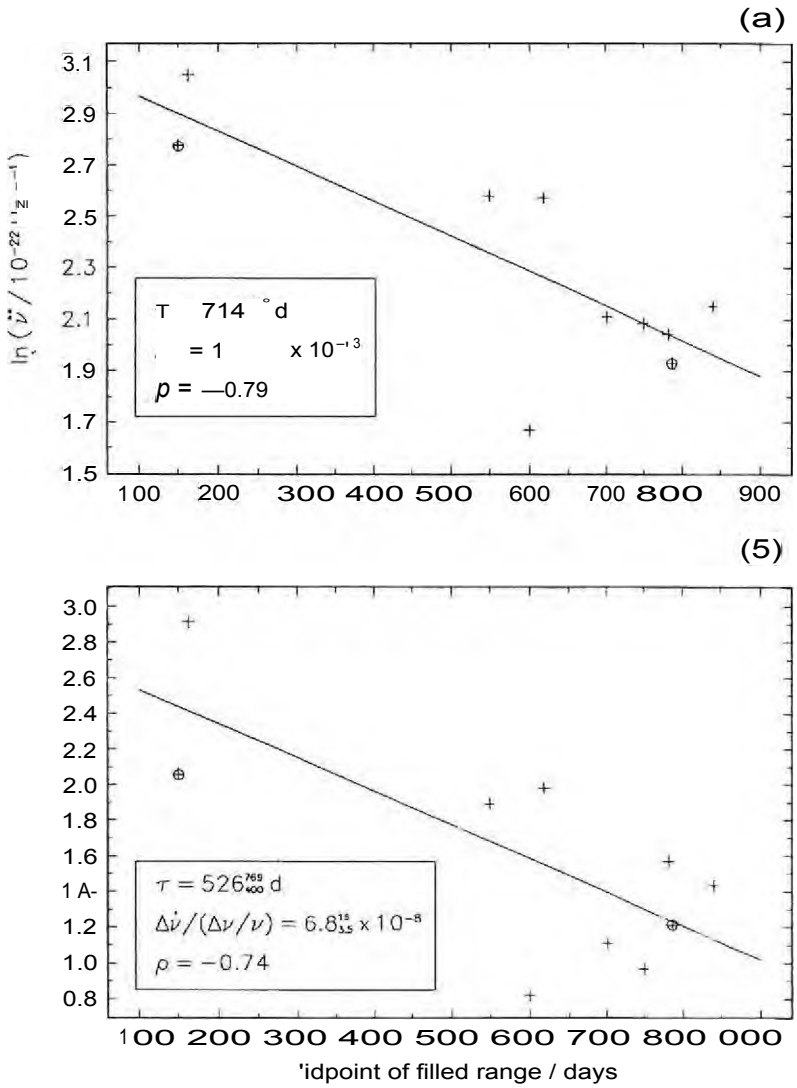

Fitted *i)* versus the midpoint of the range over which the linear model is a good fit. Parameters in boxes are from the plotted fitted line.

a If the long-term behaviour following each glitch is actually an exponential decay, with the same amplitude and time-constant 7 for each glitch, then all the points should lie on a straight line with slope 7^{-1}. Glitch-to-glitch variations in Ai> will introduce scatter about this line.
The circled points (e)) are from a fit to JPL data following the 1982 glitch up to approximately *TG* + 200d, and a fit to HartRAO data from the same glitch, from T_G + 500 to the subsequent glitch. The fact that both points lie the same distance below the fitted line indicates consistency with the plotted T (= 714d).

b Each point has been scaled by the glitch size

Figure 8-7: Pre-glitch Behaviour of *1/(0* in PSR 0833-45.

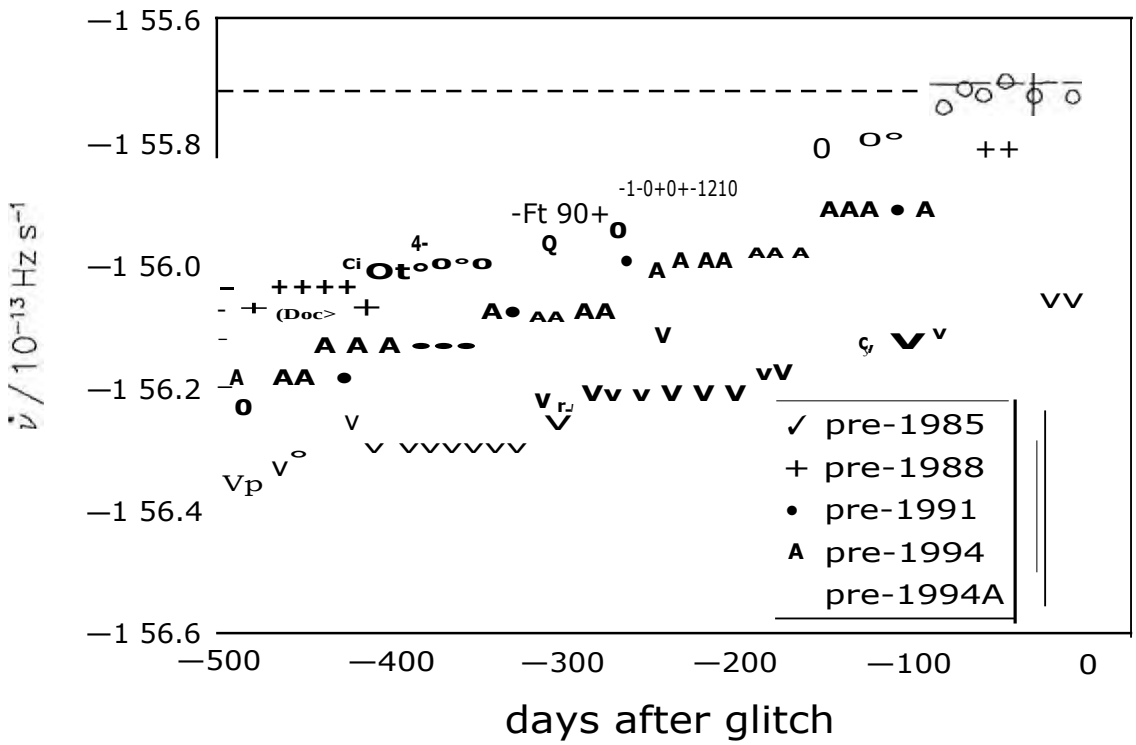

The evolution of i/(t) over the 500d immediately preceding the five large glitches observed from HartRAO. The dashed line has slope corresponding to the theoretically predicted value of $= 6.5 \times 10^{-23}$ Hzs^{-2}.

9 Transients induced by the Glitch.

As described in chapter 2, the immediate post-glitch behaviour is generally modeled with one or more simple exponential decays of the jump in *z(t)* or (equivalently) in v(t) or *cb(t)* (the transients). The theoretical model proposed by Alpar *et al.* (e.g. 1984b) also predicts a Fermi function behaviour for some components of the transient recovery. In this chapter the transients are modeled with the traditional combination of simple exponential decays. The long-term behaviour discussed in chapter 8 is also included; the final models are thus expected to describe all rotational behaviour, excluding timing noise.

9.1 The fitted Model.

Post-glitch recovery models were fitted to *i/(t)* (independent data) of each entire interglitch era. Simulations (appendix 8) show that the averaging affect of reducing the data to b(t) is not too serious. Initially, each era was fitted separately; later fits were made to the entire 11 yr. A baseline model of the form determined in chapter 8 (i.e. dependent on the particular interglitch era) was included in the fit, and the baseline parameters re-optimised, since a slight error in these parameters would cause transient-like edge effects.

The model fitted to each era is then:

$$z(t) = \quad + \mathrm{E} \quad \exp(-t/\tau_i) \qquad +V7/\,[1 \quad \frac{1}{1 + e^{-t/Tra}\,(\mathrm{eto\,Ni} - 1}\,{}_1 \qquad (^1)$$

Not all terms are included in every model.

9.1.1 Parameter Uncertainties.

These were determined by repeating the fit on 400 randomisations of the fitted model: the model was evaluated at each t-ordinate and these calculated values perturbed; the size of the perturbation was drawn from a Gaussian distribution with standard deviation equal to the assigned data error. Prior to fitting, all data errors were increased by quadratically adding the value of σ_{TN} listed in table 8-1, in order to make some allowance for the timing noise present.

Aids used in evaluating the fitted models are:

- reduced x^2 residual, x_R^2;
- plots of parameter values of 400 randomisations in which the data (not the model) were perturbed (examples are shown in appendix 8);
- correlations between the parameters obtained from these randomisations;
- plots of residuals Sii(t) and *v (t)* to the models.

9.1.2 Number of Terms in each Model.

This was determined by comparing x_R^2 for models with various numbers of exponential decay terms. x_R^2 was calculated over the first 100d of post-glitch data, since this is the time-span that affects the transient models most. The results are listed in table 9-1; they imply that:

- the 1985 glitch is adequately modeled with a single decay of *Ai);*
- three exponential decays are required to model the 1988 and 1991 glitches;
- although a single z>-term is not a perfect fit to the glitch of 1994, the inclusion of either a ii_o-term or an exponential decay does not improve the model;
- the same holds for the glitch of 1994A, although a single decay term helps matters slightly; additional decay terms do not significantly improve the model.

9.1.3 Baseline Models.

The form of the baseline models was discussed in chapter 8, for the first three glitches. There is only —30d of data following the glitch of 1994, until the 1994A event - a it-term was used as a baseline for this glitch. Following the 1994A glitch, there is less than 200d of data available. The recovery of *zi(t)* appears to flatten (i; ¬0) for -50d, shortly after the glitch; a ii model was used as a baseline, and all models fitted only up to the end of this 50 d period (i.e. up to Mil) 49659, or TG,i994A-I-68d).

Table 9-1: Test of Number of Terms in glitch Model — y^2_R.

Model	1985	1988	1991	1994	1994A
$ti_{t)}$				2.4 I 8	6.2 111
	136 8	59 15	271 1 15	2.5 I 7	5.6 I 10
baseline	42 1 8	—	271 I 15	2.4 I 8	6.2 111
baseline + 1 exp	1.3 I 6	18.7 1 13	82 I 13		5.1 I 9
baseline + 2 exp		7.1 1 11	14.9 I 11		5.2 I 5
baseline + 3 exp		1.5 1 9	1.8 1 9		

Values are x^2_R I dof, where dof is degrees of freedom.
$x^2_{\prime\prime}$ is calculated over -400d of post-glitch data.

"Baseline" models are: 1985: it+ —800d decay;
1988: it + ii_0±"Fermi function";
1991: ri_o + ii_0;
1994: ;
1994A:

The models selected for fitting each glitch individually are boxed.

1991 baseline model: From the comparison of baseline models in table 8-2, it seems that the inclusion of a z_0-term in the baseline is a significant (> 3o-) improvement. However, this term appears to be modeling timing noise and is highly dependent on the length of data fitted. Successively longer fits, all commencing at the epoch of the 1991 glitch and including the three transient terms, had varying from —10^{-}' to +10', corresponding to a variation in r of -1000 to +1000. in contrast, a similar test done on the post-1985 glitch resulted in variations of the long exponential around r = 720 ± 80d. The 1-term was thus omitted from fits to the 1991 glitch.

9.2 Results: Independent Models.

The results of fitting eqn. 1, with the number of terms determined from table 9-1, to each individual glitch, are listed in table 9-2. Figs. 94 and 9-2 show '--100d of post-glitch and v-residuals respectively. Residuals to the 1994 glitch are shown in fig. 9-4. Note that the parameters obtained for the baseline models, from these fits to all the data, are essentially the same as those obtained in chapter 8 (table 8-2) from fits that excluded the first 300d of post-glitch data, for the glitches of 1988 - 1991-

9.3 Common Parameters?

The results of table 9-2 suggest that some parameters may be common to all glitches. Alpar *et at.* have found that the recovery from each of the first nine glitches can be satisfactorily modeled by assuming three decay components with timescales that remain constant from glitch to glitch. The time-constants, obtained from fits to the first eight glitches by Alpar *et al.* (1993a) and verified, by Chau *et at.* (1993) by a fit to the 1991 glitch, are: 0.42 d, 3.2 d, and 33 d. In addition, the (model-dependent) moments of inertia associated with the two faster decays can also be restricted to the same values for all nine glitches. The moment of inertia of a linearly-coupled component is (e.g. Alpar *et at.* 1993a, Sedrakian *et al.* 1995)

$$Jill = \$27,1\text{Aftc}, \qquad (^2)$$

where Afic is the size of the spin-up.

Since the HartRAO data is of better quality (denser coverage) than that available to Alpar *et at.,* the five glitches reported here were modeled simultaneously, and various combinations of 73 and /-; were restricted to the same values for all five glitches. Results are listed in tables 9-3 (a), 9-4 (7), and 9-5 - 9-7 *(Ii).*

9.3.1 Common Timescales.

Since any physically reasonable glitch model would incorporate common decay timescales more easily than it would common inertial moments, the decay timescales were restricted first. It seems (as Alpar et *at.* found) that the timescales of all three transients can be restrained in this way. In fact, fixing the timescales to the specific values obtained by Alpar *et al.* yields residuals only slightly inferior to those of the original model in which all glitches were fitted independently. The residuals to this fit are shown in fig. 9-5. The only real difference between these residuals and those of fig. 9-1 is small systematic variations over the first —40d following the glitches of 1988 and (to a lesser extent) 1991.

Table 9-2: Glitch-recovery Models: Each Glitch individually fitted.

			1985	1988	1991	1994	1994A
baseline model:							
ii(T_G)	10^{-13} Hzs^{-1}		-155.52(3)	-156.44(3)	-156.62(4)	-156.54(3)	-156.44(3)
$1_{\cdot 0}$	10^{-22} Hzs^{-2}			+9.1(7)	+8.2(2)		
Abniiii		%		+0.11(2)			
$T_{i/i}$		days		9(6)			
t_o		days		468(6)			
		%	+0.88(2)				
T		days	790(40)				
transients:							
				+0.26(4)	+0.45(6)		
Ts°		days		70(20)	41(6)		
Aii$_5$/ii		%	+2.4(3)	+1.3(5)	+2.9(7)		+0.2(2)
T5		days	6.9(4)	5(1)	4.1(6)		10(7)
				+21(6)	+70(10)		
To.5		days		0.49(9)	0.44(4)		

The components listed in column 1 are those of eqn. 1.
TG is the glitch epoch.
In this and all subsequent tables, component subscript 50 refers to a decay over —50d ("intermediate" component of Cordes et al. 1988), etc.

Errors are 2-o- in the least significant digit quoted.

Figure 9-1: Residuals to Models fitted individually: $S_i(t)$.

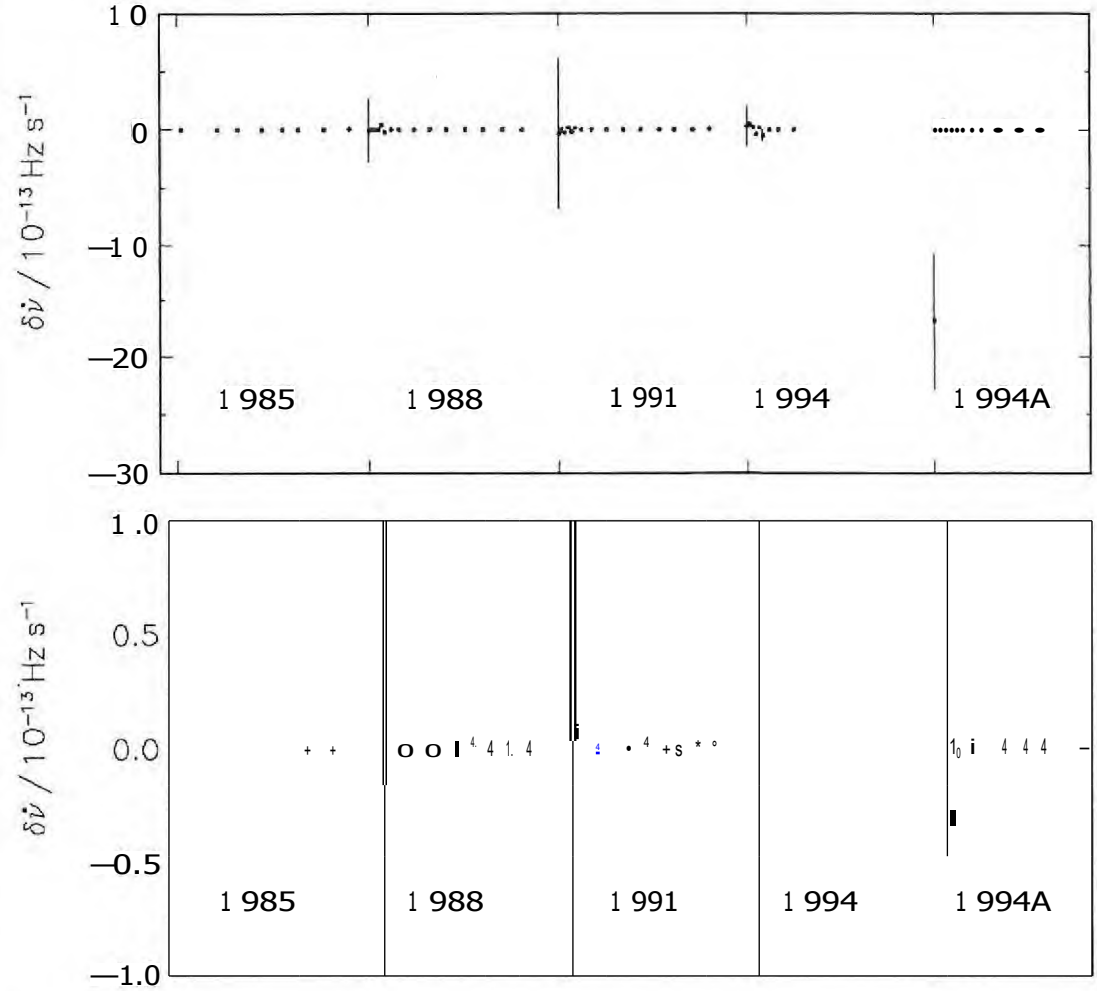

The upper panel shows all residuals.
The lower panel is an expanded view.
About 100d of data are shown following each glitch.
Model parameters are listed in table 9-2.

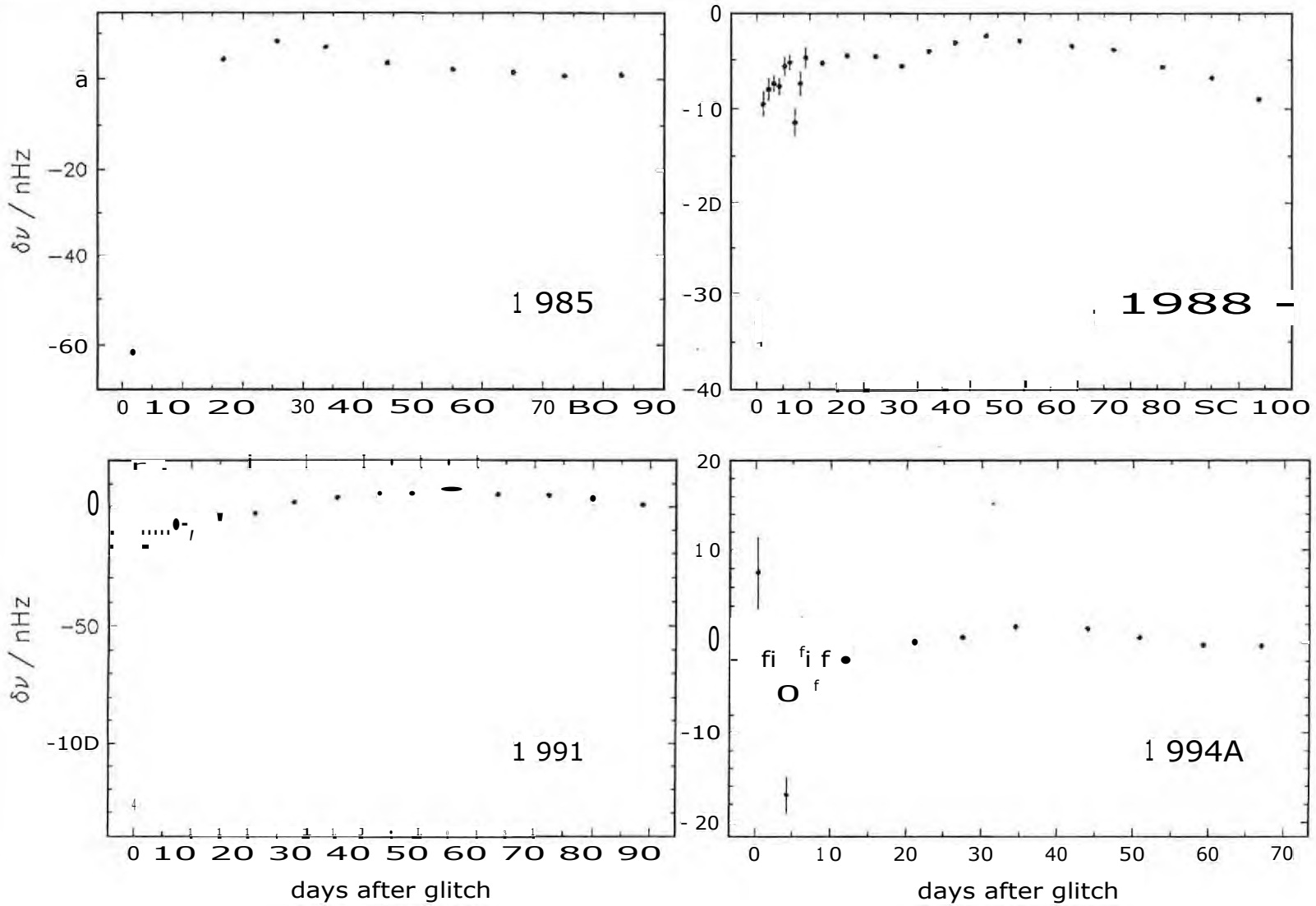

Figure 9-2: Residuals to Models fitted individually: $\delta\nu(t)$.

Model parameters are listed in table 9-2. Residuals to the first glitch of 1994 are shown in fig. 9-4.

Hoping to get better estimates of the timescales (since the HartRAO data is more densely sampled and the timescales in question are short), we then obtain all three timescales r5, $7_{0.5}$) from a simultaneous fit to all five glitches. The resulting residuals are very similar to those of Alpar *et al.*, although the timescales and amplitudes are slightly different. In other words, even though the data is presumably better, we do not seem to be able to improve on the results of Alpar *et al.* Perusal of table 9-3 gives the reason for this: the additional decay terms use up valuable degrees of freedom — the initial HartRAO fit (with each glitch fitted independently), in which the number of model parameters required was carefully determined, has more degrees of freedom. This implies that the model with simultaneously fitted Ti may be over-specified. A specific example is the glitch of 1985, for which. the amplitudes of the two shortest decays must be determined from only one point. We thus then proceed to retrieve degrees of freedom by restricting some of the decay *amplitudes,* as described below.

Before proceeding, though, we note that table 9-3 shows that the HartRAO fit with simultaneously fitted r is probably a better estimate of the timescales than the results of Alpar *et* a/. (at least for the five HartRAO glitches) — the HartRAO model weights the fit so that the better-sampled eras of post-1988 and -1991 influence the model more (line 3 of the table). Thus we retain the feature of common timescales for all decay components, as opposed to adopting the values of Alpar *et* al., while searching for common amplitudes for some of them.

9.3.2 Common Amplitudes.

The amplitude of a decay component is restrained by requiring a common moment of inertia for all glitches (eqn. 2). Most combinations (inertial moments of one of, pairs of, and all three components) were fitted. Results are shown in tables 9-3 $_{(xi)}$ and 9-5 - 9-7 PO.

The --13.5 d Component. It is immediately apparent that any fit involving a common $/_{0.5}$ (i.e. the fastest, d, component) is not satisfactory_ The residuals to the 1991 glitch, which is both large and well-sampled, cannot be kept to a reasonable level while restraining $/_{0.5}$ (lines 4, 7 and 9 of table 9-3). Also, note that for all other fits (i.e. in which $/_{0.5}$ is not restrained), 10,54988 is significantly different from /0,54991.

Alpar et *at.* found that $/_{0.5}$ = (5.9 ± 0.6) x 10'/ and $/_5$ = (1.5 + 0.1) x 10^{-3}/ for the data available to them. Residuals to a model in which both $/_{0.5}$ and $/_5$ were restricted to common values among all five glitches are shown in fig. 9-6. They are further evidence that this model is not correct. It is not clear why the inertial moments obtained by Alpar *et al.* are so different from those

obtained from the HartRAO data, although the actual decay amplitude for the 1991 glitch quoted by Chau et *al.* (1993) is smaller than that obtained from the HartRAO data.

The —5 d and ~--50 d Components. It is possible to simultaneously restrict both these components for all five HartRAO glitches. In fact, for the three fits in which either or both of the components are restricted, the resulting *I* of both components are generally similar (within the quoted errors listed in tables 9-5 - 9-7). However:

- Alpar *et al.* found that it was not possible to restrain I_{50} for the first nine glitches' (including the six not observed from HartRAO); and
- the ~50d timescale associated with I_{50} is similar to that of the general timing noise — in other words, in fits such as these, which simultaneously optimise the parameters of the baseline model, the fitting routine can adjust the baseline parameters to satisfy the requirement of restrained I_{50} and τ_{50}; this in fact happened for the 1985 glitch, in which the fitting routine increased the baseline timescale from (--800d to —1 000d.

Conclusions. We thus conclude that:

- a model that incorporates three exponential decay components with timescales of 49±8, 5.4+0.7, and 0.49+0.03d for all glitches, is a satisfactory fit to the HartRAO data;
- the inertial moment associated with the 5.4d decay is (5 + 1) x 10^{-3} / for all glitches;

Residuals to this model are shown in fig. 9-7. The errors quoted above are *2-0-;* simulations described in appendix 8 suggest that decay parameters obtained in this way can be in error by up to five times the formal 1-a error. In this case, a more realistic estimate would be:

T_{50} = 50 + 20 d
I_5 = 5 ± 2 d $\qquad I_5/I = (5 + 3) \times 10^{-3}$
$\tau_{0.5}$ = 0.49 + 0.08d

- it is not possible to similarly restrain the inertial moment associated with the 0.49d decay.

9.4 Small Glitch of 1991'.

This glitch was modeled simultaneously with the larger one of 1991. the simplest model (a single decay of *Ail)* is adequate; no extra parameters (such as a permanent offset in *it)* could be fitted, as they were highly correlated with the decay parameters of the 1991 glitch. There is thus no justification for regarding the 1991' event in *ii(t)* as anything more complicated than a short-lived perturbation to the recovery of $A1>_{1991}$, although it does appear to introduce a long-term change in v(t) (fig. 7-1). The perturbation to ii(t) has amplitude Az:/ii = (5 ± 3) x 10^{-4} and timescale T = 30 + 20d.

9.5 The Glitches of 1994.

The glitch of I994A is both unusually small and occurs unusually soon after the previous large glitch. In chapter 7, it was suggested that this event may belong in a separate class, with those of 1971' and 1991', although it is an order of magnitude larger than either of these. Fig. 9-3 shows the evolution of zi over the first 180d following all five glitches, superimposed for easy comparison. It in fact appears that *both* glitches of 1994 are atypical (when compared to the other three plotted in the figure). Note that, although fig. 9-3 does not show the full scale of the recovery of the first three glitches, all post 1994 and 1994A data are shown. The difference is not an effect of different pre-glitch conditions — all five pre-glitch values fall within the upper half of the graph. The scatter in pre-glitch values for the "typical" glitches of 1985 — 1991 is large when compared to the post-glitch behaviour for the same glitches from about 20d after the glitch. For the 1994 glitch, on the other hand, the pre-glitch value of i is the same as that for the 1988 glitch.

It appears from fig. 9-3 that the behaviour of *zi(t)* at the time of the first glitch of 1994 may be a slow transition from the pre-glitch to the post-glitch state. This is more clearly seen in the behaviour of *v(t)* (fig. 9-4); a fit to these data gives

$$\text{Aviv} = (1.0 \pm 0.3) \times 10^{-9}$$
$$= 2.0+0.9\text{d},$$

which corresponds to *L1>/ii* = —(4 + 3) x 10^{-3} (all errors quoted are 2-a).

This transient is in the opposite sense to those observed in the other large glitches, and is clearly visible above the level of the timing noise in fig. 6-5e. It could be regarded as a fraction (0.11 ±0.03)% of the spin-up that is resolved. Such a component, if present following the other glitches, would have been completely overwhelmed by the transients in *ii(t).* Lyne *et al.* (1993) report

Figure 9-3: Recovery of At': All Glitches.

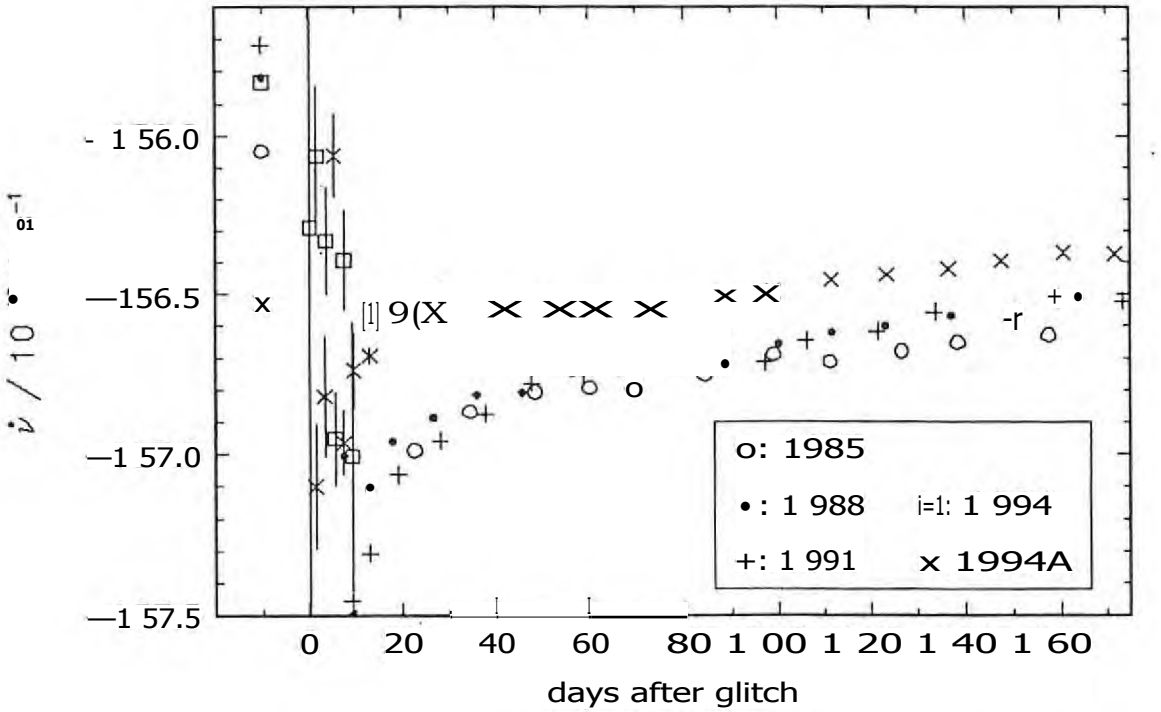

The recovery of Ari over the first 180d following the glitch. Original (i.e. unscaled and unmodeled) values are plotted. Pre-glitch values of it (from table 6-1) are shown on the left.

Figure 9-4: 1994 residuals.

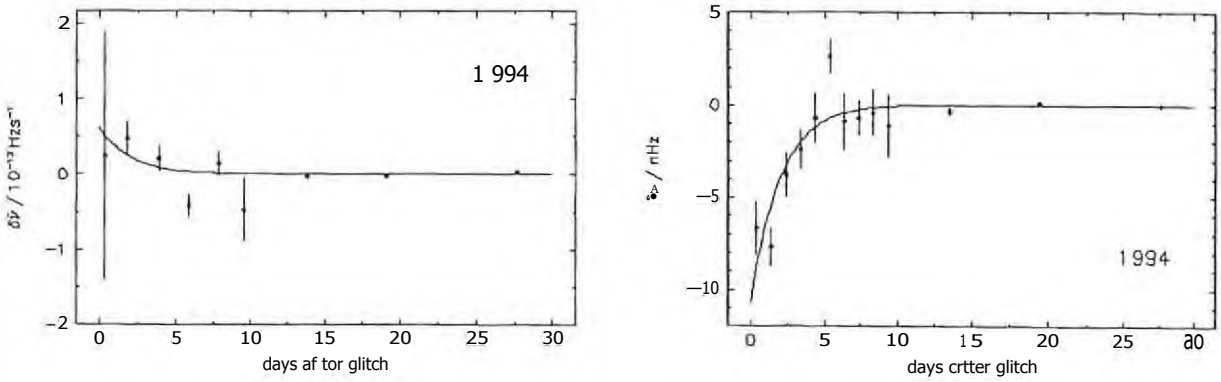

51ʳ (t) (left) and i5v(i) (right) residuals to the model listed in table 9-2 [ii0]. A transient of amplitude = 0.4% (Av/v = 10^{-9}) and timescale r 2d, obtained from a fit to 6 v(t) , is plotted over the data.

a similar feature following a glitch in the Crab pulsar; the fraction of the spin-up resolved was 27%.

The behaviour of *ii(t)* following the 1994A glitch is also rather different from that of the 1985 — 1991 glitches, as can be seen in fig. 9-3. Specifically, *r7(t)* approaches a stable value within ~25d of the glitch, at which point it appears to remain unchanged *(i;* constant) for whereupon the steady decline seen following the 1985 — 1991 glitches is resumed. Interestingly, the flattening occurs when 1/(t) reaches its pre-glitch value.

This flattening is confirmed by a fit to the phase residuals of TG,1994A + 25 d to TG,1994A ⁻F 75 d, which giv'es = +(1.310.4) x 10^{-22} Hz s^{-2}, a value way below any of the long-term interglitch values listed in table 8-2, arid comparable with the expected value +6.5 x 10^{-23} for long-term energy loss. This feature has the appearance of the non-linear term suggested by Alpar *et al.* (1984a) — no recoupling appears to be occurring over this 50 d period, whereupon behaviour similar to that following the earlier glitches resumes. However, more data is needed to confirm this.

9.6 Timing Noise following the Glitches.

Scatter in ii(t) following the large glitches is large; in at least one case 7 d after the 1988 glitch) there appears to be a small spin-down with a clear recovery (fig. 9-2); this feature is prominent in v-residuals to all post-glitch models fitted. The amplitude of the event depends on the glitch model assumed; it is $Aviv$ = —(5.6 ± 1.4) x $10^{-1°}$ *(la* error) for the best-fitting model. A less convincing "event", involving a small spin-up, is seen about the same time after the 1994A glitch.

Although such a small change in the spin-rate may seem insignificant compared to the glitches discussed here, if verified it may pose a serious challenge to most models involving vortex un-pinning as the cause of a glitch: if the region of pinning where the glitch originates is non-linearly coupled to the crust, then this region should be completely decoupled at the time of the glitch, and remain in this state until the differential velocity between the two components has regained at least its pre-glitch value. This corresponds to a time of Mk'/ 1fI which is–15d for the 1988 glitch.

9.7 Alternative Measurement of I.

Although inertial moments of various components are discussed above, the extraction of these values (e.g. tables 9-5 — 9-7) from the post-glitch behaviour depends on assumptions about the type of coupling involved between the components (e.g. linear or non-linear).

Table 9-3: Glitch Recovery Models: x^2_R from common Components.

Parameters restricted	1985		1988		1991		1994		1994A		All	
none	1.3	6	1.5	9	1.8	9	2.4	8	5.1	9	2.5	41
7_{50}=33 d , 7_5=3.2 d, $7_{0.5}$=0.42d	2.2	5	3.2	12	2.0	12	2.5	5	4.7	8	2.9	42
T50, T5, T0.5	6.0	5	2.1	11	1.8	11	2.7	5	5.8	7	3.2	39
T50, T5: T0.5, 10.5	4.4	5	2.6	12	4.1	12	8.1	5	5.7	8	4.4	43
T5O• T5, T0.5, 15	4.0	5	2.3	12	2.3	12	7.2	5	5.2	8	3.6	43
750, T5, T0.5, 150	6.6	5	2.0	12	1.6	12	3.1	5	5.7	8	3.2	43
150, T5, T0.5, 15, 10.5	3.6	6	5.0	13	6.3	13	18	6	5.0	9	6.9	47
T5ø, T5, TO.5, 150, 15	4.4	6	1.9	13	2.5	13	7.5	6	5.1	9	3.7	47
750, Ts, 70.5, /5o, /5, $1_{0.5}$	3.7	7	4.6	13	7.0	13	18	7	5.0	10	7.0	51

Values of x^2_R 1 dof are given above, for 10041 following each glitch. For individual interglitch eras, the degrees of freedom lost by including a parameter fitted across all glitches are allocated proportional to the amount of data available in that particular era.

Table 9-4: Glitch-recovery Models: common Parameters.

x^2_R	dof	T_{50} days	T_s days	$T_{G.5}$ days	$A_{/50}$//	$A_{/5}$//	$A_{/0.5}$//
2.5	41						
2.9	42	33+4	3.2+0.2	0.42			
3.2	39	49(7)	4.4(6)	0.45(3)			
4.4	43	43(5)	3.8(4)	0.48(4)			0.8(2)
3.6	43	49(8)	5.4(7)	0.49(3)		0.5(1)	
3.2	43	47(7)	4.7(6)	0.46(3)	0.8(2)		
6.9	47	48(7)	5.3(8)	0.55(4)		0.5(1)	0.9(2)
3.7	47	52(8)	5.6(7)	0.49(3)	0.8(2)	0.5(1)	
7.0	51	53(9)	5.6(8)	0.55(4)	0.8(2)	0.5(1)	0.9(2)

Results from models fitted simultaneously to all five Vela glitches reported here, while restraining some parameters to be constant for all glitches.
x^2_R, is calculated over -100d following each glitch.
Only those parameters that were restrained are listed.
The second row gives A for a model in which all timescales were fixed to those values quoted by Alpar et al. (1993a). Errors are those quoted by Chau et at, (1993).
2-cr errors in the least significant figure are given for the HartRAO results.

Table 9-5: Glitch Recovery Models: Inertial Moments (τ, 50d).

Parameters restricted	1985	1988	1991	1994	1994A
none	—	1.3(5)	0.8(2)	—	—
T_{50}=33 d, τ_5=3.2 d, $T_{0.5}$=0.42d	0.2(1)	0.83(7)	0.81(4)	1(1)	3(1)
T_{50}, T_5, $T_{0.5}$	0.1(2)	1.0(3)	0.9(2)	2(2)	4(3)
T_{50}, τ_5, $T_{0.5}$, $\tau_{0.5}$	0.4(2)	1.0(2)	0.8(2)	2(2)	3(2)
T_{50}, T_5, $T_{0.5}$, τ_5	0.4(2)	0.9(3)	0.8(2)	2(2)	3(2)
T_{50}, τ_5, $T_{0.5}$, τ_{50}	0.8(2)	0.8(2)	0.8(2)	0.8(2)	0.8(2)
T_{50}, T_5, $T_{0.5}$, τ_5, $\tau_{0.5}$	0.4(2)	0.8(3)	0.8(2)	3(2)	3(2)
T_{50}, T_5, $T_{0.5}$, τ_{50}, τ_5	0.8(2)	0.8(2)	0.8(2)	0.8(2)	0.8(2)
T_{50}, τ_5, $T_{0.5}$, τ_{50}, τ_5, $\tau_{0.5}$	0.8(2)	0,8(2)	0.8(2)	0.8(2)	0.8(2)
Chau *et al.* (1993)	0.9	0.95	1.07	—	—

Inertial moments are given as percentages.

Table 9-6: Glitch Recovery Models: Inertial Moments (τ, 5 d).

Parameters restricted	1985	1988	1991.	1994	1994A
none	1.3(2)	0.4(3)	0.5(2)	—	2(2)
τ_{50}=33d, T_5=3.2d, $\tau_{0.5}$=0.42d	18(9)	0.37(5)	0.53(5)	0.3(2)	0.4(9)
T_{50}, T_5, $T_{0.5}$	4(4)	0.4(1)	0.6(2)	0.2(3)	0.1(8)
T_{50}, τ_5, $T_{0.5}$, $\tau_{0.5}$	0.6(2)	0.3(1)	0.6(2)	0.5(3)	0.5(7)
T_{50}, τ_5, $T_{0.5}$, 15	0.5(1)	0.5(1)	0.5(1)	0.5(1)	0.5(1)
T_{50}, T_5, $T_{0.5}$, τ_{50}	0(1)	0.4(1)	0.5(2)	0.1(2)	0.6(8)
τ_{50}, T_5, $T_{0.5}$, τ_5, $\tau_{0.5}$	0.5(1)	0.5(1)	0.5(1)	0.5(1)	0.5(1)
T_{50}, τ_5, $T_{0.5}$, 15, 0.5	0.5(1)	0.5(1)	0.5(1)	0.5(1)	0.5(1)
T_{50}, τ_5, $T_{0.5}$, τ_{50}, 15, 0.5	0.5(1)	0.5(1)	0.5(1)	0.5(1)	0.5(1)
Chau *et al.* (1993)	0.15(1)	0.15(1)	0.15(1)	—	

See caption of table 9-5.

Table 9-7. Glitch Recovery Models' Inertial Moments ($\mathcal{T}$ - 0.5d).

Parameters restricted	1985	1988	1991	1994	1994A
none	—	0.7(3)	1.4(4)	—	—
$_{50}$=33d, y_5=3.2 d, $7_{0.5}$=0.42 d	100(50)	0.6(2)	1.4(2)	0.0(3)	6(3)
$\mathcal{T}_{50}$, $\mathcal{T}_5$, 70.5	10(20)	0.7(2)	1.4(3)	0.0(3)	4(3)
$\mathcal{T}_{50}$, $\mathcal{T}_5$ · $\mathcal{T}_{0.5}$. 10.5	0.8(2)	0.8(2)	0.8(2)	0.8(2)	0.8(2)
$\mathcal{T}_{50}$, $\mathcal{T}_5$, $\mathcal{T}_{0.5}$, 15	1.5(5)	0.7(2)	1.5(3)	0.3(3)	3(2)
1_{50}, 75, T0,5, 150	4(4)	0.7(2)	1.5(3)	0.1(3)	3(3)
rso , $\mathcal{T}_5$, $\mathcal{T}_{0.5}$, -$^{1}5$, $^{1}0.5$	0.9(2)	0.9(2)	0.9(2)	0.9(2)	0.9(2)
1.50, 75, 70.5. 150, /5	1.4(5)	0.7(2)	1.5(3)	0.4(3)	3(2)
T50, 75. $\mathcal{T}_{0.5}$, $^{1}50$, $^{1}5$, 10.5	0.9(2)	0.9(2)	0.9(2)	0.9(2)	0.9(2)
Chau *et al.* (1993)	0.059(6)	0.059(6)	0.059(6)	—	—

See caption of table 9-5.

Link et al. (1992) point out that a simple argument gives a less model-dependent lower limit on the magnitude of the "loose" component: basically, once $v(i)$ has returned to its pre-glitch value (at 7^{1},., which is easily determined), the observable component must once again be rotating more slowly than any "loose" component, and the inertial moment of this component can be calculated directly from ifi(T > T_r) - *npreii* 111(7' > T_r)1. Lower limits calculated in this way are given in table 9-8; the 1991 glitch provides the most stringent limit. Because of the large quantity of data available, a can be measured immediately after $T = T_r$; the minimum $h.//$ = 0.83% is however only slightly better than the value calculated by Link *et al.* for the 1975 glitch (0.81%).

9.8 Further Investigations.

Although a fairly intensive analysis of the post-glitch behaviour has been reported above, it is clear that the full benefit has not yet been extracted from this collection of data. Each result seems to turn up a new question, for instance the apparent discovery of the resolution of part of the spin-up at the 1994 glitch raises the question: could this behaviour accompany all the glitches? The difficulties experienced by other people in determining the form of the glitch recovery (summarised in chapter 2) were also experienced here -

Table 9-8: Lower Limit on Inertial Moments.

	1985	1988	1991	1994	1994A
I_{min} (%)	0.6	0.76	0.83	0.45	0.18

Lower limit on the inertial moment of the "loose" component, measured from HartRAO data according to the method suggested by Link *et al.* (1992).

decay components, especially the longer one, mimic the form of the timing noise, even when the data is reduced to ri(t). A possibly better approach would be to fit both Si/(t) and *5v(t)* simultaneously.

The tantalising hint of small changes in the spin-rate a few days after two of the large glitches cannot be followed up without better data coverage (a search for an abrupt change in slope in the phase residuals did not yield anything). This could possibly be accomplished by combining data from HartRAO with that of the Hobart group; the latter gather data of similar or better quality to the HartRAO data, and the time coverage is nearly complementary (i.e. the pulsar is visible from Tasmania for much of the time that it is below the horizon from South Africa).

Figure 9-5: Residuals to fixed r: 611(i).

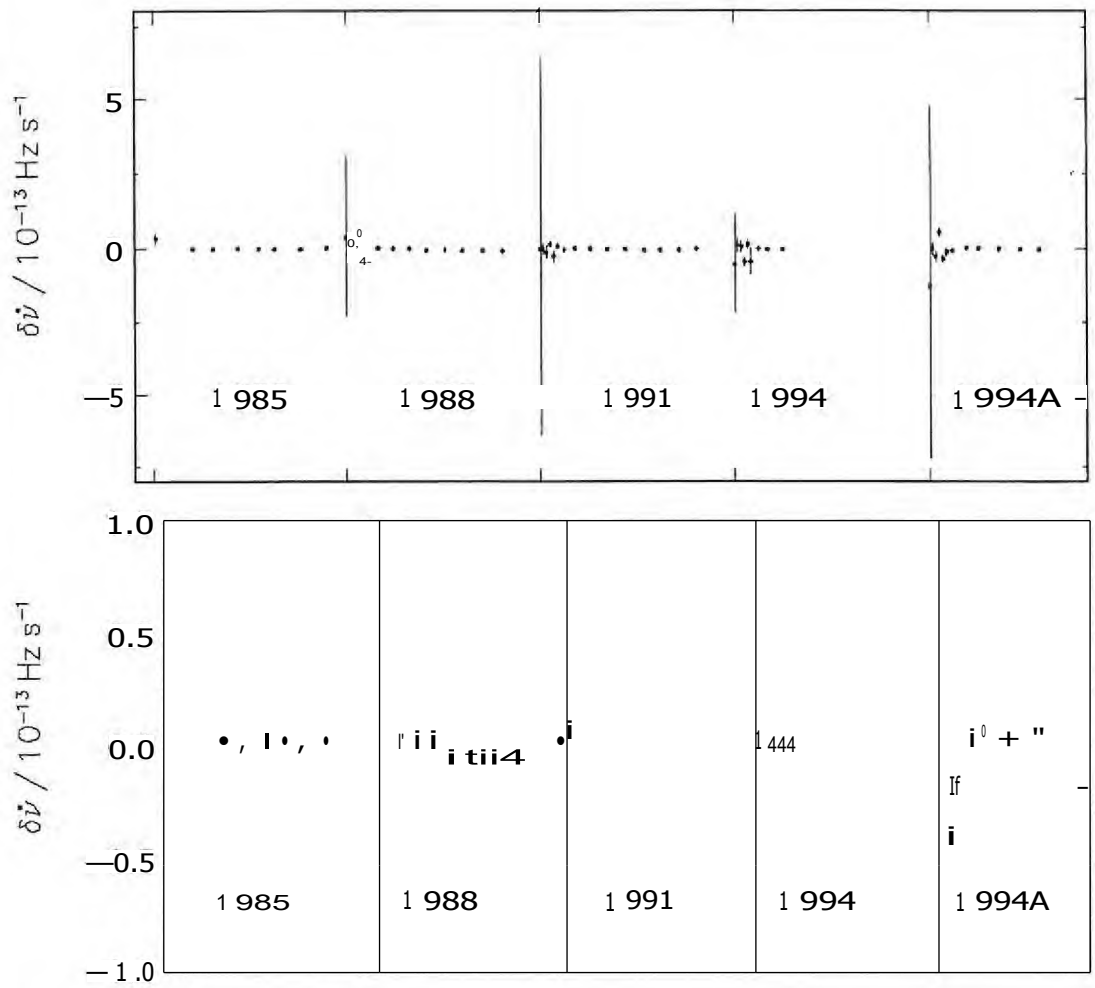

Residuals to a model in which all decay timescales were fixed to those obtained by Alpar et al.
The upper panel shows all residuals.
The lower panel is an expanded view.
About 100d of data are shown following each glitch

Figure 9-6: Residuals to restrained r, 10.5 and 1_5: $\delta\dot{\nu}(t)$.

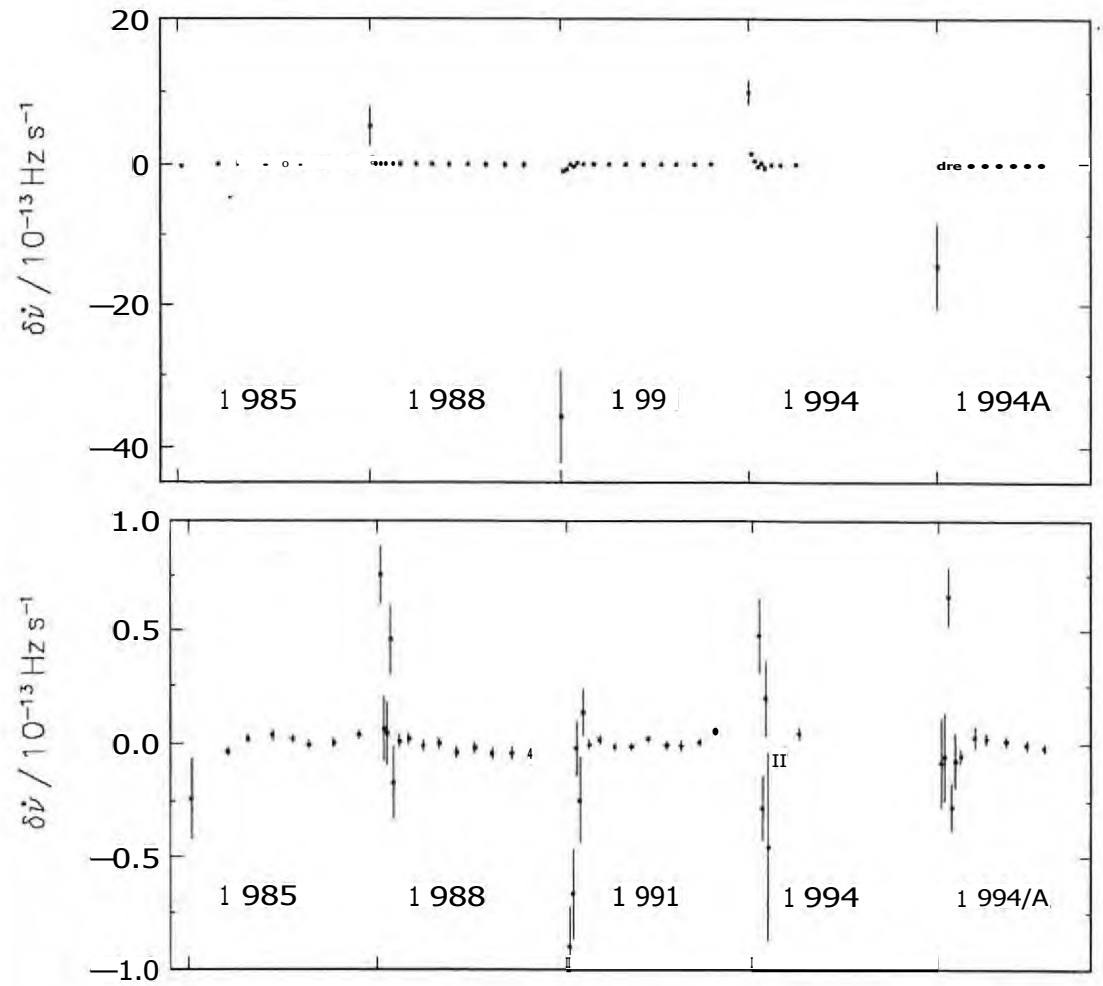

Residuals to a model in which all three decay timescales and the moment of inertia associated with the two faster decays were obtained from a simultaneous fit to all five glitches.
The upper panel shows all residuals.
The lower panel is an expanded view.
About 100d of data are shown following each glitch.

Figure 9-7: Residuals to restrained 7, 15: 61/(t).

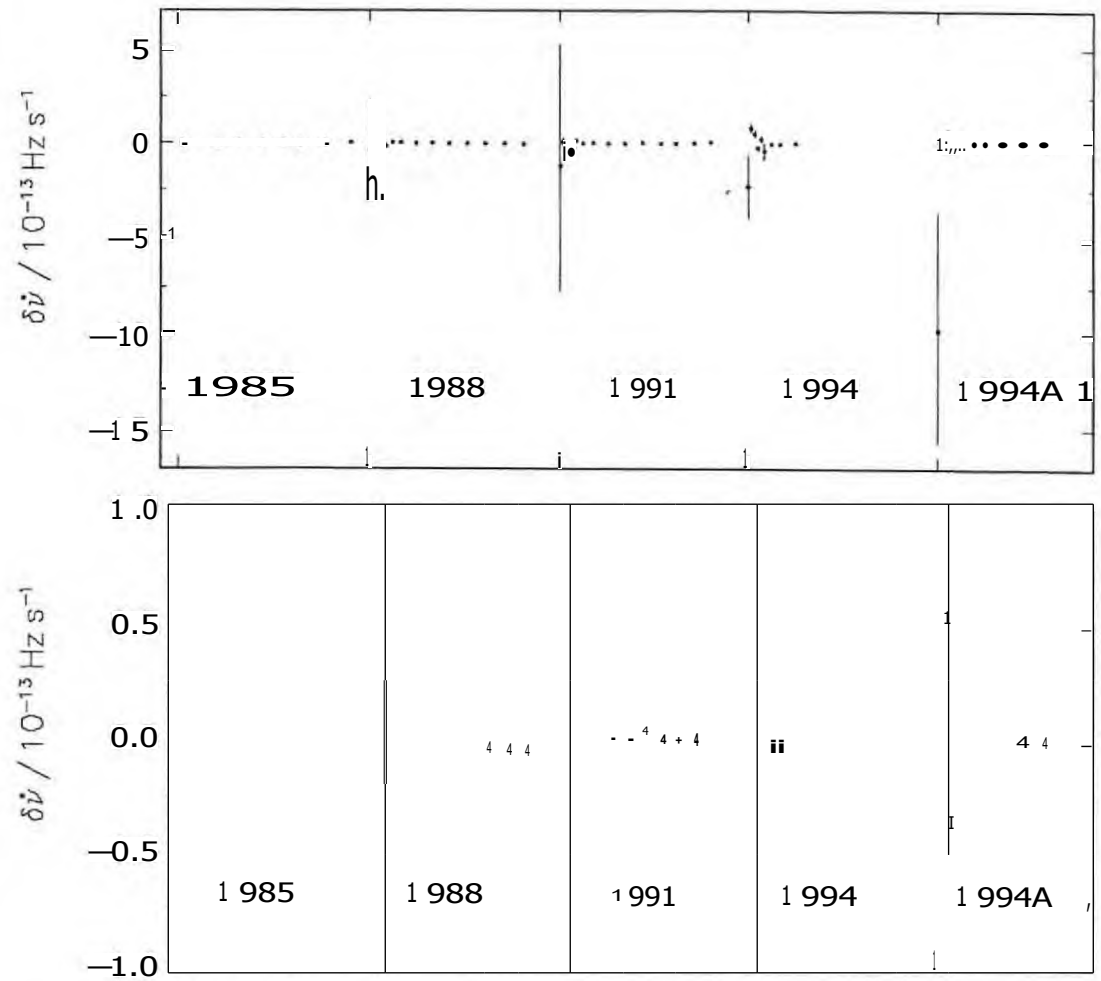

Residuals to a model in which all three decay timescales and the moment of inertia associated with the --5d decay component were obtained from a simultaneous fit to all five glitches.
The upper panel shows all residuals.
The lower panel is an expanded view.
About 100d of data are shown following each glitch.

10 DM Variations linked with Glitches?

Changes in dispersion measure coincident with a glitch would imply an external glitch trigger; the few reports of such coincidences (see chapter 2) have so far been treated with caution. McCulloch *et al.* (1990) report a delay•in pulse arrival times at one observing frequency that would imply an increase in DM of 0.016cm^{-3} pc or a change in the magnetic field configuration, around the time of the 1988 Vela glitch. T_n an attempt to determine whether such DM events do accompany glitches, HartRAO observations of the two 1994 glitches alternated every 10min between 2.3 and 1.7 GHz. The daily measurements of DM made following these two glitches are compared with measurements made over 1.4 y in fig. 10-1. Although the earlier 1994 event was followed — 6d later by a drop in DM of 0.01 cm^{-3} pc, and DM wandering of similar amplitude may follow the subsequent glitch, such variations are seen throughout the 500d covered by the plot. There is thus no evidence in the HartRAO data that such DM changes are uniquely related to glitches.

Figure 10-1. DM Behaviour in Vela.

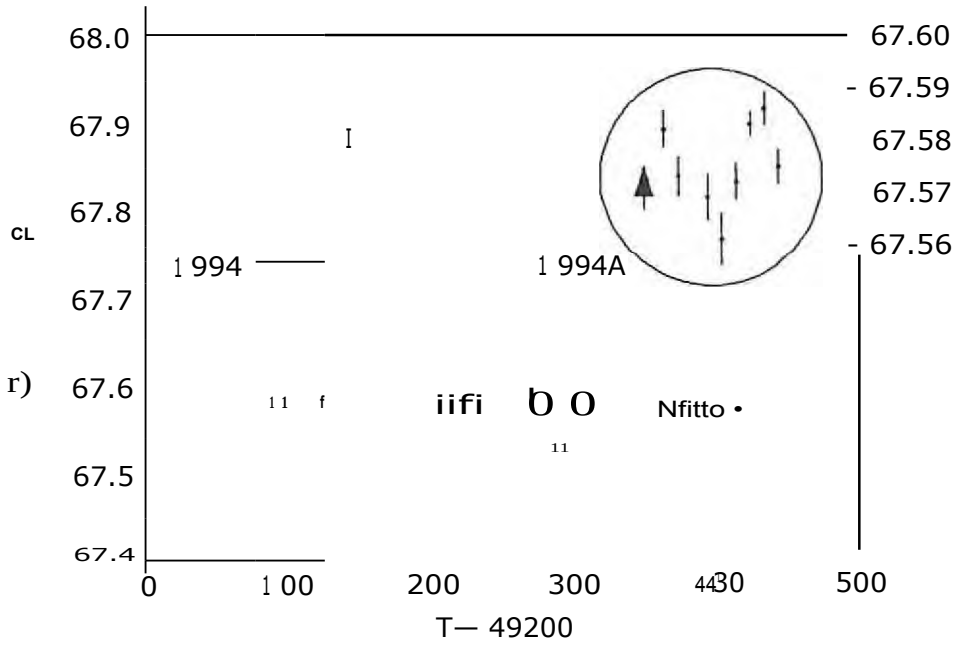

DM measured from independent id blocks (over the ten days following each of the 1994 glitches) and 10d blocks. The epochs of the two glitches are arrowed. The two 10d lengths of post-glitch data are expanded (circled); the right-hand axis gives the scale for these data.

11 Glitches in PSR 1641-45.

Two glitches occurred in this pulsar during the time covered by this thesis; one of these is similar in size to a typical Vela glitch. The parameters of both events are listed in table 6-1. The evolution of v(t) and i>(t) is shown in figs. 6-4 and 11-1 respectively. These results are discussed further below, and in Flanagan (1993).

11.1 Glitch Frequency.

Manchester et *al.* (1978) reported the only other Vela-sized glitch observed in this pulsar, in 1977. Parameters of all three events are listed, in table 11-1. There is a three-year gap between the data set of Manchester *at al.* and that of HartRAO. The difference between theyost-glitch ephemeris of Manchester *at al.* (1983) and that fitted to the early HartRAO data is Aviv = +(1.1 0.5) x 10^{-9}; i.e. it appears that no other large glitches have occurred since 1977.

PSR 1641-45 is, by nearly an order of magnitude, the oldest pulsar in which multiple Vela-sized glitches have been observed (fig. 2-1). Among the canonical pulsars, it has an ordinary spin-rate but a rather high slowing-down rate R. This is unsurprising - most glitch models involve stress build-up as the cause of the glitches.

Should the yr interglitch gap be typical for this pulsar, these observations appear to exacerbate a problem already noted for the Vela pulsar for vortex-unpinning as a glitch trigger: while the critical angular velocity difference, 44.1.1. is theoretically 1 - 10 $rads^{-1}$, the calculated value

$$\text{l} \cdot /1\ \text{ty}, \qquad (^{1})$$

where t_g is the interglitch interval, is typically 9 x10^{-3} rad s^{-1}. For PSR 1641-45, the value calculated for the one observed value of t_g is nearly two orders of magnitude smaller (1.6 x 10^{-4} $rads^{-1}$). Alpar Sz Baykal (1994) suggest that $w_{„}$ may be dependent on the local vortex density, i.e. proportional to a Scaling the observed value for Vela of I t_g accordingly gives an expected value of $w_{„}$ for 1641 of --' 2 x 10^{-3} rad s^{-1}.

The corequake model has a predicted interglitch time of (Alpar *Sz* Baykal, 1994)

$$\mathbf{tg} = \mathbf{a}^{,A,Q/S2}_{cci} \qquad (2)$$

where a is a function of the neutron star structure, proportional to the core oblateness. Scaling from the observed interglitch times of Vela (assuming

Table 11-1: Parameters of 1641-45 Glitches.

Epoch MJD		ZSLY/V X10^6	i://11 X10^2	tR,min days
43390+63	1977a	+0.191(1)	+0.16(5)	50
46453+35	1986	+0.804(1)	+0.4(4)	210
47591+6	1989	+0.0020(4)	+0.5(5)	0.5

tR,mi, is the minimum "recovery time = *Av I V* I, discussed in the text.
a: Manchester *et al. (1978).*

the same value of a for both stars) gives an expected interglitch time of 000yr for PSR 1641-45.

11.2 Post-glitch Behaviour.

Regarding the post-glitch behaviour, three features (or the lack thereof) stand out, when the z(t)-data of fig. 11-1 is compared with that of the Vela pulsar:

- no immediate post-glitch transients that are distinguishable from the general wandering by their amplitude or timescale;
- no obvious linear trend, i.e. no sign of the excess *If* seen in Vela;
- no obvious glitch-induced change in /T*:* larger than I fiiE-/ 10-3.

The first feature above can be explained by the 65d gap in observations at the time of the glitch — any transients that occurred were on a timescale of < 65d. The only other pulsar of similar age to 1641-45 in which good observational coverage of a large glitch has been reported is PSR 0355+54 (Lyne 1987). The glitch in 0355+54 was accompanied by a 44-d transient of amplitude > 6%. The same transient, accompanying the 1986 glitch in 1641-45 at the earliest possible date (at the beginning of the 65 d gap) would have been noticed as a large excess in the first post-glitch data point (fig. 11-1); this is not present in the HartRAO data. The persistent increase

Figure 11-1: PSR 1641-45: *ii(t).*

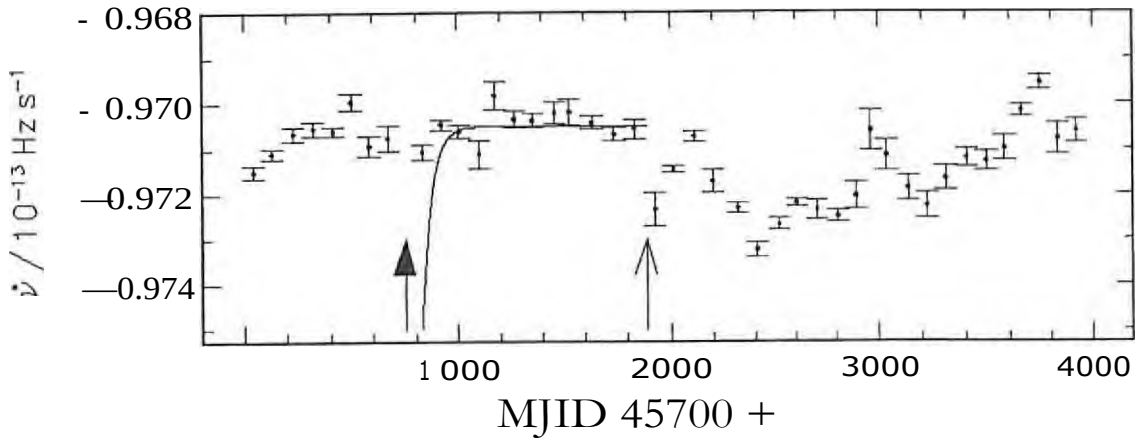

Spin-down rate ii(i) from 1984.0 to 1994.8. No model has been removed from the data. The solid arrow marks the glitch of 1986, and the open arrow that of 1989. The solid line indicates the minimum perturbation expected should the glitch have been accompanied by a transient of similar magnitude and timescale to that observed following a glitch in PSR 0355+54 by Lyne (1987) - i.e. assuming the large glitch occurred at the beginning of the 65d gap in the data. Such a transient was obviously not present in the 1641-45 data.

in ISO I of 6.2 x 10 seen following the glitch in PSR 0355+54 is also not seen accompanying the 1641 glitch.

The Vortex Creep Model: (Alpar *et al.,* e.g. 1993a) suggest that the angular momentum increase of the observed component is at the expense of that of a non-linearly coupled superfluid interior component. The non-linearity of the coupling implies that the decoupled component remains decoupled until

$$tR = (\text{An.} + {}^{8}n)i\ If^{1}1, \qquad (^{3})$$

where Al is the increase in rotation frequency of the observable component and *(5I1 the (unobserved)* decrease in that of the superfluid component. A minimum value of $_{R}$, $tR_{on}i_{n}$, can be calculated by assuming *5I1* = 0; values of $t_{R,,,,i_{7}}$ for all three observed glitches are given in table 11-1. According to this scenario, one would expect this superfluid component to remain decoupled from the observed component until at least 2R,min after the glitch. The glitch of 1986 is the only one for which observational coverage is good enough to put a limit on the inertial moment of this component (since >> the uncertainty in the glitch epoch); this limit is /„/// 10^{-3}. Conservation of

angular momentum, and the assumption that the bulk of the star is coupled to the observable component, give

$$\Delta\Omega/\Omega \gtrsim 10^{-2}\ \mathrm{rads}^{-1}, \qquad (4)$$

and a corresponding predicted time to the next glitch of t_R 600yr. This was pointed out as a problem for the vortex creep model (Flanagan, 1993). The vortex creep model can however accommodate this feature, as well as reducing the expected length of time between glitches, by incorporating a region of the superfluid component that has become permanently decoupled from the star — a "capacitor" region (Alpar *et al.* 1993a, Alpar Sz Baykal 1994, Alpar 1995). The revised scenario is then: vortices withiu a region of superfluid unpin, thus decoupling this region of superfluid; the vortices move out through the capacitor, and repin (recouple) outside this region. The angular momentum required to explain the glitch is thus derived from the entire region (including the capacitor), while the moment of inertia of the region that decouples can be much smaller.

The observation of immediate post-glitch recovery in this pulsar would be very interesting, since the response does seem to be different to that of the similarly-aged 0355+54. The observation of another glitch (and thus an additional measurement of t_g) would indicate that the one observed measurement is not unusually small, and would strongly support the concept of permanently decoupled superfluid regions, within the vortex creep model.

An apparent increase in the level of timing noise following the large glitch was also reported by Flanagan (1993). The timespan is not quite long enough to be useful. For these reasons, monitoring of PSR 1641-45 from HartRAO continues.

12 Conclusions.

A large amount of data was gathered during this project; a combination of luck and flexible scheduling of telescope time resulted in particularly good observational coverage of four large glitches in the Vela pulsar. An additional large glitch in Vela, and one in PSR 1641-45, were less well-observed. Analysis of these events, presented in this thesis, reveals some hitherto unobserved features:

a fast 11 hr) recovery component in at least two of the glitches;

a component of the spin-up that is resolved, following at least one of the glitches; although such a feature has been seen in the Crab pulsar, it has not yet been reported for Vela;

the absence of any significant remnant of Afl at the start of observations, relatively shortly after a large glitch, of PSR 1641-45, supporting the existence of "capacitor regions" proposed by Alpar *et al.* and putting limits on the presence of linearly coupled components in this pulsar.

The suggestion by Alpar et *at.* that certain parameters of the glitch recovery in Vela do not vary from glitch to glitch was followed up. The timescales of three recovery components, and a parameter probably related to the inertial moment of one of these, can be restrained in this way. However, the amplitude of the fastest recovery component clearly varies from one glitch to the next, even though the timescales observed are almost identical for both glitches. This may pose a problem for models such as the vortex creep model which assume that glitches cannot originate in regions where the coupling timescales are so short.

On the other hand, support for non-linear coupling as proposed in the vortex creep model may be obtained from observations of the latest glitch, in which recoupling appears to cease for --50 d, and then recommences.

The good coverage following the 1988 glitch revealed a possible very small glitch that may, if verified, present more of a challenge to models for glitch initiation than do the larger glitches, since it occurs within days of a large glitch.

This project was initiated in order to obtain good observational coverage of large glitches. .The attention that these results has already attracted from those involved in explaining what goes on inside pulsars (e.g. Alpar 1995, Alpar *et al.* 1990, Jones 1991) provides support for such an effort. However, the large amount of data gathered has resulted in high-quality coverage of eras between the glitches; investigation of these data has also turned up some

interesting features:

a resolved step in $\dot{N}O$, reminiscent of the "Fermi function" behaviour predicted a decade ago by Alpar et a/. but not entirely explained by their model; this is also the first time this feature has been reported in any pulsar;

an indication of persistent values of $\ddot{\nu}$, implying that models that attribute the long-term behaviour solely to linear coupling may be too simple.

A search for smaller glitches in the relatively well-sampled data was not very successful, but turned up some interesting trends, such as "quiet periods". Further investigation of such "timing noise" will be a useful but major project.

Other possible directions for future investigations, suggested by this project, include:

combining the data presented here with that obtained elsewhere, for example at Hobart; the Hobart data covers the same period but fills in the daily gaps, thus hopefully enabling better determination of glitch parameters;

applying the "glitch detection" strategy to other pulsars; the recent rash of discoveries of other young pulsars with similar glitching rates to Vela could then be taken advantage of.

The eleven Vela glitches thus far observed are starting to form a significant collection of data. Trends can now be searched for in this data-set; for instance it appears that the post-glitch behaviour of the pulsar follows a clearer trend than does the pre-glitch behaviour. The implication for glitch models is that the glitches return the pulsar to a particular state, rather than occurring when the pulsar reaches a certain state.

The two smaller but apparently atypical glitches that occurred near the end of this project will certainly provide a new challenge to the existing glitch models. Full investigation of these requires continuing observations; the project reported here is ongoing. These two glitches also remind us, yet again, that there is always a surprise in store for pulsar observers.

References

Alcock, C., Farhi, E. & Olinto, A. (1986) Ap. J. 310, 261

Alpar, M.A. (1989) in "Timing Neutron Stars", ed. Ogelman, H. & van den Heuvel, E.P.J., NATO ASI Series C262, Kluwer Academic Publishers, p431

Alpar, M.A. (1995) in "The Lives of the Neutron Stars", ed. Alpar, M.A., Kizi1o1u, U. & van Paradijs, J., NATO ASI Series C450, Kluwer Academic Publishers, p185

Alpar, M.A. & Baykal, A. (1994) MNRAS 269, 849

Alpar, M.A. & Sauls, J.A. (1988) Ap. J. 327, 723

Alpar, M.A., Langer, S.A. Si Sauls, IA. (1984) Ap. J. 282, 533

Alpar, M.A., Anderson, P.W., Pines, D. Si Shaham, J. (1984a) Ap. J. 276, 325

Alpar, M.A., Anderson, P.W., Pines, D. & Shaham, I (19841)) Ap. J. 278, 791

Alpar, M.A., Nandkumar, R. & Pines, D. (1985) Ap. J. 288, 191

Alpar, M.A., Cheng, K.S. *Si* Pines, D. (1989) Ap. J. 346, 823

Alpar, M.A., Pines, D. & Cheng, K.S. (1990) Nature 348, 707

Alpar, M.A., Ogelman, H. *k* Shaham, J. (1993) A. & A. 273, L35

Alpar, M.A., Chau, H.F., Cheng, K.S. & Pines, D. (1993a) Ap. J. 409, 345

Alpar, M.A., Chau, H.F., Cheng, K.S. Si Pines, D. (1994) Ap. J. 427, L29

Anderson, P.W. & Itoh, N. (1975) Nature 256, 25

Arzoumanian, Z., Nice, D.J., Taylor, J.H. & Thorsett, S.E. (1994) Ap. J. 422, 671

Aschenbach, B., Egger, R. & Triimper, J. (1995) Nature, 373, 587

Backer, D.C. (1989) in "Timing Neutron Stars", ed. Ogelman, H. Si van den Heuvel, E.P.J., NATO ASI Series C262, Kluwer Academic Publishers, P3

Backus, P.R., Taylor, J.H., & Damashek, M. (1982) Ap. J. 255, L63

Baym, G., Pethick, C., Pines, D. k Ruderman, M. (1969) Nature 224, 872

Baym, G. & Pethick, C. (1979) Ann. Rev. Astron. Astrophys. 17, 415

Bertsch, DI. *et al.* (1992) Nature 357, 306

Bevington, P.R. (1969) "Data Reduction and Error Analysis for the Physical Sciences", McGraw-Hill Book Company, p200

Bevington, P.R. (1969a) "Data Reduction and Error Analysis for the Physical Sciences", McGraw-Hill Book Company, Chpt. 11

Biggs, J.D. (1992) Ap. J. 394, 574

Bignami, G.F. & Caraveo, P.A. (1988) Ap. J. 325, L5

Bignami, G.F. & Caraveo, P.A. (1992) Nature 357, 287

Bildsten, L. & Epstein, R.I. (1989) Ap. J. 342, 951

Blaes, 0. M. (1994) Ap. J. Suppl. Ser. 92, 643

Blandforcl, R.D. (1992) Phil. Trans. Roy. Soc. Series A, 341, 1

Borner, G. & Cohen, J.M. (1971) Nature, Phys. Sci. 231, 146

Boynton, P.E., Groth III, E.J., Partridge, R.B. & Wilkinson, D.T. (1969) IAU Circ. No. 2179

Burnell, S.J.B. (1978) Sky & Telescope 55, 218

Caraveo, P.A. (1993) Ap. J. 415, L111

Chau, H.F. & Cheng, K.S. (1993) Phys. Rev. B47, 2707

Chau, H.F., Cheng, K.S. & Ding, K.Y. (1992) Ap. J. 399, 213

Chau, H.F., McCulloch, P.M., Nandkumar, R. & Pines, D. (1993) Ap. J. 413, L113

Chau, W.Y., Henriksen, R.N., Rayburn, D.R. (1971) Ap. J. 168, L79

Cheng, K.S., Alpar, M.A., Pines, D. & Shaham, J. (1988) Ap. J. 330, 835

Chevalier, E. (1993) Ap. J. 414, L113

Clifton, T.R. & Lyne, A.G. (1986) Nature 320, 43

Cocke, W.J., Disney, M.J. & Westerlund, B.E. (1969) Nature 222, 359

Cordes, J.M. & Downs, G.S. (1985) Ap. Suppl. Ser. 59, 343

Cordes, J.M. & Helfand, D.J. (1980) Ap. .J. 239, 640

Cordes, J.M., Downs, 0.5. & Krause-Polstorff, J. (1988) Ap. J. 330, 847

D'Alessandro, F., McCulloch, P.M., King, E.A., Hamilton, P.A. & Mc-Connell, D. (1993) MNRAS 261, 883

Datta, B. & Alpar, M.A. (1993) A. 8z A. 275, 210

Demiariski, M. & Proszyriski, M. (1983) MNRAS 202, 437

D'Odorico, S., Oosterloo, T., Zwitter, T. & Calvani, M. (1991) Nature 353, 329

Donnelly, R.J. (1988) Scientific American 259 No. 5 (Nov.), 66

Downs, G.S. (1981) Ap. J. 249, 687

Downs, G.S. (1982) Ap. J. 257, L67

Downs, G.S. & Krause-Polstorff, J. (1986) Ap. J. Suppl. Ser. 62, 81

Downs, G.S. & Reichley, P.E. (1980) Techniques for Measuring Arrival Times of Pulsar Signals I. DSN Observations from 1968 to 1980, JPL Publication 80-54, Jet Propulsion Laboratory.

Downs, G.S. & Reichley, RE. (1983) Ap. J. Suppl. Ser. 53, 169

Easson, 1. (1979) Ap. J. 228, 257

Epstein, R.I. & Baym, G. (1992) Ap. J. 387, 276

Flanagan, C.S. (1988) IAU Circ. No. 4695

Flanagan, C.S. (1990) Nature 345, 416

Flanagan, C.S. (1991) IAU Circ. No. 5311

Flanagan, C.S. (1993) MNRAS 260, 643

Flanagan, C.S. (1994) IAU Circ. No. 6038

Flanagan, C.S. (1994a) IAU Circ. No. 6064

Fomalont, E.B., Goss, W.M., Lyne, A.G. Sz Manchester, R.N. (1984) MN-RAS 210, 113

Fomalont, E.B., Goss, W.M., Lyne, A.G., Manchester, R.N. & Justtanont, K. (1992) MNRAS 258, 497

Foster, R.S., Backer, D.C. & Wolszczan, A. (1990) Ap. J. 356, 243

Foster, R.S., Fairhead, L. & Backer, D.C. (1991) Ap. J. 378, 687

Frail, D.A. & Weisberg, J.M. (1990) A. J. 100, 743

Gaede, H.J. (1988) in Proc., 2nd European Frequency and Time Forum p365

Gold, T. (1968) Nature **218,** 731

Greenstein, G. (1970) Nature 227, 791

Greenstein, G. (1979) Ap. J. 231, 880

Grath, E.J. (1975) A. J. Suppl. Ser. **29,** 453

Gullahorn, G.E. & Rankin, J.M. (1982) Ap. J. **260,** 520

Halpern, J.P. & Holt, S.S. (1992) Nature **357,** 222

Harding, **D.,** Guyer, R.A. & Greenstein, G. (1978) Ap. J. **222,** 991

Harding, A.K., Shinbrot, T. & Cordes, J.M. (1990) Ap. J. **353,** 588

Hartmann, D. in "The Lives of the Neutron Stars", ed. Alpar, M.A., Kiziloglu, U. (3..; van Paradijs, J., NATO ASI Series **C450,** Kluwer Academic Publishers, p495

Hartmann, **D.,** Hurley, K. & Niel, M. (1992) Ap. J. **387,** 622

Hewish, A. (1986) Q. Jl. R.A.S. **27,** 548

Hewish, A., Bell, S.J., Pilkington, J.D.H., Scott, P.F. & Collins, R.A. (1968) Nature **217,** 709

Johnston, S., Manchester, R.N., Lyne, A.G., Kaspi, V.M. & D'Amico, N. (1995) A. (cz A. **293,** 795

Jones, P.B. (1988) MNRAS **235,** 545

Jones, P.B. (1990) MNRAS **243,** 257

Jones, P.B. (1990a) MNRAS **244,** 675

Jones, P.B. (1990b) MNRAS **246,** 315

Jones, P.B. (1991) Ap. **J. 373,** 208

Jones, P.B. (1992) MNRAS **257,** 501

Jones, P.B. (1993) MNRAS **263,** 619

Kaspi, V.M., Manchester, R.N., Johnston, S., Lyne, A.G. & D'Arnico, N. (1992) Ap. J. **399,** L155

Kaspi, V.M., Lyne, A.G., Manchester, R.N., Johnston, S., D'Amico, N. & Shemar, S.L. (1993) Ap. J. 409, L57

Kaspi, V.M., Manchester, R.N., Siegman, B., Johnston, S. & Lyne, A.G. (1994) Ap. J. 422, L83

Klekociuk, A.R., Flanagan, C., McCulloch, P.M. & Hamilton, P.A. (1986) Proceedings of the AIP at Adelaide, August 25-29

Krause, J.D. (1986) "Radio Astronomy", 2nd edition (Cygnus-Quasar Books), Chpt. 9

Krishnamohan, S. & Downs, G.S. (1983) Ap. 1 265, 372

Kulkarni, S.R. & Frail, D.A. (1993) Nature 365, 33

Large, Mi., Vaughan, A.E., Mills, B.Y. (1968) Nature 220, 340

Lindsey, W.C. & Chie, C.M. (1976) Proc. IEEE 64, 1652

Link, B.K. & Epstein, R.I. (1991) Ap. J. 373, 592

Link, B., Epstein, R.I. & van Riper, K.A. (1992) Nature 359, 616

Lohsen, E.H.G. (1981) A. 8z A. Suppl. Ser. 44, 1

Lyne A.G. (1987) Nature 326, 569

Lyne, A.G. (1995) in "The Lives of the Neutron Stars", ed. Alpar, M.A., Kiziloglu, U. 84 van Paradijs, J., NATO ASI Series C450, Kluwer Academic Publishers, p167

Lyne, A.G. & Graham-Smith, F. (1990) "Pulsar Astronomy", Cambridge University Press

Lyne, A.G. & Lorimer, D.R. (1994) Nature 369, 127

Lyne, A.G. & Manchester, R.N. (1988) MNRAS 234, 477

Lyne, A.G. & Pritchard, R.S. (1987) MNRAS 229, 223

Lyne, A.G. 84 Pritchard, R.S. (1989) IAU Circ. No. 4845

Lyne, A.G., Smith, F.G. & Pritchard, R.S. (1992) Nature 359, 706

Lyne, A.G., Pritchard, R.S. & Graham-Smith, F. (1993) MNRAS 265, 1003

Manchester, R.N. & Taylor, J.H. (1974) Ap. J. 191, L63

Manchester, R.N., Goss, W.M., Newton, L.M. & Hamilton, P.A. (1976) Proc. A.S.A., 3, 81

Manchester, R.N., Newton, **L.M.,** Goss, W.M. & Hamilton, P.A. (1978) MNRAS **184,** 35P

Manchester, R.N. *et al.* (1978a) MNRAS **184,** 159

Manchester, R.N., Hamilton, P.A. 8z McCulloch, P.M. (1980) MNRAS **192,** 153

Manchester, R.N., Newton, L.M., Hamilton, P.A. & Goss, W.M. (1983) MNRAS **202,** 269

McCulloch, P.M. & Hamilton, P.A. (1992) in "IAU Colloquium No. 128: The rnagnetospheric structure and emission mechanisms of radio pulsars", ed. Hankins, T.H., Rankin, J.M. & Gil, J.A., Pedagogical University Press, Zielona Gora (Poland), p42

McCulloch, P.M., Hamilton, **P.A.,** Royle, G.W.R. & Manchester, R.N. (1983) Nature **302,** 319

McCulloch, P.M., Klekociuk, A.R., Hamilton, RA. & Royle, G.W.R. (1987) Aust. J. Phys. **40,** 725

McCulloch, P.M., Hamilton, P.A., McConnell, D. & King, E.A. (1990) Nature **346,** 822

McKenna, J. & Lyne, A.G. (1990) Nature **343,** 349

Michel, F.C. (1970) Ap. J. **159,** L25

Mochizulci, Y. & Izuyama, T. (1995) Ap. J. 440, 263

Newton, L.M., Manchester, R.N. & Cooke, D.J. (1981) MNRAS **194,** 841

Nice, D. (1990) IAU Circ. No. **5135** •

Ogelman, H. & Zimmermann, H.-U., (1989) A. & A. **214,** 179

Ogelman, H., Koch-Miramond, L. & Auriere, M. (1989) Ap. .1. **342,** L83

Ogelman, H., Basinger, G. & Triimper, J. (1991) IAU Circ. No. 5162

Ogelman, H., Finley, J.P. & Zimmermann, H.U. (1993) Nature **361,** 136

Paczyliski, B. (1989) Nature **337,** 689

Phillips, J.A. (1991) Ap. J. **373,** L63

Pines, D. & Alpar, M.A. (1983) Nature **316,** 27

Pines, D., Shaham, J. & Ruderrnan, M. (1972) Nature, Phys. Sci. 237, 83

Press, W.H., Flannery, BY., Teukolsky, S.A. & Vetterling, W.T. (1986) in "Numerical Recipes: The Art of Scientific Computing", Cambridge University Press, p203

Press, NCH., Flannery, B.P., Teukolsky, S.A. & Vetterling, W.T. (1986a) in "Numerical Recipes: The Art of Scientific Computing", Cambridge University Press, p503

Radhakrishn.an, V., & Manchester, R.N. (1969) Nature **222,** 228

Rankin, J.M. (1983) Ap. J. **274,** 333

Rankin, J.M. (1993) Ap. **J.** Suppl. Ser. **85,** 145

Rankin, J.M., & Counselman III, C.C. (1973) Ap. J. **181,** 875.

Reichley, P.E., & Downs, G.S. (1969) Nature 222, 229

Roberts, D.H., & Sturrock, P.A. (1972) Ap. J. **173,** L33.

Ruderman, M.A. (1969) Nature **223,** 597

Ruderman, M. (1976) Ap. J. 203, 213

Ruderman, M. (1991) Ap. J. 366, 261

Ruderman, M. (1991a) Ap. J. 382, 587

Ruderman, M.A. & Sutherland, P.G. (1974) Ap. J. **190,** 137

Rutman, **J.** (1978) Proc. **IEEE 66,** 1048

Sauls, J. (1989) in "Timing Neutron Stars", ed. Ogelman., H. & van den Heuvel, E.P.J., NATO ASI Series **C262,** Kluwer Academic Publishers, p457

Scargle, J.D. & Harlan, E.A. (1970) Ap. J. **159,** LI43

Sedrakian, A.D. & Sedrakian, D.M. (1995) Ap. J. **447,** 305

Sedrakian, A.D., Sedrakian, DM., Cordes, J.M. & Terzian, Y. (1995) Ap. J. **447,** 324

Shabanova, T.V. (1990) Soy. Astron. **34,** 372

Shemar, S.L. (1995) in "The Lives of the Neutron Stars", ed. Alpar, M.A., Kiziloglu, U. & van Paradijs, **J.,** NATO ASI Series **C450,** Kluwer Academic Publishers, p177

Siegman, B.C., Manchester, R.N. & Durdin, **J.M.** (1993) MNRAS **202,** 449

Simonetti, J.H., Cordes, J.M. & Heeschen, D.S. (1985) Ap. J. **296,** 46

Smith, F.G. (1991) Comments Astrophys. **15,** 207

Srinivasan, G. (1989) A. & A. Rev. 1, 209

Staelin, D.M., & Reifenstein, E.C. (1968) Science **162,** 1481

Takatsuka, T. & Tamagaki, R. (1989) Prog Theor Phys **82,** 945

Taylor, J.H. (1990) in "Workshop on Impact of Pulsar Timing on Relativity and Cosmology" held at T.JCB

Taylor, Manchester, R.N. Sz Lyne, A.G. (1993) Ap. J. Suppl. Set. **88,** 529

Taylor, **J.H. &** Stinebring, D.R. (1986) Ann. Rev. Astron. Astrophys. **24,** 285

Taylor, **J.H. &** Weisberg, J.M. (1989) Ap. J. **345,** 434

Thorne, K. S. &tytkow, A. N. (1977) Ap. J. **212,** 832

Tingay, S.J. *et al.* (1995) Nature **374,** 141

Tramper, J., Kahabka, P., ogelman, H., Pietsch, W. & Voges, W. (1986) Ap. J. **300,** L63

Tamer, 0.T., Dayton, **B.,** Long, J., O'Neill, T., Zych, A. & White, R.S. (1984) Nature **310,** 214

van Riper, K.A., Epstein, R.I., & Miller, G.S. (1991) Ap. J. **381,** L47

Wallace, P.T. *et al.* (1977) Nature **266,** 692

White, N.E. (1989) Astron. Astrophys. Rev. **1,** 85

Appendix 1: Notation.

Spin-rate and Spin-period - *P, ii*, Q.

Throughout this thesis, the symbols *P* (spin-period), v (spin-rate) and 12 (= 27rv) are used to describe the rotation rate of a pulsar. HartRAO data is analysed in terms of *v* and its derivatives V, ü and V. Occasionally, for example when describing data analysed elsewhere, *P* and its derivatives are used. Models explaining pulsar behaviour are often explained in terms of SI and its derivatives. The notation Si and v are sometimes used interchangeably in this context, since they differ only by a scaling factor (27r).

Changes in Spin-rate – A and *6.*

When discussing models, Ap refers to an observable change in parameter p, and 629 to an inferred but not directly observable change.

In a different context (for instance when discussing structure functions) *p* refers to the parameter under analysis and Sp to residuals after removal of a model.

Symbols used.

p density;

T temperature;

E_{ff} neutron Fermi energy;

M_e solar mass;

ic quantum of vorticity

= h/2m_n;

m_{it} neutron mass;

R is the vorticity vector, parallel to the rotation axis;

Lti = — C¹C

= the difference between superfluid and crustal lattice rotation rates;

Wcr is a critical value of (Ar, above which the pinning force is exceeded by the Magnus force:

$$wcr = \frac{Ep}{pnr(b'} \qquad (1)$$

A superfluid energy gap;

Ep pinning energy — the energy difference between the pinned and unpinned states, per pinning site; *Ep* is a function of the vortex geometry and superfluid parameters such as density;

6 superfluid coherence length;

the vortex core radius --, the superfluid coherence length;

b the distance between successive pinning centres along the vortex line;

v_o typical microscopic velocity of the vortex lines 10^7 cm s^{-1}-)

Appendix 2: Pulsar Timer Software.

On the command S *Ns Np*
where *Ns* is the number of samples per period, and
Np is the number of periods to integrate
execute the following:

work out start of data storage, and other sampling parameters;
clear RAM used for data storage;
disable all interrupts (including Ipps interrupt on which clock is updated);
wait for next lpps transition;
enable interrupts (to allow time-update routine to act on 1pps interrupt);
disable all interrupts (including Ipps);
gate through lpps signal to initiate sampling hardware;
set counter *ip = Np;*
while (Ip 0 0) do
set counter */s* = /Vs;
while (Is 0 0) do
wait for AID conversion to complete;
read output of AiD converter;
add data into RAM location corresponding to */s;*
Is is — 1;

Ip = —1;

output "F" for Finished.

Appendix 3: PLS77, the Observing Program.

Equipment Checks

```
instruct PT to carry out a memory check;
instruct PT to test for the presence of the station 1 Hz signal;
set the sampling frequency to 5 kHz and instruct PT to verify the sampling rate;
if (not automated) then
    request operator to set up signal level;
check presence of calibrating noise diode:
    tun on noise diode and look for a positive change in signal level;
    if this test fails, then switch to alternate observing frequency and try again;
if (not automated) then
    request operator to verify HP1000 clock against station clock;

ALARM = FALSE;
for each pulsar in source list do:
    read NPLSAR, F_obs, N1NT, CAL?, PLOT?, GCHECK? from source list;
    get co-ordinates, ephemeris, T_o♭, , N p for NPLSAR from source-file PULSAR;
    precess co-ordinates to current date;
    set up correct local oscillator frequency for F.

    for each of N_INT integrations do:
        track this pulsar;
        if (not ALARM) and (CAL?) then
            if this is the first integration then
                calibrate [measure noise diode deflection in PT units];
            else
                calibration = most recent calibration;
        set PT clock to HP1000 clock;
        measure offset between 1 Hz and HP1000 clock;
        work out current pulsar rotation period PERIOD from ephemeris;
        correct PERIOD for doppler shift caused by velocity of antenna wrt pulsar;
        work out no. of samples Ns per PERIOD;
        set sampling frequency to (PERIOD / Ns)';
        instruct PT to do on-line integration of N p x Ns samples;
        wait for PT to complete this integration;
        retrieve data from PT;
        if (not ALARM) and (PLOT? or GCHECK?) then
            write data to temporary disk file on HP1000;
```

```
            if GCHECK? then
                do glitch detection;
                if ALARM then
                    turn on audible antenna alarm;

            if PLOT? then
                plot data in temporary file;
                if GCHECK? then
                    mark predicted arrival time on plot;
        if (not ALARM) and CAL? then
            calibrate;
        write data to disk file on HP1000;
        write details (sampling frequency etc.) to log file;
    if (not ALARM) then
        skip to next source in source-list;
    else
        glitch alarm on: keep observing this source while it is visible;
```

In the above:

PT is the Pulsar Timer;

NPLSAR is the name of the pulsar;

F_obs is the observing frequency;

Np is the number of consecutive periods to integrate over;

PERIOD is the current apparent period of pulsar NPLSAR;

NINT is the number of integrations, each Np X PERIOD long, per observation;

CAL? is true to calibrate this observation;

PLOT? is true to plot this observation;

GCHECK? is true to do a "glitch detection" check on this observation;

rob, is the post-detection filter constant;

Appendix 4: PGDET, the Glitch-detection Program.

observe the pulsar;
ALARM = TRUE;
UPDATE = TRUE *cancel later if necessary*
read pulsar name, position, ephemeris, etc. from PULSAR source file;
ALARM = ALARM and (name=0833-45) or (name=1641-45);
only take action for these two pulsars
read latest pulse-phase offset relative to current ephemeris, rb_{prey}, from PULSAR source file;
because of timing noise, O will slowly drift from 0
ALARM = ALARM and (OPT„ WOO)
allows for resetting of alarm when ephemeris is updated
calculate pulse arrival time t_{068}:
Avoid false alarms caused by off-source pointing or badly set signal level
calculate signal-to-noise ratio (SNR) of observation;
if (name=0833-45) then
ALARM = ALARM and (SNR > 7);
UPDATE = UPDATE and (SNR > 7);
if (name=1641-45) then
ALARM = ALARM and (SNR > 3);
UPDATE = UPDATE and (SNR > 3);
if (name0833-45) and (name1641-45) then
ALARM ALARM and (SNR > 1);
UPDATE = UPDATE and (SNR > 1);
transform L_obs to the equivalent arrival time at the solar-system barycenter;
calculate predicted arrival time, $t_{r„d}$, of this pulse, from current ephemeris;
calculate observed phase residual wrt current ephemeris:
006.5 = (tobs — tpredVP;
= prev Oobs,
if (na me=0833-45) or (name=1641-45) then
A(kmax = 1%;
else
AOmax = 2%;
if AO > A4₄ then
print warning;
if ALARM then
turn on audible antenna alarm;
UPDATE = FALSE;
if UPDATE then
update PULSAR source file with O_obs.

Appendix 5: Commands recognised by the **P**ulsar Timer

NAME	FORMAT	FUNCTION
SAMPLE	S *Ns Np*	Halt updating of the clock; Store *Ns* samples of the input into memory; Add the next (*Np* — 1) sets of *Ns* samples to the first set.
SETUP TIME	T *dddd hh mm ss*	Set the Pulsar Timer clock
PRINT TIME	P	Output the time on every second
OUTPUT DATA	E	Output the accumulated data, the parameters N_s and *Np,* and the start time, from the last SAMPLE command
SETUP τ		Select a post-detection timeconstant
GRAPH DATA	G	Output N_s accumulated data samples to oscilloscope output
LED TEST	L	Turn on front-panel LEDs for three seconds
RAM TEST	C	Test memory chips used for data storage
D/A TEST	D	Output a ramp signal to both analogue outputs
INPUT VIEW	I	Sample input; write to analogue meter
BUS TEST	B	Output A..Z on the HPIB

SAMPLING FREQUENCY TEST	F *N,,*	Count sampling pukes for *Nsec*
1PPS TEST	K	Check for presence of 1pps pulses
HOLD	**H**	Put timer into HOLD state — turn off all outputs
DEBUG	M	Transfer control to DEBUG, the primitive operating system

Appendix 6: Least-squares Fitting Routine

All model fitting is done using a version of CURFIT (Bevington 1969a) that has been modified by the author for more general use:

- An array of flags, one per fitted parameter, is passed to the subroutine. If the flag corresponding to parameter$_i$ is set, parameter$_s$ is held constant; only parameters corresponding to unset flags are fitted;
- Any problems encountered while accessing data to be fitted are passed back to the calling program via an OK parameter;
- Non-consecutive subsections of the data can be fitted. For example, models can be fitted to data at only one observing frequency.

CURFIT fits any function for which the first partial derivative with respect to each of the fitted parameters can be calculated at each value of the independent variable. It is an implementation of the Levenberg-Marquardt algorithm which combines two methods of searching for the x^2 minimum. One method, used in early iterations when the parameter values are likely to be relatively far from optimum, involves evaluating the gradient of the X^2 surface, and adjusting the parameters so as to move along the direction of steepest descent. The second search method, used when the minimum is approached and the slope less, approximates the fitting function with a first order expansion in a Taylor series, and fits this using a standard analytical least-squares method.

Output from CURFIT includes the reduced x^2, $x^2_R = x^2 idof$, with (laic the number of degrees of freedom of the fit, and estimates of the parameter errors. A "goodness of fit" parameter, Q, can be calculated by evaluating the probability of obtaining the measured value of x^2_R from this data if the model is the correct one: $Q = Q(dof/2, x^2/2)$, where $Q(dof/2, x^2/2)$ is the incomplete gamma function. If the calculated value of Q *is* to be useful, sensible estimates of the data errors must be provided to the routine. The interpretation of Q also assumes that data errors are normally distributed; in practice, this is not so, and low values of Q (as low as 0.001) are generally deemed acceptable (Press *et* a/. 1986a). Press *et al.* also point out that x^2_R will not have a x^2-distribution if the model is non-linear in its parameters and the data-set small enough that the parameter uncertainties are large.

The results reported in this thesis use weighted CURFIT fits. Care is taken to estimate data errors correctly, so that the "goodness of fit" parameter can be used to evaluate the results. However, estimates of parameter errors are generally obtained from randomisation methods rather than the values provided by CURFIT.

Appendix 7: Structure Functions.

Structure function analysis was developed within the time- and frequency-standards community to characterise clock noise (e.g. Lindsey S4 Chie 1976). This tool is now routinely used by astronomers to investigate flux variations (e.g. Simonetti et al, 1985) and pulsar timing behaviour (e.g. Cordes & Downs 1985).

A structure function plot is basically of variance measured over a timescale T versus *T*. The definition (e.g. Lindsey & Chie) is via the *Nth* increment,

$$A^N x(t,T) = \sum_{k=} \mathbf{E}(-1)^k \qquad x(t\ (N — k)r); \qquad (1)$$

the Nth-order structure function of *x* is then

$$Dn(T) =< (Ant, -0)^2 > \qquad (2)$$

Interpretation of /V).

The utility of structure functions arises from their ability to probe structure over a range of timescales. For instance, a log-log plot of D1')(7-) will

- be zero if *x(t)* is a polynomial of order *Trt < N;*
- have a slope dependent on the order of the polynomial and independent of time arid 7 if *x(t)* is a polynomial of order m = *N;* form = 1, $D1^1$)(7-) has a slope of 2;
- display more complicated behaviour for *x(t)* a polynomial of order rn > *N;*
- have a slope of 1 if the underlying noise process is a random walk in *x;*
- have a slope of 3 if the underlying noise process is a random walk in and *N*> 2;
- have a slope of 5 if the underlying noise process is a random walk in and *N* > 3.

Specifically useful for the analysis of the long-term behaviour of *i/(t)* in chapter 8.

- a linear trend in *i/(t)* should be identifiable by $D_i^{)} oc\ 7^{-2}$ (slope of 2 in the log-log plot) and **independent** of T;

- correlated noise in *ii(t)* should be identifiable by similar slopes in both D(1) and 1*.

However, structure functions can only be *consistent with* a particular interpretation of the data; in any case, data will generally be a combination of a range of behaviours.

Calculation of $D_{\text{„}}^{Ir)}$.

Structure functions of *1/(0* and Sii(t) discussed in chapter 8 were calculated as follows:

- set $r_{mi_{v}}$ = median inter-data spacing;
- set T_{ma_r} = AT **for** *N = 1*
  AT/2 for *N* = 2

  where AT is the length of the data being analysed, arid
  N is the order of the structure function.

- select intermediate lags *ri* spaced logarithmically from r_{min} to
- for each pair of points, calculate ***A(t,T);***
- accumulate this result into the logarithmically nearest bin.

Appendix 8: Generated Data.

Sets of data containing post-glitch transients were generated and analysed as an aid in interpreting the sometimes confusing results obtained from fits to post-glitch v(t) and *zi(t).* These are described below.

Noise-free, Single Transient.

These data were used to check whether the averaging introduced by the creation of v- and 1.-series from blocks of arrival times affects the parameters of the fitted exponential decays.

The Generated Data: Five days of arrival times were generated using a model that consisted of a large amplitude (di/ -= 100 x 10^{-13} Hz s^{-1}) fast (7- varying from 0.1 **to 0.8d)** transient, i/ = 0, **and** *i)* **0.** The arrival times start immediately after the glitch, and are generated over 12h per day. v(t) and zi(t) were extracted from these arrival times using the same block lengths as used for the real data, i.e.:

v(t): one value from each 12h block of data;

one value from the 12h of data immediately after the glitch, and there afterone value from each 2d of data (independent series); or
one value from the first 12h of data; one value from halfway through the first 12h block to halfway through the second 12h block; thereafter the data are blocked into 2d blocks, with the start times of consecutive blocks shifted by id (i.e. oversampled by a factor of two) (non-independent series).

The Results: The resulting *v(t)* and *ii(t)* are plotted, together with the models used to generate the data, in fig. 1. Parameters of models fitted to the independent series are also shown in the figure. The results show that the averaging is not too large, and is worst in the second value of *ii(t)* (non-independent series), which is calculated from a 24h block of data; this point is not used in any of the model fits discussed in chapter 9. When the model parameters obtained from fits to this data are compared with the true model parameters, it appears that the timescale obtained from fits to the independent series of *b(t)* are consistently overestimated, by a factor of **15%** for the 0.2d decays. This is probably because the fit relies excessively on the first point. Fitted amplitudes are affected less.

The block lengths used are therefore not expected to introduce a bias into the results, but tirnescales will be consistently over-estimated, especially for faster transients, due to the poor sampling introduced by the conversion to *U.*

Figure 1: Generated Noise-free Data.

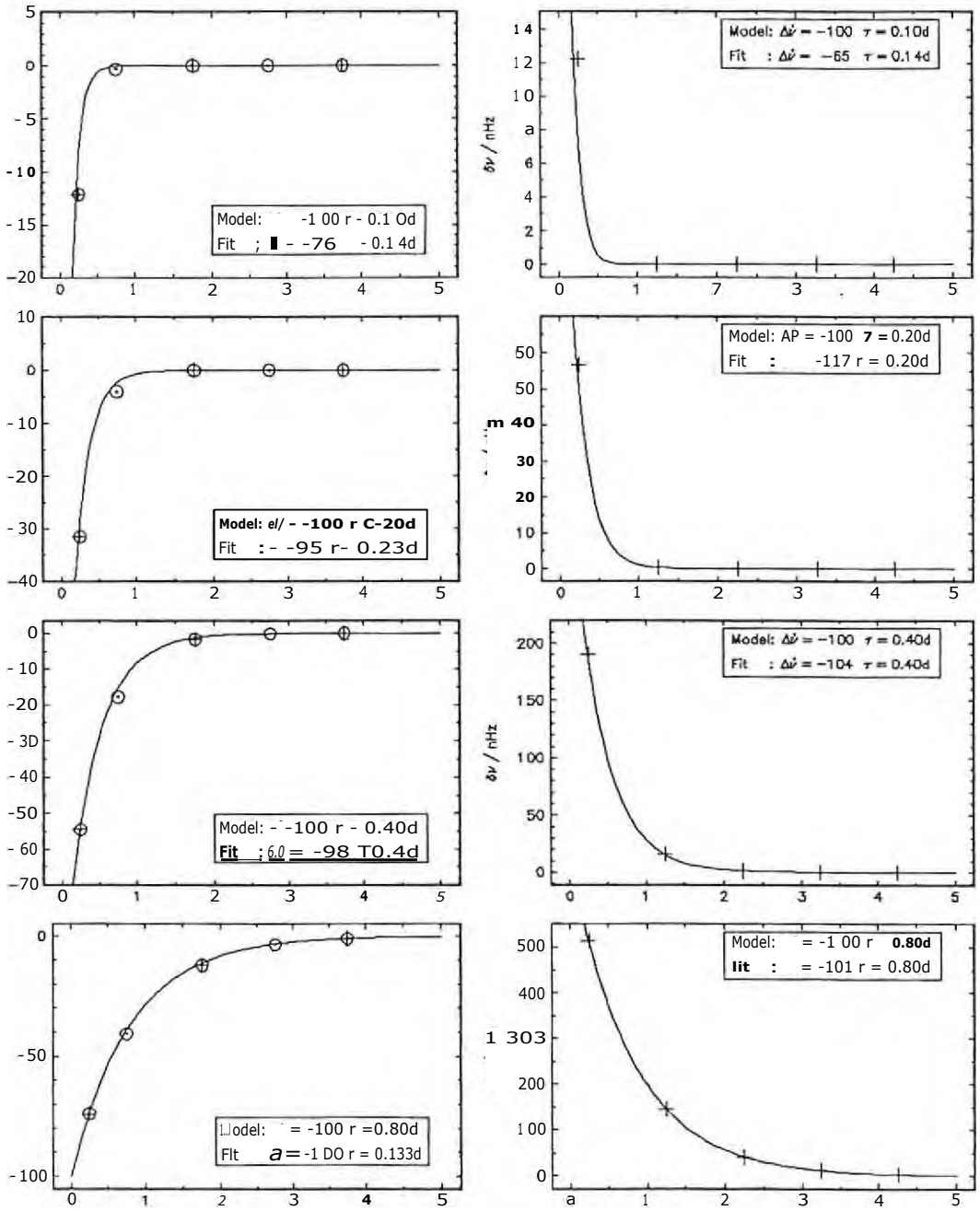

Series of *ii(t)* (left) and *v(t)* (right) obtained from generated data as described in the text. Solid lines show the true model. Independent series are indicated with plus (+) and non-independent series with circles (0). Parameters of the true model and those obtained from a fit to the independent series are given. Amplitudes (AO are in units of 10^{-13} Hzs.

Two-component Transients with Timing Noise.

A more realistic series of arrival times was generated using the sampling times following the earlier 1994 glitch. These data were used to check the affect of noise on the calculated parameters of the transients, and to investigate whether the apparent lack of transients accompanying this glitch can be ascribed to the relatively long gap (4.3 hr) between the glitch epoch and the start of observations.

The Generated Data: Dual-frequency arrival times (i.e. at 2.3 and 1.6 GHz) were generated over the entire 31 d interglitch period, from a model with = 0, constant DM, and two simple exponential decays with timescales 0.5 d and 5.0 d and a range of amplitudes. Random Gaussian noise of rms amplitude 0.15mP (the same as the measured value for the real data) was added to the arrival times. These arrival times were analysed in the same way as the real data from this glitch; errors calculated for *i/(i)* were increased by quadratically adding 0.02 x $^{10-13}$ Hz s^{-1} prior to modeling.

The Results: The results are shown as residuals 8// and to the true model (fig. 3) and to a variety of models fitted to i(t) (fig. 4). Model parameters are listed in table 1. Some of the residuals to the true model in fig. 3 have small non-random variations, possibly induced by data processing.

One indication of these simulations is that should a pair of fast transients of similar amplitude and timescale to those following the 1988 glitch be present following the 1994 glitch, they would be detected, even though the observational coverage is worse. It may however be difficult to distinguish the timescale of the faster transient, Transients of smaller amplitude would however be missed.

The 8v residuals to the two-component fits give some guidance for adjusting the component parameters obtained from modeling *//M*. A transient of the form

$$zi(t) = \quad \exp(-t/r_i) \qquad (1)$$

translates into

$$v(t) = \quad \exp(-0T_;). \qquad (2)$$

One would expect that if either i> or 7_i is over- (under-)estimated, //-residuals would have a negative (positive) transient. In one case (fig. 4s) the errors in AV and T cancel, giving an apparently correct, fit (according to the v-residuals). Except for cases such as this, it appears from the generated data that

- parameters obtained from modeling *ri(t)* can be in error by up to five times the formal lo--error (for observational coverage similar to that used in generating this data);
- the parameter estimates can be corrected to some extent by examining plots of *v;*
- for a 5 d decay, the amplitude (Al') should be corrected;
- for a 0.5 d decay, the timescale is more likely to be in error (consistent with the results of the first set of simulations).

The distribution of parameters from the randomised fits shows similar behaviour to that of the fits to the real data, in that they are occasionally clustered. This is shown in fig. 2, for two cases — one in which the model is inadequate (one transient fitted). This clustering unfortunately is not seen in every instance of an underspecified model. The second case shows that this type of clustering is also sometimes seen even when the model includes the correct number of terms. Thus clustering (or lack thereof) in randomised fit parameters is not a reliable diagnostic of an adequate model.

Figure 2: Results of Randomised Fits.

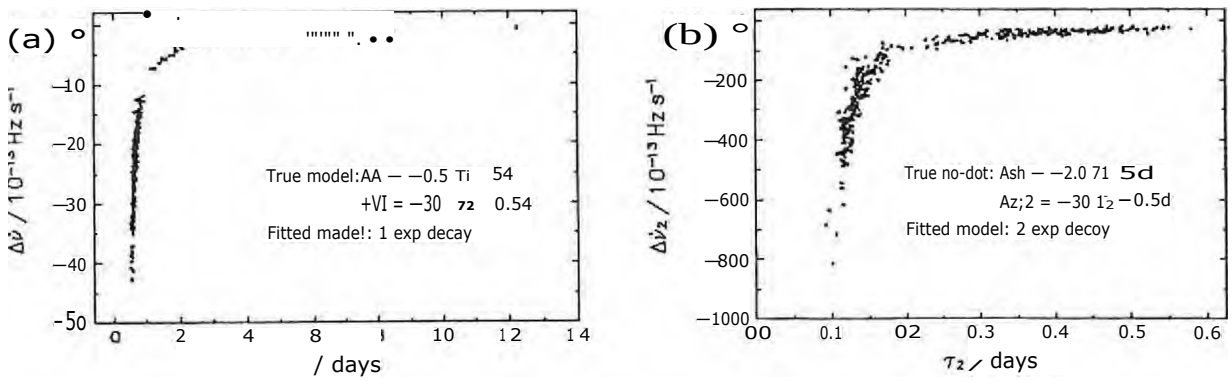

Distribution of fitted parameters from 400 fits in which the data were randomly perturbed by an amount proportional to the assigned errors prior to each fit.

a Parameters of the single exponential decay fitted cluster into two groups, corresponding to the parameters of the actual transients present

b Parameters of the faster transient fitted cluster into two groups, even though the faster of these two transients is not present in the data.

Table 1: Parameters of Fits to Generated Glitch Data.

	Model				Fit				
	Au_1	r_1	A1/2	z_2	χ^2_R				T2
	-0.5	5	-10	0.5	2.1				
	-0.5	5	-30	0.5	8.9				
	-0.5	5	-100	0.5	76				
	-0.5	5	-100	0.5	0.76	-88(7)	0.58(2)		
	-2.0	5	-10	0.5	19				
	-2.0	5	-10	0.5	2.5	-2.7(3)	4.7(5)		
	-2.0	5	-10	0.5	1.2	-2.6(2)	4.9(6)	-160(80)	0.13(1)
#	-2.0	5	-30	0.5	26				
#	-2.0	5	-30	0.5	5.7	-3.1(4)	4.5(6)		
#	-2.0	5	-30	0.5	2.5	-2.5(3)	5.3(7)	-40(10)	0.4(1)
#	-2.0	5	-30	0.5	2.6	-2.9(4)	4.8(6)	-200(100)	0.13(1)
	-2.0	5	-100	0.5	115				
	-2.0	5	-100	0.5	6.7	-86(7)	0.64(2)		
	-2.0	5	-100	0.5	2.5	-1.3(3)	7(1)	-90(6)	0.59(2)
	-4.0	5	-10	0.5	48				
	-4.0	5	-10	0.5	3.0	-4.8(5)	4.2(5)		
	-4.0	5	-10	0.5	1.6	-2.5(4)	6.0(9)	-10(4)	0.9(2)
	-4.0	5	-30	0.5	68				
	-4.0	5	-30	0.5	4.6	-5.6(4)	4.4(3)		
	-4.0	5	-30	0.5	0.78	-5.0(2)	4.7(3)	-37(7)	0.36(6)
	-4.0	5	-100	0.5	164				
	-4.0	5	-100	0.5	4.1	-5.3(7)	4.5(4)	-110(10)	0.46(3)

Parameters for models fitted to i.(i) obtained from generated data following the 1994 glitch.
Errors are the lo width of the distribution of parameters from fits to 400 randomisations of the u>-data.
χ^2_R is the reduced χ^2 residual.
Amplitudes (AO are in units of 10^{-13} Flzs^{-1}, and timescales (r) in days.
marks models that include transients of similar amplitude to those detected following the glitch of 1988.

Figure 3: Generated Realistic Data: True Residuals.

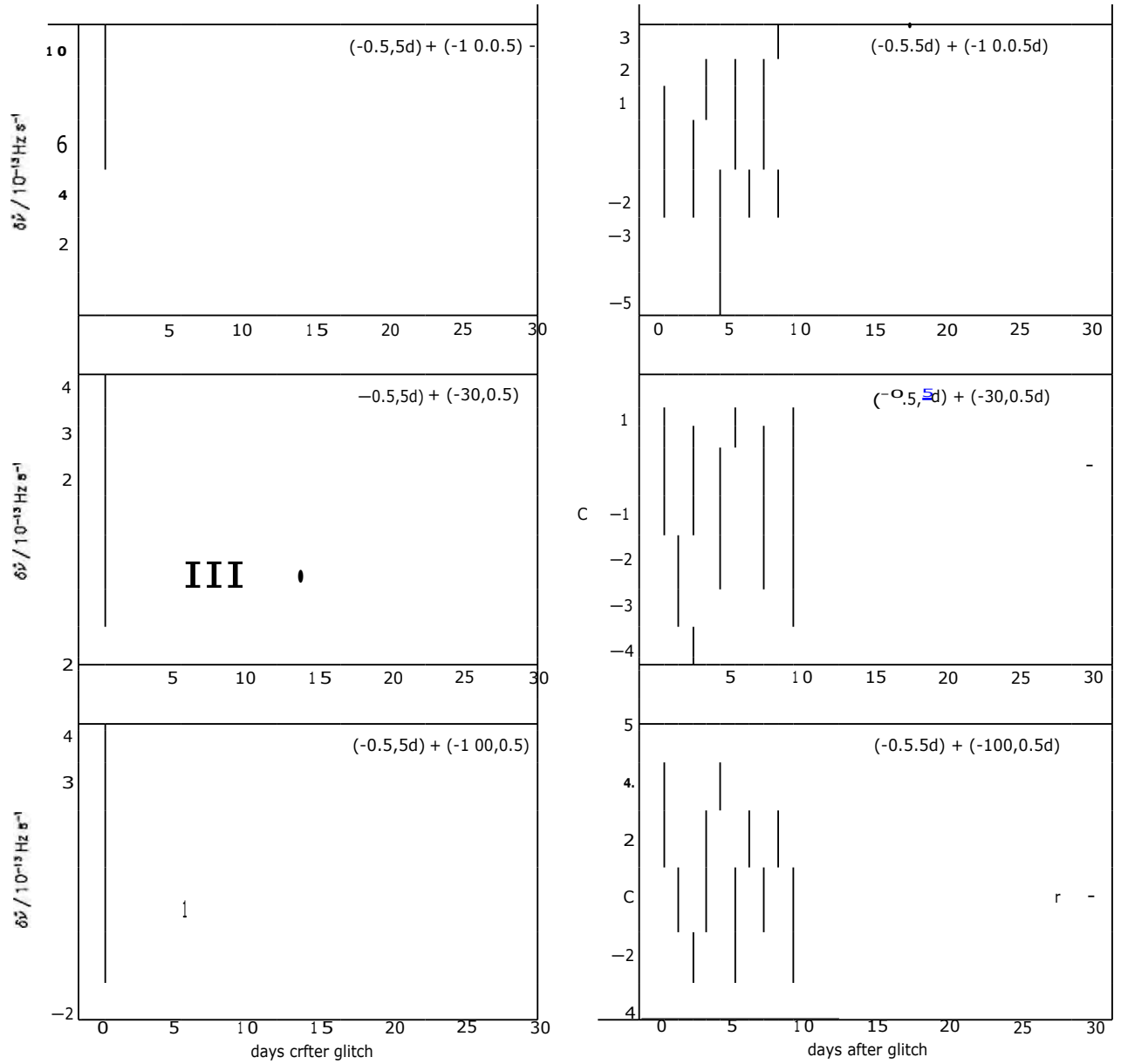

Residuals 451/(0 (left) and *8v(i)* (right) to the two-component recovery models used to generate arrival-time data following the 1994 glitch. Model parameters are in the form *(amplitude, timescale); amplitude* is in units of 10^{-13} Hzs^{-1}. Where no fitted model is given, only a i'$_0$-term was fitted.

Figure 3: *coned*

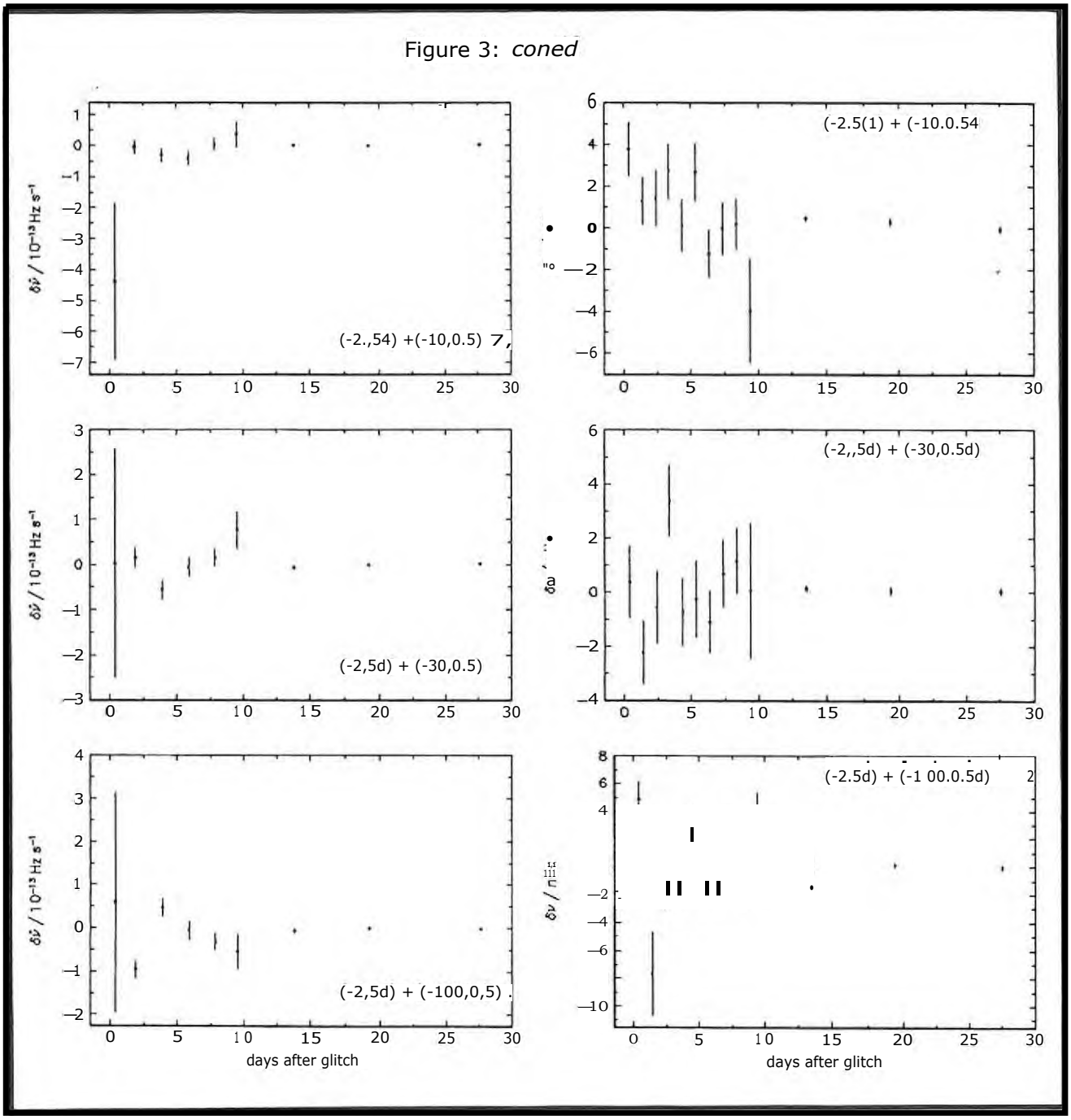

Figure 3: *cont'd*

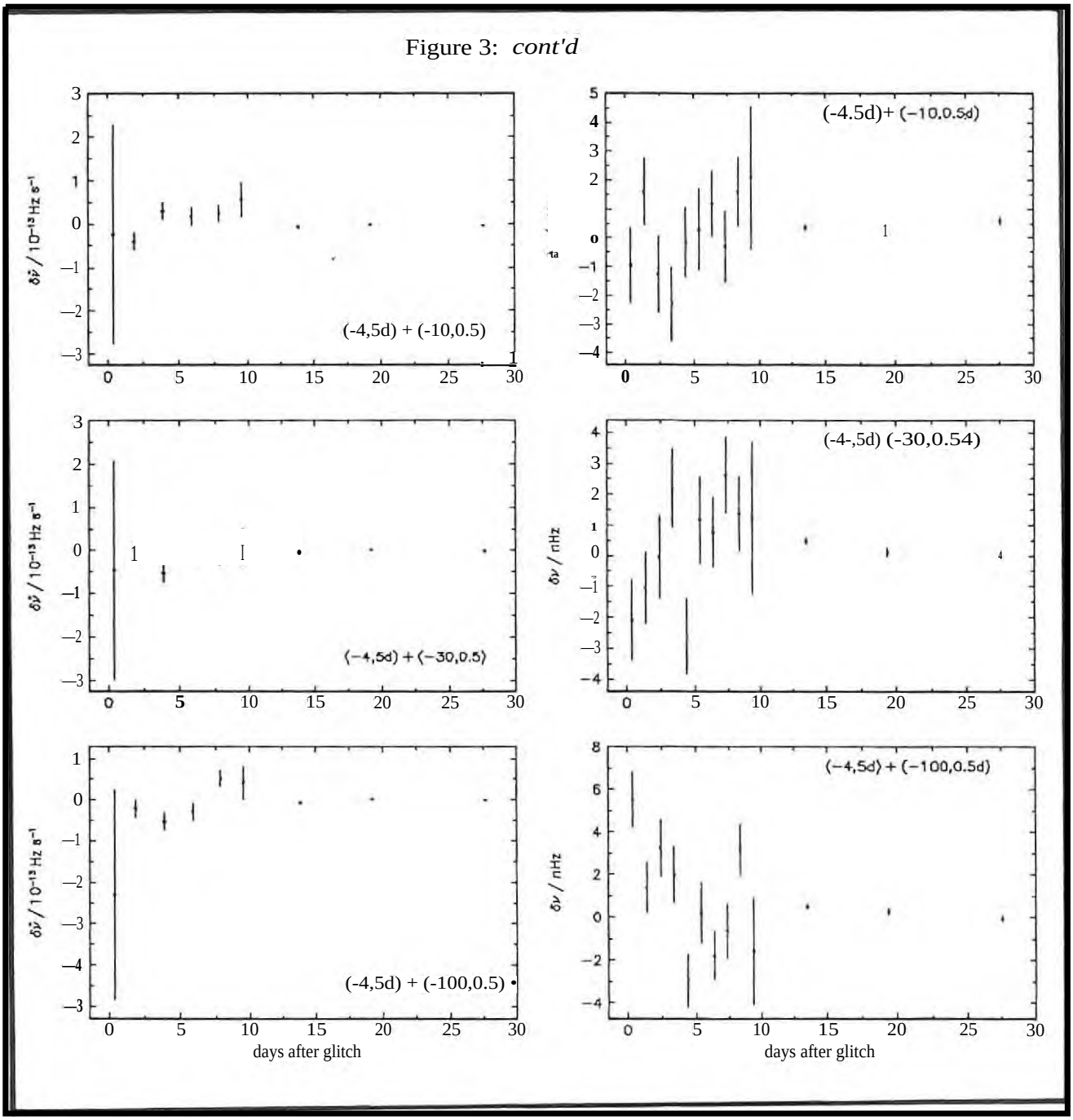

Figure 4: Generated Realistic Data: Residuals to Fitted ii Models.

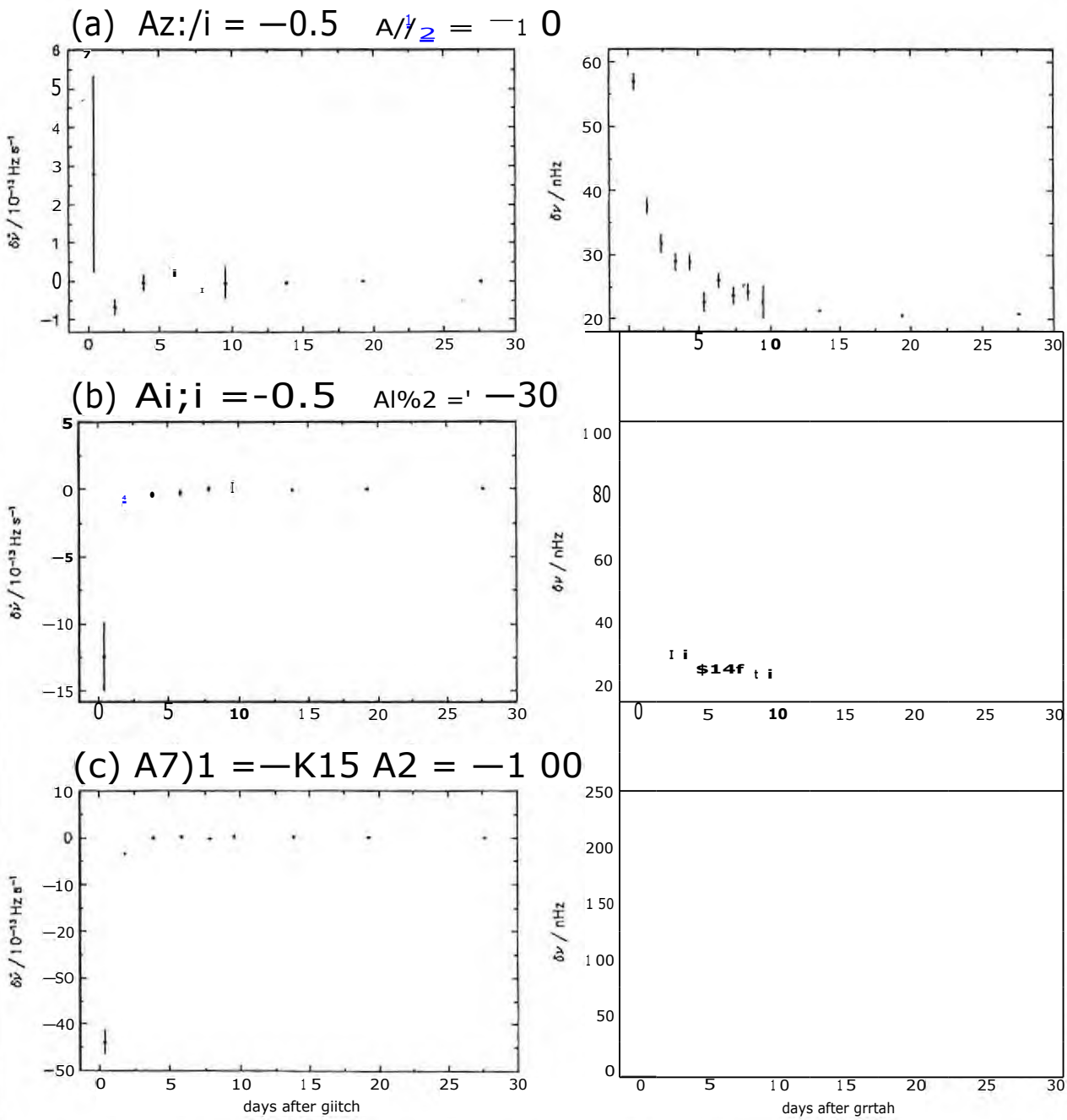

Residuals *6ii(t)* (left) and *bv(i)* (right) to models fitted to independent *i>(t)* obtained from generated arrival-time data following the 1994 glitch. Amplitudes of the two transients used to generate the data are given above each pair of plots, in units of 10^{-13} Hzs^{-1}; timescales are r_1 = 5 d and r_2 = 0.5d throughout. 1u-errors are quoted for the parameters of the fitted models.

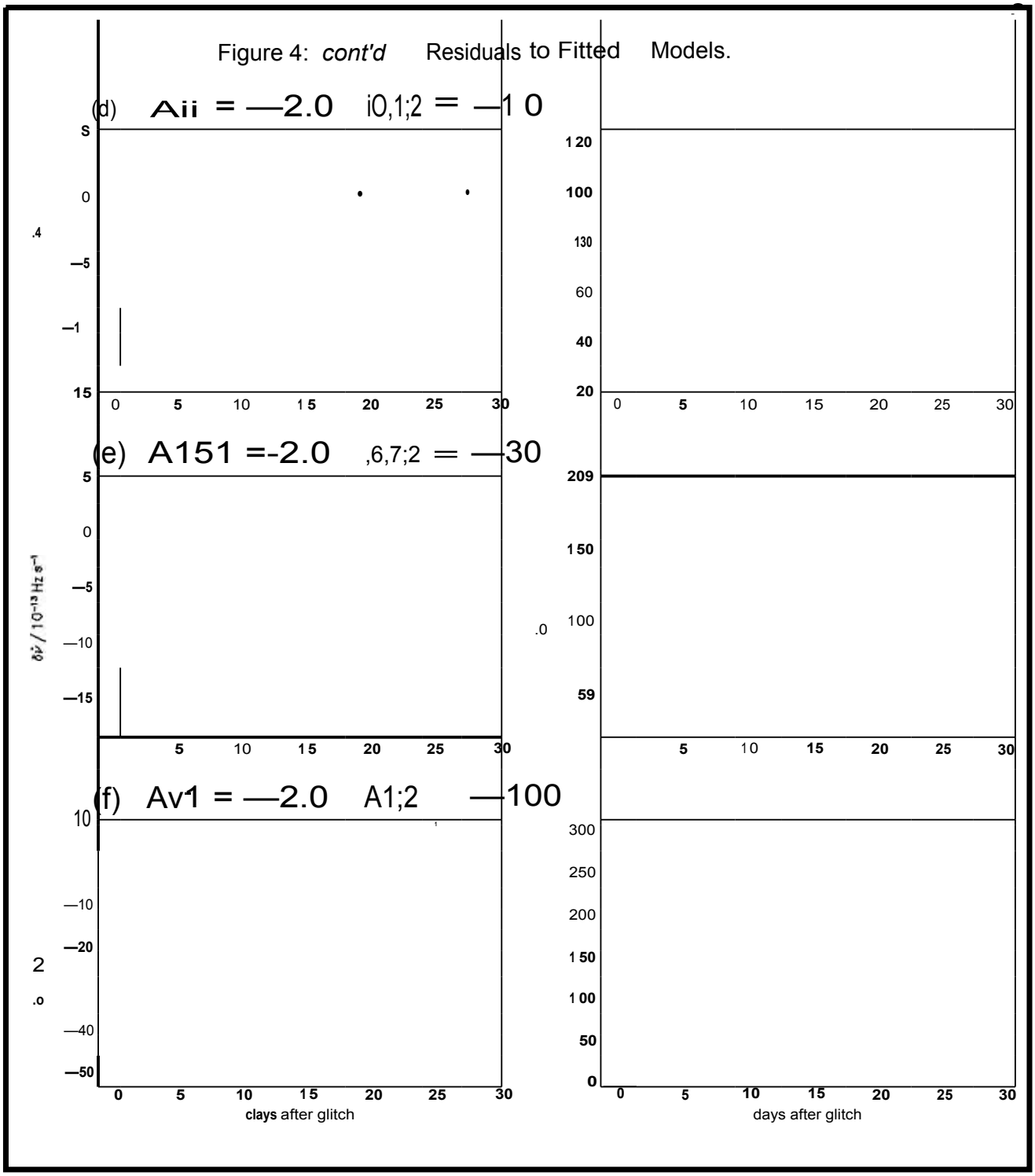

Figure 4: *cont'd* Residuals to Fitted Models.

Figure 4: *cont'd* Residuals to Fitted Models.

(g) A —2.0 LI/2 = —1 0

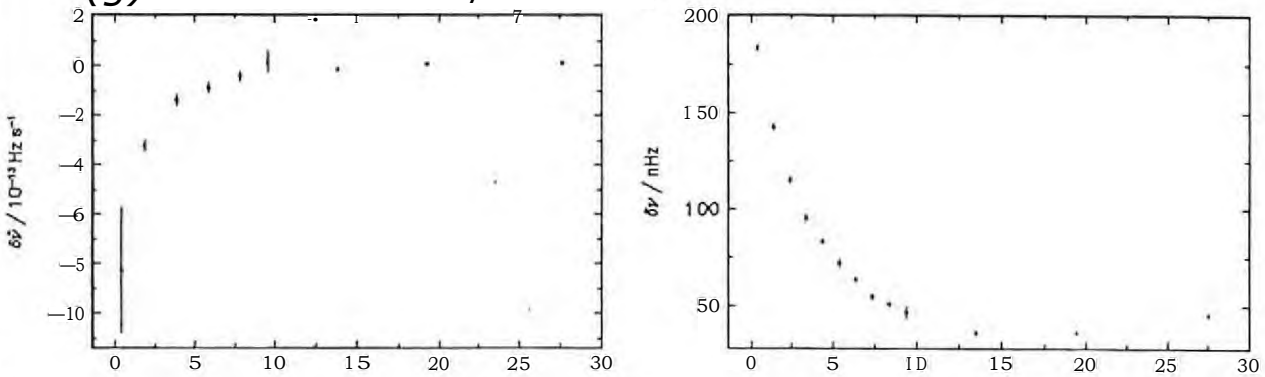

(h) Aii = —2.0 A1%2 = —30

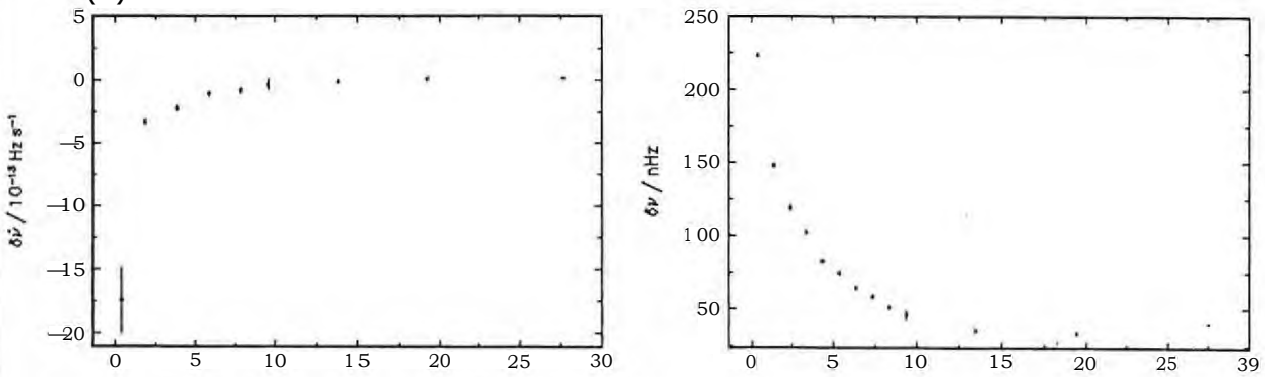

(1) Avi =-2.0 Av2 = —100

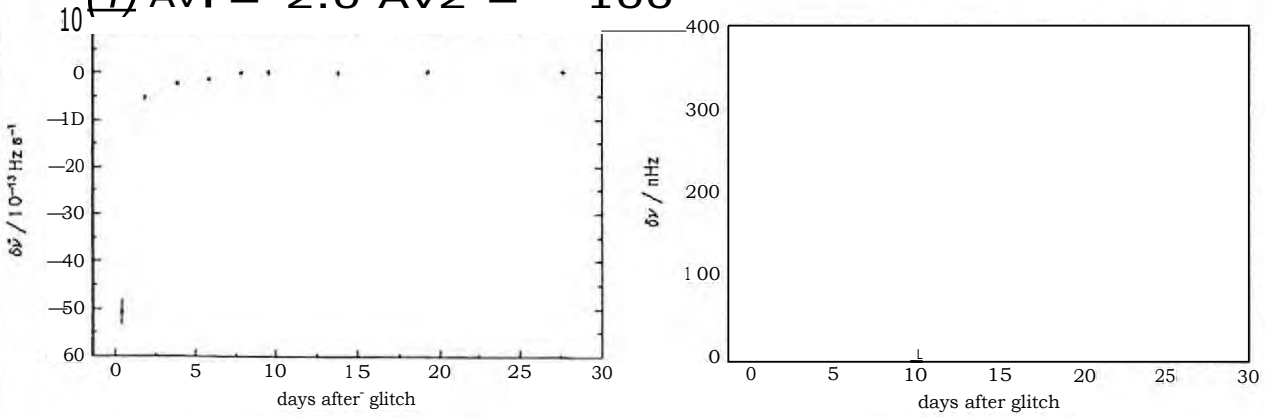

Figure 4: *cont'd* Residuals to Fitted i/ + 1-decay Models.

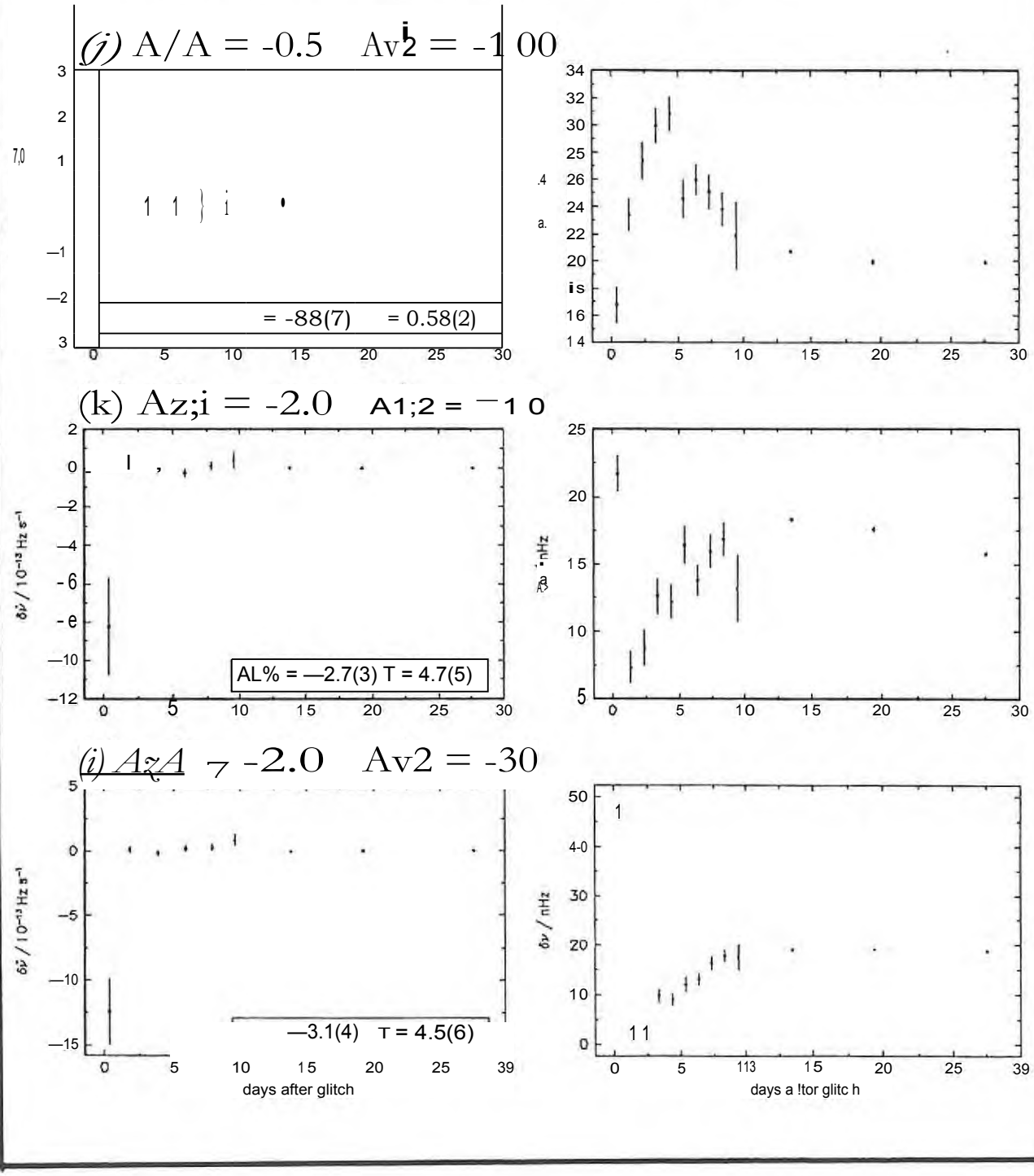

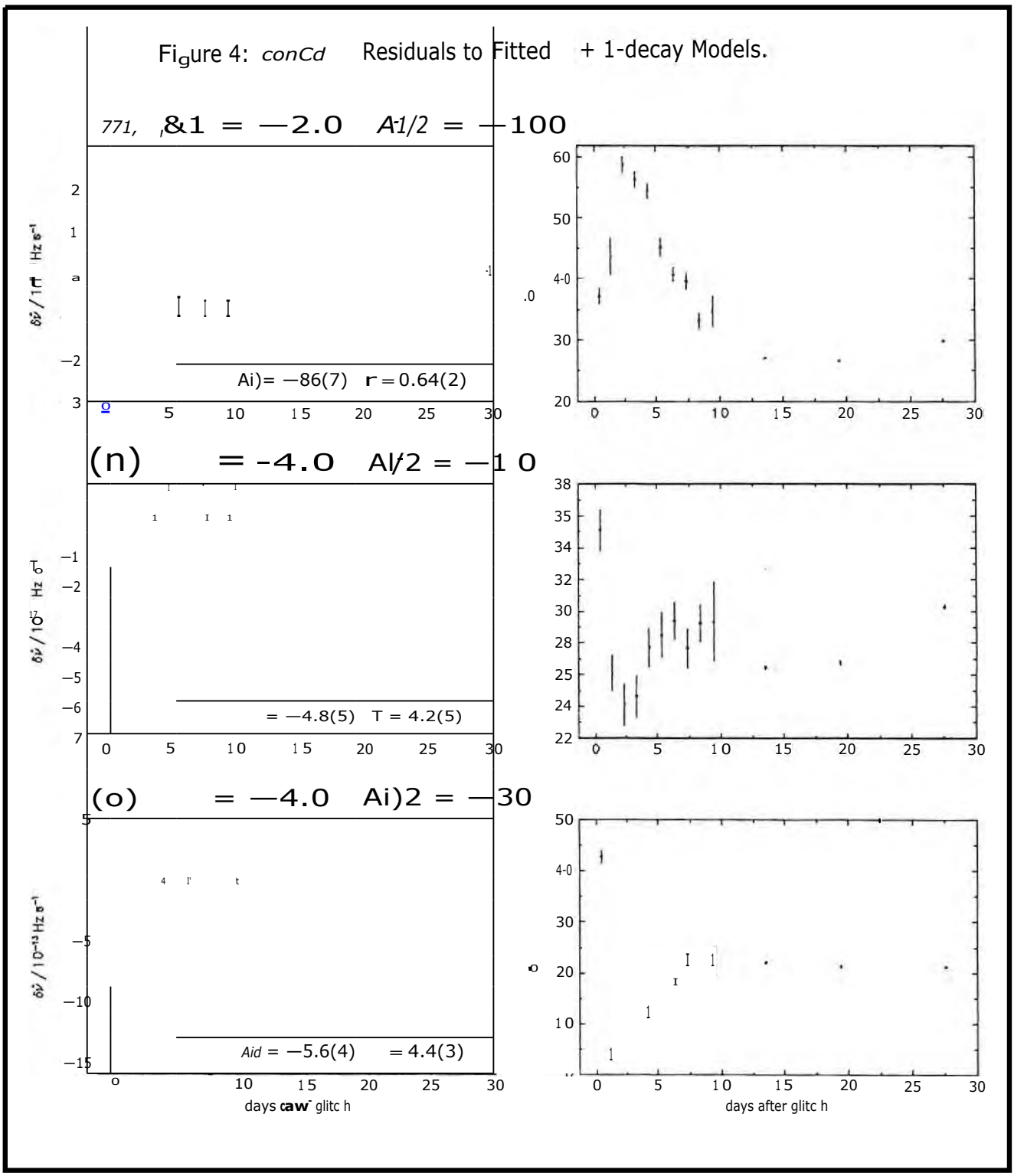
Figure 4: conCd Residuals to Fitted + 1-decay Models.
771, &1 = —2.0 A1/2 = —100
Ai)= —86(7) r = 0.64(2)
(n) = -4.0 Al/2 = —1 0
= —4.8(5) T = 4.2(5)
(o) = —4.0 Ai)2 = —30
Aid = —5.6(4) = 4.4(3)
days caw glitc h
days after glitc h

Figure 4: *cont'd* Residuals to Fitted 1/ + 2-decay Models.

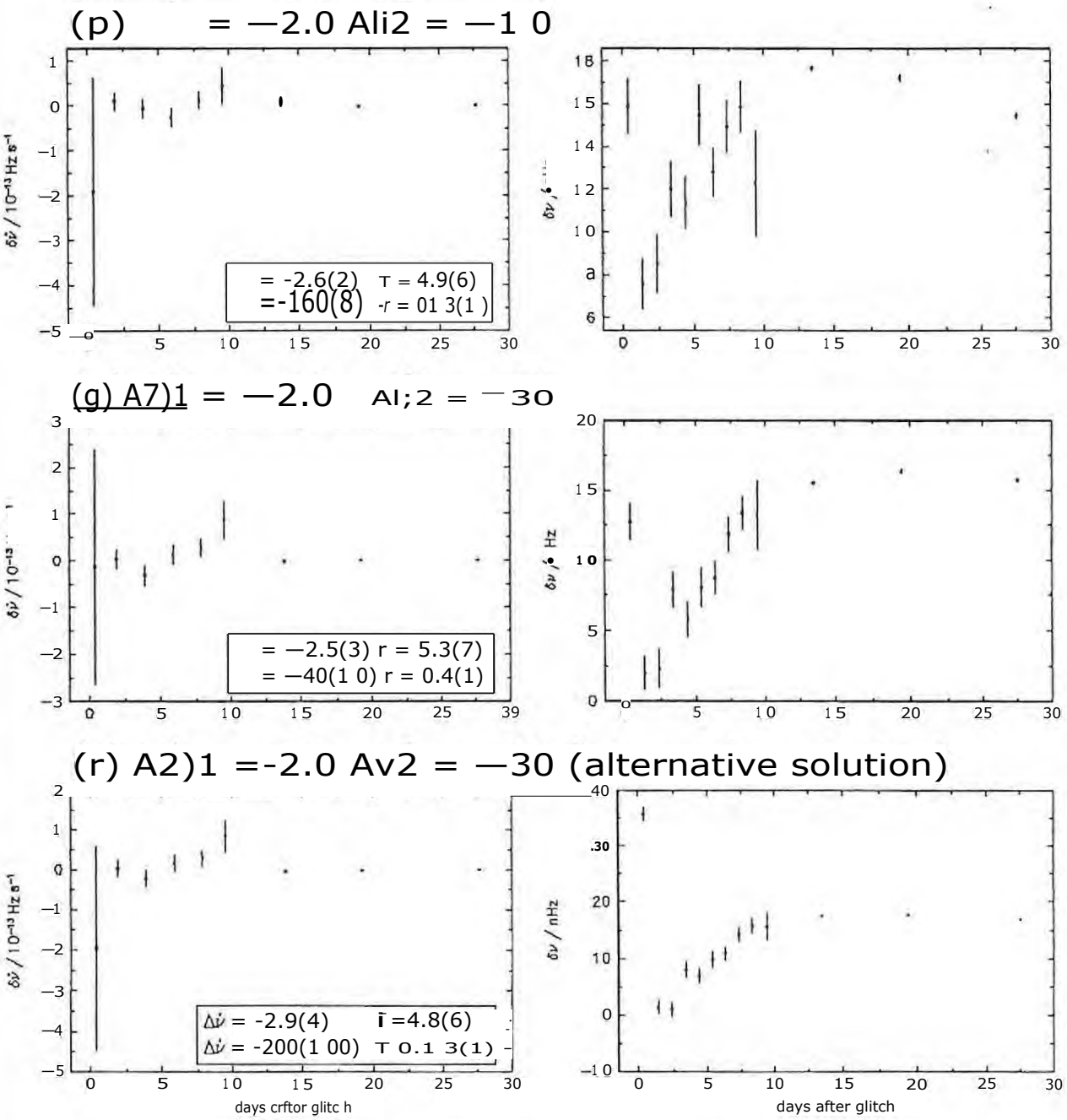

Figure 4: *cont'd* Residuals to Fitted 1*f* + 2-decay Models.